frontiers | Research Topics

Double-edged swords: Important factors connecting metabolic disorders and cancer development - from basic research to translational applications

Edited by
Che-Pei Kung, Conghui Yao, Thibaut Barnoud and Maureen Murphy

Published in
Frontiers in Oncology
Frontiers in Endocrinology

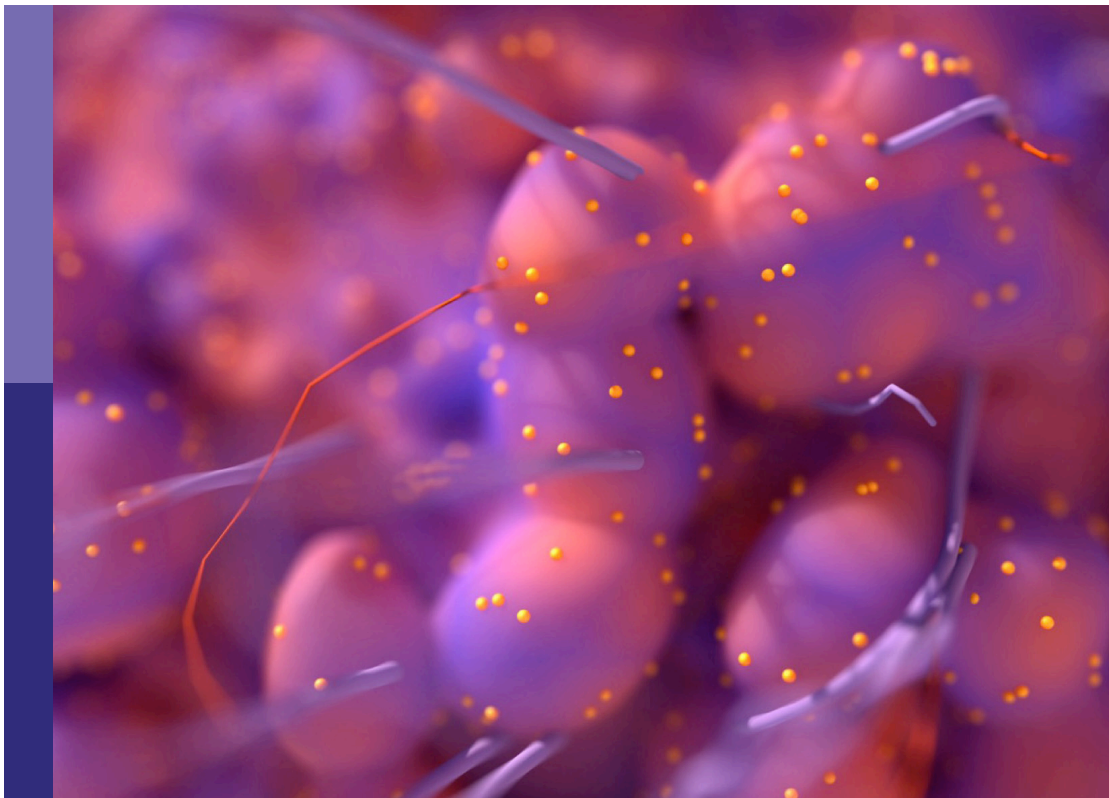

ISSN 1664-8714
ISBN 978-2-83251-939-4
DOI 10.3389/978-2-83251-939-4

About Frontiers

Frontiers is more than just an open access publisher of scholarly articles: it is a pioneering approach to the world of academia, radically improving the way scholarly research is managed. The grand vision of Frontiers is a world where all people have an equal opportunity to seek, share and generate knowledge. Frontiers provides immediate and permanent online open access to all its publications, but this alone is not enough to realize our grand goals.

Frontiers journal series

The Frontiers journal series is a multi-tier and interdisciplinary set of open-access, online journals, promising a paradigm shift from the current review, selection and dissemination processes in academic publishing. All Frontiers journals are driven by researchers for researchers; therefore, they constitute a service to the scholarly community. At the same time, the *Frontiers journal series* operates on a revolutionary invention, the tiered publishing system, initially addressing specific communities of scholars, and gradually climbing up to broader public understanding, thus serving the interests of the lay society, too.

Dedication to quality

Each Frontiers article is a landmark of the highest quality, thanks to genuinely collaborative interactions between authors and review editors, who include some of the world's best academicians. Research must be certified by peers before entering a stream of knowledge that may eventually reach the public - and shape society; therefore, Frontiers only applies the most rigorous and unbiased reviews. Frontiers revolutionizes research publishing by freely delivering the most outstanding research, evaluated with no bias from both the academic and social point of view. By applying the most advanced information technologies, Frontiers is catapulting scholarly publishing into a new generation.

What are Frontiers Research Topics?

Frontiers Research Topics are very popular trademarks of the *Frontiers journals series*: they are collections of at least ten articles, all centered on a particular subject. With their unique mix of varied contributions from Original Research to Review Articles, Frontiers Research Topics unify the most influential researchers, the latest key findings and historical advances in a hot research area.

Find out more on how to host your own Frontiers Research Topic or contribute to one as an author by contacting the Frontiers editorial office: frontiersin.org/about/contact

Double-edged swords: Important factors connecting metabolic disorders and cancer development - from basic research to translational applications

Topic editors

Che-Pei Kung — Washington University in St. Louis, United States
Conghui Yao — Harvard Medical School, United States
Thibaut Barnoud — Medical University of South Carolina, United States
Maureen Murphy — Wistar Institute, United States

Citation

Kung, C.-P., Yao, C., Barnoud, T., Murphy, M., eds. (2023). *Double-edged swords: Important factors connecting metabolic disorders and cancer development - from basic research to translational applications*. Lausanne: Frontiers Media SA.
doi: 10.3389/978-2-83251-939-4

Table of contents

frontiers | Frontiers in Endocrinology

TYPE Editorial
PUBLISHED 02 March 2023
DOI 10.3389/fendo.2023.1168700

OPEN ACCESS

EDITED AND REVIEWED BY
Antonino Belfiore,
University of Catania, Italy

*CORRESPONDENCE
Che-Pei Kung
patkung@wustl.edu

SPECIALTY SECTION
This article was submitted to Cancer Endocrinology, a section of the journal Frontiers in Endocrinology

RECEIVED 17 February 2023
ACCEPTED 22 February 2023
PUBLISHED 02 March 2023

CITATION
Kung C-P, Barnoud T, Yao C-H and Murphy ME (2023) Editorial: Double-edged swords: Important factors connecting metabolic disorders and cancer development – from basic research to translational applications. *Front. Endocrinol.* 14:1168700. doi: 10.3389/fendo.2023.1168700

Editorial: Double-edged swords: Important factors connecting metabolic disorders and cancer development – from basic research to translational applications

Che-Pei Kung[1]*, Thibaut Barnoud[2], Cong-Hui Yao[3] and Maureen E. Murphy[4]

[1]Division of Molecular Oncology, Department of Medicine, School of Medicine, Washington University in St. Louis, Saint Louis, MO, United States, [2]Department of Biochemistry and Molecular Biology, College of Medicine, Medical University of South Carolina, Charleston, SC, United States, [3]Department of Cell Biology, Blavatnik Institute, Harvard Medical School, Boston, MA, United States, [4]Program in Molecular and Cellular Oncogenesis, The Wistar Institute, Philadelphia, PA, United States

KEYWORDS

metabolism, cancer, translational research, MetS (metabolic syndrome), microbiome, obesity, p53, metabolomics

Editorial on the Research Topic

Double-edged swords: Important factors connecting metabolic disorders and cancer development - from basic research to translational applications

The relationship between metabolic dysfunction and cancer development has been informed by research of epidemiology, endocrinology, cancer biology, chemistry, genomics, and metabolomics. By revealing both distinctive and shared mechanisms, the articles in this issue, including both original research studies and reviews, point to opportunities to discover new diagnostic and therapeutic strategies.

The relationship between metabolic syndromes (MetS) and cancer is multi-faceted (1). One field of interest is to link existing MetS with cancer prognosis. In *"Effects of Metabolic Syndrome and Its Components on the Prognosis of Endometrial Cancer"*, Yang et al. explored the effects of MetS on the prognosis of endometrial cancer (EC) in over 500 patients, and found that combining high-density lipoprotein cholesterol with tumor stage and grade improved the prediction power for patient survival.

MetS also impacts other clinical outcomes in cancer patients. In *"Effect and Management of Excess Weight in the Context of Fertility-Sparing Treatments in Patients with Atypical Endometrial Hyperplasia and Endometrial Cancer: Eight-Year Experience of 227 Cases"*, Shan et al. investigated the clinical outcomes of cancer therapy and fertility-sparing treatments (FSTs) in overweight EC patients. They showed that the combination of gonadotropin-releasing hormone agonist and levonorgestrel intrauterine device resulted in better disease-free survival for overweight patients. Moreover, patients with normal weight achieved a better pregnancy

rate through FSTs, while overweight patients benefited from ovulation induction to improve fertility success.

In *"Hepatocellular Carcinoma and Obesity, Type 2 Diabetes Mellitus, Cardiovascular Disease: Causing Factors, Molecular Links, and Treatment Options"*, Zhang et al. summarized the current literature linking MetS, including diabetes, obesity, and cardiovascular disease, to the development of non-alcoholic fatty liver disease and HCC. They discussed signaling pathways involved and their potential as therapeutic targets. Can we take advantage of this knowledge to develop better diagnostic tools? That is the question Cao et al. explored in "Metabolic Profiling Identified a Novel Biomarker Panel for Metabolic Syndrome-Positive Hepatocellular Cancer", in which they used targeted metabolomic analysis to identify biomarkers for MetS-positive HCC. A panel including L-gluamic acid, pipecolic acid and alpha-fetoprotein was identified as a potential diagnostic tool for MetS-positive HCC. With recent advances in metabolomic technologies, more examples like this could become reality in aiding early diagnosis and personalized therapy of cancer (2).

Outside of clinical settings, we have also highlighted preclinical investigations studying roles of metabolic pathways in cancer progression and therapy response. The tumor suppressor p53 plays versatile roles in regulating metabolic dysfunction and cancer (3). In *"Mutant p53-microRNA-200c-ZEB2-Axis-Induced CPT1C Elevation Contributes to Metabolic Reprogramming and Tumor Progression in Basal-Like Breast Cancers"*, Wang et al. provided new insight about how mutant p53 (Mutp53) contributes to tumor progression in basal-like breast cancers. They demonstrated that Mutp53 enhances fatty acid oxidation through dysregulating the miR-200c-ZEB2 axis to induce CPT1C, resulting in epithelial-mesenchymal transition phenotypes and increased cancer stemness. These data suggest that Mutp53-driven metabolic reprogramming could be an effective therapeutic target. In a complementary Mini-Review article *"p53-Mediated Indirect Regulation on Cellular Metabolism: From the Mechanism of Pathogenesis to the Development of Cancer Therapeutics"*, Wang and Chao summarized the indirect regulation of cellular metabolism by wild-type and mutant p53 through 1) transcriptional targets, 2) protein-protein interaction with other transcription factors, and 3) other signaling pathways. These findings support the premise that improving understanding of these mechanisms can inform novel therapeutic strategies through the concept of synthetic lethality.

One of the most studied cancer-regulating metabolic mechanisms is the Warburg effect, describing cancers' propensity to use glycolysis for their survival (4). In *"FBP1/miR-24-1/enhancer axis activation blocks renal cell carcinoma progression via Warburg effect"*, Ju et al. showed that FBP1, a rate-limiting enzyme regulating gluconeogenesis and whose downregulation in renal cell carcinoma (RCC) is linked to poor survival, can be activated to slow down RCC progression. This can be achieved through employing miR-24-1, a nuclear activating miRNA, to activate FBP1 and repress the Warburg effect in RCC cells.

Metabolic alterations also regulate treatment response of cancer. In *"Lapatinib Suppresses HER2-Overexpressed Cholangiocarcinoma and Overcomes ABCB1– Mediated Gemcitabine Chemoresistance"*, Bai et al. showed that HER2-targeting lapatinib overcomes gemcitabine resistance in cholangiocarcinoma (CCA). Gemcitabine works as a nucleoside analog to suppress cancer cell proliferation, and the authors showed that the active metabolite of gemcitabine, dFdCTP, is a substrate of ATP-binding cassette subfamily B member 1 (ABCB1). Gemcitabine-treated CCA cells develop a negative feedback loop by upregulating ABCB1 to cause gemcitabine resistance, which can be circumvented by the combination of lapatinib and gemcitabine.

The relationship between metabolism and tumorigenesis is more than one-directional. Oncogenes and tumor suppressors can also play important roles in the development of metabolic diseases (5, Chen et al.). In *"Tumor Suppressor Par-4 Regulates Complement Factor C3 and Obesity"*, Araujo et al. used both *in vitro* and *in vivo* models to show that another tumor suppressor, prostate apoptosis response-4 (Par-4), contributes to the development of obesity. Par-4 suppresses p53 and its target, complement factor c3, to regulate fat storage in adipocytes. Mice with Par-4 deletion developed obesity even with standard diet. Lower expression of Par-4 was found in obese patients and associated with increased risk of developing obesity later in life.

Finally, the microbiome can dictate our susceptibility to metabolic dysfunction and cancer (6). In *"Connecting the Dots Between the Gut–IGF-1–Prostate Axis: A Role of IGF-1 in Prostate Carcinogenesis"*, Matsushita et al. summarized the relationship between prostate cancer (PCa) and Insulin-like growth factor 1 (IGF-1) to exemplify this concept. They highlighted the recent finding that short-chain fatty acids produced by the gut microbiota increase IGF-1 production, resulting in PCa progression through activation of downstream signaling pathways (7). They suggest that specialized dietary interventions could be implemented for prevention and treatment of PCa through optimizing the gut microbiome.

With fast-growing interest from scientific communities of different disciplines to understand the relationship between metabolic disorder and cancer development, this Research Topic hopefully serves as a precursor and medium to facilitate more nuanced, even provocative discussions to re-think and innovate actionable strategies to reduce the burden of human disease.

Author contributions

C-PK drafted the manuscript. C-PK, TB, C-HY, and MEM reviewed and revised the manuscript. All authors contributed to the article and approved the submitted version.

Acknowledgments

We sincerely thank all the reviewers for offering their time and effort for this project, and the editorial team at Frontiers for their help and professionalism throughout this process.

Conflict of interest

The authors declare that the research was conducted in the absence of any commercial or financial relationships that could be construed as a potential conflict of interest.

Publisher's note

References

1. Uzunlulu M, Telci Caklili O, Oguz A. Association between metabolic syndrome and cancer. *Ann Nutr Metab* (2016) 68(3):173–9. doi: 10.1159/000443743

2. Yao CH, Wang L, Stancliffe E, Sindelar M, Cho K, Yin W, et al. Dose-response metabolomics to understand biochemical mechanisms and off-target drug effects with the TOXcms software. *Anal Chem* (2020) 92(2):1856–64. doi: 10.1021/acs.analchem.9b03811

3. Barnoud T, Indeglia A, Murphy ME. Shifting the paradigms for tumor suppression: lessons from the p53 field. *Oncogene* (2021) 40(25):4281–90. doi: 10.1038/s41388-021-01852-z

4. DeBerardinis RJ, Chandel NS. We need to talk about the warburg effect. *Nat Metab* (2020) 2(2):127–9. doi: 10.1038/s42255-020-0172-2

5. Kung CP, Murphy ME. The role of the p53 tumor suppressor in metabolism and diabetes. *J Endocrinol* (2016) 231(2):R61–75. doi: 10.1530/JOE-16-0324

6. Cullin N, Azevedo Antunes C, Straussman R, Stein-Thoeringer CK, Elinav E. Microbiome and cancer. *Cancer Cell* (2021) 39(10):1317–41. doi: 10.1016/j.ccell.2021.08.006

7. Matsushita M, Fujita K, Hayashi T, Kayama H, Motooka D, Hase H, et al. Gut microbiota-derived short-chain fatty acids promote prostate cancer growth *via* IGF1 signaling. *Cancer Res* (2021) 81(15):4014–26. doi: 10.1158/0008-5472.CAN-20-4090

frontiers in Oncology

ORIGINAL RESEARCH
published: 05 November 2021
doi: 10.3389/fonc.2021.749881

Effect and Management of Excess Weight in the Context of Fertility-Sparing Treatments in Patients With Atypical Endometrial Hyperplasia and Endometrial Cancer: Eight-Year Experience of 227 Cases

Ying Shan[1,2†], Meng Qin[1,2†], Jie Yin[1,2], Yan Cai[1,2], Yan Li[1,2], Yu Gu[1,2], Wei Wang[1,2], Yong-xue Wang[1,2], Jia-yu Chen[12], Ying Jin[1,2] and Ling-ya Pan[1,2*]*

[1] Department of Obstetrics and Gynecology, Peking Union Medical College Hospital, Chinese Academy of Medical Sciences and Peking Union Medical College, Beijing, China, [2] National Clinical Research Center for Obstetric & Gynecologic Diseases, Beijing, China

Objective: To investigate the oncologic and reproductive outcomes of fertility-sparing treatments (FSTs) in atypical endometrial hyperplasia (AEH) and endometrial cancer (EC) patients with excess weight (EW).

Methods: This retrospective study comprised patients with AEH or EC who achieved a complete response (CR) after FST from 2010 to 2018. The clinical characteristics, oncological and reproductive outcomes were compared between the excess weight (EW) group (body mass index (BMI)≥25 kg/m^2) and normal weight (NW) group (BMI<25 kg/m^2). The risk factors associated with recurrence and unsuccessful pregnancy in patients with EW were analyzed.

Results: Overall, 227 patients were enrolled, including 139 (61.2%) in EW group and 88 (38.8%) in NW group. In patients with EW, the pregnancy rate, the live birth rate and the relapse rate were 29.8%, 23.4%, and 30.9%, respectively. In patients with NW, these rates were 61.1%, 47.2%, and 31.8%, respectively. No significant differences were observed in the time to remission (P=0.865) and disease-free survival (DFS) (P=0.750). Patients in NW group achieved a better pregnancy rate than patients in the EW group (P=0.034). The patients with EW using ovulation induction to increase fertility tended to have a shorter time to pregnancy (P=0.042). However, no significant risk factors associated with unsuccessful pregnancy were identified after the multivariate analysis. In terms of DFS, the combination of gonadotropin-releasing hormone agonist (GnRH-a) and LNG-IUD was better for patients with EW than GnRH-a or oral progestin therapy alone (P=0.044, adjusted hazard ratio (HR)=0.432, 95% confidence interval (CI): 0.152-1.229), especially for patients with EW diagnosed with EC (P=0.032).

OPEN ACCESS

Edited by:
Che-Pei Kung, Washington University School of Medicine in St. Louis, United States

Reviewed by:
Gulzhanat Aimagambetova, Nazarbayev University, Kazakhstan
Mathieu Luyckx, Cliniques Universitaires Saint-Luc, Belgium

***Correspondence:**
Ling-ya Pan
panly@pumch.cn
Ying Jin
jinying@pumch.cn

†These authors have contributed equally to this work

Specialty section:
This article was submitted to Cancer Metabolism, a section of the journal Frontiers in Oncology

Received: *30 July 2021*
Accepted: *22 October 2021*
Published: *05 November 2021*

Citation:
Shan Y, Qin M, Yin J, Cai Y, Li Y, Gu Y, Wang W, Wang Y-x, Chen J-y, Jin Y and Pan L-y (2021) Effect and Management of Excess Weight in the Context of Fertility-Sparing Treatments in Patients With Atypical Endometrial Hyperplasia and Endometrial Cancer: Eight-Year Experience of 227 Cases. Front. Oncol. 11:749881. doi: 10.3389/fonc.2021.749881

Conclusion: FSTs for overweight and obese patients should be more individualized. GnRH-a and/or LNG-IUD may be options prior to FSTs in patients with EW. Further prospective studies are needed.

Keywords: fertility-sparing treatments, atypical endometrial hyperplasia (AEH), endometrial cancer (EC), excess weight, levonorgestrel intrauterine devices, gonadotropin-releasing hormone agonist (GnRH- a)

INTRODUCTION

Endometrial cancer (EC) is one of the most common malignant tumors in females (1). EC usually arises in postmenopausal women, but approximately 10% of EC patients are younger than 40 years old (2). Atypical endometrial hyperplasia (AEH) prior to EC represents a continuously changing disease process as AEH is a precancerous lesion of EC. The risk of AEH progressing to EC within fifteen years has been reported to be as high as 29.0% (3, 4). Thus, therapy for both AEH and EC should warrant attention.

In recent years, the incidence of young patients with AEH and EC has increased worldwide, and fertility-sparing treatments (FSTs) to preserve reproductive function are urgently needed (5). Approximately 80% of young EC patients have well-differentiated type I disease at a very early stage and high-estrogen exposure backgrounds, presenting the possibility of progestin-based therapy (6). The National Comprehensive Cancer Network (NCCN) has provided FST options for the management of AEH and EC patients who meet five specific criteria (7). The common recommended conservative treatments for AEH and EC include high-dose oral progestin and levonorgestrel intrauterine devices (LNG-IUDs). After FST, most AEH and EC patients can achieve a higher complete response (CR) rate and lower relapse rate and then successfully undergo delivery (8). Nevertheless, approximately one-quarter of females still suffer from recurrence problems. Gallos et al. showed that the relapse rates of patients with EC and AEH after FST were 40.6% and 26%, respectively, in a meta-analysis of 34 observational studies (9). The curative effect and prognostic outcomes after recurrence were not satisfactory. Therefore, the risk factors for recurrence must be identified to decrease the risk of recurrence.

The relationship between obesity and endometrial cancer (EC) has been established and accepted for decades. Overweight and obesity are evaluated by body mass index (BMI), which is a measurement of a person's weight with respect to his or her height. The World Health Organization (WHO) defines an adult who has a BMI between 25 kg/m^2 and 29.9 kg/m^2 as overweight and an adult who has a BMI of 30 kg/m^2 or higher as obese (10). On the one hand, the risk of EC increases with increasing weight according to several previous reports (11). Compared with normal-weight women, the relative risk (RR) and odds ratio for developing EC were 1.34 and 1.43 in overweight women and 2.54 and 3.33 in obese women, respectively (12). The previous study from our single team reported that age ≥35 years, obesity, prolonged time to CR, and consistent infertility after conservative treatment were associated with an increased risk of recurrence (9). In addition, although the mortality rate of EC is low, the RR of death is significantly higher for obese EC patients than for those with a normal BMI (RR 2.53 for BMI 30–34 kg/m^2, RR 6.25 for BMI > 40 kg/m^2) (13). Thus, we can solve most of treatment and recurrence problems related to FSTs if we can solve the treatment problems encountered in obese patients with AEH and EC. On the other hand, FSTs for obese patients are challenging. Obese patients with EC often have multiple complications, such as polycystic ovarian syndrome (PCOS), diabetes mellitus (DM), and hypertension. Moreover, obesity not only is a risk factor for developing EC but may also significantly impact pregnancy (14). High-dose oral progestin, as the most common FST, has side effects, including weight gain, abnormal lipid metabolism, and compromised liver function. These side effects limit its application in overweight patients and may lead to an increased risk of recurrence (15). Recently, the use of gonadotropin-releasing hormone agonist (GnRH-a) has become widely popularized for obese patients in clinical practice, but NCCN guidelines do not provide specific treatment recommendations (16).

Therefore, we performed this retrospective study to explore the oncologic and reproductive results of FSTs in patients with excess weight (EW) with AEH and EC, as well as risk factors for unsuccessful and recurrent pregnancy. Developing more suitable management strategies is important for such populations.

MATERIALS AND METHODS

Study Population

This retrospective study included all patients with AEH and EC who received FSTs between January 2010 and December 2018 at Peking Union Medical College Hospital (PUMCH). Patients with EW were defined as having a BMI equal to or greater than 25 kg/m^2. In our institution, patients were considered candidates for FST when they met the following criteria, which were almost consistent with NCCN guidelines (7): 1) age younger than 40 years old and a strong desire for fertility preservation; 2) a diagnosis of EC of a well-differentiated type (G1) or AEH through dilation and curettage (D&C) with or without hysteroscopy, with confirmation of the pathological diagnosis by at least two experienced gynecological pathologists; 3) a tumor confined to the endometrium with no evidence of myometrial invasion as evaluated by transvaginal ultrasonography and pelvic magnetic resonance imaging (MRI); 4) Estrogen receptor (ER) and progesterone receptor (PR) positivity; 5) a normal serum CA125 level; 6) no contraindications for progestin therapy or other medical therapy; 7) fertility function assessment prior to FST; and 8) an understanding through

counseling that fertility-sparing option is not a standard of care for the treatment of EC and provision of written informed consent. This study was conducted with the approval of the Ethics Committee of PUMCH.

Data Collection

All included patients were provided counseling regarding their FST options, including the side effects of the drugs and potential risks of recurrence or progression. Patients who met the study inclusion criteria were divided into two groups: the excess weight (EW) group, BMI of which was equal to or more than 25 kg/m^2; the normal weight (NW) group, BMI of which was less than 25 kg/m^2. In this study, the treatment methods were divided into four groups: 1) MPA; 2) MA; 3) GnRH-a; and 4) GnRH-a+LNG-IUD. Oral progestin therapy is one of the most common primary FSTs and includes medroxyprogesterone acetate (MPA) at doses of 250-500 mg/day or megestrol acetate (MA) at doses of 160-480 mg/day. If a patient with EC or with extended lesion, GnRH-a was administered for three to six cycles (3.6 mg/3.75 mg) by subcutaneous injection as the first treatment according to experience. In addition, an LNG-IUD could be placed in combination for treatment. The patients using common therapy in combination with letrozole or only LNG-IUD were in a small number, which were excluded from this study to avoid results bias. The response to treatment was assessed every 3-6 months using pathological specimens, which were obtained *via* D&C and hysteroscopy. CR was defined as the absence of endometrial hyperplasia or carcinoma. Patients were recommended to receive regular maintenance treatment after CR while waiting for fertility or not having fertility willing, which included LNG-IUD or low-dose oral progestin. The ultrasound should be administered every 3 to 6 months during maintenance therapy.

All willing patients with immediate fertility after a CR were transferred to the specialized reproductive center to undergo counseling regarding reproductive treatment options. In a general way, the patients with a preferable ovarian reserve and successful ovulation, as well as smooth fallopian tubes, were encouraged to conceive spontaneously. Patients with anovulation were recommended track their sex life and induce ovulation with letrozole, which was administered at a dose of 2.5 mg/day for 5 days. For patients with a reduced ovarian reserve, anovulation, or PCOS, assisted reproductive technology (ART) was encouraged as early as possible. These methods included intrauterine insemination (IUI) or *in vitro* fertilization and embryo transfer (IVF-ET). The time to pregnancy was defined as the time interval between the date that CR was achieved and the date that a pregnancy was confirmed by ultrasound examination or the final follow-up.

Recurrence was defined as initial lesions (AEH or EC) reappearing in the specimen after complete remission or a disease lesion reappearing in the endometrium and/or myometrium on imaging examination. Patients with EW were divided into two groups: the recurrence group and the control group. Disease-free survival (DFS) was defined as the time interval between the date that CR was achieved and the date of recurrence or the final follow-up. For this study, patients with any of the following characteristics were excluded: 1) received other treatments except MA, MPA and GnRHa ± LNG-IUD; 2) did not achieve CR after FST; 3) were not regularly evaluated every three months *via* D&C or hysteroscopy during the treatment period; and 4) were not followed up regularly after CR at PUMCH or a local hospital.

Statistical Analysis

All statistical analyses were performed using SPSS software (version 23.0; SPSS Inc., Chicago, IL, USA), and graphs were generated using GraphPad Prism software for Macbook (version 7.0; GraphPad software Inc., San Diego, USA). Student's t-tests and Mann-Whitney U tests were used to compare continuous variables. Pearson's chi-squared tests and Fisher's exact tests were used to compare categorical variables (17). Survival analysis was performed using Kaplan-Meier curves and the log-rank test. Each factor related to survival outcomes was individually evaluated using a Cox regression model in a univariate analysis. Then, all variables with P values <0.200 and meaningful variables based on the univariate analysis were included in the Cox proportional hazards regression model in a multivariate analysis. The associations of these variables with follow-up outcomes was evaluated by hazard ratios (HRs) and 95% confidence intervals (CIs). Statistical significance was set at $P<0.050$.

RESULTS

The Clinical Characteristics, Treatment Choices, and Follow-up Outcomes of the Included Patients

Table 1 shows the clinical and pathological characteristics of AEH and EC patients after FST between EW and the NW group. Overall, 227 patients who met the inclusion criteria were included in this retrospective analysis. The NW group contained 88 (38.8%) patients, while the EW group contained 139 (61.2%) patients, including 74 (53.2%) patients with a 25≤BMI<30 kg/m^2 and 65 (46.8%) patients with a BMI≥30 kg/m^2. The mean BMI of all patients was 26.8(± 5.2) kg/m^2 (ranging from 18.0 to 46.5 kg/m^2), and the mean age was 31.5 (± 4.7) years. A total of 29.1% of patients had complications, including PCOS (20.7%), DM (5.3%), and others (3.1%). A total of 63.0% of patients were diagnosed with AEH, and 37.0% were diagnosed with EC. The median follow-up time was 41.7 (± 23.0) months. No significant differences were observed in complications (P=0.120), menstruation cycle (P=0.190), previous pregnancy (P=0.050), previous delivery (P=0.063), and histology (P=0.902). Therefore, most of variables were equally comparable for the survival analysis.

The treatment, follow-up and reproductive outcomes of the included patients are shown in **Table 2**. The treatment methods were divided into four groups: MPA (40.1%), MA (17.2%), GnRH-a (17.6%), and GnRH-a+LNG-IUD (25.1%). A total of 51.1% of patients received regular maintenance treatment, including LNG-IUDs (73.3%) and Duphaston (26.7%). The

TABLE 1 | The clinical characteristics of AEH and EC patients after FST between the excess weight group and normal weight group.

Variable	Total (N = 227)	Excess weight group (N = 139)	Normal weight group (N = 88)	*P*
BMI (kg/m^2)				
Mean ± SD	26.8 ± 5.2	30.1 ± 3.9	21.7 ± 1.8	
Range	18.0-46.5	25.0-46.5	18.0-24.8	
Age (year)	31.5 ± 4.7	32.2 ± 4.5	30.4 ± 4.8	0.028
≤35	182 (80.2%)	105 (75.5%)	77 (87.5%)	
>35	45 (19.8%)	34 (24.5%)	11 (12.5%)	
Complications				0.120
No	161 (70.9%)	91 (65.5%)	70 (79.5%)	
PCOS	47 (20.7%)	33 (23.7%)	14 (15.9%)	
Diabetes mellitus	12 (5.3%)	9 (6.5%)	3 (3.5%)	
Others	7 (3.1%)	6 (4.3%)	1 (1.1%)	
Menstruation cycle				0.190
Regular	114 (50.2%)	65 (46.8%)	49 (55.7%)	
Irregular	113 (49.8%)	74 (53.2%)	39 (44.3%)	
Previous pregnancy				0.050
No	150 (66.1%)	85 (61.2%)	65 (73.9%)	
Yes	77 (33.9%)	54 (38.8%)	23 (26.1%)	
Previous delivery				0.063
No	182 (80.2%)	106 (76.3%)	76 (86.4%)	
Yes	45 (19.8%)	33 (23.7%)	12 (13.6%)	
Histology				0.902
AEH	143 (63.0%)	88 (63.3%)	55 (62.5%)	
EC	84 (37.0%)	51 (36.7%)	33 (37.5%)	
Follow-up time (Months)	41.7 ± 23.0	39.7 ± 21.5	44.8 ± 25.0	

Data are presented as number (%) or mean (± SD) or median (± IQR). BMI, body mass index; PCOS, polycystic ovary syndrome; AEH, atypical endometrial hyperplasia; EC, endometrial cancer.

mean time to a CR was 8.7 (± 5.6) months, and 22% patients need more than 12 months. The time to remission among the four treatment types did not significantly differ (*P*=0.597) in patients with EW, as shown in **Figure 2A**. A total of 33.8% of patients with EW had an immediate pregnancy intention after remission and attempted to become pregnant by different methods. Among these patients with EW, 27.7% of patients spontaneously became pregnant, 23.4% used ovulation induction, and the others used IVF-ET to improve their chances of conceiving. In patients with EW, the pregnancy rate, the live birth rate and the relapse rate were respectively 29.8%, 23.4%, and 30.9%. While in patients with NW, the pregnancy rate, the live birth rate and the relapse rate were respectively 61.1%, 47.2%, and 31.8%. There were no significant differences of the time to remission between EW group and NW group in **Figure 1A** (*P*=0.865). The patients in NW group showed similar DFS with patients in EW group in **Figure 1B** (*P*=0.750, HR=0.926, 95% CI: 0.577-1.485). However, the patients in NW group had better pregnancy rate than in EW group (*P*=0.034, HR=2.023, 95% CI: 1.047-3.909), as shown in **Figure 1C**.

Risk Factors Associated With Unsuccessful Pregnancy Among the Included Patients With EW

The risk factors associated with unsuccessful pregnancy among AEH and EC patients with EW after FSTs with pregnancy intention were further analyzed. In the univariate analysis shown in **Table 3**, the *P* values of the following two factors were less than 0.050: histology (*P*=0.009), and pregnancy method (*P*=0.042). In **Figure 2B**, the patients with EW who used letrozole for ovulation induction to promote conception had the shortest time to pregnancy, followed by those who used IVF-ET and those who achieved spontaneous pregnancy. However, there were no significant risk factors associated with unsuccessful pregnancy after the multivariate analysis.

Similarly, in the subgroup analysis of initial pathology, the oncologic outcomes of the included patients with EW characterized by the pregnancy method were further analyzed. There were no significant differences among three pregnancy methods in AEH (P=0.456) and EC (P=0.111) patients with EW, which were respectively shown in **Figures S1A, B**.

Risk Factors Associated With Recurrence Among the Included Patients With EW

We analyzed the risk factors associated with recurrence for AEH and EC patients with EW after FSTs. In the univariate analysis, as shown in **Table 4**, the *P* values of the following two factors were less than 0.050: the absence of regular maintenance treatment (*P*=0.017) and treatment type (*P*=0.015). In **Figure 2C**, the patients with EW treated with GnRH-a+LNG-IUD had the best DFS (HR=0.309, 95%CI: 0.122-0.778), followed by those treated with GnRH-a and MPA, and the worst DFS was observed in patients treated with MA. After multivariate analysis, the treatment type was the risk factors associated with recurrence for AEH and EC patients with EW (*P*=0.044, adjusted HR=0.432, 95% CI: 0.152-1.229).

In the subgroup analysis of initial pathology, we further analyzed the oncologic outcomes of the included patients with EW characterized by treatment method. Similar tendencies for oncologic outcomes among EC patients with EW (*P*=0.032) are shown in **Figure S1D**. However, there was no significant

TABLE 2 | The treatment, follow-up and reproductive outcomes of AEH and EC patients after FST between the excess weight group and normal weight group.

Variable	Total (N = 227)	Excess weight group (N = 139)	Normal weight group (N = 388)	*P*
Treatment				0.001
MPA	91 (40.1%)	44 (31.7.%)	47 (53.4%)	
MA	39 (17.2%)	21 (15.1%)	18 (20.5%)	
GnRH-a	40 (17.6%)	28 (20.1%)	12 (13.6%)	
GnRH-a+LNG-IUD	57 (25.1%)	46 (33.1%)	11 (12.5%)	
Time to CR (Months)	8.7 ± 5.6	8.6 ± 5.6	8.8 ± 5.6	0.865
<6	89 (39.2%)	56 (40.3%)	33 (37.5%)	
≥6, <12	88 (38.8%)	52 (37.4%)	36 (40.9%)	
≥12	50 (22.0%)	31 (22.3%)	19 (21.6%)	
Regular maintenance treatment				0.993
No	111 (48.9%)	68 (48.9%)	43 (48.9%)	
Yes	116 (51.1%)	71 (51.1%)	45 (51.1%)	
LNG-IUDs	85 (73.3%)	53 (74.6%)	32 (71.1%)	
Duphaston	31 (26.7%)	18 (25.4%)	13 (28.9%)	
Pregnancy Method				
without pregnancy intention	144 (63.4%)	92 (66.2%)	52 (59.1%)	0.279
with pregnancy intention	83 (36.6%)	47 (33.8%)	36 (40.9%)	0.084
spontaneous	24 (29.0%)	13 (27.7%)	11 (30.6%)	
ovulation induction	19 (22.9%)	11 (23.4%)	8 (22.2%)	
IVF-ET	40 (48.1%)	23 (48.9%)	17 (47.2%)	
Pregnancy outcome				
without pregnancy intention	144 (63.4%)	92 (66.2%)	52 (59.1%)	0.279
with pregnancy intention	83 (36.6%)	47 (33.8%)	36 (40.9%)	0.017
Live birth	28 (33.7%)	11 (23.4%)	17 (47.2%)	
Spontaneous abortion	8 (9.6%)	3 (6.4%)	5 (13.9%)	
Non-pregnant	47 (56.7%)	33 (70.2%)	14 (38.9%)	
Recurrence				0.889
No	156 (68.7%)	96 (69.1%)	60 (68.2%)	
Yes	71 (31.3%)	43 (30.9%)	28 (31.8%)	
Recurrent histology				0.617
AEH	54 (76.1%)	31 (72.1%)	23 (82.1%)	
EC	17 (23.9%)	12 (27.9%)	5 (17.9%)	

Data are presented as number (%). MPA, Medroxyprogesterone; MA, Megestrol acetate; LNG-IUD, levonorgestrel intrauterine device; GnRH-a, Gonadotropin releasing hormone agonist; CR; complete remission; AEH, atypical endometrial hyperplasia; EC, endometrial cancer; IVF-EF, In vitro fertilization and embryo transfer.

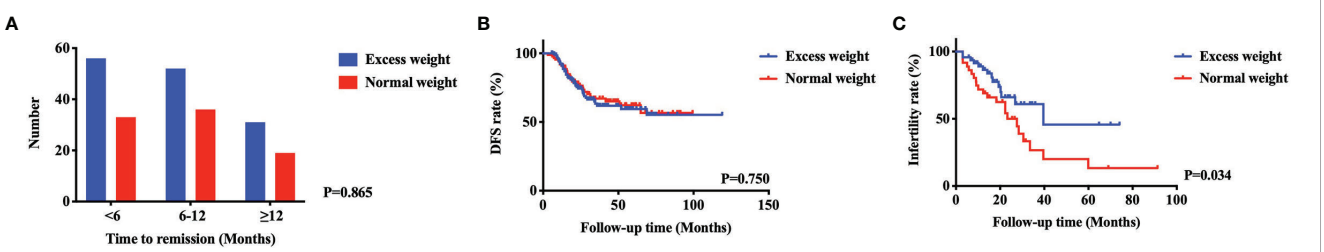

FIGURE 1 | The comparison of AEH and EC patients after FST between excess weight group and normal weight group. There were no significant differences of the time to remission **(A)** and DFS **(B)** between two groups. The patients in NW group had better pregnancy rate than in EW group **(C)**.

difference among four treatment methods in AEH patients with EW (P=0.289), as shown in **Figure S1C**.

DISCUSSION

BMI plays an important role in the occurrence and development of AEH and EC. Approximately two-thirds of EC patients are obese, and the risk of EC is 2- to 5-times higher among obese women, which can be explained by the fact that increased sex hormone production from adipose tissue causes unopposed estrogen stimulation in the endometrial lining, similar to what occurs in breast cancer (6). Our previous study reported that obesity is not a risk factor for recurrence in AEH and EC patients after FST, although EW led to a higher incidence rate of EC and AEH (9). Gonthier et al. also showed that obese patients with AEH and EC also had similar CR rates and relapse rates compared with nonobese patients (18). However, a study

TABLE 3 | The univariate analysis and multivariate analysis of risk factors associated with infertility for AEH and EC patients of excess weight after FST with pregnancy intention.

Variables	N	Univariate analysis			Multivariate analysis		
		HR	95% CI	*Pp*	HR	95%CI	*P*
Age (year)				0.089			
≤35	35	1					
>35	12	0.171	0.022-1.313				
Complications				0.964			
No	32	1					
PCOS	10	0.681	0.147-3.148				
		0.227					
Diabetes mellitus	2	1.057	0.130-8.580				
Others	3	1.106	0.140-8.711				
Menstruation cycle				0.161			
Regular	21	1					
Irregular	26	2.294	0.718-7.331				
Previous pregnancy				0.367			
No	30	1					
Yes	17	0.579	0.176 -1.899				
Histology				0.009			0.052
AEH	29	1			1		
EC	18	4.385	1.445-13.306		3.270	0.992-10.780	
Regular maintenance treatment				0.662			
No	19	1					
Yes	28	1.296	0.405-4.151				
Treatment				0.714			
MPA	11	1					
MA	10	1.165	0.258-5.270				
GnRH-a	11	1.304	0.282-6.027				
GnRH-a +LNG-IUD	15	0.559	0.112-2.789				
Recurrence				0.098			
No	26	1					
Yes	21	2.568	0.841-7.840				
Pregnancy				0.042			0.229
spontaneous	13	1			1		
ovulation induction	11	5.696	1.092-29.722		3.020	0.518-17.599	
IVF-ET	23	1.623	0.324-8.139		1.137	0.217-5.967	

PCOS, polycystic ovary syndrome; AEH, atypical endometrial hyperplasia; EC, endometrial cancer; MPA, Medroxyprogesterone; MA, Megestrol acetate; LNG-IUD, levonorgestrel intrauterine device; GnRH-a, Gonadotropin releasing hormone agonist; IVF-EF, In vitro fertilization and embryo transfer.

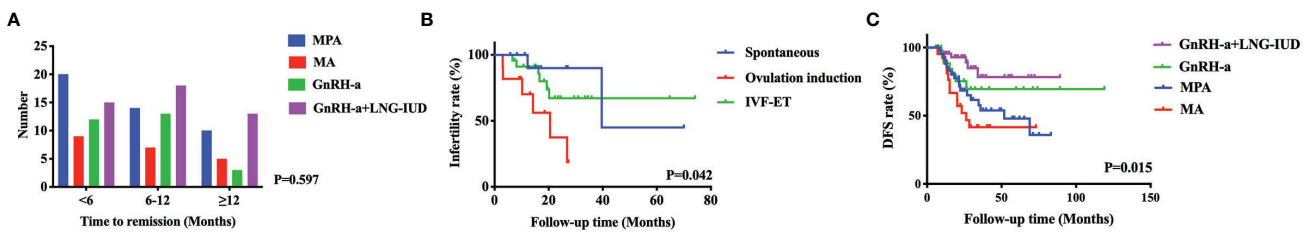

FIGURE 2 | The risk factors associated with infertility for AEH and EC patients of excess weight with pregnancy intention. The time to remission among the four treatment types did not significantly differ in patients with EW **(A)**. In the univariate analysis, the patients with EW who used ovulation induction to promote conception had the shortest time to pregnancy, followed by those who used IVF-ET and those who achieved spontaneous pregnancy **(B)**. The patients with EW treated with GnRH-a+ LNG-IUD had the best DFS, followed by those treated with GnRH-a and MPA, and the worst DFS was observed in patients treated with MA **(C)**.

performed by von Greunigen and the Gynecologic Oncology Group (GOG) showed that obesity increases the risk of mortality among women with a diagnosis of EC (19). In addition, obese patients often also have insulin resistance or cardiovascular diseases, which may lead to a longer therapeutic duration and poor prognosis for AEH and EC patients after FST (20). Therefore, overweight and obesity are nonnegligible risk factors during therapy for AEH and EC.

For AEH or EC patients without any contraindications receiving FSTs, the common treatment is high-dose progestin (21).

TABLE 4 | The univariate analysis and multivariate analysis of risk factors associated with recurrence for AEH and EC patients of excess weight after FST.

Variables	N	Univariate analysis			Multivariate analysis		
		HR	95% CI	*Pp*	HR	95%CI	*P*
Age (year)				0.380			
≤35	105	1					
>35	34	1.349	0.691-2.632				
Complications				0.111			
No	91	1					
PCOS	33	0.306	0.109-0.863				
Diabetes mellitus	9	0. 0.442	0.106-1.842				
Others	6	0.703	0.169-2.930				
Menstruation cycle				0.097			
Regular	65	1					
Irregular	74	1.737	0.905-3.333				
Previous pregnancy				0.362			
No	85	1					
Yes	54	1.322	0.725-2.412				
Histology				0.089			
AEH	88	1					
EC	51	0.552	0.278-1.095				
Regular maintenance treatment				0.017			0.181
No	68	1			1		
Yes	71	0.474	0.257-0.877		0.614	0.300-1.255	
Treatment				0.015			0.044
MPA	44	1			1		
MA	21	1.416	0.681-2.943		1.730	0.790-3.789	
GnRH-a	28	0.613	0.256-1.470		0.755	0.301-1.894	
GnRH-a+LNG-IUD	46	0.309	0.122-0.778		0.432	0.152-1.229	

PCOS, polycystic ovary syndrome; AEH, atypical endometrial hyperplasia; EC, endometrial cancer; MPA, Medroxyprogesterone; MA, Megestrol acetate; LNG-IUD, levonorgestrel intrauterine device; GnRH-a, Gonadotropin releasing hormone agonist.

However, the most common side effect of high-dose oral progestin is an increase in BMI, which creates a very large challenge for overweight patients trying to control their body weight (22). In addition, high-dose oral progestin may lead to elevated liver enzymes, which is also a very unfavorable condition for obese patients, especially those with DM or hypertension (23). Cholakian et al. showed that in patients with a BMI ≥ 35 kg/m^2, MA was associated with more weight gain than LNG-IUDs (+2.2 *vs* -5.40 kg, *P*=0.05) (24). Regarding conservative treatment for EC, weight change is one of the evaluation indices for treatment effect and prognostic outcomes (25). Park et al. reported that a BMI≥25 kg/m^2 before and after treatment is an important predictor for poor treatment response and high recurrence rate (25). The treatments for obesity include diet control, exercise, drugs, and bariatric surgery (26). The NCCN guidelines have indicated the importance of effective weight control and healthy lifestyle management for overweight patients. In our institution, overweight patients are also required to seek advice for weight loss in the nutrition department while undergoing FSTs. It is essential for patients to maintain a normal BMI during progestin treatment. Therefore, oral progestin may not be an optimal option for overweight AEH and EC patients, as the most common side effect is weight gain (22).

GnRH-a and LNG-IUDs as effective and acceptable forms of treatment have been used for multiple purposes by thousands of women worldwide. In our study, the combined use of GnRH-a and LNG-IUDs yielded the best DFS trend among treatments, especially for overweight EC patients. On the one hand, this result can be explained by a lower probability of weight gain with an GnRH-a and LNG-IUD. Cholakian et al. reported that the median weight change during therapy was greater with MA than with LNG-IUDs (+2.95 *vs*. +0.05 kg, *P*=0.03) (24). On the other hand, LNG-IUDs played an important role in maintaining endometrial thinning. Additionally, GnRH-a can inhibit the hypothalamic pituitary-gonadal axis in the central nervous system. Thus, the combination of LNG-IUDs and GnRH-a was a comparably effective method to suppress the production of estrogen from both the ovaries and peripheral tissue. Other studies have reported results similar to those of our study. A systematic review of 19 articles showed that LNG-IUDs had an advantage over oral progestin (27). Women with AEH were more likely to show regression with an LNG-IUD than with oral progestin. Furthermore, GnRH is an effective fertility-sparing strategy for women with AEH and EC due to the low recurrence rate of these diseases and the absence of progressive disease; this method achieved a good long-term uterine preservation rate and a high pregnancy rate (16, 28). Therefore, the abovementioned studies and our study provide evidence that LNG-IUDs and GnRH-a are preferred in the treatment of overweight and obese patients with AEH and EC (16).

On the one hand, letrozole belongs to a class of medications known as aromatase inhibitors and acts by blocking estrogen production and causing the pituitary gland to increase its stimulation of ovarian follicles (29). NCCN guidelines have

recommended that letrozole can be used to enhance ovulation as the first-line treatment (7). Additionally, letrozole has been reported to be an effective ovulation induction agent in higher-BMI women (30). Obese patients usually have PCOS or ovulation disorders, which are important risk factors for infertility. Insulin resistance caused by obesity may exacerbate hyperandrogenism, and hyperandrogenism can increase the resistance to insulin, thus forming a vicious cycle (31). Letrozole can inhibit the growth of nondominant follicles and promote the development of single follicles (32). Letrozole has a short drug half-life and is thought to cause fewer antiestrogenic side effects on estrogen target organs than clomiphene citrate because ERs are not directly affected (33). In summary, letrozole can increase the sensitivity of patients to gonadotropin and improve impaired ovarian function due to obesity (34, 35). In our study, overweight patients using letrozole for ovulation induction to promote conception may have improved pregnancy outcomes to some extent, while IVF-ET was not an optimal choice. This can be explained by the fact that most patients using IVF-ET may indeed have infertility syndromes, and the successful pregnancy rate was originally lower. According to guidelines recommendations, obese patients should not undergo IVF until their BMI drops to below 30 kg/m^2. On the other hand, letrozole can be used for FST in patients with AEH and EC from European Society of Gynecological Oncology (ESGO) guideline (36). This kind of treatment has been reported in our institution, as well as in some literatures (37–40). A previous study reported that the combination of GnRH-a and aromatase inhibitors showed a beneficial long-term outcome in young obese EC patients who wished to receive FST (40). However, the use of letrozole for FST was in a small number, and not more high evidence-based studies supported. Thus, in our institution, letrozole was mainly applied to induce ovulation in most overweight patients.

The results of our study showed that for patients with EW, maintenance treatment tend to reduce the recurrence rate of AEH and EC and increase the likelihood of maintaining regular menstruation, regardless of pregnancy intention after CR (21). The main maintenance treatments in this study were LNG-IUDs or low-dose oral progestin. Our previous studies have confirmed that regular oral progestin also significantly prolonged the DFS (RR=4.726; 95% CI: 2.672– 8.359) of young patients with AEH and EC (41). Wang et al. also showed that maintenance therapy was an independent protective factor for recurrence (P=0.001), while DM was an independent risk factor for recurrence (P=0.003) (42). Park et al. reported that if patients want to maintain fertility after childbirth, they can choose to use periodic oral contraceptives or LNG-IUDs to prevent recurrence (43). Therefore, it is considerable to use regular maintenance treatment after remission, regardless of whether the patients are considered normal weight or excess weight.

Nonetheless, there are several limitations in this study. First, unknown potential confounders and selection biases may be present in this retrospective institutional study due to the long period of data collection. However, we attempted to define the patient inclusion criteria carefully to ensure that all data were collected in a similar way and to always ensure uniformity between the two groups stratified by BMI. Moreover, we balanced confounding factors in the EW group with a Cox multivariate regression analysis when heterogeneities were present in the baseline factors. We also divided the dataset into homogenous subgroups and performed a stratification analysis. Second, the conservative treatments for AEH and EC patients are relatively unique. There has been no uniform standard for FST until now. This study retrospectively summarized the characteristics of existing cases and proposed guidelines. In clinical practice, gynecologic oncologists should pay more attention to the weight loss of overweight patients and adopt more personalized treatment options for such patients (11). For obese patients who have no histological response to the primary therapy for over 6-12 months, an alternative therapy strategy should be actively applied. Overweight patients should be informed that they may have an elevated risk of failed conservative treatment (44). In the future, we will continue to analyze more AEH and EC patients after FSTs and collect more information from new patients.

CONCLUSION

In conclusion, most patients with AEH and EC who undergo FSTs are overweight and obese. The combination of GnRH-a and LNG-IUD produced better outcomes in patients with EW than GnRH-a or oral progestin therapy alone, especially for patients with EW diagnosed with EC. GnRH-a and/or LNG-IUD may be options prior to FSTs in patients with EW due to the low relapse rates of AEC and EC. Furthermore, patients with EW using ovulation induction to boost fertility tend to have a shorter time to pregnancy. The use of regular maintenance treatment after remission is recommended. Fertility-sparing management should not necessarily be contraindicated in overweight and obese patients, but the therapy and reproductive strategy should be more individualized. Further prospective studies are needed to investigate the underlying factors associated with oncologic and pregnancy outcomes.

DATA AVAILABILITY STATEMENT

The raw data supporting the conclusions of this article will be made available by the authors, without undue reservation.

ETHICS STATEMENT

This study was conducted with the approval of the Ethics Committee of Peking Union Medical College Hospital. The patients/participants provided their written informed consent to participate in this study.

AUTHOR CONTRIBUTIONS

Study concepts: L-yP, and YJ. Study design: YS, MQ, L-yP, and YJ. Data acquisition: YS, MQ, YG, and WW. Quality control of data

and algorithms: JY, Y-yC, and YL. Data analysis and interpretation: YS, MQ, and Y-xW. Statistical analysis: YS, MQ, and YC. Manuscript preparation: YS and MQ. Manuscript editing: All authors. Manuscript review: L-yP, YJ, and JY. All authors contributed to the article and approved the submitted version.

FUNDING

This project was supported by The Fund of The National Key R&D Program of China 2016YFC1303700 (Affiliated project 2016YFC1303701, 2016.9-2020.12). Furthermore, this project was also supported by CAMS Innovation Fund for Medical Sciences (CIFMS-2017-I2M-1-002, 2017.01-2020.12). Besides, MQ was supported by China Scholarship Council (201906210463).

SUPPLEMENTARY MATERIAL

The Supplementary Material for this article can be found online at: https://www.frontiersin.org/articles/10.3389/fonc.2021.749881/full#supplementary-material

REFERENCES

1. Zhu G, Falahat R, Wang K, Mailloux A, Artzi N, Mule JJ. Tumor-Associated Tertiary Lymphoid Structures: Gene-Expression Profiling and Their Bioengineering. *Front Immunol* (2017) 8:767. doi: 10.3389/fimmu.2017.00767
2. Tangjitgamol S, Anderson BO, See HT, Lertbutsayanukul C, Sirisabya N, Manchana T, et al. Management of Endometrial Cancer in Asia: Consensus Statement From the Asian Oncology Summit 2009. *Lancet Oncol* (2009) 10 (11):1119–27. doi: 10.1016/S1470-2045(09)70290-6
3. Committee on Gynecologic Practice Society of Gynecologic Oncology. The American College of Obstetricians and Gynecologists Committee Opinion No. 631. Endometrial Intraepithelial Neoplasia. *Obstetrics Gynecol* (2015) 125 (5):1272–8. doi: 10.1097/01.aog.0000465189.50026.20
4. Bray F, Ferlay J, Soerjomataram I, Siegel RL, Torre LA, Jemal A. Global Cancer Statistics 2018: GLOBOCAN Estimates of Incidence and Mortality Worldwide for 36 Cancers in 185 Countries. *CA: Cancer J For Clin* (2018) 68 (6):394–424. doi: 10.3322/caac.21492
5. Braun MM, Overbeek-Wager EA, Grumbo RJ. Diagnosis and Management of Endometrial Cancer. *Am Family Physician* (2016) 93(6):468–74.
6. Lee WL, Lee FK, Su WH, Tsui KH, Kuo CD, Hsieh SL, et al. Hormone Therapy for Younger Patients With Endometrial Cancer. *Taiwanese J Obstetrics Gynecol* (2012) 51(4):495–505. doi: 10.1016/j.tjog.2012.09.003
7. Koh WJ, Abu-Rustum NR, Bean S, Bradley K, Campos SM, Cho KR, et al. Uterine Neoplasms, Version 1.2018, NCCN Clinical Practice Guidelines in Oncology. *J Natl Compr Cancer Network JNCCN* (2018) 16(2):170–99. doi: 10.6004/jnccn.2018.0006
8. Gallos ID, Yap J, Rajkhowa M, Luesley DM, Coomarasamy A, Gupta JK. Regression, Relapse, and Live Birth Rates With Fertility-Sparing Therapy for Endometrial Cancer and Atypical Complex Endometrial Hyperplasia: A Systematic Review and Metaanalysis. *Am J Obstetrics Gynecol* (2012) 207 (4):266. doi: 10.1016/j.ajog.2012.08.011
9. Yim GW, Kim SW, Nam EJ, Kim S, Kim YT. Learning Curve Analysis of Robot-Assisted Radical Hysterectomy for Cervical Cancer: Initial Experience at a Single Institution. *J Gynecol Oncol* (2013) 24(4):303–12. doi: 10.3802/jgo.2013.24.4.303
10. Romero-Corral A, Somers VK, Sierra-Johnson J, Thomas RJ, Collazo-Clavell ML, Korinek J, et al. Accuracy of Body Mass Index in Diagnosing Obesity in the Adult General Population. *Int J Obes (Lond)* (2008) 32(6):959–66. doi: 10.1038/ijo.2008.11
11. Papatla K, Huang M, Slomovitz B. The Obese Endometrial Cancer Patient: How do We Effectively Improve Morbidity and Mortality in This Patient Population? *Ann Oncol* (2016) 27(11):1988–94. doi: 10.1093/annonc/mdw310
12. Jenabi E, Poorolajal J. The Effect of Body Mass Index on Endometrial Cancer: A Meta-Analysis. *Public Health* (2015) 129(7):872–80. doi: 10.1016/j.puhe.2015.04.017
13. Liu PH, Wu K, Ng K, Zauber AG, Nguyen LH, Song M, et al. Association of Obesity With Risk of Early-Onset Colorectal Cancer Among Women. *JAMA Oncol* (2019) 5(1):37–44. doi: 10.1001/jamaoncol.2018.4280
14. Ali AT. Risk Factors for Endometrial Cancer. *Ceska Gynekologie* (2013) 78 (5):448–59.
15. Bouwman F, Smits A, Lopes A, Das N, Pollard A, Massuger L, et al. The Impact of BMI on Surgical Complications and Outcomes in Endometrial Cancer Surgery–An Institutional Study and Systematic Review of the Literature. *Gynecologic Oncol* (2015) 139(2):369–76. doi: 10.1016/j.ygyno.2015.09.020
16. Zhou H, Cao D, Yang J, Shen K, Lang J. Gonadotropin-Releasing Hormone Agonist Combined With a Levonorgestrel-Releasing Intrauterine System or Letrozole for Fertility-Preserving Treatment of Endometrial Carcinoma and Complex Atypical Hyperplasia in Young Women. *Int J Gynecological Cancer* (2017) 27(6):1178–82. doi: 10.1097/igc.0000000000001008
17. du Prel J-B, Röhrig B, Hommel G, Blettner M. Choosing Statistical Tests: Part 12 of a Series on Evaluation of Scientific Publications. *Dtsch Arztebl Int* (2010) 107(19):343–8. doi: 10.3238/arztebl.2010.0343
18. Gonthier C, Walker F, Luton D, Yazbeck C, Madelenat P, Koskas M. Impact of Obesity on the Results of Fertility-Sparing Management for Atypical Hyperplasia and Grade 1 Endometrial Cancer. *Gynecologic Oncol* (2014) 133(1):33–7. doi: 10.1016/j.ygyno.2013.11.007
19. von Gruenigen VE, Tian C, Frasure H, Waggoner S, Keys H, Barakat RR. Treatment Effects, Disease Recurrence, and Survival in Obese Women With Early Endometrial Carcinoma: A Gynecologic Oncology Group Study. *Cancer* (2006) 107(12):2786–91. doi: 10.1002/cncr.22351
20. Yang B, Xie L, Zhang H, Zhu Q, Du Y, Luo X, et al. Insulin Resistance and Overweight Prolonged Fertility-Sparing Treatment Duration in Endometrial Atypical Hyperplasia Patients. *J Gynecologic Oncol* (2018) 29(3):e35. doi: 10.3802/jgo.2018.29.e35
21. Gressel GM, Parkash V, Pal L. Management Options and Fertility-Preserving Therapy for Premenopausal Endometrial Hyperplasia and Early-Stage Endometrial Cancer. *Int J Gynaecol Obstetrics* (2015) 131(3):234–9. doi: 10.1016/j.ijgo.2015.06.031
22. Li M, Guo T, Cui R, Feng Y, Bai H, Zhang Z. Weight Control Is Vital for Patients With Early-Stage Endometrial Cancer or Complex Atypical Hyperplasia Who Have Received Progestin Therapy to Spare Fertility: A Systematic Review and Meta-Analysis. *Cancer Manage Res* (2019) 11:4005–21. doi: 10.2147/cmar.s194607
23. Raffone A, Travaglino A, Saccone G, Di Maio A, Mollo A, Mascolo M, et al. Diabetes Mellitus and Responsiveness of Endometrial Hyperplasia and Early Endometrial Cancer to Conservative Treatment. *Gynecological Endocrinol* (2019) 35(11):932–7. doi: 10.1080/09513590.2019.1624716
24. Cholakian D, Hacker K, Fader AN, Gehrig PA, Tanner EJ3rd. Effect of Oral *Versus* Intrauterine Progestins on Weight in Women Undergoing Fertility Preserving Therapy for Complex Atypical Hyperplasia or Endometrial Cancer. *Gynecologic Oncol* (2016) 140(2):234–8. doi: 10.1016/j.ygyno.2015.12.010
25. Park JY, Seong SJ, Kim TJ, Kim JW, Bae DS, Nam JH. Significance of Body Weight Change During Fertility-Sparing Progestin Therapy in Young Women With Early Endometrial Cancer. *Gynecologic Oncol* (2017) 146(1):39–43. doi: 10.1016/j.ygyno.2017.05.002
26. Ward KK, Roncancio AM, Shah NR, Davis MA, Saenz CC, McHale MT, et al. Bariatric Surgery Decreases the Risk of Uterine Malignancy. *Gynecologic Oncol* (2014) 133(1):63–6. doi: 10.1016/j.ygyno.2013.11.012
27. Nwanodi O. Progestin Intrauterine Devices and Metformin: Endometrial Hyperplasia and Early Stage Endometrial Cancer Medical Management. *Healthcare (Basel Switzerland)* (2017) 5(3):30. doi: 10.3390/healthcare5030030
28. Tock S, Jadoul P, Squifflet JL, Marbaix E, Baurain JF, Luyckx M. Fertility Sparing Treatment in Patients With Early Stage Endometrial Cancer, Using a Combination of Surgery and GnRH Agonist: A Monocentric Retrospective

Study and Review of the Literature. *Front Med* (2018) 5:240. doi: 10.3389/fmed.2018.00240
29. Bedaiwy MA, Mousa NA, Esfandiari N, Forman R, Casper RF. Follicular Phase Dynamics With Combined Aromatase Inhibitor and Follicle Stimulating Hormone Treatment. *J Clin Endocrinol Metab* (2007) 92 (3):825–33. doi: 10.1210/jc.2006-1673
30. McKnight KK, Nodler JL, Cooper JJ Jr, Chapman VR, Cliver SP, Bates GW Jr. Body Mass Index-Associated Differences in Response to Ovulation Induction With Letrozole. *Fertil steril* (2011) 96(5):1206–8. doi: 10.1016/j.fertnstert.2011.08.002
31. Okamura Y, Saito F, Takaishi K, Motohara T, Honda R, Ohba T, et al. Polycystic Ovary Syndrome: Early Diagnosis and Intervention Are Necessary for Fertility Preservation in Young Women With Endometrial Cancer Under 35 Years of Age. *Reprod Med Biol* (2017) 16(1):67–71. doi: 10.1002/rmb2.12012
32. Tanbo T, Mellembakken J, Bjercke S, Ring E, Åbyholm T, Fedorcsak P. Ovulation Induction in Polycystic Ovary Syndrome. *Acta Obstetricia Gynecol Scand* (2018) 97(10):1162–7. doi: 10.1111/aogs.13395
33. Balen AH, Morley LC, Misso M, Franks S, Legro RS, Wijeyaratne CN, et al. The Management of Anovulatory Infertility in Women With Polycystic Ovary Syndrome: An Analysis of the Evidence to Support the Development of Global WHO Guidance. *Hum Reprod Update* (2016) 22(6):687–708. doi: 10.1093/humupd/dmw025
34. Costello MF, Garad RM, Hart R, Homer H, Johnson L, Jordan C, et al. A Review of Second- and Third-Line Infertility Treatments and Supporting Evidence in Women With Polycystic Ovary Syndrome. *Med Sci (Basel Switzerland)* (2019) 7(7):75. doi: 10.3390/medsci7070075
35. Casper RF, Mitwally MF. A Historical Perspective of Aromatase Inhibitors for Ovulation Induction. *Fertil Steril* (2012) 98(6):1352–5. doi: 10.1016/j.fertnstert.2012.10.008
36. Rodolakis A, Biliatis I, Morice P, Reed N, Mangler M, Kesic V, et al. European Society of Gynecological Oncology Task Force for Fertility Preservation: Clinical Recommendations for Fertility-Sparing Management in Young Endometrial Cancer Patients. *Int J Gynecological Cancer* (2015) 25(7):1258–65. doi: 10.1097/igc.0000000000000493
37. Barker LC, Brand IR, Crawford SM. Sustained Effect of the Aromatase Inhibitors Anastrozole and Letrozole on Endometrial Thickness in Patients With Endometrial Hyperplasia and Endometrial Carcinoma. *Curr Med Res Opin* (2009) 25(5):1105–9. doi: 10.1185/03007990902860549
38. Tabatabaie A, Karimi Zarchi M, Dehghani-Tafti M, Miratashi-Yazdi A, Teimoori S, Dehghani A. Comparing Letrozole With Medroxyprogesterone Acetate (MPA) as Hormonal Therapy for Simple Endometrial Hyperplasia Without Atypia in Adult and Middle-Aged Women. *Eur J Gynaecol Oncol* (2013) 34(6):552–5.
39. Azim A, Oktay K. Letrozole for Ovulation Induction and Fertility Preservation by Embryo Cryopreservation in Young Women With Endometrial Carcinoma. *Fertil Steril* (2007) 88(3):657–64. doi: 10.1016/j.fertnstert.2006.12.068
40. Zhang Z, Huang H, Feng F, Wang J, Cheng N. A Pilot Study of Gonadotropin-Releasing Hormone Agonist Combined With Aromatase Inhibitor as Fertility-Sparing Treatment in Obese Patients With Endometrial Cancer. *J Gynecologic Oncol* (2019) 30(4):e61. doi: 10.3802/jgo.2019.30.e61
41. Yin J, Ma S, Shan Y, Wang Y, Li Y, Jin Y, et al. Risk Factors for Recurrence in Patients With Atypical Endometrial Hyperplasia and Endometrioid Adenocarcinoma After Fertility-Sparing Treatments. *Cancer Prev Res (Philadelphia Pa)* (2020) 13(4):403–10. doi: 10.1158/1940-6207.capr-19-0399
42. Wang Y, Zhou R, Wang H, Liu H, Wang J. Impact of Treatment Duration in Fertility-Preserving Management of Endometrial Cancer or Atypical Endometrial Hyperplasia. *Int J Gynecol Cancer* (2019) 29(4):699–704. doi: 10.1136/ijgc-2018-000081
43. Park H, Seok JM, Yoon BS, Seong SJ, Kim JY, Shim JY, et al. Effectiveness of High-Dose Progestin and Long-Term Outcomes in Young Women With Early-Stage, Well-Differentiated Endometrioid Adenocarcinoma of Uterine Endometrium. *Arch Gynecol Obstetrics* (2012) 285(2):473–8. doi: 10.1007/s00404-011-1959-x
44. Chen M, Jin Y, Li Y, Bi Y, Shan Y, Pan L. Oncologic and Reproductive Outcomes After Fertility-Sparing Management With Oral Progestin for Women With Complex Endometrial Hyperplasia and Endometrial Cancer. *Int J Gynaecol Obstetrics* (2016) 132(1):34–8. doi: 10.1016/j.ijgo.2015.06.046

Conflict of Interest: The authors declare that the research was conducted in the absence of any commercial or financial relationships that could be construed as a potential conflict of interest.

frontiers in Endocrinology

ORIGINAL RESEARCH
published: 16 December 2021
doi: 10.3389/fendo.2021.780769

Effects of Metabolic Syndrome and Its Components on the Prognosis of Endometrial Cancer

Xiao Yang†, Xingchen Li†, Yangyang Dong†, Yuan Fan, Yuan Cheng, Lirong Zhai, Shuyi Zhang, Jingyi Zhou and Jianliu Wang**

Department of Obstetrics and Gynecology, Peking University People's Hospital, Beijing, China

OPEN ACCESS

Edited by:
Thibaut Barnoud, Medical University of South Carolina, United States

Reviewed by:
Gulzhanat Aimagambetova, Nazarbayev University, Kazakhstan
Yaping Shao, Dalian Medical University, China
Vincenzo Marotta, AOU S. Giovanni di Dio e Ruggi D'Aragona, Italy

****Correspondence:***
Jianliu Wang
wangjianliu@pkuph.edu.cn
Jingyi Zhou
sy_zhoujingyi@hsc.pku.edu.cn

†These authors have contributed equally to this work

Specialty section:
This article was submitted to Cancer Endocrinology, a section of the journal Frontiers in Endocrinology

Received: *21 September 2021*
Accepted: *16 November 2021*
Published: *16 December 2021*

Citation:
Yang X, Li X, Dong Y, Fan Y, Cheng Y, Zhai L, Zhang S, Zhou J and Wang J (2021) Effects of Metabolic Syndrome and Its Components on the Prognosis of Endometrial Cancer. Front. Endocrinol. 12:780769. doi: 10.3389/fendo.2021.780769

Objective: To explore the effects of metabolic syndrome (MetS) on the prognosis of endometrial cancer (EC) and to identify key components of MetS associated with EC.

Methods: A total of 506 patients surgically diagnosed with EC were analyzed in this study. These patients were diagnosed with EC in the Department of Obstetrics and Gynecology at the People's Hospital of Peking University between 2010 and 2016. The follow-up time was cut off at December 2019. MetS was characterized based on standards provided by the Chinese Diabetes Society in 2004.

Results: Among the 506 EC patients analyzed, 153 patients were diagnosed with MetS. MetS patients were more likely to be older and postmenopausal. MetS was positively related to tumor grade, stage, LNM, LVSI, and MI. The univariate analysis showed that MetS was closely related to the OS (HR = 2.14; P = 0.032) and RFS (HR = 1.80; P = 0.045) of EC patients. K–M analysis also indicated that EC patients with MetS had shorter OS and RFS than EC patients without MetS. More specifically, patients that had ≥3 components showed a worse outcome compared with patients only having 0 or 1–2 components (P <0.05). In the multivariate-adjust model, after adjusting for age, histotype, tumor grade, and stage, HDL-C was found to be associated with increased risk of death related to EC (HR = 2.2, P = 0.034). However, MetS did not significantly correlate with this. ROC analysis revealed that the area under the ROC curve of combined factors (HDL-C + grade + stage) was better than traditional stage or grade at 1-, 3-, and 5-year survival rates. From this, a nomogram based on HDL-C, grade, and stage was constructed to predict survival of EC patients. Calibration curve analysis and decision curve analysis (DCA) showed the nomogram we constructed could better predict the survival of EC patients.

Conclusion: MetS is closely related to poor prognosis in EC patients. The prevalence of individual MetS components increase with worse outcomes in EC patients. A nomogram based on HDL-C, grade, and stage has good ability to predict survival of EC patients.

Keywords: endometrial cancer, metabolic syndrome, clinicopathological characteristics, overall survival, recurrence-free survival

INTRODUCTION

Endometrial cancer (EC) is one of the most common gynecological malignancies. The latest cancer statistics from the SEER data showed that the estimated new EC cases in the United States increased by 66,570, and the estimated deaths increased by 12,940 in 2021, and the incidence rate was fourth among female malignant tumors and sixth in terms of deaths (1, 2). With lifestyle changes and the increased incidence of metabolic diseases (obesity, diabetes, and hypertension), the incidence and mortality rates of EC has been increasing worldwide. This EC incidence rate is expected to increase to 42.13 cases per 100,000 in the United States by 2030 (3). The mortality rates of EC increased 21% from 1999 to 2016 in the United States (4). Early stage EC patients show a more favorable prognosis, while advanced stage patients or cases of recurrence show a five-year survival rate less than 50% (5, 6). Therefore, it is of great clinical significance to explore the factors affecting the prognosis or recurrence of EC.

Recently, many risk factors have been linked to the occurrence of EC, such as obesity, diabetes and hyperinsulinemia. Epidemiological studies showed that the risk of EC was 2.45-fold higher in overweight patients (BMI ≥25 kg/m^2) and 2.12-fold higher in diabetic patients (7). In addition, a sedentary lifestyle, Lynch syndrome, nulliparity, early menarche, and anovulatory conditions were also found to be potential risk factors for EC. Obesity-related insulin resistance is also a key factor associated with EC (8). At the same time, insulin resistance also leads to diabetes. Thus, obesity and diabetes may have common factors related to EC. It is well known that insulin directly promotes cell proliferation through the PI3K/Akt and Ras/MAPK pathways (9). There are many studies continually confirming that metabolic syndrome (MetS) consisted of obesity, diabetes/hyperglycemia, insulin resistance, hyperlipidemia, hypertension, and other metabolic abnormalities is closely related to the increased risk of various cancers, including prostate, colorectal and breast cancers (10–12). Also, MetS has been considered an important risk factor for EC. A recent meta-analysis showed that MetS diagnosed according to the NCEP-ATP III and IDF standards was closely related to an increased risk for EC (ORs) = 1.62 and ORs = 1.45, respectively (13). In addition, a Canadian population-based study showed that MetS was closely related to poor survival and disease-free survival in EC patients (14). However, few studies have explored the effects of MetS and its components on the prognosis of EC based on the Chinese population.

In our study, to evaluate the association between MetS and EC, we firstly explored the association between MetS and clinicopathological characteristics of EC patients. Then, we studied the effects of both MetS as a whole and its individual components on the prognosis of EC to provide new evidence for the association between MetS and EC. We also aimed to identify the key components of MetS associated with EC.

METHODS

Patients Clinical Data

A retrospective study was performed that included 560 patients surgically confirmed to have EC at the Department of Obstetrics and Gynecology, People's Hospital of Peking University between 2010 and 2016. Fifty-four patients were excluded from this study due to a family history of malignancy or missing data. MetS clinical data, clinicopathologic characteristics, and general patient information were collected. The recurrence and survival status of each patient was recorded, and the overall survival (OS) and recurrence-free survival (RFS) times were calculated. December 2019 was used as a cut-off for follow-up time. The study protocol was approved by the ethics committee of the Peking University People's Hospital (2015PHB116-01).

Defining MetS

MetS was defined based on the 2004 Chinese Diabetes Society standard, which explains that three or more of the following conditions must be present in a patient: 1) Overweight and/or obese: BMI ≥25.0 kg/m^2; 2) Hyperglycemia: fasting blood glucose ≥6.1 mmol/L and (or) 2 h PG ≥7.8 mmol/L, or (and) those diagnosed as diabetic and were being treated; 3) Hypertension: blood pressure ≥140/90 mmHg, or (and) those diagnosed as having hypertension and were being treated; and 4) Dyslipidemia: Fasting triglycerides ≥1.69 mmol/l and/or HDL-C <0.9 mmol/l for males and <1.0 mmol/l for females.

Statistical Analysis

The clinical statistical analysis was performed using EmpowerStats (http://www.empowerstats.com/). A P <0.05 was considered as statistically significant. The odds ratio (OR), hazard ratios (HRs), and 95% confidence intervals (CIs) were also calculated. Kaplan–Meier (K–M) survival curves were generated using Graphpad Prism 8.0. The time-dependent receiver operating characteristic (ROC) curve was analyzed using the "survivalROC" package in R. The nomogram was constructed using the "regplot" package in R. Calibration curves and decision curve analysis (DCA) were performed to evaluate the prediction accuracy of the prognostic model.

RESULTS

Patient Clinicopathological Characteristics

The clinical and pathological characteristics of 506 patients are presented in **Table 1**. According to the definition of MetS, there were 153 patients with MetS (30.20%) and 388 without MetS (69.80%). Out of the total number of patients, 39.70% had hyperglycemia and 56.30% had a BMI ≥25 kg/m^2. In addition, the percentage of patients with hypertension and dyslipidemia was 41.30% and 49.60%, respectively. According to the different MetS components, EC patients were characterized as follows: 0 components for 73 cases (14.4%), 1–2 components for 280 cases (55.3%) and ≥3 components for 153 cases (30.2%). Lymph node metastasis (LNM) positive, Lymph-vascular space invasion (LVSI) positive, deep-myometrial infiltration (MI), were found in 11.1, 17.2, and 33.4% of patients, respectively (**Table 1**).

Association Between MetS and Clinicopathological Characteristics

Further, we analyzed the association between MetS and clinicopathological characteristics (**Table 2**). The results

TABLE 1 | Clinical and pathological characteristics for 506 EC patients. .

Characteristics	Number of patients(%)
Age	55.76 ± 9.56
<55 years	220 (43.48)
≥55 years	286 (56.52)
Menopause	
Premenopausal status	184 (36.40)
Postmenopausal status	322 (63.60)
Histotype	
EEA	436 (86.20)
SEA	70 (13.80)
Grade	
1	169 (33.40)
2–3	337 (66.60)
Stage	
I	402(79.40)
II–IV	104 (20.60)
LNM	
Negative	364 (71.9)
Positive	56 (11.1)
NA	86 (17)
LVSI	
Negative	419 (82.8)
Positive	87 (17.2)
MI	
Superficial	337 (66.6)
Deep	169 (33.4)
Ascites tumor	
Negative	352 (69.6)
Positive	35 (6.9)
NA	119 (23.5)
MetS	
Without	353 (69.80)
With	153 (30.20)
MetS components	
0 components	73 (14.4)
1–2 components	280 (55.3)
≥3 components	153 (30.2)
Blood glucose	
Normal glycemia	305 (60.30)
Hyperglycemia	201 (39.70)
BMI	
<25 kg/m^2	221 (43.70)
≥25 kg/m^2	285 (56.30)
Hypertension	
Without	297 (58.70)
With	209 (41.30)
Dyslipidemia	
Without	255 (50.40)
With	251 (49.60)
TG	
<1.69 mmol/l	339 (67%)
≥1.69 mmol/l	167 (33%)
HDL-C	
≥1.0 mmol/l	369 (72.92%)
<1.0 mmol/l	137 (27.08%)

showed that patients with MetS had more elderly (≥55 years, 71.24% vs 50.14%, P <0.05) and postmenopausal proportion (72.55% vs 59.77%, P <0.05) than patients without MetS. The proportion of MetS patients with high grade (2–3) and advanced stage (II–IV) EC was greater than patients without MetS (30.72% vs 20.40%, 33.99% vs 14.73%, P <0.05). In addition, patients with MetS had higher positive rate of LNM, LVSI, and deep-MI proportion (25.98% vs 7.85%, 24.84% vs 13.88%, 44.44% vs 28.61%, P <0.05). These results suggested that EC patients with MetS have increased tumor aggressiveness.

Effects of MetS and its Components on OS and RFS of EC Patients

To explore the effects of MetS and its components on OS and RFS in EC patients, we firstly performed the univariate analysis as shown in **Table 3**. Results indicated that MetS was closely related to OS (HR = 2.14; 95%CI: 1.07–4.28; P = 0.032) and RFS (HR = 1.80; 95%CI: 1.0–3.3; P = 0.045) of EC patients. The K–M analysis showed that EC patients with MetS had shorter OS and RFS rates compared to patients without MetS (**Figures 1A, B**). The OS time decreased in patients who had ≥3 components vs 1–2 or 0 components (P = 0.045), while there was no apparent difference observed for RFS rates (P = 0.0691) (**Figures 1C, D**). In addition, there was a significant correlation between OS and dyslipidemia (HR = 3.20; 95%CI: 1.44–7.12; P = 0.004), HDL-C <1.0 mmol/l (HR = 3.24; 95%CI: 1.62–6.49; P = 0.0009). EC patients with dyslipidemia or HDL-C <1.0 mmol/l had shorter OS and RFS rates compared to EC patients with normolipidemia or an HDL-C ≥1.0 mmol/l (**Figures 1E–H**). Patients with dyslipidemia and an HDL-C < 1.0 mmol/l also were more likely to have recurrence. Using univariate analysis, we also found that age, histotype, tumor grade, and tumor stage were associated with OS and RFS. Altogether, these results suggested that MetS was associated with poor prognosis in EC patients. Among the MetS components, dyslipidemia, especially an HDL-C <1.0mmol/l, was significantly correlated with poor prognosis in EC patients.

Cox multivariate analysis showed associations between MetS and its components and OS or RFS after adjusting for basic factors (**Tables 4**, **5**). These results indicated that dyslipidemia and HDL-C <1.0mmol/l were significantly associated with worse OS and RFS after adjusting for age. However, after adjusting for age, histotype, grade, and stage, only HDL-C was associated with an increased risk of EC-related deaths (HR = 2.2, 95%CI: 1.1–4.4; P = 0.034), and there was no significant difference observed for RFS. These results suggested that among MetS components, HDL-C was an independent risk factor for EC.

ROC Analysis and Construction of a Nomogram

To further evaluate the ability of HDL-C in predicting EC patient prognosis, we performed ROC analysis as shown in **Figures 2A–C**. These results showed that the area under curve (AUC) of HDL-C was 0.626, 0.599, and 0.648 at 1-, 3-, and 5-years, respectively. It is important to note that the AUC of combine factors (HDL-C + grade + stage) was 0.853, 0.882, and 0.902 at 1-, 3-, and 5-years, respectively, which was better than any single factor. This suggests that this combination better predicts the prognosis of EC patients compared to using traditional stage or grade.

Nomograms are used for multiple-parameter diagnosis or to predict tumorigenesis or development (15). To provide clinicians with a method to quantitatively predict the prognosis of EC patients, we constructed a nomogram based on HDL-C, grade, and stage to predict 1- and 3-year survival rates of EC patients

TABLE 2 | MetS associated with clinicopathological characteristics of EC patients.

Characteristics	Without MetS 353 (69.80%)	With MetS 153 (30.20%)	P-value
Age			**0.000**
<55 years	176 (49.86)	44 (28.76)	
≥55 years	177 (50.14)	109 (71.24)	
Menopause			**0.006**
Premenopausal status	142 (40.23)	42 (27.45)	
Postmenopausal status	211 (59.77)	111 (72.55)	
Histotype			0.175
EEA	309 (87.54)	127 (83.01)	
SEA	44 (12.46)	26 (16.99)	
Grade			**0.012**
1	281 (79.60)	106 (69.28)	
2–3	72 (20.40)	47 (30.72)	
Stage			**0.000**
I	301 (85.27)	101 (66.01)	
II–IV	52 (14.73)	52 (33.99)	
LNM			**0.000**
Negative	270 (92.15)	94 (74.02)	
Positive	23 (7.85)	33 (25.98)	
LVSI			**0.003**
Negative	304 (86.12)	115 (75.16)	
Positive	49 (13.88)	38 (24.84)	
MI			**0.001**
Superficial	252 (71.39)	85 (55.56)	
Deep	101 (28.61)	68 (44.44)	
Ascites tumor			0.904
Negative	248 (90.84)	104 (91.23)	
Positive	25 (9.16)	10 (8.77)	

The bold values means the P-value < 0.05.

(**Figure 2D**). A total number of points was calculated for each patient based on these different parameters. The higher the total number, the worse the prognosis of the patient. Furthermore, calibration curve analysis showed that the nomogram-predicted probability of survival was closed to actual survival at 1-, 3-, and 5 years (**Figure 2E**). The DCA analysis also indicated that the combine factors (HDL-C + grade + stage) showed a better ability to predict survival compared to HDL-C, stage, grade or stage + grade (**Figure 2F**). Taken together, this constructed nomogram can better predict EC patient survival.

DISCUSSION

In this retrospective study, we explored the association between MetS and clinicopathological characteristics of EC patients. Also, the effect of MetS and its components on the prognosis of EC was studied. We found that MetS was positively related to several clinicopathological characteristics, such as tumor grade, stage, LNM, etc. Our results also indicated that MetS was associated with a 2.14-fold increased risk of death and a 1.8-fold increased risk of recurrence in EC patients, although these correlations were not significant using the multivariate-adjust model. Among the MetS components, only HDL-C was found to be associated with OS of EC patients in the multivariate-adjust model. Then, a nomogram combining HDL-C, grade, and stage was constructed to predict prognosis. To our knowledge, this retrospective study is the first to explore the association between MetS and its components on the prognosis of EC patients in a Chinese population, and the nomogram constructed has good ability to predict survival of EC patients.

It is known that MetS, hyperglycemia, obesity, hypertension, and dyslipidemia are high-risk factors for cardiovascular and other diseases. In addition, a great number of studies confirmed that MetS is associated with cancer development and cancer-related mortality (16). A meta-analysis, including 38,940 cases, showed that although ages, populations, and the definitions of MetS differed, MetS was associated with increased cancer risk. These cancers included liver, colorectal and bladder cancers in men and breast and colorectal cancers in women (17). A 14-year follow-up study showed that MetS was associated with a 56% greater age-adjusted risk in cancer mortality (18). However, the role of MetS in some cancers remains controversial. One study reported that there was no correlation between MetS and renal cell carcinoma. In contrast, another study reported that there was a slight correlation between MetS and renal cell carcinoma, which may be a result of the population size used in this study versus the other study showing no correlations (19, 20). Also, MetS was found to be associated with increased risk for EC. Our study found that MetS was closely associated with advanced stage, high grade, positive LNM, positive LVSI, and deep MI, suggesting that MetS may contribute to increased aggressiveness of tumors. It was reported that the prevalence of MetS in postmenopausal women with endometrial hyperplasia and EC was higher than what was observed in premenopausal women (21). Furthermore, our study found that patients with MetS had

TABLE 3 | Univariate analysis of OS and RFS for EC patients.

Variable	OS			RFS		
	HR	95%CI	P-value	HR	95%CI	P-value
Age						
<55 years	1.0	Ref		1.0	Ref	
≥55 years	2.87	1.24–6.65	**0.014**	2.1	1.1–4.1	**0.025**
Menopause						
Premenopausal status	1.0	Ref		1.0	Ref	
Postmenopausal status	1.52	0.70–3.28	0.291	2.0	1.0–4.0	0.055
Histotype						
Type I	1.0	Ref		1.0	Ref	
Type II	9.02	4.50–18.09	**<0.001**	8.8	4.9–16.0	**<0.001**
Grade						
1	1.0	Ref		1.0	Ref	
2–3	13.92	6.02–32.20	**<0.001**	11.9	6.0–23.7	**<0.001**
Stage						
I	1.0	Ref		1.0	Ref	
II–IV	16.41	7.09–37.96	**0.001**	10.0	5.3–19.0	**<0.001**
MetS						
No	1.0	Ref		1.0	Ref	
Yes	2.14	1.07–4.28	**0.032**	1.8	1.0–3.3	**0.045**
MetS components						
0 components	1.0	Ref		1.0	Ref	
1–2 components	4.06	0.54–30.63	0.174	1.9	0.6–6.3	0.305
≥3 components	7.36	0.97–55.70	0.053	3.1	0.9–10.6	0.066
Blood glucose						
Normal glycemia	1.0	Ref		1.0	Ref	
Hyperglycemia	1.06	0.8747	0.875	1.1	0.6–2.0	0.824
BMI						
<25 kg/m^2	1.0	Ref		1.0	Ref	
≥25 kg/m^2	1.31	0.64–2.68	0.458	1.4	0.7–2.5	0.308
Hypertension						
Without	1.0	Ref		1.0	Ref	
With	1.30	0.65–2.61	0.457	1.1	0.6–2.0	0.728
Dyslipidemia						
Without	1.0	Ref		1.0	Ref	
With	3.20	1.44–7.12	**0.004**	2.6	1.3–4.9	**0.004**
TG						
<1.69 mmol/l	1.0	Ref		1.0	Ref	
≥1.69 mmol/l	0.92	0.43–1.94	0.820	0.8	0.4–1.6	0.617
HDL-C						
≥1.0 mmol/l	1.0	Ref		1.0	Ref	
<1.0 mmol/l	3.24	1.62–6.49	**0.0009**	2.6	1.5–4.8	**0.001**

The bold values means the P-value < 0.05.

more elder and postmenopausal proportion compared to patients without MetS, which is consistent with previous studies.

Even though many studies explored the relationship between MetS and the risk of various cancers, there are few studies investigating the relationship between MetS and cancer mortality. Esposito et al. showed that MetS was associated with an increased risk and mortality of colon cancer in both men and women (11). A SEER database study also reported that MetS was associated with a lower cancer-specific survival in early stage EC cases (HR = 1.28, 95%CI: 1.09–1.53) (16). Besides, patients with 1 or 2 MetS components have worse survival rates compared to those with 0 components, based on a breast cancer study (22). However, there are no reports understanding the relationship between MetS components and OS in EC. In our study, univariate analysis showed that compared with people without MetS, EC patients with MetS showed significant correlations with both OS and RFS. Among the components of MetS, dyslipidemia and HDL-C were also related with OS and RFS in EC patients. In addition, K–M survival analysis showed that patients with MetS, dyslipidemia, and HDL-C levels <1.0 mmol/l showed lower OS and RFS rates compared to patients without MetS, dyslipidemia, and HDL-C levels ≥1.0 mmol/l, respectively. Interestingly, with the number of MetS components increased, the OS of patients with EC decreased. We found that patients with ≥3 components showed shorter OS rates compared to patients with 0 or 1–2 components. Our results are consistent with conclusions reported in previous studies, suggesting the most severe the metabolism disorder, the worse the prognosis of EC patients.

The mechanism behind MetS in promoting EC remains unclear, although it may be attributed to long-term hyperglycemia, obesity, dyslipidemia, insulin, and inflammatory cytokines (23). Previous studies showed that insulin resistance/hyperinsulinemia, abnormal endogenous estrogen signaling, inflammatory cytokines, and adipocytokines (IL-6, TNF-α, adiponectin, visfatin, and leptin)

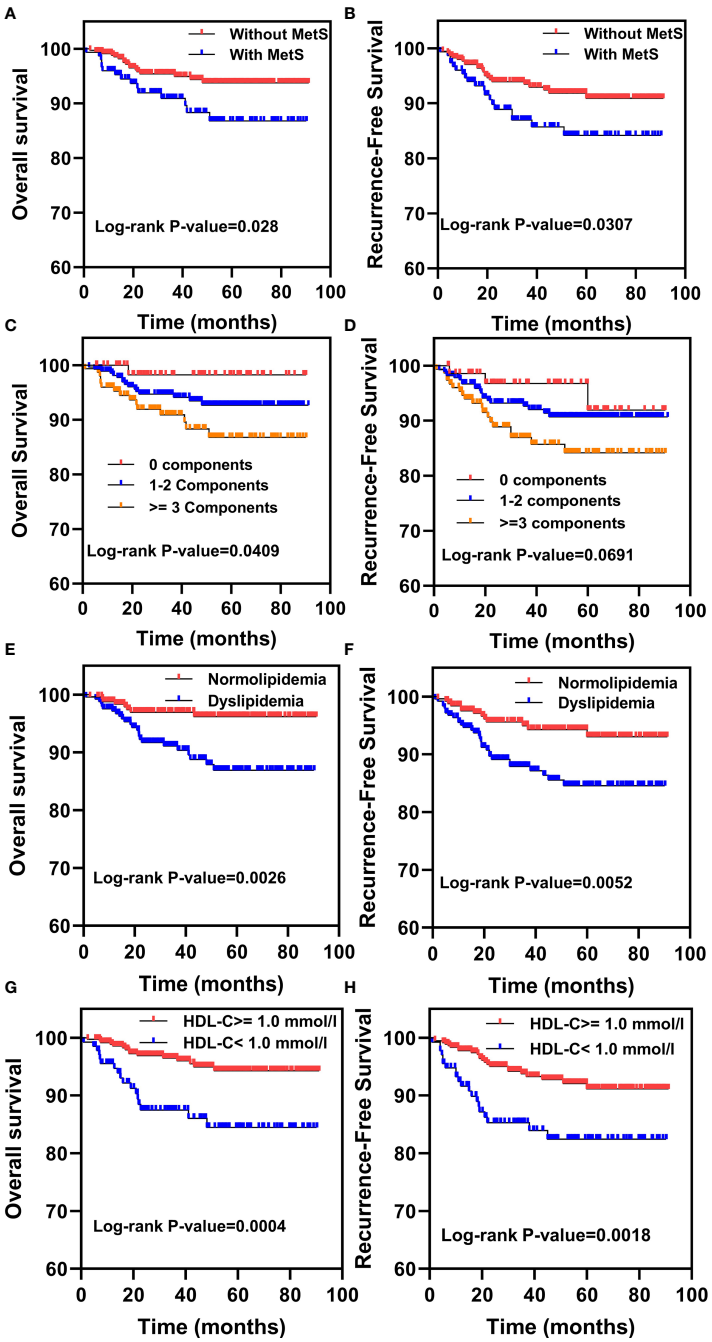

FIGURE 1 | Kaplan–Meier analysis for overall survival (OS) and recurrence-free survival (RFS) in EC patients with MetS and its components. **(A, B)** The Kaplan–Meier survival analysis of the OS and RFS between EC patients with or without MetS. **(C, D)** Kaplan–Meier survival analysis of the OS and RFS between EC patients with 0 components, 1–2 components or ≥3 components. **(E, F)** The Kaplan–Meier survival analysis of the OS and RFS between EC patients with normolipidemia and dyslipidemia. **(G, H)** The Kaplan–Meier survival analysis of the OS and RFS between EC patients with HDL-C ≥1.0mmol/l and HDL-C <1.0mmol/l.

may be the main mechanisms behind obesity that is associated with EC (24). Epidemiological studies indicate that obesity-related insulin resistance is a potential risk factor for EC. Insulin and insulin-like growth factor-1 promote the proliferation and migration of EC cells through the PI3K/Akt and RAS/MAPK pathways (9). Decreased serum adiponectin levels or increased visfatin levels are independent risk factors for EC. The ratio of visfatin to adiponectin has a certain reference value for the diagnosis of EC. Adiponectin may activate the expression of the downstream LKB1-AMPK/S6 signal axis by binding to AdipoRs, thereby inhibiting the proliferation, adhesion and invasion of EC cells (25). Epidemiological studies also indicated that there was a

TABLE 4 | Cox multivariate analysis of OS for MetS and its components in EC patients.

Variable	OS-adjust I			OS-adjust II		
	HR	95%CI	P-value	HR	95%CI	P-value
MetS						
Without	1.0	Ref		1.0	Ref	
With	1.80	0.9–3.7	0.097	1.3	0.6–2.6	0.518
BMI						
<25 kg/m^2	1.0	Ref		1.0	Ref	
≥25 kg/m^2	1.3	0.6–2.6	0.497	1.5	0.7–3.0	0.301
Hypertension						
Without	1.0	Ref		1.0	Ref	
With	1.1	0.5–2.1	0.890	1.2	0.6–2.5	0.574
Blood glucose						
Normal glycemia	1.0	Ref		1.0	Ref	
Hyperglycemia	0.9	0.4–1.8	0.675	1.0	0.5–2.1	0.960
Dyslipidemia						
Without	1.0	Ref		1.0	Ref	
With	3.1	1.4–6.9	**0.006**	1.6	0.7–3.7	0.246
TG						
<1.69 mmol/l	1.0	Ref		1.0	Ref	
≥1.69 mmol/l	0.9	0.4–1.8	0.714	0.76	0.6	0.3–1.2
HDL-C						
≥1.0 mmol/l	1.0	Ref		1.0	Ref	
<1.0 mmol/l	3.6	1.8–7.2	**<0.001**	2.2	1.1–4.4	**0.034**
MetS components						
0 components	1.0	Ref		1.0	Ref	
1–2 components	3.4	0.4–25.6	0.241	5.9	0.8–45.4	0.088
≥3 components	5.4	0.7–41.7	0.105	6.0	0.8–46.7	0.088

Adjust I for: Age.
Adjust II for: Age, Histotype, Grade, Stage.
The bold values means the P-value < 0.05.

TABLE 5 | Cox multivariate analysis of RFS for MetS and its components in EC patients.

Variable	RFS-adjust I			RFS-adjust II		
	HR	95%CI	P-value	HR	95%CI	P-value
MetS						
Without	1.0	Ref		1.0	Ref	
With	1.6	0.9–3.0	0.120	1.09	0.58–2.03	0.792
BMI						
<25 kg/m^2	1.0	Ref		1.0	Ref	
≥25 kg/m^2	1.4	0.7–2.5	0.333	1.61	0.86–3.00	0.133
Hypertension						
Without	1.0	Ref		1.0	Ref	
With	0.9	0.5–1.7	0.830	1.02	0.55–1.89	0.956
Blood glucose						
Normal glycemia	1.0	Ref		1.0	Ref	
Hyperglycemia	0.9	0.5–1.7	0.755	1.00	0.54–1.85	0.995
Dyslipidemia						
Without	1.0	Ref		1.0	Ref	
With	2.5	1.3–4.8	**0.006**	1.38	0.71–2.74	0.337
TG						
<1.69 mmol/l	1.0	Ref		1.0	Ref	
≥1.69 mmol/l	0.8	0.4–1.6	0.535	0.58	0.30–1.13	0.110
HDL-C						
≥1.0 mmol/l	1.0	Ref		1.0	Ref	
<1.0 mmol/l	2.8	1.5–5.0	**<0.001**	1.65	0.90–3.02	0.105
MetS components						
0 components	1.0	Ref		1.0	Ref	
1–2 components	1.6	0.5–5.5	0.429	2.90	0.84–9.97	0.091
≥3 components	2.5	0.7–8.6	0.153	2.61	0.74–9.18	0.134

Adjust I for: Age.
Adjust II for: Age, Histotype, Grade, Stage.
The bold values means the P-value < 0.05.

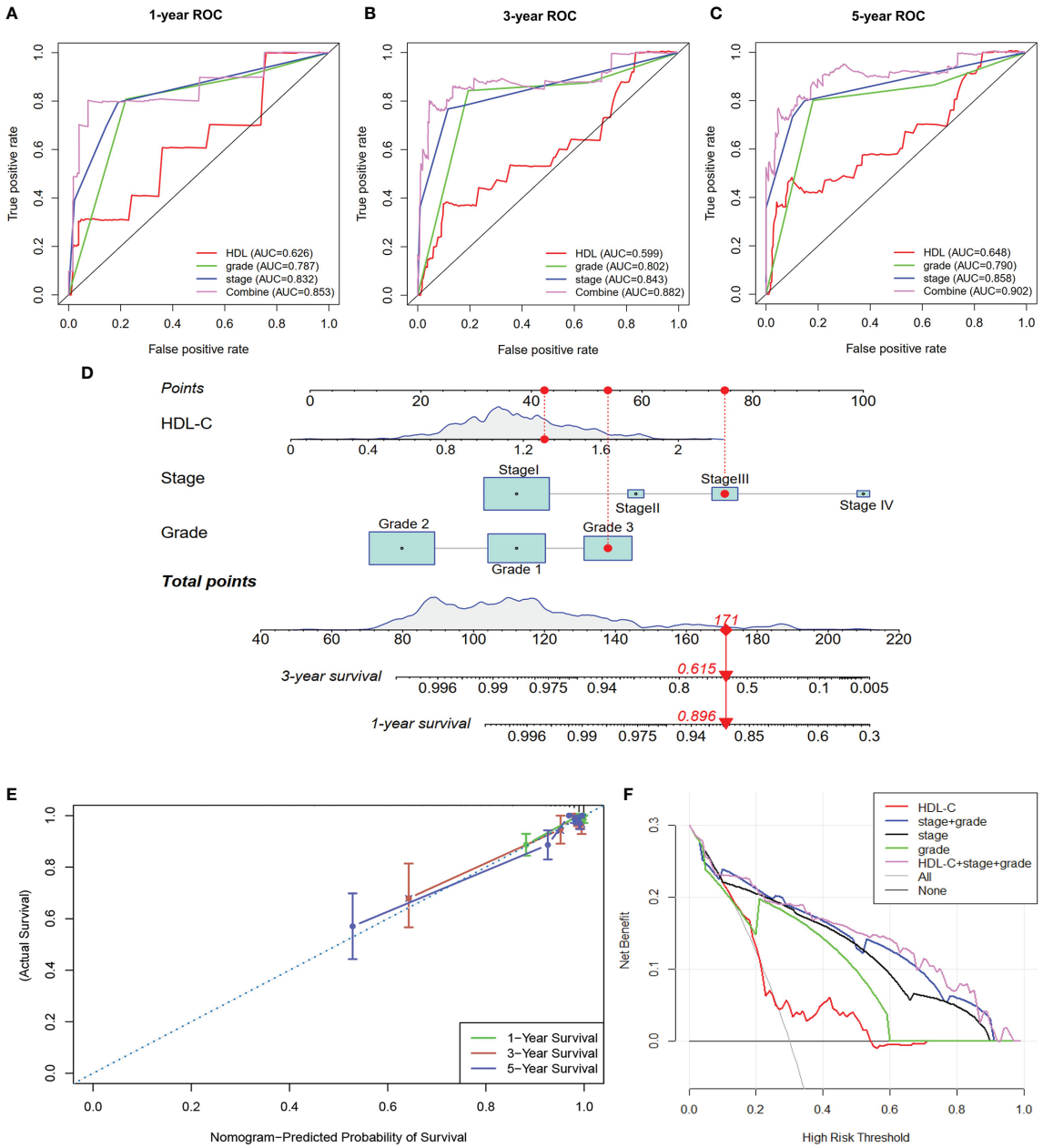

FIGURE 2 | (**A–C**) ROC analysis were performed to evaluate the ability of HDL-C in predicting EC patient prognosis at 1-, 3-, and 5-years. (**D**) A nomogram was constructed based on HDL-C, grade, and stage to predict 1- and 3-year survival rates of EC patients. (**E, F**) Calibration curve analysis and DCA analysis of the nomogram.

significant correlation between diabetes mellitus and the incidence of EC. It is important to note that this association remained after adjusting for obesity (26). The exact molecular mechanisms behind the association between diabetes and cancer is not clear. However, some studies confirmed that hyperglycemia, the insulin/insulin-like growth factor (IGF) axis and inflammatory cytokines play important roles in promoting EC proliferation and invasion (27). Hyperglycemia may also directly promote hyperinsulinemia and indirectly induce tumor development by increasing IGF-1 function. In addition, an increasing number of studies found that metformin, an antidiabetic drug, inhibited the growth of EC by inhibiting the AMPK and PI3K/Akt/mTOR signaling pathways (28). Even though previous work showed that each component of MetS is associated with cancer development, it is not known whether these effects are additive or synergistic. It has been reported that visfatin upregulated the expression of insulin receptor (IR) and insulin receptor substrate (IRS) 1/2, both of which cooperated with insulin to activate the PI3K/Akt and MAPK/ERK1/2 signaling pathways, thereby

promoting proliferation of endometrial cancer cell and inhibiting apoptosis in EC. In addition, obesity, hyperlipidemia, and hyperglycemia, as important pathogenic factors of MetS, promoted the occurrence and development of malignant tumors by inducing insulin resistance (29). Altogether, multiple molecular mechanisms associated with MetS may be closely related to the increased risk and deaths associated with EC.

To explore the key factors associated with EC in relation to MetS components, multivariate analysis was performed. In addition to MetS and its components, there was an association between age, histotype, grade, and stage associated with OS and RFS in EC patients. Therefore, age, histotype, grade, and stage were adjusted. In the multivariate-adjust model, we found that only HDL-C was associated with an increased risk for death related to EC. Meanwhile, MetS did not show a significant correlation EC death even though it was reported that MetS is an independent prognostic factor for EC patients in a study including 385 cases (18). Differences in conclusions may be explained by sample sizes used in these studies. One study reported that the TG/HDL-c ratio may be a potential marker for EC (30). Furthermore, ROC analysis found that a combination of factors (HDL-C + grade + stage) better predict EC patient prognosis in comparing to stage or grade. It is known that tumor grade and stage are important factors to evaluate the prognosis of EC patients (31). However, other important factors, such as metabolic disorders, are also closely related to patient survival and prognosis. More and more nomogram prognostic models have been established to predict the prognosis of patients (32). In our study, we used R software to generate a nomogram based on stage, grade, and HDL-C, so as to intuitively and visually predicting the survival of patients with EC. The calibration curves also showed that in the nomogram the predicted value had high consistency with the actual value. DCA is a simple method used to assess the feasibility and benefit of prediction tools (33). In our study, the DCA confirmed that our nomogram model was superior to stage, grade, HDL-C and stage + grade when it comes to predicting the survival of EC patients.

However, our study faced several limitations. First, waist circumference information was not recorded in our study, which limits the analysis of different definitions of MetS and EC. We defined MetS according to the Chinese Diabetes Society standard from 2004, which is suitable for Chinese population characteristics. Second, further studies with a larger sample size are needed to confirm our results. Similarly, the nomogram we constructed needed to be validated in other cohorts. Lastly, the molecular mechanisms behind these relationships need. to be further explored.

In conclusion, through a retrospective study of 506 endometrial cancers, our study indicated that MetS is closely related to clinicopathological characteristics. In addition, MetS and its components such as dyslipidemia, was associated with poor outcomes in EC patients. The prevalence of the individual components of MetS increases with worse outcomes in EC patients. Furthermore, a nomogram combined HDL-C, grade, and stage was constructed and the nomogram has good ability to predict EC patient survival. Our study supports that improving MetS is expected to improve the prognosis of patients with EC.

DATA AVAILABILITY STATEMENT

The raw data supporting the conclusions of this article are available from the corresponding author upon request

ETHICS STATEMENT

The studies involving human participants were reviewed and approved by the Peking University People's Hospital. The patients/participants provided their written informed consent to participate in this study. Written informed consent was obtained from the individual(s) for the publication of any potentially identifiable images or data included in this article.

AUTHOR CONTRIBUTIONS

XY: Project development, analysis and manuscript writing. XL: Project development and data analysis. YD, YF, YC, LZ, and SZ: Data collection. JW and JZ: Project development, supervision and manuscript revising. All authors contributed to the article and approved the submitted version.

FUNDING

This work was supported by the National Key Technology R&D Program of China (Nos. 2019YFC1005200 and 2019YFC1005201), the Natural Science Foundation of Beijing (No. 7202213) and the National Natural Science Foundation of China (No. 82072861, 81672571, and 81874108).

REFERENCES

1. Siegel RL, Miller KD, Jemal A. Cancer Statistics, 2018. *CA Cancer J Clin* (2018) 68:7–30. doi: 10.3322/caac.21442
2. Terzic M, Aimagambetova G, Kunz J, Bapayeva G, Aitbayeva B, Terzic S, et al. Molecular Basis of Endometriosis and Endometrial Cancer: Current Knowledge and Future Perspectives. *Int J Mol Sci* (2021) 22:9274. doi: 10.3390/ijms22179274
3. Sheikh MA, Althouse AD, Freese KE, Soisson S, Edwards RP, Welburn S, et al. USA Endometrial Cancer Projections to 2030: Should We be Concerned? *Future Oncol* (2014) 10:2561–8. doi: 10.2217/fon.14.192
4. Henley SJ, Miller JW, Dowling NF, Benard VB, Richardson LC. Uterine Cancer Incidence and Mortality - United States, 1999-2016. *MMWR Morb Mortal Wkly Rep* (2018) 67:1333–8. doi: 10.15585/mmwr.mm6748a1
5. Gadducci A, Cosio S, Fabrini MG, Guerrieri ME, Greco C, Genazzani AR. Analysis of Failures in Patients With FIGO Stage IIIc1-IIIc2 Endometrial Cancer. *Anticancer Res* (2012) 32:201–5.
6. Sorbe B, Juresta C, Ahlin C. Natural History of Recurrences in Endometrial Carcinoma. *Oncol Lett* (2014) 8:1800–6. doi: 10.3892/ol.2014.2362
7. Morice P, Leary A, Creutzberg C, Abu-Rustum N, Darai E. Endometrial Cancer. *Lancet* (2016) 387:1094–108. doi: 10.1016/S0140-6736(15)00130-0

8. Corzo C, Barrientos Santillan N, Westin SN, Ramirez PT. Updates on Conservative Management of Endometrial Cancer. *J Minim Invasive Gynecol* (2018) 25:308–13. doi: 10.1016/j.jmig.2017.07.022
9. Mu N, Zhu Y, Wang Y, Zhang H, Xue F. Insulin Resistance: A Significant Risk Factor of Endometrial Cancer. *Gynecol Oncol* (2012) 125:751–7. doi: 10.1016/j.ygyno.2012.03.032
10. Hammarsten J, Damber JE, Haghsheno MA, Mellstrom D, Peeker R. A Stage-Dependent Link Between Metabolic Syndrome Components and Incident Prostate Cancer. *Nat Rev Urol* (2018) 15:321–33. doi: 10.1038/nrurol.2018.8
11. Esposito K, Chiodini P, Capuano A, Bellastella G, Maiorino MI, Rafaniello C, et al. Colorectal Cancer Association With Metabolic Syndrome and its Components: A Systematic Review With Meta-Analysis. *Endocrine* (2013) 44:634–47. doi: 10.1007/s12020-013-9939-5
12. Dibaba DT, Ogunsina K, Braithwaite D, Akinyemiju T. Metabolic Syndrome and Risk of Breast Cancer Mortality by Menopause, Obesity, and Subtype. *Breast Cancer Res Treat* (2019) 174:209–18. doi: 10.1007/s10549-018-5056-8
13. Wang L, Du ZH, Qiao JM, Gao S. Association Between Metabolic Syndrome and Endometrial Cancer Risk: A Systematic Review and Meta-Analysis of Observational Studies. *Aging (Albany NY)* (2020) 12:9825–39. doi: 10.18632/aging.103247
14. Kokts-Porietis RL, McNeil J, Nelson G, Courneya KS, Cook LS, Friedenreich CM. Prospective Cohort Study of Metabolic Syndrome and Endometrial Cancer Survival. *Gynecol Oncol* (2020) 158:727–33. doi: 10.1016/j.ygyno.2020.06.488
15. Iasonos A, Schrag D, Raj GV, Panageas KS. How to Build and Interpret a Nomogram for Cancer Prognosis. *J Clin Oncol* (2008) 26:1364–70. doi: 10.1200/JCO.2007.12.9791
16. Jin J, Dalwadi SM, Masand RP, Hall TR, Anderson ML, Ludwig MS. Association Between Metabolic Syndrome and Endometrial Cancer Survival in a SEER-Medicare Linked Database. *Am J Clin Oncol* (2020) 43:411–7. doi: 10.1097/COC.0000000000000686
17. Esposito K, Chiodini P, Colao A, Lenzi A, Giugliano D. Metabolic Syndrome and Risk of Cancer: A Systematic Review and Meta-Analysis. *Diabetes Care* (2012) 35:2402–11. doi: 10.2337/dc12-0336
18. Jaggers JR, Sui X, Hooker SP, LaMonte MJ, Matthews CE, Hand GA, et al. Metabolic Syndrome and Risk of Cancer Mortality in Men. *Eur J Cancer* (2009) 45:1831–8. doi: 10.1016/j.ejca.2009.01.031
19. Esposito K, Chiodini P, Capuano A, Bellastella G, Maiorino MI, Parretta E, et al. Effect of Metabolic Syndrome and Its Components on Prostate Cancer Risk: Meta-Analysis. *J Endocrinol Invest* (2013) 36:132–9. doi: 10.1007/BF03346748
20. Gacci M, Russo GI, De Nunzio C, Sebastianelli A, Salvi M, Vignozzi L, et al. Meta-Analysis of Metabolic Syndrome and Prostate Cancer. *Prostate Cancer Prostatic Dis* (2017) 20:146–55. doi: 10.1038/pcan.2017.1
21. Ozdemir S, Batmaz G, Ates S, Celik C, Incesu F, Peru C. Relation of Metabolic Syndrome With Endometrial Pathologies in Patients With Abnormal Uterine Bleeding. *Gynecol Endocrinol* (2015) 31:725–9. doi: 10.3109/09513590.2015.1058355
22. Buono G, Crispo A, Giuliano M, De Angelis C, Schettini F, Forestieri V, et al. Metabolic Syndrome and Early Stage Breast Cancer Outcome: Results From a Prospective Observational Study. *Breast Cancer Res Treat* (2020) 182:401–9. doi: 10.1007/s10549-020-05701-7
23. Yang X, Wang J. The Role of Metabolic Syndrome in Endometrial Cancer: A Review. *Front Oncol* (2019) 9:744. doi: 10.3389/fonc.2019.00744
24. Calle EE, Kaaks R. Overweight, Obesity and Cancer: Epidemiological Evidence and Proposed Mechanisms. *Nat Rev Cancer* (2004) 4:579–91. doi: 10.1038/nrc1408
25. Moon HS, Chamberland JP, Aronis K, Tseleni-Balafouta S, Mantzoros CS. Direct Role of Adiponectin and Adiponectin Receptors in Endometrial Cancer: *In Vitro* and Ex Vivo Studies in Humans. *Mol Cancer Ther* (2011) 10:2234–43. doi: 10.1158/1535-7163.MCT-11-0545
26. Lucenteforte E, Bosetti C, Talamini R, Montella M, Zucchetto A, Pelucchi C, et al. Diabetes and Endometrial Cancer: Effect Modification by Body Weight, Physical Activity and Hypertension. *Br J Cancer* (2007) 97:995–8. doi: 10.1038/sj.bjc.6603933
27. Avgerinos KI, Spyrou N, Mantzoros CS, Dalamaga M. Obesity and Cancer Risk: Emerging Biological Mechanisms and Perspectives. *Metabolism* (2019) 92:121–35. doi: 10.1016/j.metabol.2018.11.001
28. Zhao Y, Sun H, Feng M, Zhao J, Zhao X, Wan Q, et al. Metformin is Associated With Reduced Cell Proliferation in Human Endometrial Cancer by Inbibiting PI3K/AKT/mTOR Signaling. *Gynecol Endocrinol* (2018) 34:428–32. doi: 10.1080/09513590.2017.1409714
29. Deng T, Lyon CJ, Bergin S, Caligiuri MA, Hsueh WA. Obesity, Inflammation, and Cancer. *Annu Rev Pathol* (2016) 11:421–49. doi: 10.1146/annurev-pathol-012615-044359
30. Luo YZ, Yang Z, Qiu YL, Li XH, Qin LQ, Su QS, et al. Pretreatment Triglycerides-to-High Density Lipoprotein Cholesterol Ratio in Postmenopausal Women With Endometrial Cancer. *Kaohsiung J Med Sci* (2019) 35:303–9. doi: 10.1002/kjm2.12033
31. Tejerizo-Garcia A, Jimenez-Lopez JS, Munoz-Gonzalez JL, Bartolome-Sotillos S, Marqueta-Marques L, Lopez-Gonzalez G, et al. Overall Survival and Disease-Free Survival in Endometrial Cancer: Prognostic Factors in 276 Patients. *Oncol Targets Ther* (2013) 9:1305–13. doi: 10.2147/OTT.S51532
32. Wu J, Zhang H, Li L, Hu M, Chen L, Xu B, et al. A Nomogram for Predicting Overall Survival in Patients With Low-Grade Endometrial Stromal Sarcoma: A Population-Based Analysis. *Cancer Commun (Lond)* (2020) 40:301–12. doi: 10.1002/cac2.12067
33. Zhang Z, Rousson V, Lee WC, Ferdynus C, Chen M, Qian X, et al. Decision Curve Analysis: A Technical Note. *Ann Transl Med* (2018) 6:308. doi: 10.21037/atm.2018.07.02

Conflict of Interest: The authors declare that the research was conducted in the absence of any commercial or financial relationships that could be construed as a potential conflict of interest.

frontiers in Endocrinology

MINI REVIEW
published: 23 December 2021
doi: 10.3389/fendo.2021.808526

Hepatocellular Carcinoma and Obesity, Type 2 Diabetes Mellitus, Cardiovascular Disease: Causing Factors, Molecular Links, and Treatment Options

Chunye Zhang[1†], *Shuai Liu*[2†] *and Ming Yang*[3*†]

[1] Department of Veterinary Pathobiology, University of Missouri, Columbia, MO, United States, [2] The First Affiliated Hospital, Zhejiang University, Hangzhou, China, [3] Department of Surgery, University of Missouri, Columbia, MO, United States

OPEN ACCESS

Edited by:
Che-Pei Kung,
Washington University School of Medicine in St. Louis, United States

Reviewed by:
Ferdinando Carlo Sasso,
Università della Campania Luigi Vanvitelli, Italy
Norbert Stefan,
University of Tübingen, Germany

***Correspondence:**
Ming Yang
yangmin@health.missouri.edu

[†]These authors share first authorship

Specialty section:
This article was submitted to Cancer Endocrinology, a section of the journal Frontiers in Endocrinology

Received: 03 November 2021
Accepted: 07 December 2021
Published: 23 December 2021

Citation:
Zhang C, Liu S and Yang M (2021) Hepatocellular Carcinoma and Obesity, Type 2 Diabetes Mellitus, Cardiovascular Disease: Causing Factors, Molecular Links, and Treatment Options. Front. Endocrinol. 12:808526. doi: 10.3389/fendo.2021.808526

Hepatocellular carcinoma (HCC) is the most common type of primary liver cancer, which will affect more than a million people by the year 2025. However, current treatment options have limited benefits. Nonalcoholic fatty liver disease (NAFLD) is the fastest growing factor that causes HCC in western countries, including the United States. In addition, NAFLD co-morbidities including obesity, type 2 diabetes mellitus (T2DM), and cardiovascular diseases (CVDs) promote HCC development. Alteration of metabolites and inflammation in the tumor microenvironment plays a pivotal role in HCC progression. However, the underlying molecular mechanisms are still not totally clear. Herein, in this review, we explored the latest molecules that are involved in obesity, T2DM, and CVDs-mediated progression of HCC, as they share some common pathologic features. Meanwhile, several therapeutic options by targeting these key factors and molecules were discussed for HCC treatment. Overall, obesity, T2DM, and CVDs as chronic metabolic disease factors are tightly implicated in the development of HCC and its progression. Molecules and factors involved in these NAFLD comorbidities are potential therapeutic targets for HCC treatment.

Keywords: hepatocellular carcinoma, obesity, type 2 diabetes mellitus, cardiovascular diseases, nonalcoholic fatty liver disease, signaling pathway, treatment

INTRODUCTION

Hepatocellular carcinoma is the most common type of primary liver cancer, with a global case number larger than one million by 2025 (1). Factors including hepatitis viral infection, nonalcoholic fatty liver disease (NAFLD), alcohol abuse, and dietary toxins (e.g., aflatoxins) can cause the initiation and development of HCC (2). Both genetic and epigenetic factors can promote HCC progression (3), such as mutation of programmed cell death-1 (PDCD1, rs10204525 C > T mutation) and DNA methylation.

NAFLD is the fastest growing factor that causes HCC in western countries, including the United States (4). Many metabolic disorders, including obesity, type 2 diabetes mellitus (T2DM), and

cardiovascular diseases (CVDs), are comorbidities of NAFLD or its advanced stage nonalcoholic steatohepatitis (NASH) (5). Gut microbiota and their-associated factors such as metabolites and components play important roles in the pathogenesis of obesity, T2DM, CVDs, NAFLD, and HCC (6–9). For example, feeding a high fat/high cholesterol diet (HFHC) can lead to fatty liver, NASH, fibrosis, and subsequential HCC in mice (10). Gut microbiota such as genera *Mucispirillum* and *Desulfovibrio* were increased, while genera *Bifidobacterium* and *Bacteroides* were dramatically decreased in HFHC-fed mice. In addition, gut microbial metabolites taurocholic acid and 3-indolepropionic acid were increased and decreased, separately, during NAFLD-HCC development (10). Overgrowth of nonvirulent lipopolysaccharide (LPS)-producing bacterial strains, such as *Enterobacter cloacae*, *Escherichia coli*, and *Klebsiella pneumoniae* from obese patients with severe fatty liver can induce NAFLD in germ-free mice fed a high-fat diet (HFD), but not HFD alone (11).

Chronic intestinal inflammation and malfunction of gut barrier associated with change of gut microbiota impact enteric hormones, adiposity, insulin resistance, and metabolic functions of intestine and other organs, such as *via* G protein-coupled receptors (12, 13). Accumulating evidence shows that GPCR signaling pathway play critically important roles in obesity, T2DM, and CVDs (14, 15). For example, phenylacetylglutamine, a gut-microbiota derived metabolite, can modulate cellular functions during CVD *via* GPCRs, such as α2A, α2B, and β2-adrenergic receptors (16). In addition to gut microbiota, several other factors such as chronic inflammation, insulin resistance, alteration of metabolites have been reported to be associated with obesity, T2DM, CVDs, as well as NAFLD, which can induce HCC initiation and progression. However, in specific situation, the risk factor may have different effect on these comorbidities. For example, genetic risk alleles (e.g., 148Met in the patatin-like phospholipase domain-containing protein 3, PNPLA3) in NAFLD are associated with protecting function in CVDs (17).

Herein, in this review, we summarize the relationships of obesity, T2DM, and CVDs with HCC, and uncover some signaling pathways and treatment options. The causing factors and treatment options of NAFLD-related HCC have been reported in another paper recently (3).

OBESITY AND HCC

Obesity is a causing factor for many cancers (18), including HCC with a moderate magnitude in obesity-associated cancers. For example, dysbiosis of gut microbiota is shown to be associated with obesity, resulting in an increase of lipoteichoic acid (LTA) (19). LTA, a Gram-positive bacterial membrane component, can promote HCC development by enhancing senescent hepatic stellate cells (HSCs) (19). In addition, LTA function together with deoxycholic acid (DCA), a secondary bile acid produced by gut microbiota, to upregulate the expression of SASP factors and cyclooxygenase-2 (COX2) through Toll-like receptor 2 (TLR2), resulting in COX2-mediated prostaglandin E2 (PGE2) production to inhibit antitumor immunity (19, 20). Furthermore, obesity can modulate intestinal hormone secretion to impact liver function. For example, a high level of glucose-dependent insulinotropic polypeptide (GIP), an intestinal enteroendocrine K cell-secreted hormone, contributes to hepatic steatosis and liver injury by modulating the expression of microRNAs (miRNAs) (21). Overall, obesity can promote HCC progression through modulating metabolites, inflammation, immunity, and autophagy in the tumor microenvironment, as discussed below.

Metabolites

Obesity-mediated metabolic change in the tumor microenvironment can suppress anti-tumor immunity (22). In addition, obesity induces the alteration of gut microbiota, which impacts anti-HCC immune therapies (23). For example, obesity induced by a HFD compromised the effect of cytotoxic $CD8^+$ T cells in the tumor microenvironment by reprogramming fat intake in tumor cells *via* reducing prolyl hydroxylase-3 (PHD3) expression (7). Obesity can modulate glucose metabolism to promote HCC progression. Saturated fatty acids such as palmitate impact cancer stem cell properties, production of reactive oxidative species, and glucose metabolism to enhance HCC initiation and progression (24, 25). In addition, feeding a HFD promoted the production of lactate when the mice received glucose (25). T-regulatory cells (Tregs) can proliferate in lactate-rich environments, which mediates suppression effector T cell function (26). In addition, feeding a HFD in carcinogen diethylnitrosamine (DEN)-injected promoted the development of HCC compared to mice fed a control diet, with increased secretion of lactate (25).

Chronic Inflammation

Low-grade chronic inflammation displays a key role in obesity and metabolic disorder (27). Inflammation impacts the activation of innate and adaptive immunity and modulates the progression of fibrosis and angiogenesis. For example, obesity-induced aberrant biosynthesis of glycosaminoglycan (GAG) which functions as one of the damage-associated molecular patterns (DAMPs) to promote hepatic inflammation and HCC *via* nuclear factor kappa B (NF-κB) signaling, in tumor suppressor gene exostosin-like 2-deficient mice (28). Adipose tissue caused by obesity can secrete diverse adipokines, such as leptin, adiponectin, and resistin, as well as proinflammatory cytokines, resulting in insulin resistance and chronic low-grade inflammation in different tissues, including liver tissue (29). For example, emerging evidence shows that leptin plays essential roles in cancer development by increasing tumor cell proliferation, metastasis, chemoresistance and promoting angiogenesis *via* binding its receptor to regulate many downstream signaling pathways (30, 31), as well as promoting NASH and liver fibrosis (32). Obesity impacts adipocytes to secrete proinflammatory cytokines such as interleukin (IL)-6 and tumor necrosis factor-α (TNF-α), and lipotoxicity induces hepatocyte death to activate Kupffer cells to produce those cytokines (33). Obesity-associated HCC development depended on the increased tumor-promoting cytokines IL-6 and TNF, inducing liver inflammation and activation of oncogenic signal transducer and activator of transcription 3 (STAT3) signaling in

mice (34). The mRNA expression of Toll-like receptor 4 (TLR4) was positively correlated with IL-6 and IL-10 mRNA expression in obese HCC patients. Treatment with resatorvid, a TLR4 inhibitor, inhibited HCC growth in mice with deletion of phosphatase and tensin homolog (PTEN) in hepatocytes (35).

Plasma S100 calcium-binding protein A4 (S100A4) levels were positively associated with insulin resistance in prepubertal non-diabetic obese children, which has been shown to be associated with inflammation (36). Plasma levels of FGF-21 are higher in obese adolescents than lean controls, especially in those with fatty liver (37). Feeding a high fat, high sucrose (HFHS) diet, fibroblast growth factor 21 (FGF21) deficient mice developed advanced steatosis and liver fibrosis, with liver inflammation compared to wild-type mice (38).

Immune Modulation

Obesity modulates intrahepatic immunity to induce an immunotolerant microenvironment, which results in HCC progression. For example, obese mice had a higher frequency of PD-1^+ T cells in the liver compared to control mice (39). In addition, the expression of Ki67 in hepatic T cells in obese mice was reduced compared to that in control mice, post-*ex vivo* stimulation with anti-mouse CD3 antibody, as well as reduced interferon (IFN)-γ and TNF-α production, indicating functional exhaustion. The frequency of PD-1^+ T cells and Ki67$^+$ T cells in the peripheral blood of obese (BMI ≥ 30) volunteers were increased and decreased, respectively, compared to that in non-obese (BMI < 30) human healthy controls following *ex vivo* stimulation (39). Similarly, a recent study showed that PD1$^+$CD8$^+$ T cells were increased in the livers of mice with NASH, promoting NASH-HCC progression (40). In addition, Ma et al. reported that obesity caused hepatic lipid accumulation and loss of CD4$^+$ T cells, which plays a critical role in NAFLD-HCC progression (41). A recent study from this group also showed that loss of liver CD4$^+$ T cells impaired immunotherapies such as RNA vaccine (M30) and anti-OX40 antibody-mediated treatment against tumor cell growth in the liver (42). Furthermore, there are several other subtypes of T cells play important roles in the NALFD or NAFLD-HCC pathogenesis (43).

Autophagy

Autophagy-related protein 4b (Apg4b)-deficient mice, with limited autophagy function, showed a bodyweight gain compared to wild-type mice when the mice were challenged with a high-fat diet consisting of 42% fat or with a standard rodent diet with 30% sucrose supplementation in drinking water (44). Apg4b-deficient mice also displayed more accumulation of visceral and hepatic fat, low glucose tolerance, and reduced insulin responses. By modulating autophagy, lipid metabolism, endoplasmic reticulum (ER) stress, and mitochondrial dysfunction can be regulated to ameliorate obesity-associated pathogenesis (45).

Excessive production of reactive oxygen species (ROS) plays a pivotal role in the pathogenesis of obesity, which promotes obesity-related metabolic disorders, including diabetes, NAFLD, and HCC (45). Autophagy can be turned off to rescue ROS-induced cell damage (46). Furthermore, autophagy-related genes were also shown to be aberrantly expressed in cholangiocarcinoma (47), the secondary most liver cancer. Treatment with hydroxychloroquine can induce cell apoptosis and inhibit cholangiocarcinoma cell proliferation by increasing ROS accumulation through inhibiting autophagy (47).

T2DM AND HCC

T2DM has been reported to be an independent factor that is associated with increased risk for HCC for both men and women in the U.S (48)., as well as Asian countries. For example, in Japan, the concurrence of HCC with T2DM and obesity is reported in hepatitis B virus surface antigen-negative or hepatitis C virus antibody-negative patients (49). Another report also showed that HCC-caused mortality was higher than other cancer-associated death in T2DM patients in Japan (50). Some differentially methylated genes (DMGs) were co-expressed in HCC and T2DM, such as ST3 beta-galactoside alpha-2,3-sialyltransferase 2 (ST3GAL2) and glycerophosphodiester phosphodiesterase domain containing 2 (GDPD2). And also, these DMGs were implicated in the signaling pathways including biosynthesis of glycosaminoglycan and unsaturated fatty acids (51). In addition, patients with NAFLD showed a higher risk of incident T2DM than those without NAFLD, even more in those with advanced high NAFLD fibrosis scores (52). Even after transarterial chemoembolization (TACE), a shorter interval time of progression and higher risk of cancer-specific mortality were found in HCC patients with T2DM who underwent TACE than patients without T2DM, especially in patients with cirrhosis (53).

A recent study showed that the prevalence of NAFLD in T2DM patients was 100%, while the prevalence of NASH was 96.82% (54). This study also showed that the HOMA-IR score (homeostatic model assessment for insulin resistance) was significantly higher in NASH patients than that in NALFD patients, which may cause a higher co-incidence of NASH with T2DM. Factors in T2DM pathogenesis impact HCC initiation and progression, including insulin/insulin-like growth factor (IGF) related factors (55, 56), proinflammatory cytokines (57), oxidative stress (58), gut microbiota dysbiosis (8, 59), angiogenesis (60), cell apoptosis (61), autophagy (62), which are summarized in **Table 1**.

CVDS AND HCC

Cardiovascular diseases (CVDs) are a group of disorders of the heart and blood vessels. CVDs and their outcomes include myocardial infarction, angina, transient ischemic attack, stroke, claudication, and heart failure (79). Chronic liver disease can increase the development of CVD events. For example, a meta-analysis of studies on the effects of NAFLD and the risk of CVD showed that patients with NAFLD have a significantly increased risk of fatal and non-fatal CVD incidences than those without NAFLD (80). Hepatokines such as α2-HS-glycoprotein secreted in the liver during NAFLD contribute to both CVDs and T2DM

TABLE 1 | The underlying molecular mechanisms of HCC progression in T2DM patients or CVDs.

Factors	Function	References
Type 2 diabetes mellitus (T2DM)		
Insulin/insulin-like growth factor (IGF) related factors	Liver specific-knockout insulin receptor substrate (IRS) 1, one of the molecules responsible for insulin/IGF signaling transduce in the liver, reduced DEN-induced hepatocarcinogenesis and inflammation.	(55)
	HCC tumor cells-acquired resistance to sorafenib was associated with higher levels of IGF and fibroblast growth factor (FGF). Inhibiting IGF and FGF signaling pathways delayed tumor growth.	(56)
Proinflammatory cytokines	T2DM can induce liver inflammation evidenced by an increase of proinflammatory cytokines NF-κB, TNF-α, IL-6, and IL-1β, which is associated with cell apoptosis and oxidative stress, all factor promoting HCC progression.	(57)
Oxidative stress	Treatment with *Codonopsis lanceolata* polysaccharide improved high fat/high sucrose diet-induced insulin resistance *via* activating antioxidant nuclear factor erythroid 2-related factor 2 signaling and enzymes, such as superoxide dismutase and catalase.	(58)
Gut microbiota dysbiosis	Gut microbiota plays an important role in the pathogenesis of T2DM. For example, *Bifidobacterium* genus is commonly reported to be negatively associated with T2DM, while it was also reduced in NAFLD-related HCC patients.	(8, 59)
Angiogenesis	Treatment with sodium-glucose cotransporter 2 inhibitor (SGLT2i) canagliflozin (100 mg/day) induced a spontaneous regression of HCC in a cirrhotic patient with T2DM, with a reduction in angiogenesis-related cytokines, such as angiopoietin-1/2 and platelet-derived growth factor-AA (PDGF-AA).	(60)
Cell apoptosis	Hepatic expression of pro-apoptotic protein Bad was increased during the development of T2DM in mice, while anti-apoptotic protein Bcl-2 was not increased.	(61)
Autophagy	Treatment with fenofibrate, a peroxisome proliferator-activated receptor alpha (PPARα) agonist, can activate autophagy and reduce liver fat accumulation by upregulating transcription factors E3 and EB in HFD-fed mice.	(62)
Cardiovascular diseases (CVDs)		
Inflammation	Low-grade chronic inflammation, dysbiosis of gut microbiota, infection, and genetic factors can lead to the development of obesity and CVDs, as well as insulin resistance and NAFLD, factors causing HCC.	(63–65)
Oxidative stress	Oxidative stress closely associated with inflammation is another major contributor to CVDs due to lack of antioxidant enzymes, such as superoxide dismutase and glutathione peroxidase, and overexpression of reactive oxygen species-producing enzymes, such as NADPH oxidase.	(66, 67)
Gut microbiota and relative metabolites	High levels of gut-derived metabolite trimethylamine-N-Oxide (TMAO) increased the risk of cardiovascular disease, which is also associated with NASH and primary liver cancer.	(68–70)
Metabolic disorders	Increased plasma cholesterol, especially low-density lipoprotein cholesterol (LDL-C), is associated with a higher risk of coronary artery disease (CAD). Insulin resistance impacts systemic lipid metabolism, which can lead to high levels of plasma triglycerides and low levels of high-density of lipoprotein, associated with CVD development.	(71–73)
Cell apoptosis	Apoptotic factors such as Bax and Bcl-2 are shown to be altered in different CVDs, associated with the change of inflammation and oxidative stress. In addition to apoptosis, ferroptosis and pyroptosis with a robust inflammatory response also play important roles in the progression of CVDs.	(74–76)
Viral Infections	A study showed that viral infection (HCV and/or HBV) significantly increased the 10-year cardiovascular risk and CVD events in patients with metabolic-associated fatty liver disease (MAFLD).	(77)
Autophagy	Intracellular and extracellular signals triggered by autophagy are involved in the pathogenesis of CVDs, which can be regulated by epigenetic factors such as microRNAs and long non-coding RNAs.	(78)

as distinct pathogenic factors from skeletal muscle and adipose tissue (81). Not only liver diseases can impact the progression of CVDs, but cardiovascular complications can in turn affect hepatic function and disease progression (66). There are many co-factors of CVDs and HCC, such as inflammation (63–65), oxidative stress (66, 67), gut microbiota and their relative metabolites (68–70), metabolic dysfunction (71–73), cell apoptosis (74–76), viral infections (77), and autophagy (78) (**Table 1**). Due to their correlation, medicines for the treatment of heart disease could be applied to treat liver disease. For example, statins, β-Hydroxy β-methylglutaryl-CoA (HMG-CoA) reductase inhibitors with function to reduce the risk of CVD morbidity and mortality, show a beneficial effect on liver disease, including NASH and HCC (82, 83).

SIGNALING PATHWAYS AND PROCESSES

Obesity, T2DM, and CVDs share some signaling pathways to promote NAFLD-related HCC progression. Thus, some examples of canonical signaling pathways and new findings will be discussed in the following context.

Wnt/β-Catenin

Wnt/β-catenin signaling is implicated in adipose tissue lipogenesis (84), activation of hepatic stellate cells (HSCs) or liver fibrosis (85), and ischemic myocardium (86). In primary liver cancers, including HCC, Wnt/β-catenin signaling is often activated to induce cancer cell growth and metastasis (87).

IKK-β/NF-κB

In obesity-associated HCC, liver inflammation and ER stress are associated with higher expression of inositol-requiring enzyme 1α (IRE1α). IRE1α, the unfolded protein response (UPR) signal transducer in ER, can activate nuclear factor kappa B kinase subunit beta (IKK-β)/NF-κB signaling pathway to promote TNF and IL-6 expression, resulting in HCC progression (88).

MiRNAs

The expression of miR-34a was upregulated in fatty liver and palmitate acid (PA)-treated BNL CL.2 cells, which can induce hepatocyte senescence *via* downregulating cyclin-dependent kinase 6 (CDK6) expression (89). Hydrodynamic injection of miR-15a/16-1 (containing the miR-15a and miR-16-1) can prevent HCC in both protein kinase B (AKT)/Ras and c-Myc

mice with overexpression of activated forms of AKT and NRas oncogenes (AKT/Ras) or c-Myc, *via* suppressing Tregs function to increase the effect of cytotoxic T cells (90). As the most abundant miRNAs in the liver, miR-122 has been reported to be significantly suppressed in HCC cell lines and tumor tissues. Overexpression of miR-122 can increase HCC cell radiosensitivity and sensitivity to chemotherapy medicines (91).

FABP5/HIF-1α

Proteomics analysis showed that hypoxia-inducible factor-1 alpha (HIF-1α), a transcription factor, is a binding protein of fatty acid-binding protein 5 (FABP5) (92). In addition, fatty acid (e.g., oleic acid) can activate FABP5/HIF-1α signaling to modulate lipid metabolism reprogramming to promote HCC progression, as well as the proliferation of HCC cells.

STAT3 Signaling Pathway

Signal transducer and activator of transcription 3 (STAT3) signaling pathway is involved in apoptosis, migration, and epithelial-mesenchymal transition (EMT) of HCC cells (93, 94). Surgical procedure-induced overexpression of IL-11 promoted tumor cell growth and recurrence of HCC *via* activating STAT3 signaling, while blocking IL-11/STAT3 signaling dampened HCC recurrence after surgical resection (95).

PI3K/Akt

Aberrant activation and inhibition of phosphatidylinositol-4,5-bisphosphate 3-kinase (PI3K)/AKT signaling pathway are associated with HCC cell proliferation (96) and apoptosis (97), respectively. One study showed that protein arginine methyltransferase 9 can regulate EMT to increase HCC cell migration and invasion by activating Snail expression through PI3K/AKT signaling pathway (98).

PPARs

Peroxisome proliferator-activated receptors (PPARs), including PPAR-α (99), PPAR-β/δ (100), and PPAR-γ (101), are involved in HCC growth and metastasis. PPARs can be regulated by microRNAs (miRNAs) to regulate tumor cell proliferation, migration, and invasion. For example, miR-1468 can promote HCC progression by activating PPAR-γ/AKT signaling pathway (102).

VEGF/VEGFR Signaling

Vascular endothelial growth factor (VEGF) or its receptor (VEGFR) plays an important role in angiogenesis in HCC. A cohort study in Turkish showed that HCC patients with low levels of serum VEGF-A (<100 pg/mL) had a higher overall survival (OS) rate compared to patients with high levels of serum VEGF-A (≥100 pg/mL), indicating as an independent predictor for OS in HCC patients (103). Treatment of bioactive compound VS 8 can induce human HCC cell line HepG2 cell apoptosis and inhibit the expression of EMT-induced transcription factors in $CD44^+CD133^+$ cancer stem cells, by inhibiting VEGF/VEGFR-2 signaling pathway (104).

TREATMENTS

Prevention and treatment options for HCC include lifestyle change, dietary supplement, modulation of gut microbiota, anti-inflammation and anti-oxidative stress medicines, anti-obesity and anti-diabetic treatments, anti-angiogenesis, as well as natural products-mediated therapies, which are summarized in **Figure 1**.

Lifestyle Change

Unhealthy lifestyles, such as over-nutrition, smoking, drinking, and lack of exercise, are risk factors causing cancer development and progression (105). One study showed that consumption of caffeinated coffee with an extra two cups daily was positively associated with reduction in the risk of HCC, which was also shown with consumption of decaffeinated coffee to some extent (106). Another study showed that intermediate-salt (6-10 g/day) or high-salt (>10 g/day) intake displayed a higher risk to develop primary liver cancer compared to low-salt intake (<6 g/day), after adjusting other potential cofactors such as fatty liver, hypertension, and diabetes (107). Lifestyle intervention can effectively result in low body fat mass, reduction of visceral adiposity, and a decrease of metabolic diseases, including NAFLD, CVD, and T2DM (108, 109); therefore, change of lifestyle plays an essential role in preventing HCC development.

Environmental or dietary exposure to aflatoxin B1, a genotoxic hepatocarcinogen, can also drive a high risk of HCC (110, 111). Aflatoxin contamination in food has been reported in food products, such as groundnuts, maize, wheat, and cocoa, which is associated with fungal growth (112). Therefore, consumption with fresh and non-contaminated food is also critically important to reduce potential risk of HCC.

Dietary Supplement

Supplement of eicosapentaenoic acid (EPA), an omega-3 polyunsaturated fatty acid, reduced the development of obesity-related HCC in mice *via* suppressing the expression of STAT3 to inhibit tumor growth (113). Another study also omega-3 supplementation can decrease hepatic *de novo* lipogenesis while increasing fatty acid oxidation (114). Both *in vitro* and *in vivo* studies show that Se and selenoproteins exert immunomodulatory function against HCC by modulating oxidative stress, inflammation, angiogenesis, cell proliferation, and apoptosis (115).

Bariatric Surgery and FMT

Strategies *via* modulating gut microbiota are able to change anti-cancer immune response and inhibit factors causing HCC development, including bariatric surgery (BS) and fecal microbiota transplantation (FMT). For example, BS can inhibit the onset of NASH and HCC in a large propensity-matched cohort study after 7.1 years of follow-up (116), which can ameliorate NASH features including steatosis, hepatocyte ballooning, and lobular inflammation (117). Another meta-analysis with a comprehensive literature review also showed that BS was associated with a decreased HCC risk (118).

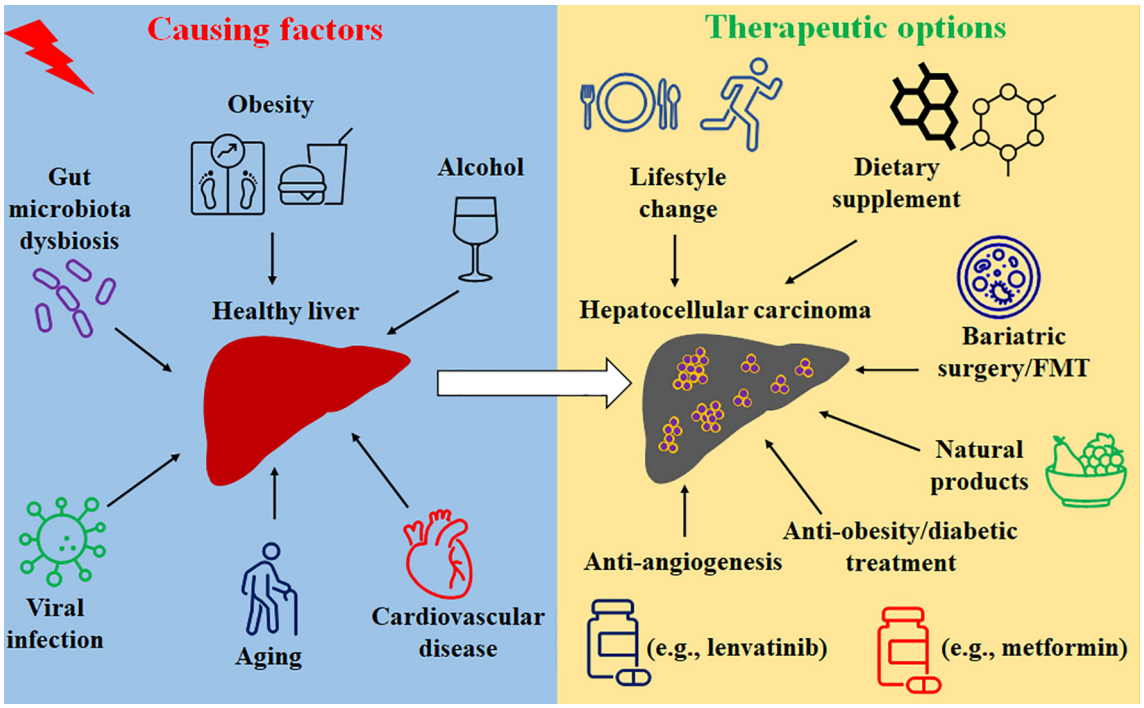

FIGURE 1 | The causing factors and treatment options of HCC.

Another review paper explored the potential of FMT in the prevention of NAFLD/NASH and improving the anti-cancer immune response (119).

Anti-Inflammation and Anti-Oxidative Stress

We and other researchers show that natural anti-oxidative and anti-inflammatory product astaxanthin can modulate intrahepatic and systemic inflammation and oxidative stress to inhibit NASH and liver fibrosis (120). Molecular mechanism study showed that metformin treatment inhibited the expression of IL-12-mediated proliferation, migration, and invasion of HCC cells and attenuated ectopic IL-22 expression-caused HCC progression by activating the Hippo signaling pathway (121). In addition, it has been shown that astaxanthin inhibits the alcoholic fatty liver disease (AFLD) *via* modulating gut microbiota, resulting in a decrease of phyla Bacteroidetes and Proteobacteria and genera *Butyricimonas*, *Bilophila*, and *Parabacteroides*, while inducing an increase of phylum Verrucomicrobia and genus *Akkermansia* compared to control group (122).

Aspirin, a nonsteroidal anti-inflammatory drug, can reduce pain, fever, and reduce the risk of a heart attack. A prospective study showed that daily aspirin use inhibited the progression of NASH and advanced fibrosis in NAFLD patients (123). In addition, Ricciotti et al. reported that as an adjuvant, aspirin has the ability to reduce the recurrence of HCC, which is associated with anti-inflammatory and antiplatelet functions (124).

Anti-Obesity and Anti-Diabetic Treatments

A retrospective study showed that the incidence of HCC was significantly lower in T2DM patients with cirrhosis with metformin treatment (17.4% in total of 125 patients) compared to patients without metformin treatment (37.4% in total of 128 patients) (125). For HCC patients, metformin treatment extended the median survival time from 3.88 years to 6.9 years (125). Another meta-analysis study showed that metformin treatment can significantly prolong the OS of HCC patients with T2DM after curative therapy (126). Metformin treatment can reduce HCC risk, but the effective dose has racial disparity in HCC patients with T2DM but without chronic liver disease (127).

Several studies showed that the combination of anti-diabetic drug liraglutide with human umbilical cord mesenchymal stem cell (hUC-MSCs) can modulate glycolipid metabolism, insulin resistance, and liver injury in rats with T2DM *via* inhibiting pancreatic beta-cell apoptosis, TLR4/NF-κB signaling pathway, and oxidative stress (128, 129). Furthermore, cholesterol-lowering drugs such as statin show beneficial effects against HCC development (130) or recurrence (131).

Anti-Angiogenesis

Angiogenesis resulting from an imbalance of factors such as VEGF/VEGFR signaling can advance HCC progression. The approved anti-angiogenic drugs (AAD) such as sorafenib, regorafenib, and lenvatinib have been shown to have a therapeutic effect on HCC (5). However, proteinuria caused by AAD can impact their effect against HCC. Angiotensin-converting

enzyme inhibitors have been applied to reduce AAD-related proteinuria (132), but these inhibitors show inhibiting effects to the efficacy of AADs. In addition, some studies showed that T2DM patients with HCC who received metformin are resistant to sorafenib treatment (133, 134), having poor progression-free survival (PFS) and OS.

Natural Products-Mediated Therapies

Treatment with hirsutine, an indole alkaloid isolated from *Uncaria rhynchophylla*, can attenuate HFD-induced hepatic steatosis, peripheral hyperglycemia, cardiac hypertrophy, and insulin resistance, *via* activating PI3K/AKT pathway (135). Another study showed that freshly dried mulberry fruits can avoid hyperphagia and reduce body weight gain and visceral fat accumulation, ameliorating hypertrophy of arterial and cardiac walls, aortic collagen fiber, and hepatic lipid accumulation in HFD-fed mice (136).

Furthermore, eradication of viral infection is also helpful to reduce metabolic disorders. For example, hepatitis C virus (HCV) eradication treated with direct-acting antivirals can reduce the incidence of T2DM by improving insulin resistance and restoring glucose homeostasis altered during viral infection (137). In addition, HCV clearance was also independently associated with a decreased risk of cardiovascular events (138), as well as major cardiovascular events in prediabetic patients (139). Therefore, anti-HCV treatment is helpful for metabolic disease-associated progression of HCC.

CONCLUSIONS

NAFLD comorbidities obesity, T2DM, and CVDs are risk factors that contribute to HCC initiation and progression. The incidence of metabolic disease-associated HCC is increased in the past decade, due to the increase of NAFLD and its comorbidities. Pathogenic factors such as abnormal metabolites, inflammatory factors, and immune modulations are underlying mechanisms for metabolic dysfunction associated with HCC pathogenesis. Currently, many treatment options show promising effects in HCC. However, the benefit of treatments such as sorafenib is still limited. In addition, an inappropriate combination of treatments even may reduce the effect of monotherapy. More clinical trials are awaited to explore the potential treatments for metabolic disease-associated HCC. A better understanding of the underlying mechanism of how these metabolic dysfunctions promote HCC initiation and progression is helpful to provide precision medicine care personally.

AUTHOR CONTRIBUTIONS

Conceptualization and data collection: CZ, SL, and MY. Original draft preparation, review, and editing: CZ, SL, and MY. All authors contributed to the article and approved the submitted version.

REFERENCES

1. Llovet JM, Kelley RK, Villanueva A, Singal AG, Pikarsky E, Roayaie S, et al. Hepatocellular Carcinoma. *Nat Rev Dis Primers* (2021) 7(1):6. doi: 10.1038/s41572-020-00240-3
2. Yang JD, Hainaut P, Gores GJ, Amadou A, Plymoth A, Roberts LR. A Global View of Hepatocellular Carcinoma: Trends, Risk, Prevention and Management. *Nat Rev Gastroenterol Hepatol* (2019) 16(10):589–604. doi: 10.1038/s41575-019-0186-y
3. Zhang C, Yang M. The Emerging Factors and Treatment Options for NAFLD-Related Hepatocellular Carcinoma. *Cancers (Basel)* (2021) 13 (15):3740. doi: 10.3390/cancers13153740
4. Huang DQ, El-Serag HB, Loomba R. Global Epidemiology of NAFLD-Related HCC: Trends, Predictions, Risk Factors and Prevention. *Nat Rev Gastroenterol Hepatol* (2021) 18(4):223–38. doi: 10.1038/s41575-020-00381-6
5. Zhang C, Yang M. Current Options and Future Directions for NAFLD and NASH Treatment. *Int J Mol Sci* (2021) 22(14):7571. doi: 10.3390/ijms22147571
6. Canfora EE, Meex RCR, Venema K, Blaak EE. Gut Microbial Metabolites in Obesity, NAFLD and T2DM. *Nat Rev Endocrinol* (2019) 15(5):261–73. doi: 10.1038/s41574-019-0156-z
7. Tang WH, Kitai T, Hazen SL. Gut Microbiota in Cardiovascular Health and Disease. *Circ Res* (2017) 120(7):1183–96. doi: 10.1161/circresaha.117.309715
8. Ponziani FR, Bhoori S, Castelli C, Putignani L, Rivoltini L, Del Chierico F, et al. Hepatocellular Carcinoma Is Associated With Gut Microbiota Profile and Inflammation in Nonalcoholic Fatty Liver Disease. *Hepatology* (2019) 69(1):107–20. doi: 10.1002/hep.30036
9. Ren Z, Li A, Jiang J, Zhou L, Yu Z, Lu H, et al. Gut Microbiome Analysis as a Tool Towards Targeted Non-Invasive Biomarkers for Early Hepatocellular Carcinoma. *Gut* (2019) 68(6):1014–23. doi: 10.1136/gutjnl-2017-315084
10. Zhang X, Coker OO, Chu ESH, Fu K, Lau HCH, Wang Y-X, et al. Dietary Cholesterol Drives Fatty Liver-Associated Liver Cancer by Modulating Gut Microbiota and Metabolites. *Gut* (2021) 70(4):761. doi: 10.1136/gutjnl-2019-319664
11. Fei N, Bruneau A, Zhang X, Wang R, Wang J, Rabot S, et al. Endotoxin Producers Overgrowing in Human Gut Microbiota as the Causative Agents for Nonalcoholic Fatty Liver Disease. *mBio* (2020) 11(1):e03263–19. doi: 10.1128/mBio.03263-19
12. Patterson E, Ryan PM, Cryan JF, Dinan TG, Ross RP, Fitzgerald GF, et al. Gut Microbiota, Obesity and Diabetes. *Postgrad Med J* (2016) 92(1087):286–300. doi: 10.1136/postgradmedj-2015-133285
13. Yang M, Zhang C-Y. G Protein-Coupled Receptors as Potential Targets for Nonalcoholic Fatty Liver Disease Treatment. *World J Gastroenterol* (2021) 27(8):677–91. doi: 10.3748/wjg.v27.i8.677
14. Oliveira de Souza C, Sun X, Oh D. Metabolic Functions of G Protein-Coupled Receptors and β-Arrestin-Mediated Signaling Pathways in the Pathophysiology of Type 2 Diabetes and Obesity. *Front Endocrinol (Lausanne)* (2021) 12:715877. doi: 10.3389/fendo.2021.715877
15. Plouffe B, Thomsen ARB, Irannejad R. Emerging Role of Compartmentalized G Protein-Coupled Receptor Signaling in the Cardiovascular Field. *ACS Pharmacol Trans Sci* (2020) 3(2):221–36. doi: 10.1021/acsptsci.0c00006
16. Nemet I, Saha PP, Gupta N, Zhu W, Romano KA, Skye SM, et al. A Cardiovascular Disease-Linked Gut Microbial Metabolite Acts *via* Adrenergic Receptors. *Cell* (2020) 180(5):862–77.e22. doi: 10.1016/j.cell.2020.02.016
17. Stefan N, Häring HU, Cusi K. Non-Alcoholic Fatty Liver Disease: Causes, Diagnosis, Cardiometabolic Consequences, and Treatment Strategies. *Lancet Diabetes Endocrinol* (2019) 7(4):313–24. doi: 10.1016/s2213-8587(18)30154-2
18. Colditz GA, Peterson LL. Obesity and Cancer: Evidence, Impact, and Future Directions. *Clin Chem* (2018) 64(1):154–62. doi: 10.1373/clinchem.2017.277376
19. Loo TM, Kamachi F, Watanabe Y, Yoshimoto S, Kanda H, Arai Y, et al. Gut Microbiota Promotes Obesity-Associated Liver Cancer Through PGE2-Mediated Suppression of Antitumor Immunity. *Cancer Discov* (2017) 7 (5):522–38. doi: 10.1158/2159-8290.cd-16-0932
20. Yoshimoto S, Loo TM, Atarashi K, Kanda H, Sato S, Oyadomari S, et al. Obesity-Induced Gut Microbial Metabolite Promotes Liver Cancer Through Senescence Secretome. *Nature* (2013) 499(7456):97–101. doi: 10.1038/nature12347

21. Góralska J, Raźny U, Polus A, Dziewońska A, Gruca A, Zdzienicka A, et al. Malczewska-Malec: Enhanced GIP Secretion in Obesity Is Associated With Biochemical Alteration and miRNA Contribution to the Development of Liver Steatosis. *Nutrients* (2020) 12(2):476. doi: 10.3390/nu12020476
22. Ringel AE, Drijvers JM, Baker GJ, Catozzi A, García-Cañaveras JC, Gassaway BM, et al. Obesity Shapes Metabolism in the Tumor Microenvironment to Suppress Anti-Tumor Immunity. *Cell* (2020) 183 (7):1848–66.e26. doi: 10.1016/j.cell.2020.11.009
23. Zhang C, Yang M, Ericsson AC. The Potential Gut Microbiota-Mediated Treatment Options for Liver Cancer. *Front Oncol* (2020) 10:524205. doi: 10.3389/fonc.2020.524205
24. Chong LW, Tsai CL, Yang KC, Liao CC, Hsu YC. Targeting Protein Palmitoylation Decreases Palmitate–Induced Sphere Formation of Human Liver Cancer Cells. *Mol Med Rep* (2020) 22(2):939–47. doi: 10.3892/mmr.2020.11172
25. Broadfield LA, Duarte JAG, Schmieder R, Broekaert D, Veys K, Planque M, et al. Fat Induces Glucose Metabolism in Nontransformed Liver Cells and Promotes Liver Tumorigenesis. *Cancer Res* (2021) 81(8):1988–2001. doi: 10.1158/0008-5472.Can-20-1954
26. Angelin A, Gil-de-Gómez L, Dahiya S, Jiao J, Guo L, Levine MH, et al. Foxp3 Reprograms T Cell Metabolism to Function in Low-Glucose, High-Lactate Environments. *Cell Metab* (2017) 25(6):1282–93.e7. doi: 10.1016/j.cmet.2016.12.018
27. Saltiel AR, Olefsky JM. Inflammatory Mechanisms Linking Obesity and Metabolic Disease. *J Clin Invest* (2017) 127(1):1–4. doi: 10.1172/jci92035
28. Nadanaka S, Hashiguchi T, Kitagawa H. Aberrant Glycosaminoglycan Biosynthesis by Tumor Suppressor EXTL2 Deficiency Promotes Liver Inflammation and Tumorigenesis Through Toll-Like 4 Receptor Signaling. *FASEB J* (2020) 34(6):8385–401. doi: 10.1096/fj.201902076R
29. Rajesh Y, Sarkar D. Association of Adipose Tissue and Adipokines With Development of Obesity-Induced Liver Cancer. *Int J Mol Sci* (2021) 22 (4):2163. doi: 10.3390/ijms22042163
30. Lin TC, Hsiao M. Leptin and Cancer: Updated Functional Roles in Carcinogenesis, Therapeutic Niches, and Developments. *Int J Mol Sci* (2021) 22(6):2870. doi: 10.3390/ijms22062870
31. Ribatti D, Belloni AS, Nico B, Di Comite M, Crivellato E, Vacca A. Leptin-Leptin Receptor Are Involved in Angiogenesis in Human Hepatocellular Carcinoma. *Peptides* (2008) 29(9):1596–602. doi: 10.1016/j.peptides.2008.05.011
32. Jiménez-Cortegana C, García-Galey A, Tami M, Del Pino P, Carmona I, López S, et al. Role of Leptin in Non-Alcoholic Fatty Liver Disease. *Biomedicines* (2021) 9(7):762. doi: 10.3390/biomedicines9070762
33. Parthasarathy G, Revelo X, MalhiH. Pathogenesis of Nonalcoholic Steatohepatitis: An Overview. *Hepatol Commun* (2020) 4(4):478–92. doi: 10.1002/hep4.1479
34. Park EJ, Lee JH, Yu GY, He G, Ali SR, Holzer RG, et al. Dietary and Genetic Obesity Promote Liver Inflammation and Tumorigenesis by Enhancing IL-6 and TNF Expression. *Cell* (2010) 140(2):197–208. doi: 10.1016/j.cell.2009.12.052
35. Nguyen J, Jiao J, Smoot K, Watt GP, Zhao C, Song X, et al. Toll-Like Receptor 4: A Target for Chemoprevention of Hepatocellular Carcinoma in Obesity and Steatohepatitis. *Oncotarget* (2018) 9(50):29495–507. doi: 10.18632/oncotarget.25685
36. Anguita-Ruiz A, Mendez-Gutierrez A, Ruperez AI, Leis R, Bueno G, Gil-Campos M, et al. The Protein S100A4 as a Novel Marker of Insulin Resistance in Prepubertal and Pubertal Children With Obesity. *Metabolism* (2020) 105:154187. doi: 10.1016/j.metabol.2020.154187
37. Giannini C, Feldstein AE, Santoro N, Kim G, Kursawe R, Pierpont B, et al. Circulating Levels of FGF-21 in Obese Youth: Associations With Liver Fat Content and Markers of Liver Damage. *J Clin Endocrinol Metab* (2013) 98 (7):2993–3000. doi: 10.1210/jc.2013-1250%JTheJournalofClinicalEndocrinology&Metabolism
38. Singhal G, Kumar G, Chan S, Fisher FM, Ma Y, Vardeh HG, et al. Deficiency of Fibroblast Growth Factor 21 (FGF21) Promotes Hepatocellular Carcinoma (HCC) in Mice on a Long Term Obesogenic Diet. *Mol Metab* (2018) 13:56–66. doi: 10.1016/j.molmet.2018.03.002
39. Wang Z, Aguilar EG, Luna JI, Dunai C, Khuat LT, Le CT, et al. Paradoxical Effects of Obesity on T Cell Function During Tumor Progression and PD-1 Checkpoint Blockade. *Nat Med* (2019) 25(1):141–51. doi: 10.1038/s41591-018-0221-5
40. Pfister D, Núñez NG, Pinyol R, Govaere O, Pinter M, Szydlowska M, et al. NASH Limits Anti-Tumour Surveillance in Immunotherapy-Treated HCC. *Nature* (2021) 592(7854):450–6. doi: 10.1038/s41586-021-03362-0
41. Ma C, Kesarwala AH, Eggert T, Medina-Echeverz J, Kleiner DE, Jin P, et al. NAFLD Causes Selective CD4(+) T Lymphocyte Loss and Promotes Hepatocarcinogenesis. *Nature* (2016) 531(7593):253–7. doi: 10.1038/nature16969
42. Heinrich B, Brown ZJ, Diggs LP, Vormehr M, Ma C, Subramanyam V, et al. Steatohepatitis Impairs T-Cell-Directed Immunotherapies Against Liver Tumors in Mice. *Gastroenterology* (2021) 160(1):331–45.e6. doi: 10.1053/j.gastro.2020.09.031
43. Zhang C, Yang M. Targeting T Cell Subtypes for NAFLD and NAFLD-Related HCC Treatment: An Opinion. *Front Med* (2021) 8:789859. doi: 10.3389/fmed.2021.789859
44. Fernández Á F, Bárcena C, Martínez-García GG, Tamargo-Gómez I, Suárez MF, Pietrocola F, et al. Autophagy Couteracts Weight Gain, Lipotoxicity and Pancreatic β-Cell Death Upon Hypercaloric Pro-Diabetic Regimens. *Cell Death Dis* (2017) 8(8):e2970. doi: 10.1038/cddis.2017.373
45. Pietrocola F, Bravo-San Pedro JM. Targeting Autophagy to Counteract Obesity-Associated Oxidative Stress. *Antioxid (Basel)* (2021) 10(1):102. doi: 10.3390/antiox10010102
46. Forte M, Bianchi F, Cotugno M, Marchitti S, Stanzione R, Maglione V, et al. An Interplay Between UCP2 and ROS Protects Cells From High-Salt-Induced Injury Through Autophagy Stimulation. *Cell Death Dis* (2021) 12 (10):919. doi: 10.1038/s41419-021-04188-4
47. Chen J, Pan Q, Bai Y, Chen X, Zhou Y. Hydroxychloroquine Induces Apoptosis in Cholangiocarcinoma *via* Reactive Oxygen Species Accumulation Induced by Autophagy Inhibition. *Front Mol Biosci* (2021) 8:720370. doi: 10.3389/fmolb.2021.720370
48. Simon TG, King LY, Chong DQ, Nguyen LH, Ma Y, VoPham T, et al. Diabetes, Metabolic Comorbidities, and Risk of Hepatocellular Carcinoma: Results From Two Prospective Cohort Studies. *Hepatology* (2018) 67 (5):1797–806. doi: 10.1002/hep.29660
49. Umetsu S, Mizukami H, Saito T, Uchida C, Igawa A, Kudo K, et al. Diabetes, an Independent Poor Prognostic Factor of Non-B Non-C Hepatocellular Carcinoma, Correlates With Dihydropyrimidinase-Like 3 Promoter Methylation. *Sci Rep* (2020) 10(1):1156. doi: 10.1038/s41598-020-57883-1
50. Shima T, Uto H, Ueki K, Kohgo Y, Yasui K, Nakamura N, et al. Hepatocellular Carcinoma as a Leading Cause of Cancer-Related Deaths in Japanese Type 2 Diabetes Mellitus Patients. *J Gastroenterol* (2019) 54 (1):64–77. doi: 10.1007/s00535-018-1494-7
51. Wei H, Wang J, Li W, Ma R, Xu Z, Luo Z, et al. The Underlying Pathophysiology Association Between the Type 2-Diabetic and Hepatocellular Carcinoma. *J Cell Physiol* (2019) 234(7):10835–41. doi: 10.1002/jcp.27919
52. Mantovani A, Byrne CD, Bonora E, Targher G. Nonalcoholic Fatty Liver Disease and Risk of Incident Type 2 Diabetes: A Meta-Analysis. *Diabetes Care* (2018) 41(2):372–82. doi: 10.2337/dc17-1902
53. Liu G, Xia F, Fan G, Yu J, Bao L, Zhang C, et al. Type 2 Diabetes Mellitus Worsens the Prognosis of Intermediate-Stage Hepatocellular Carcinoma After Transarterial Chemoembolization. *Diabetes Res Clin Pract* (2020) 169:108375. doi: 10.1016/j.diabres.2020.108375
54. Masarone M, Rosato V, Aglitti A, Bucci T, Caruso R, Salvatore T, et al. Liver Biopsy in Type 2 Diabetes Mellitus: Steatohepatitis Represents the Sole Feature of Liver Damage. *PloS One* (2017) 12(6):e0178473. doi: 10.1371/journal.pone.0178473
55. Sakurai Y, Kubota N, Takamoto I, Obata A, Iwamoto M, Hayashi T, et al. Role of Insulin Receptor Substrates in the Progression of Hepatocellular Carcinoma. *Sci Rep* (2017) 7(1):5387. doi: 10.1038/s41598-017-03299-3
56. Tovar V, Cornella H, Moeini A, Vidal S, Hoshida Y, Sia D, et al. Tumour Initiating Cells and IGF/FGF Signalling Contribute to Sorafenib Resistance in Hepatocellular Carcinoma. *Gut* (2017) 66(3):530–40. doi: 10.1136/gutjnl-2015-309501
57. Hamouda HA, Mansour SM, Elyamany MF. Vitamin D Combined With Pioglitazone Mitigates Type-2 Diabetes-Induced Hepatic Injury Through Targeting Inflammation, Apoptosis, and Oxidative Stress. *Inflammation* (2021). doi: 10.1007/s10753-021-01535-7

58. Zhang Y, Wang H, Zhang L, Yuan Y, Yu D. Codonopsis Lanceolata Polysaccharide CLPS Alleviates High Fat/High Sucrose Diet-Induced Insulin Resistance *via* Anti-Oxidative Stress. *Int J Biol Macromol* (2020) 145:944–9. doi: 10.1016/j.ijbiomac.2019.09.185
59. Gurung M, Li Z, You H, Rodrigues R, Jump DB, Morgun A, et al. Role of Gut Microbiota in Type 2 Diabetes Pathophysiology. *EBioMedicine* (2020) 51:102590. doi: 10.1016/j.ebiom.2019.11.051
60. Kawaguchi T, Nakano D, Okamura S, Shimose S, Hayakawa M, Niizeki T, et al. Spontaneous Regression of Hepatocellular Carcinoma With Reduction in Angiogenesis-Related Cytokines After Treatment With Sodium-Glucose Cotransporter 2 Inhibitor in a Cirrhotic Patient With Diabetes Mellitus. *Hepatol Res* (2019) 49(4):479–86. doi: 10.1111/hepr.13247
61. Michurina SV, Ishchenko IY, Arkhipov SA, Cherepanova MA, Vasendin DV, Zavjalov EL. Apoptosis in the Liver of Male Db/Db Mice During the Development of Obesity and Type 2 Diabetes. *Vavilovskii Zhurnal Genet Selektsii* (2020) 24(4):435–40. doi: 10.18699/VJ20.43-o
62. Yoo J, Jeong IK, Ahn KJ, Chung HY, Hwang YC. Fenofibrate, a Pparα Agonist, Reduces Hepatic Fat Accumulation Through the Upregulation of TFEB-Mediated Lipophagy. *Metabolism* (2021) 120:154798. doi: 10.1016/j.metabol.2021.154798
63. Soysal P, Arik F, Smith L, Jackson SE, Isik AT. Inflammation, Frailty and Cardiovascular Disease. *Adv Exp Med Biol* (2020) 1216:55–64. doi: 10.1007/978-3-030-33330-0_7
64. Suresh D, Srinivas AN, Kumar DP. Etiology of Hepatocellular Carcinoma: Special Focus on Fatty Liver Disease. *Front Oncol* (2020) 10:601710. doi: 10.3389/fonc.2020.601710
65. Giraud J, Saleh M. Host-Microbiota Interactions in Liver Inflammation and Cancer. *Cancers (Basel)* (2021) 13(17):4342. doi: 10.3390/cancers13174342
66. Matyas C, Haskó G, Liaudet L, Trojnar E, Pacher P. Interplay of Cardiovascular Mediators, Oxidative Stress and Inflammation in Liver Disease and Its Complications. *Nat Rev Cardiol* (2021) 18(2):117–35. doi: 10.1038/s41569-020-0433-5
67. Steven S, Frenis K, Oelze M, Kalinovic S, Kuntic M, Bayo Jimenez MT, et al. Vascular Inflammation and Oxidative Stress: Major Triggers for Cardiovascular Disease. *Oxid Med Cell Longev* (2019) 2019:7092151. doi: 10.1155/2019/7092151
68. Roncal C, Martínez-Aguilar E, Orbe J, Ravassa S, Fernandez-Montero A, Saenz-Pipaon G, et al. Trimethylamine-N-Oxide (TMAO) Predicts Cardiovascular Mortality in Peripheral Artery Disease. *Sci Rep* (2019) 9 (1):15580. doi: 10.1038/s41598-019-52082-z
69. Liu ZY, Tan XY, Li QJ, Liao GC, Fang AP, Zhang DM, et al. Trimethylamine N-Oxide, a Gut Microbiota-Dependent Metabolite of Choline, Is Positively Associated With the Risk of Primary Liver Cancer: A Case-Control Study. *Nutr Metab (Lond)* (2018) 15:81. doi: 10.1186/s12986-018-0319-2
70. León-Mimila P, Villamil-Ramírez H, Li XS, Shih DM, Hui ST, Ocampo-Medina E, et al. Trimethylamine N-Oxide Levels Are Associated With NASH in Obese Subjects With Type 2 Diabetes. *Diabetes Metab* (2021) 47 (2):101183. doi: 10.1016/j.diabet.2020.07.010
71. Cohain AT, Barrington WT, Jordan DM, Beckmann ND, Argmann CA, Houten SM, et al. An Integrative Multiomic Network Model Links Lipid Metabolism to Glucose Regulation in Coronary Artery Disease. *Nat Commun* (2021) 12(1):547. doi: 10.1038/s41467-020-20750-8
72. Ponce de León-Ballesteros G, Sánchez-Aguilar HA, Aguilar-Salinas CA, Herrera MF. Reaching LDL-C Targets in Patients With Moderate, High, and Very High Risk for Cardiovascular Disease After Bariatric Surgery According to Different Guidelines. *Obes Surg* (2021) 31(5):2087–96. doi: 10.1007/s11695-021-05221-3
73. Ormazabal V, Nair S, Elfeky O, Aguayo C, Salomon C, Zuñiga FA. Association Between Insulin Resistance and the Development of Cardiovascular Disease. *Cardiovasc Diabetol* (2018) 17(1):122. doi: 10.1186/s12933-018-0762-4
74. Mohammadi A, Balizadeh Karami AR, Dehghan Mashtani V, Sahraei T, Bandani Tarashoki Z, Khattavian E, et al. Evaluation of Oxidative Stress, Apoptosis, and Expression of MicroRNA-208a and MicroRNA-1 in Cardiovascular Patients. *Rep Biochem Mol Biol* (2021) 10(2):183–96. doi: 10.52547/rbmb.10.2.183
75. Chen X, Li X, Xu X, Li L, Liang N, Zhang L, et al. Ferroptosis and Cardiovascular Disease: Role of Free Radical-Induced Lipid Peroxidation. *Free Radic Res* (2021) 55(4):405–15. doi: 10.1080/10715762.2021.1876856
76. Gao J, Chen X, Wei P, Wang Y, Li P, Shao K. Regulation of Pyroptosis in Cardiovascular Pathologies: Role of Noncoding RNAs. *Mol Ther Nucleic Acids* (2021) 25:220–36. doi: 10.1016/j.omtn.2021.05.016
77. Guerreiro GTS, Longo L, Fonseca MA, de Souza VEG, Álvares-da-Silva MR. Does the Risk of Cardiovascular Events Differ Between Biopsy-Proven NAFLD and MAFLD? *Hepatol Int* (2021) 15(2):380–91. doi: 10.1007/s12072-021-10157-y
78. Bu S, Singh KK. Epigenetic Regulation of Autophagy in Cardiovascular Pathobiology. *Int J Mol Sci* (2021) 22(12):6544. doi: 10.3390/ijms22126544
79. Weiner DE, Tabatabai S, Tighiouart H, Elsayed E, Bansal N, Griffith J, et al. Cardiovascular Outcomes and All-Cause Mortality: Exploring the Interaction Between CKD and Cardiovascular Disease. *Am J Kidney Dis* (2006) 48(3):392–401. doi: 10.1053/j.ajkd.2006.05.021
80. Targher G, Byrne CD, Lonardo A, Zoppini G, Barbui C. Non-Alcoholic Fatty Liver Disease and Risk of Incident Cardiovascular Disease: A Meta-Analysis. *J Hepatol* (2016) 65(3):589–600. doi: 10.1016/j.jhep.2016.05.013
81. Stefan N, Häring HU. The Role of Hepatokines in Metabolism. *Nat Rev Endocrinol* (2013) 9(3):144–52. doi: 10.1038/nrendo.2012.258
82. Alipour Talesh G, Trézéguet V, Merched A. Hepatocellular Carcinoma and Statins. *Biochemistry* (2020) 59(37):3393–400. doi: 10.1021/acs.biochem.0c00476
83. Kawaguchi Y, Sakamoto Y, Ito D, Ito K, Arita J, Akamatsu N, et al. Statin Use Is Associated With a Reduced Risk of Hepatocellular Carcinoma Recurrence After Initial Liver Resection. *Biosci Trends* (2017) 11(5):574–80. doi: 10.5582/bst.2017.01191
84. Bagchi DP, Nishii A, Li Z, DelProposto JB, Corsa CA, Mori H, et al. Wnt/β-Catenin Signaling Regulates Adipose Tissue Lipogenesis and Adipocyte-Specific Loss Is Rigorously Defended by Neighboring Stromal-Vascular Cells. *Mol Metab* (2020) 42:101078. doi: 10.1016/j.molmet.2020.101078
85. Jia WQ, Zhou TC, Dai JW, Liu ZN, Zhang YF, Zang DD, et al. CD73 Regulates Hepatic Stellate Cells Activation and Proliferation Through Wnt/β-Catenin Signaling Pathway. *Eur J Pharmacol* (2021) 890:173667. doi: 10.1016/j.ejphar.2020.173667
86. Haybar H, Khodadi E, Shahrabi S. Wnt/β-Catenin in Ischemic Myocardium: Interactions and Signaling Pathways as a Therapeutic Target. *Heart Fail Rev* (2019) 24(3):411–9. doi: 10.1007/s10741-018-9759-z
87. Perugorria MJ, Olaizola P, Labiano I, Esparza-Baquer A, Marzioni M, Marin JJG, et al. Wnt-β-Catenin Signalling in Liver Development, Health and Disease. *Nat Rev Gastroenterol Hepatol* (2019) 16(2):121–36. doi: 10.1038/s41575-018-0075-9
88. Wu Y, Shan B, Dai J, Xia Z, Cai J, Chen T, et al. Dual Role for Inositol-Requiring Enzyme 1α in Promoting the Development of Hepatocellular Carcinoma During Diet-Induced Obesity in Mice. *Hepatology* (2018) 68 (2):533–46. doi: 10.1002/hep.29871
89. Qin YE, Duan L, He Y, Yuan C, Wang T, Yuan D, et al. Saturated Fatty Acids Promote Hepatocytic Senecence Through Regulation of miR-34a/Cyclin-Dependent Kinase 6. *Mol Nutr Food Res* (2020) 64:e2000383. doi: 10.1002/mnfr.202000383
90. Liu N, Chang CW, Steer CJ, Wang XW, Song G. MicroRNA-15a/16-1 Prevents Hepatocellular Carcinoma by Disrupting the Communication Between Kupffer Cells and Tregs. *Gastroenterology* (2021). doi: 10.1053/j.gastro.2021.10.015
91. Xu G, Bu S, Wang X, Ge H. MiR-122 Radiosensitize Hepatocellular Carcinoma Cells by Suppressing Cyclin G1. *Int J Radiat Biol* (2021) 1–7. doi: 10.1080/09553002.2021.1987561
92. Seo J, Jeong D-W, Park J-W, Lee K-W, Fukuda J, Chun Y-S. Fatty-Acid-Induced FABP5/HIF-1 Reprograms Lipid Metabolism and Enhances the Proliferation of Liver Cancer Cells. *Commun Biol* (2020) 3(1):638. doi: 10.1038/s42003-020-01367-5
93. Liu Y, Liu L, Zhou Y, Zhou P, Yan Q, Chen X, et al. CKLF1 Enhances Inflammation-Mediated Carcinogenesis and Prevents Doxorubicin-Induced Apoptosis *via* IL6/STAT3 Signaling in HCC. *Clin Cancer Res* (2019) 25 (13):4141–54. doi: 10.1158/1078-0432.Ccr-18-3510
94. Yao RR, Li JH, Zhang R, Chen RX, Wang YH. M2-Polarized Tumor-Associated Macrophages Facilitated Migration and Epithelial-Mesenchymal Transition of HCC Cells *via* the TLR4/STAT3 Signaling Pathway. *World J Surg Oncol* (2018) 16(1):9. doi: 10.1186/s12957-018-1312-y

95. Wang D, Zheng X, Fu B, Nian Z, Qian Y, Sun R, et al. Hepatectomy Promotes Recurrence of Liver Cancer by Enhancing IL-11-STAT3 Signaling. *EBioMedicine* (2019) 46:119–32. doi: 10.1016/j.ebiom.2019.07.058
96. Gong C, Ai J, Fan Y, Gao J, Liu W, Feng Q, et al. NCAPG Promotes The Proliferation Of Hepatocellular Carcinoma Through PI3K/AKT Signaling. *Onco Targets Ther* (2019) 12:8537–52. doi: 10.2147/ott.S217916
97. Liu JS, Huo CY, Cao HH, Fan CL, Hu JY, Deng LJ, et al. Aloperine Induces Apoptosis and G2/M Cell Cycle Arrest in Hepatocellular Carcinoma Cells Through the PI3K/Akt Signaling Pathway. *Phytomedicine* (2019) 61:152843. doi: 10.1016/j.phymed.2019.152843
98. Jiang H, Zhou Z, Jin S, Xu K, Zhang H, Xu J, et al. PRMT9 Promotes Hepatocellular Carcinoma Invasion and Metastasis *via* Activating PI3K/Akt/GSK-3β/Snail Signaling. *Cancer Sci* (2018) 109(5):1414–27. doi: 10.1111/cas.13598
99. Zhang Q, Zhang Y, Sun S, Wang K, Qian J, Cui Z, et al. ACOX2 Is a Prognostic Marker and Impedes the Progression of Hepatocellular Carcinoma *via* Pparα Pathway. *Cell Death Dis* (2021) 12(1):15. doi: 10.1038/s41419-020-03291-2
100. Li Z, Li H, Zhao ZB, Zhu W, Feng PP, Zhu XW, et al. SIRT4 Silencing in Tumor-Associated Macrophages Promotes HCC Development *via* Pparδ Signalling-Mediated Alternative Activation of Macrophages. *J Exp Clin Cancer Res* (2019) 38(1):469. doi: 10.1186/s13046-019-1456-9
101. Feng J, Dai W, Mao Y, Wu L, Li J, Chen K, et al. Simvastatin Re-Sensitizes Hepatocellular Carcinoma Cells to Sorafenib by Inhibiting HIF-1α/PPAR-γ/PKM2-Mediated Glycolysis. *J Exp Clin Cancer Res* (2020) 39(1):24. doi: 10.1186/s13046-020-1528-x
102. Wu H, Ng R, Chen X, Steer CJ, Song G. MicroRNA-21 Is a Potential Link Between Non-Alcoholic Fatty Liver Disease and Hepatocellular Carcinoma *via* Modulation of the HBP1-P53-Srebp1c Pathway. *Gut* (2016) 65(11):1850–60. doi: 10.1136/gutjnl-2014-308430
103. Lacin S, Yalcin S. The Prognostic Value of Circulating VEGF-A Level in Patients With Hepatocellular Cancer. *Technol Cancer Res Treat* (2020) 19:1533033820971677. doi: 10.1177/1533033820971677
104. Modi SJ, Kulkarni VM. Discovery of VEGFR-2 Inhibitors Exerting Significant Anticancer Activity Against CD44+ and CD133+ Cancer Stem Cells (CSCs): Reversal of TGF-β Induced Epithelial-Mesenchymal Transition (EMT) in Hepatocellular Carcinoma. *Eur J Med Chem* (2020) 207:112851. doi: 10.1016/j.ejmech.2020.112851
105. Anstee QM, Reeves HL, Kotsiliti E, Govaere O, Heikenwalder M. From NASH to HCC: Current Concepts and Future Challenges. *Nat Rev Gastroenterol Hepatol* (2019) 16(7):411–28. doi: 10.1038/s41575-019-0145-7
106. Kennedy OJ, Roderick P, Buchanan R, Fallowfield JA, Hayes PC, Parkes J. Coffee, Including Caffeinated and Decaffeinated Coffee, and the Risk of Hepatocellular Carcinoma: A Systematic Review and Dose-Response Meta-Analysis. *BMJ Open* (2017) 7(5):e013739. doi: 10.1136/bmjopen-2016-013739
107. Sun M, Cui H, Liang M, Wang W, Wang Y, Liu X, et al. Perceived Dietary Salt Intake and the Risk of Primary Liver Cancer: A Population-Based Prospective Study. *J Hum Nutr Diet* (2020) 33(6):833–40. doi: 10.1111/jhn.12761
108. Romero-Gómez M, Zelber-Sagi S, Trenell M. Treatment of NAFLD With Diet, Physical Activity and Exercise. *J Hepatol* (2017) 67(4):829–46. doi: 10.1016/j.jhep.2017.05.016
109. Stefan N. Causes, Consequences, and Treatment of Metabolically Unhealthy Fat Distribution. *Lancet Diabetes Endocrinol* (2020) 8(7):616–27. doi: 10.1016/s2213-8587(20)30110-8
110. Wu HC, Shen J, Siegel A, Santella RM. Environmental Exposure and Clinical Correlates of Hepatocellular Carcinoma in New York City: A Case Only Study. *Cancer Causes Control* (2021). doi: 10.1007/s10552-021-01494-2
111. Hamid AS, Tesfamariam IG, Zhang Y, Zhang ZG. Aflatoxin B1-Induced Hepatocellular Carcinoma in Developing Countries: Geographical Distribution, Mechanism of Action and Prevention. *Oncol Lett* (2013) 5(4):1087–92. doi: 10.3892/ol.2013.1169
112. Mahato DK, Lee KE, Kamle M, Devi S, Dewangan KN, Kumar P, et al. Aflatoxins in Food and Feed: An Overview on Prevalence, Detection and Control Strategies. *Front Microbiol* (2019) 10:2266. doi: 10.3389/fmicb.2019.02266
113. Inoue-Yamauchi A, Itagaki H, Oda H. Eicosapentaenoic Acid Attenuates Obesity-Related Hepatocellular Carcinogenesis. *Carcinogenesis* (2018) 39(1):28–35. doi: 10.1093/carcin/bgx112
114. Green CJ, Pramfalk C, Charlton CA, Gunn PJ, Cornfield T, Pavlides M, et al. Hepatic De Novo Lipogenesis Is Suppressed and Fat Oxidation Is Increased by Omega-3 Fatty Acids at the Expense of Glucose Metabolism. *BMJ Open Diabetes Res Care* (2020) 8(1). doi: 10.1136/bmjdrc-2019-000871
115. Wu BK, Chen QH, Pan D, Chang B, Sang LX. A Novel Therapeutic Strategy for Hepatocellular Carcinoma: Immunomodulatory Mechanisms of Selenium and/or Selenoproteins on a Shift Towards Anti-Cancer. *Int Immunopharmacol* (2021) 96:107790. doi: 10.1016/j.intimp.2021.107790
116. Kwak M, Mehaffey JH, Hawkins RB, Hsu A, Schirmer B, Hallowell PT. Bariatric Surgery Is Associated With Reduction in Non-Alcoholic Steatohepatitis and Hepatocellular Carcinoma: A Propensity Matched Analysis. *Am J Surg* (2020) 219(3):504–7. doi: 10.1016/j.amjsurg.2019.09.006
117. Lassailly G, Caiazzo R, Buob D, Pigeyre M, Verkindt H, Labreuche J, et al. Bariatric Surgery Reduces Features of Nonalcoholic Steatohepatitis in Morbidly Obese Patients. *Gastroenterology* (2015) 149(2):379–88; quiz e15-6. doi: 10.1053/j.gastro.2015.04.014
118. Ramai D, Singh J, Lester J, Khan SR, Chandan S, Tartaglia N, et al. Systematic Review With Meta-Analysis: Bariatric Surgery Reduces the Incidence of Hepatocellular Carcinoma. *Aliment Pharmacol Ther* (2021) 53(9):977–84. doi: 10.1111/apt.16335
119. Delaune V, Orci LA, Lacotte S, Peloso A, Schrenzel J, Lazarevic V, et al. Fecal Microbiota Transplantation: A Promising Strategy in Preventing the Progression of Non-Alcoholic Steatohepatitis and Improving the Anti-Cancer Immune Response. *Expert Opin Biol Ther* (2018) 18(10):1061–71. doi: 10.1080/14712598.2018.1518424
120. Yang M, Kimchi ET, Staveley-O'Carroll KF, Li G. Astaxanthin Prevents Diet-Induced NASH Progression by Shaping Intrahepatic Immunity. *Int J Mol Sci* (2021) 22(20):11037. doi: 10.3390/ijms222011037
121. Zhao D, Xia L, Geng W, Xu D, Zhong C, Zhang J, et al. Metformin Suppresses Interleukin-22 Induced Hepatocellular Carcinoma by Upregulating Hippo Signaling Pathway. *J Gastroenterol Hepatol* (2021). doi: 10.1111/jgh.15674
122. Liu H, Liu M, Fu X, Zhang Z, Zhu L, Zheng X, et al. Astaxanthin Prevents Alcoholic Fatty Liver Disease by Modulating Mouse Gut Microbiota. *Nutrients* (2018) 10(9):1298. doi: 10.3390/nu10091298
123. Simon TG, Henson J, Osganian S, Masia R, Chan AT, Chung RT, et al. Daily Aspirin Use Associated With Reduced Risk For Fibrosis Progression In Patients With Nonalcoholic Fatty Liver Disease. *Clin Gastroenterol Hepatol* (2019) 17(13):2776–2784.e4. doi: 10.1016/j.cgh.2019.04.061
124. Ricciotti E, Wangensteen KJ, FitzGerald GA. Aspirin in Hepatocellular Carcinoma. *Cancer Res* (2021) 81(14):3751–61. doi: 10.1158/0008-5472.Can-21-0758
125. Tangjarusritaratorn T, Tangjittipokin W, Kunavisarut T. Incidence and Survival of Hepatocellular Carcinoma in Type 2 Diabetes Patients With Cirrhosis Who Were Treated With and Without Metformin. *Diabetes Metab Syndr Obes* (2021) 14:1563–74. doi: 10.2147/dmso.S295753
126. Zhou J, Ke Y, Lei X, Wu T, Li Y, Bao T, et al. Meta-Analysis: The Efficacy of Metformin and Other Anti-Hyperglycemic Agents in Prolonging the Survival of Hepatocellular Carcinoma Patients With Type 2 Diabetes. *Ann Hepatol* (2020) 19(3):320–8. doi: 10.1016/j.aohep.2019.11.008
127. Wang CP, Kuhn J, Shah DP, Schmidt S, Lam YF, MacCarthy D, et al. Metformin Modifies Disparity in Hepatocellular Carcinoma Incidence in Men With Type 2 Diabetes But Without Chronic Liver Diseases. *Cancer Med* (2019) 8(6):3206–15. doi: 10.1002/cam4.2142
128. Wang W, Wu RD, Chen P, Xu XJ, Shi XZ, Huang LH, et al. Liraglutide Combined With Human Umbilical Cord Mesenchymal Stem Cell Transplantation Inhibits Beta-Cell Apoptosis *via* Mediating the ASK1/JNK/BAX Pathway in Rats With Type 2 Diabetes. *Diabetes Metab Res Rev* (2020) 36(2):e3212. doi: 10.1002/dmrr.3212
129. Xu X, Wang W, Lin L, Chen P. Liraglutide in Combination With Human Umbilical Cord Mesenchymal Stem Cell Could Improve Liver Lesions by Modulating TLR4/NF-kB Inflammatory Pathway and Oxidative Stress in T2DM/NAFLD Rats. *Tissue Cell* (2020) 66:101382. doi: 10.1016/j.tice.2020.101382

130. Kim G, Jang SY, Han E, Lee YH, Park SY, Nam CM, et al. Effect of Statin on Hepatocellular Carcinoma in Patients With Type 2 Diabetes: A Nationwide Nested Case-Control Study. *Int J Cancer* (2017) 140(4):798–806. doi: 10.1002/ijc.30506
131. Yang SY, Wang CC, Chen KD, Liu YW, Lin CC, Chuang CH, et al. Statin Use Is Associated With a Lower Risk of Recurrence After Curative Resection in BCLC Stage 0-A Hepatocellular Carcinoma. *BMC Cancer* (2021) 21(1):70. doi: 10.1186/s12885-021-07796-7
132. Zhang S, Cao M, Hou Z, Gu X, Chen Y, Chen L, et al. Angiotensin-Converting Enzyme Inhibitors Have Adverse Effects in Anti-Angiogenesis Therapy for Hepatocellular Carcinoma. *Cancer Lett* (2021) 501:147–61. doi: 10.1016/j.canlet.2020.12.031
133. Casadei Gardini A, Marisi G, Scarpi E, Scartozzi M, Faloppi L, Silvestris N, et al. Effects of Metformin on Clinical Outcome in Diabetic Patients With Advanced HCC Receiving Sorafenib. *Expert Opin Pharmacother* (2015) 16 (18):2719–25. doi: 10.1517/14656566.2015.1102887
134. Casadei Gardini A, Faloppi L, De Matteis S, Foschi FG, Silvestris N, Tovoli F, et al. Metformin and Insulin Impact on Clinical Outcome in Patients With Advanced Hepatocellular Carcinoma Receiving Sorafenib: Validation Study and Biological Rationale. *Eur J Cancer* (2017) 86:106–14. doi: 10.1016/j.ejca.2017.09.003
135. Hu W, Li M, Sun W, Li Q, Xi H, Qiu Y, et al. Hirsutine Ameliorates Hepatic and Cardiac Insulin Resistance in High-Fat Diet-Induced Diabetic Mice and. *Vitro models Pharmacol Res* (2021) 105917. doi: 10.1016/j.phrs.2021.105917
136. Chaiwong S, Chatturong U, Chanasong R, Deetud W, To-On K, Puntheeranurak S, et al. Dried Mulberry Fruit Ameliorates Cardiovascular and Liver Histopathological Changes in High-Fat Diet-Induced Hyperlipidemic Mice. *J Tradit Complement Med* (2021) 11(4):356–68. doi: 10.1016/j.jtcme.2021.02.006
137. Adinolfi LE, Petta S, Fracanzani AL, Nevola R, Coppola C, Narciso V, et al. Reduced Incidence of Type 2 Diabetes in Patients With Chronic Hepatitis C Virus Infection Cleared by Direct-Acting Antiviral Therapy: A Prospective Study. *Diabetes Obes Metab* (2020) 22(12):2408–16. doi: 10.1111/dom.14168
138. Adinolfi LE, Petta S, Fracanzani AL, Coppola C, Narciso V, Nevola R, et al. Impact of Hepatitis C Virus Clearance by Direct-Acting Antiviral Treatment on the Incidence of Major Cardiovascular Events: A Prospective Multicentre Study. *Atherosclerosis* (2020) 296:40–7. doi: 10.1016/j.atherosclerosis.2020.01.010
139. Sasso FC, Pafundi PC, Caturano A, Galiero R, Vetrano E, Nevola R, et al. Impact of Direct Acting Antivirals (DAAs) on Cardiovascular Events in HCV Cohort With Pre-Diabetes. *Nutr Metab Cardiovasc Dis* (2021) 31 (8):2345–53. doi: 10.1016/j.numecd.2021.04.016

Conflict of Interest: The authors declare that the research was conducted in the absence of any commercial or financial relationships that could be construed as a potential conflict of interest.

Publisher's Note: All claims expressed in this article are solely those of the authors and do not necessarily represent those of their affiliated organizations, or those of the publisher, the editors and the reviewers. Any product that may be evaluated in this article, or claim that may be made by its manufacturer, is not guaranteed or endorsed by the publisher.

frontiers in Endocrinology

ORIGINAL RESEARCH
published: 26 January 2022
doi: 10.3389/fendo.2021.816748

Metabolic Profiling Identified a Novel Biomarker Panel for Metabolic Syndrome-Positive Hepatocellular Cancer

Lin-Lin Cao[1], Yi Han[1], Yuanxiao Wang[1], Lin Pei[1], Zhihong Yue[1], Li Qin[1], Boyu Liu[2], Jingwen Cui[3], Mei Jia[1] and Hui Wang[1]*

[1] Department of Clinical Laboratory, Peking University People's Hospital, Beijing, China, [2] Department of Pharmacy, Peking University People's Hospital, Beijing, China, [3] SCIEX Analytical Instrument Trading Co., Shanghai, China

Metabolic syndrome (MetS) is an independent risk factor for hepatocellular cancer (HCC). Currently, there is no highly sensitive and specific biomarkers for HCC surveillance in MetS population. Metabolomics has been reported as a powerful technology for biomarker discovery. In the present study, we aimed to explore novel biomarkers with high sensitivity and specificity for MetS-positive [MetS(+)] HCC by metabolomic analysis. At first, many serum metabolites were found dysregulated in MetS(+) HCC individuals. Validation of the dysregulated metabolites by targeted metabolite analyses revealed that serum L-glutamic acid (L-glu), pipecolic acid (PA) and 7-methylguanine (7-mG) were increased in MetS(+) HCC compared to MetS group. Then a biomarker panel including L-glu, PA and alpha-fetoprotein (AFP) was identified as a novel biomarker for the diagnosis of MetS(+) HCC. Receiver operating characteristic (ROC) curve was drawn and the area under the ROC curve (AUC) was 0.87 for discriminating MetS(+) HCC from MetS group. The biomarker panel was capable of detecting small (AUC = 0.82) and early-stage (AUC = 0.78) tumors as well. Moreover, it exhibited great diagnostic performance (AUC = 0.93) for discriminating MetS(+) HCC from other MetS-associated cancers, including colorectal cancer and gastric cancer. Collectively, our study establishes a novel diagnostic tool for MetS(+) HCC.

Keywords: hepatocellular cancer, metabolic syndrome, metabolomics, L-glutamic acid, pipecolic acid

OPEN ACCESS

Edited by:
Conghui Yao,
Harvard Medical School, United States

Reviewed by:
Ming Yang,
University of Missouri, United States
Mary Taub,
University at Buffalo, United States
Zhenyu Huo,
Guangzhou Medical University, China

****Correspondence:***
Lin-Lin Cao
caoll@bjmu.edu.cn

Specialty section:
This article was submitted to Cancer Endocrinology, a section of the journal Frontiers in Endocrinology

Received: *17 November 2021*
Accepted: *14 December 2021*
Published: *26 January 2022*

Citation:
Cao L-L, Han Y, Wang Y, Pei L, Yue Z, Qin L, Liu B, Cui J, Jia M and Wang H (2022) Metabolic Profiling Identified a Novel Biomarker Panel for Metabolic Syndrome-Positive Hepatocellular Cancer. Front. Endocrinol. 12:816748. doi: 10.3389/fendo.2021.816748

INTRODUCTION

Hepatocellular cancer (HCC) is the most common primary liver cancer and represents a seriously threat to human health. It is estimated to be the fourth-most frequent cause of cancer mortality in the world (1, 2). Although considerable progress has been achieved in the diagnosis and treatment of HCC during the past few decades, the prognosis of HCC is still very poor, possibly due to the lack of obvious symptoms in the early stages and the delay in diagnosis of the disease (2). It has been reported that tumors diagnosed at early stages are suitable for curative therapy, with a median overall survival (OS) of exceeding 60 months, whereas the median OS of patients with advanced-stage HCC is only 11 months (3). Therefore, early detection of HCC in high-risk populations is essential to improve the prognosis of HCC patients.

It has been widely known that the hepatitis B virus (HBV) and hepatitis C virus (HCV) are the most important risk factors for HCC at present. However, their importance is gradually decreasing, which is due to the vaccination of newborns and the effective treatment of both HBV and HCV infections (4). Increasing evidence shows that metabolic syndrome (MetS) is also a significant risk factor for HCC, regardless of other risk factors (5–7). MetS is a cluster of metabolic abnormalities including insulin resistance, dyslipidemia, hypertension and central obesity. It has been demonstrated that MetS is associated with a 1.81-fold increased risk of HCC (8), indicating the necessity of monitoring the MetS population to ameliorate HCC risk. However, there is no specific biomarker for early detection of HCC in MetS patients at present. Serum alpha-fetoprotein (AFP) is the most widely used biomarker for HCC diagnosis, but its diagnostic accuracy is not satisfactory (2). Some other circulating biomarkers, such as microRNAs (9), specific proteins (10, 11) and differentially DNA methylation (12, 13), have been identified as potential biomarkers for HCC diagnosis, but they are not specific for MetS-positive [MetS(+)] HCC and not suitable for HCC surveillance in MetS population. Therefore, it is critical to explore novel biomarkers for MetS(+) HCC.

Metabolomics, which serves as a powerful platform focusing on the comprehensive profiling of small metabolites, has provided a promising technology for biomarker discovery (14). The liver is one of the most important metabolic centers of humans, and regulates many important metabolic processes. Therefore, there is no doubt that HCC occurrence is accompanied by changes in the levels of numerous metabolites, and metabolomic analysis is particularly useful for HCC diagnosis by determining dysregulated metabolites (15). A lot of effort has been devoted to the metabolomic study on HCC using various specimens, including liver tissue, serum and urine, and many metabolites have been reported as biomarkers for HCC diagnosis and prognosis (16–21). However, most studies have focused on HBV- and HCV-associated HCC, and there is still a lack of research on the metabolic biomarkers of MetS(+) HCC.

In this study, we aimed to explore the dysregulated metabolites in MetS(+) HCC compared to MetS patients, and find potential biomarkers for HCC surveillance in MetS population. Serum metabolite profiles in MetS patients and MetS(+) HCC patients were determined by untargeted metabolomic analysis. The metabolites that were differentially expressed in MetS(+) HCC compared with MetS patients were validated by targeted metabolite analyses. In addition, diagnostic values of these biomarkers and their correlation with clinicopathologic variables of patients were also evaluated. Overall, our study explored candidate metabolite biomarkers for the diagnosis of MetS(+) HCC.

MATERIALS AND METHODS

Study Population

In the present study, a total of 407 participants, including patients with HCC, colorectal cancer (CRC), gastric cancer (GC), MetS, and healthy controls (HC) were recruited in Peking University People's Hospital. In the discovery stage, 32 MetS patients and 43 MetS(+) HCC patients were included and subjected to metabolomic analyses. In the validation stage, 94 HCs, 100 MetS patients, 66 MetS(+) HCC patients, 42 MetS(+) CRC patients and 30 MetS(+) GC patients were included and subjected to targeted metabolite analyses. This study was approved by the Ethics Committee of Peking University People's Hospital and complied with the principles of the Declaration of Helsinki. Informed consents were obtained from all recruited participants.

The presence of MetS was defined as three or more of the following metabolic situations (22): (1) Central obesity: waist circumstance ≥ 90 cm in men or ≥ 85cm in women; (2) Hyperglycemia: fasting glucose (FG) ≥ 6.1 mmol/L or 2-h glucose in oral glucose tolerance test (OGTT) ≥ 7.8 mmol/L and/or confirmed diabetes that is under treatment; (3) Hypertension: blood pressure ≥ 130/85 mmHg and/or confirmed hypertension with antihypertensive therapy; (4) Fasting triglycerides (TG) ≥ 1.70 mmol/L; (5) Fasting high-density lipoprotein cholesterol (HDL-C) < 1.04 mmol/L. The diagnosis of patients with HCC, CRC and GC were confirmed by histopathology, and patients with other types of malignancy were excluded. In addition, all patients with HCC, CRC and GC included in this study had MetS. The enrolled HC subjects were healthy people who had received physical examinations. Peripheral blood samples were collected under fasting conditions before surgery. The demographic and clinical characteristics were collected from medical records and summarized in **Table 1**.

Chemicals and Reagents

All solvents used in this study were of high-performance liquid chromatography (HPLC) grade. Acetonitrile was purchased from Fisher Chemical. Methanol, ammonia hydroxide and formic acid were purchased from Sigma-Aldrich. Distilled water was purchased from Watsons. Ammonium acetate was purchased from Aladdin. The isotopically-labelled internal standard mixture used in metabolomic analyses was from Biotree Biomedical Technology. L-glutamic acid (L-glu), citrulline (Citru), pipecolic acid (PA), 7-methylguanine (7-mG) and L-glu-2,3,3,4,4-d5 were purchased from Sigma-Aldrich as well.

Measurement of Clinical Indicators

The peripheral blood sample was collected and serum was separated by centrifuging at 4000 rpm for 5 minutes for each individual. Serum levels of FG, TG, HDL-C were measured by AU5832 automatic biochemical analyzer (Beckman Coulter). Serum HBV surface antigen (HBsAg) was detected by the automatic chemiluminescent microparticle immunoassay analyzer ARCHITECT i2000 SR (Abbott Laboratories). The concentration of serum AFP was determined by an electrochemiluminescence immunoassay in Cobas e801 system (Roche Diagnostics). All measurements were performed with original manufacturers' reagents according to the manufacturers' instructions.

Metabolomic Analyses

The pretreatment of serum samples was as follows. 100 μL of serum sample was mixed with 400 μL of extract solution (acetonitrile: methanol = 1: 1, containing isotopically-labelled

TABLE 1 | The demographic and clinical variables of individuals included in this study.

	Discovery Cohort			Validation Cohort			
Variables	MetS N=32	MetS(+) HCC N=43	HC N=94	MetS N=100	MetS(+) HCC N=66	MetS(+) CRC N=42	MetS(+) GC N=30
Age	56.47 ± 11.37	59.09 ± 11.76	43.56 ± 15.02	54.39 ± 12.04	58.59 ± 9.94	66.31 ± 10.43	69.23 ± 11.36
Gender Male/Female	20/12	36/7	32/62	71/29	53/13	29/13	20/10
AFP >7/≤7 ng/ml	4/28	27/16	2/92	10/90	41/25	2/40	7/23
FG (mmol/L)	7.43 ± 1.43	6.91 ± 2.28	4.99 ± 0.42	8.60 ± 2.37	6.94 ± 2.70	5.46 ± 1.63	6.64 ± 3.51
TG (mmol/L)	1.77 ± 0.61	1.38 ± 0.61	1.03 ± 0.30	2.85 ± 1.34	1.45 ± 0.71	1.63 ± 0.51	1.56 ± 0.53
HDL-C (mmol/L)	0.99 ± 0.18	0.92 ± 0.25	1.29 ± 0.15	0.89 ± 0.08	0.94 ± 0.24	0.92 ± 0.18	0.96 ± 0.23
Central obesity +/-	16/16	22/21	10/84	44/56	40/26	31/11	22/8
Hypertension +/-	20/12	32/11	8/86	75/25	44/22	31/11	16/14

internal standard mixture) by vortexing for 30 seconds. Then the sample was sonicated for 10 min in ice-water bath, and incubated for 1 hour at -40°C to precipitate proteins. Subsequently, the sample was centrifuged at 12000 rpm for 15 min at 4°C. The supernatant was transferred into a fresh glass vial for metabolomic analysis. The quality control (QC) sample was prepared by mixing the supernatants from all of the samples in equal amounts.

Metabolomic analyses were performed using a UPLC system (Vanquish, Thermo Fisher Scientific) coupled to a Q Exactive HFX mass spectrometer (Orbitrap MS, Thermo Fisher Scientific). An ACQUITY UPLC BEH Amide column (2.1 mm × 100 mm, 1.7 μm, Waters) was used for analysis. The mobile phase A consisted of 25 mmol/L ammonium acetate and 25 mmol/L ammonia hydroxide in water (pH = 9.75), and the mobile phase B was 100% acetonitrile. The auto-sampler temperature was maintained at 4°C, and the column temperature was set at 30°C. The injection volume was set at 2 μL, and the flow rate was set at 0.5 mL/min. The following elution gradient was applied: 0-0.5 min, 95% B; 0.5-7 min, 95%-65% B; 7-8 min, 65%-40% B; 8-9 min, 40% B; 9-9.1 min, 40%-95% B; 9.1-12 min, 95% B. The ion spray voltage was set at 3600 V in the ESI+ mode and −3200 V in the ESI − mode. The capillary temperature was set at 350°C. The sheath gas flow rate was set at 30 arbitrary units and the aux gas flow rate was set at 25 arbitrary units. The mass scan range was set from 70 to 1050 m/z. The full MS resolution was set at 120000. A stepped normalized collisional energy (10, 30, 60 eV) approach was applied for effective fragmentation. The acquisition software Xcalibur (Thermo Fisher Scientific) was used to acquire MS/MS spectra on information-dependent acquisition (IDA) mode.

Targeted Metabolite Analyses

Calibration standard mixtures and QC samples were prepared according to the following procedures. At first, twenty serum samples were mixed in equal amounts. Then seven standard mixtures of L-glu, Citru, PA and 7-mG were prepared by 10-fold serial dilutions using the mixed serum to eliminate the matrix effect. The concentrations of these standard mixtures were determined with reference to the serum concentration ranges of these metabolites described in previous studies (23–26). QC samples (low-level and high-level) were prepared by spiking appropriate concentrations of L-glu, Citru, PA and 7-mG into the mixed serum.

Subsequently, the pretreatment of calibration standard mixtures, QC samples and serum samples was performed as follows. 100 μL of serum sample was mixed with 200 μL of extract solution (acetonitrile: methanol = 1: 1, containing isotopically-labelled internal standard L-glu-2,3,3,4,4-d5) by vortexing for 60 seconds, and centrifuged at 12000 rpm for 15 min at 4°C. Then 200 μL of the supernatant was diluted by adding 800 μL of water, and the diluted sample could be directly used for targeted metabolite analysis.

Targeted metabolite analyses were performed using a Jasper HPLC system coupled to a Triple Quad 4500MD (SCIEX). A Kinetex F5 column (3 mm × 100 mm, 2.6 μm, Phenomenex) was used for analysis. The mobile phase A consisted of 10 mmol/L ammonium acetate and 0.05% formic acid in water, and the mobile phase B consisted of 5 mmol/L ammonium acetate and 0.05% formic acid in 90% acetonitrile. The auto-sampler temperature was maintained at 4°C, and the column temperature was set at 40°C. The injection volume was set at 5 μL, and the flow rate was set at 0.4 mL/min. The following elution gradient was applied: 0-1 min, 6% B; 1-2 min, 6%-98% B; 2-3.5 min, 98% B; 3.5-3.6 min, 98%-6% B; 3.6-5 min, 6% B. The MS detection was carried out with a Turbo Spray probe in positive ion mode. The metabolites were tuned individually to get optimal signals, and multiple reaction monitoring (MRM) mode was used to monitor the specific metabolite transitions. The MRM settings are shown in **Supplementary Table 1**. The ion spray voltage was set at 5500 V, and the capillary temperature was set at 400°C. The curtain gas flow rate was set at 25 arbitrary units and the collision gas flow rate was set at 9 arbitrary units. The acquisition software Analyst MD 1.6.3 (SCIEX) was used to acquire MS/MS spectra, and MultiQuant MD 3.0.3 (SCIEX) was used for quantification.

Statistical Analysis

The metabolomic raw data were converted to the mzXML format with ProteoWizard software (27) version 3.0 (https://proteowizard.sourceforge.io/) and processed with an in-house program, which was developed using R software version 3.6.3 and based on XCMS software version 3.6.1. In-house MS2 database was applied for metabolite annotation. The resulting dataset including the information of sample name, peak number and normalized peak area was subjected to multivariate analysis using SIMCA 16.0.2 software package (Sartorius Stedim Data Analytics AB). An unsupervised principal component

analysis (PCA) with unit variance scaling was performed to visualize the distribution of the samples and assess the stability of the study. A supervised model of orthogonal projections to latent structures-discriminate analysis (OPLS-DA) with unit variance scaling was applied to maximize the distance between groups and find significantly dysregulated metabolites. A 7-fold cross validation was used to evaluate the reliability of our model. A permutation test was proceeded 200 times to estimate the risk of overfitting.

Then the score of variable importance in the projection (VIP) of the first principal component in OPLS-DA model was calculated. The metabolites with VIP > 1, $p < 0.05$ (student's t test) and |log_fold change (FC)| (the absolute value of log_FC) > 1 were considered as significantly dysregulated metabolites. Hierarchical clustering analysis was performed to represent the pattern of the dysregulated metabolites among samples, and the volcano plot was constructed to visualize these metabolites. In addition, the MetaboAnalyst database (http://www.metaboanalyst.ca/) were used to reveal the critical disturbed metabolic pathways in MetS(+) HCC. The chord plot and correlation analysis were conducted using R software version 3.6.3.

For targeted metabolite analysis, data were analyzed using GraphPad Prime 5.01 (GraphPad Software) or SPSS 20.0 software (IBM). All data were expressed as mean ± standard deviation (SD). Student's t test or Mann-Whitney U test was applied to evaluate the differences between two groups, depending on whether the data followed the Gaussian distribution. Receiver operating characteristic (ROC) curves were drawn and the areas under the ROC curves (AUCs) were determined to evaluate the diagnostic performances of the dysregulated metabolites. Youden's Indices were calculated to determine the cut-off points with optimal sensitivity and specificity. The correlations between the metabolites and clinical indicators were also investigated. The p value < 0.05 was regarded as statistically significant.

RESULTS

Serum Metabolic Profiling Identified Significantly Dysregulated Metabolites in MetS(+) HCC

Metabolic profiling of serum samples from patients with MetS and MetS(+) HCC in the discovery cohort was performed, and pooled QC samples were inserted into batches to evaluate the stability of the analytical method. Representative base peak chromatograms from ESI+ and ESI- mode were displayed in **Supplementary Figure 1**. The QC samples were clustered together in the PCA score plot (**Figure 1A**), indicating that the present analytical method was stable and repeatable. In addition, the reliability of the metabolomic analyses was further confirmed by the high correlation coefficients of the QC samples under the ESI+ and ESI- mode (**Supplementary Figure 2**). Subsequently, the supervised OPLS-DA model was applied to explore the metabolic changes in MetS(+) HCC patients compared to MetS population. As shown in **Figure 1B**, the HCC group was clearly separated from the MetS group in the OPLS-DA score plot, and the cumulative R^2Y and Q^2 were 0.92 and 0.82 respectively, representing a high predictive ability of the model. Then the permutation test was conducted 200 times and no overfitting was observed as the cumulative R^2Y-intercept and Q^2-intercept were 0.56 and -1.10 respectively (**Figure 1C**).

The dysregulated metabolites were selected according to the conditions of VIP > 1, $p < 0.05$ and |log_FC| > 1, and a total of 27 candidate metabolites including 24 upregulated and 3 downregulated in MetS(+) HCC patients were identified (**Supplementary Table 2**). The result of hierarchical clustering depicted the distinguishable profiling of the dysregulated metabolites between MetS and MetS(+) HCC group (**Figure 2A**), and a volcano plot was constructed for visualizing these metabolites (**Figure 2B**). In addition, pathway analysis was conducted using MetaboAnalyst database, and several metabolic pathways, including arginine biosynthesis, histidine metabolism, glycine, serine and threonine metabolism, and D-glutamine and D-glutamate metabolism, were revealed to be disturbed in MetS (+) HCC compared to MetS patients (**Figure 2C**). Moreover, the chord plot and correlation analysis showed that there were varying levels of correlation among these metabolites (**Figures 2D, E**).

Validation of Dysregulated Metabolites by Targeted Metabolite Analyses

Among these 27 dysregulated metabolites, L-glu, Citru, PA and 7-mG have been reported to be associated with HCC (28–31). To validate the metabolic profiling results, a new method for simultaneous quantification of L-glu, Citru, PA and 7-mG by liquid chromatography tandem mass spectrometry (LC-MS/MS) was developed, and the results of methodology validation suggested the precision and accuracy of the LC-MS/MS method was acceptable (**Supplementary Table 3**). Consistently, the levels of L-glu (**Figure 3A**), PA (**Figure 3C**) and 7-mG (**Figure 3D**) were significantly increased in MetS(+) HCC patients compared to MetS individuals in the discovery cohort. However, there was no significant difference in the levels of Citru between the two groups (**Figure 3B**). In addition, an independent validation cohort was introduced to further confirm the above results. As shown in **Figures 3E–G**, the levels of L-glu, PA and 7-mG were also upregulated significantly in the MetS(+) HCC patients compared to MetS and HC individuals. Interestingly, we found that L-glu and 7-mG were upregulated significantly in MetS compared to HC individuals, while PA showed no significant difference between MetS and HC group, indicating that the levels of L-glu and 7-mG, but not PA, were further affected as a consequence of the MetS in HCC patients. Moreover, as MetS was closely associated with the occurrence of CRC and GC as well as HCC (32, 33), CRC and GC patients were included in this study to assess the specificity of these potential biomarkers for MetS(+) HCC. The results showed that the levels of L-glu, PA and 7-mG in MetS(+) CRC and MetS(+) GC patients were significantly lower than those in MetS(+) HCC patients, suggesting the specificity of these metabolites for the detection

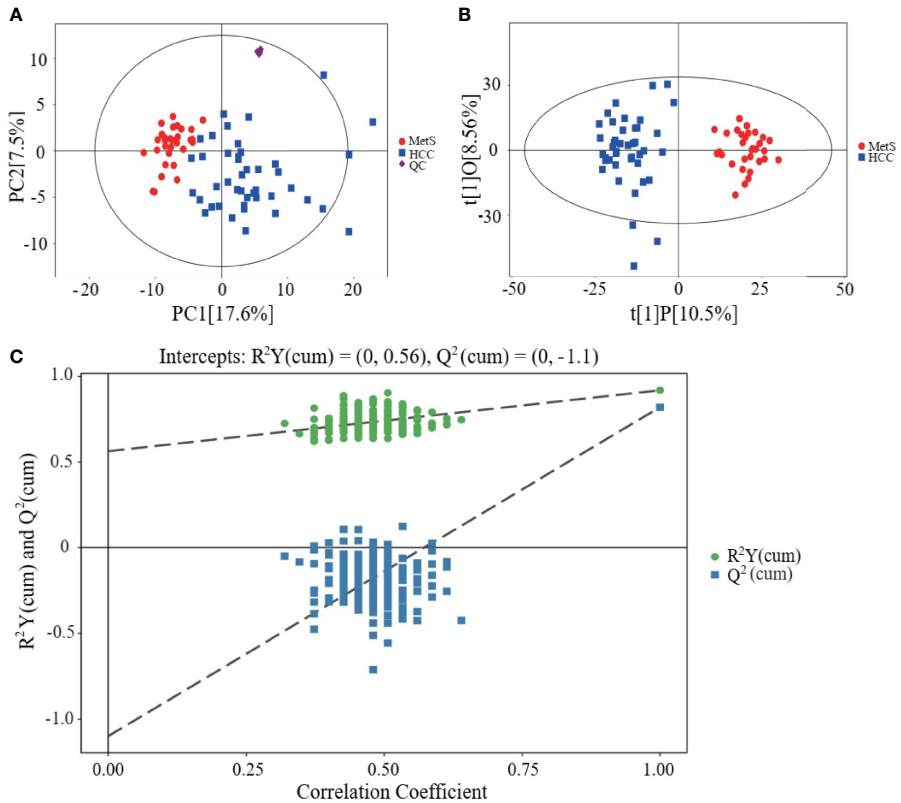

FIGURE 1 | Metabolic profiling of serum samples from patients with MetS and MetS(+) HCC. **(A)** Score plot of principal component analysis (PCA) based on the combinational data of ESI+ and ESI- modes. **(B)** Score plot of orthogonal projections to latent structures-discriminate analysis (OPLS-DA). **(C)** Statistical validation of the OPLS-DA model in 200 random permutation tests.

of MetS(+) HCC. These results suggested that L-glu, PA and 7-mG were specifically upregulated in MetS(+) HCC.

Evaluation of the Diagnostic Performances of L-glu, PA, and 7-mG

Then we evaluated the diagnostic potential of L-glu, PA and 7-mG in MetS(+) HCC using ROC curves. As shown in **Figure 4A** and **Table 2**, L-glu exhibited an AUC of 0.75 in discriminating MetS(+) HCC patients from MetS individuals, and the optimal sensitivity and specificity were 51.52% and 95.00%, respectively. The diagnostic accuracy of L-glu was high (0.95) for MetS patients, but low (0.52) for MetS(+) HCC patients (**Figure 4F**). In addition, PA exhibited an AUC of 0.75 as well, and the optimal sensitivity and specificity were 65.15% and 75.00%, respectively (**Figure 4B** and **Table 2**). The diagnostic accuracy of PA was 0.75 for MetS patients and 0.65 for MetS(+) HCC patients (**Figure 4F**). However, 7-mG showed poor diagnostic performance with an AUC of 0.56 in discriminating MetS(+) HCC patients from MetS individuals (**Figure 4C** and **Table 2**).

As the diagnostic efficacy of AFP was limited (AUC 0.73, sensitivity 62.12% and specificity 76% at the cut-off value of 7.0 ng/ml) (**Figure 4D** and **Table 2**), especially for AFP-negative [AFP (-)] HCC (34), we evaluated the diagnostic potential of L-glu and PA in AFP(-) MetS(+) HCC patients. As shown in **Supplementary Figure 3**, L-glu exhibited an AUC of 0.73 and PA exhibited an AUC of 0.68 in discriminating AFP(-) MetS(+) HCC patients from MetS individuals. Next, we determined whether the combination of L-glu, PA and AFP could improve the accurate diagnosis rate of MetS(+) HCC. Logistic regression based on L-glu, PA and AFP for MetS(+) HCC diagnosis was used to construct a model. This biomarker panel for the detection of MetS(+) HCC was constructed as follows: logit [p = HCC] = 0.0017 × [L-glu] + 0.0021 × [PA] + 0.1216 × [AFP] − 5.6391. As shown in **Figure 4E**, the biomarker panel exhibited better diagnostic performance than AFP alone in differentiating MetS(+) HCC patients from MetS individuals (AUC 0.87, sensitivity 78.79% and specificity 91.00% at the optimal cut-off point) (**Figure 4E** and **Table 2**). More importantly, the biomarker panel showed better diagnostic accuracy than any single biomarker. For MetS and MetS(+) HCC patients, the diagnostic accuracy of the biomarker panel was 0.91 and 0.79, respectively (**Figure 4F**). In general, the diagnostic accuracy of the biomarker panel was similar to that of L-glutamic acid alone (0.91 vs 0.95), but much higher than that of pipecolic acid alone (0.91 vs 0.75) or AFP (0.91 vs 0.75) for MetS patients. Consistently, the diagnostic accuracy of the biomarker panel was much higher than that of L-glutamic acid alone (0.79 vs 0.52), pipecolic acid alone (0.79 vs 0.65) or AFP (0.79 vs 0.62) for MetS(+) HCC patients.

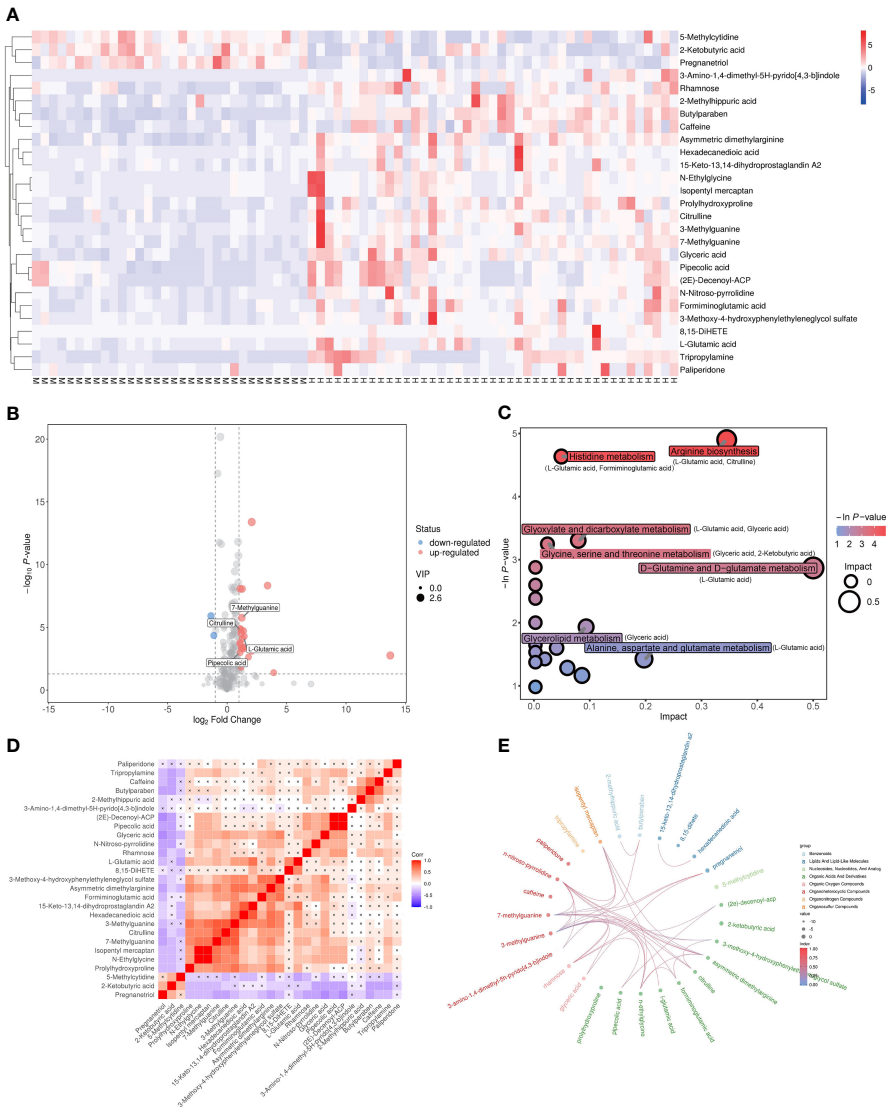

FIGURE 2 | Dysregulated metabolites between MetS and MetS(+) HCC patients identified in metabolic profiling. **(A)** Hierarchical clustering showing the dysregulated metabolites between MetS and MetS(+) HCC patients. Each column represents a sample, and each row represents a metabolite. M represents MetS individual, and H represents MetS(+) HCC patient. 'Red' indicates a high level, and 'blue' indicates a low level. **(B)** The volcano plot depicts the difference of metabolites between MetS and MetS(+) HCC patients. Red points (up-regulated) and blue points(down-regulated) refer to significant dysregulation according to fold change > 2.0 and p value < 0.05. **(C)** Pathway enrichment analysis of differential metabolites identified in MetS(+) HCC versus MetS group. **(D)** Correlation analysis of differential metabolites identified in MetS(+) HCC versus MetS group. 'Red' indicates a positive correlation, and 'blue' indicates a negative correlation. **(E)** Chord plot analysis of differential metabolites identified in MetS(+) HCC versus MetS group.

Subsequently, correlation analyses of the score of the biomarker panel with clinical characteristics were performed. As shown in **Table 3**, the biomarker panel was significantly correlated with tumor number, and the higher the score of the biomarker panel was, the more intrahepatic metastases might occur. However, no significant correlation of the score of the biomarker panel with other clinical characteristics of HCC patients was observed, such as tumor size, clinical stage, HBV and HCV status, cirrhosis, alcohol consumption, Child-Pugh classification and the metabolic situations. Together, these results suggested that the biomarker panel including L-glu, PA and AFP had good diagnostic performance for the detection of MetS(+) HCC in MetS population, and it might be associated with multiple intrahepatic metastases of HCC.

Diagnostic Performance of the Biomarker Panel in Small and Early-Stage MetS(+) HCC

As small and early-stage HCC patients are often difficult to detect, we evaluated the diagnostic value of the biomarker panel in these tumors. As shown in **Figure 5A** and **Table 4**, the

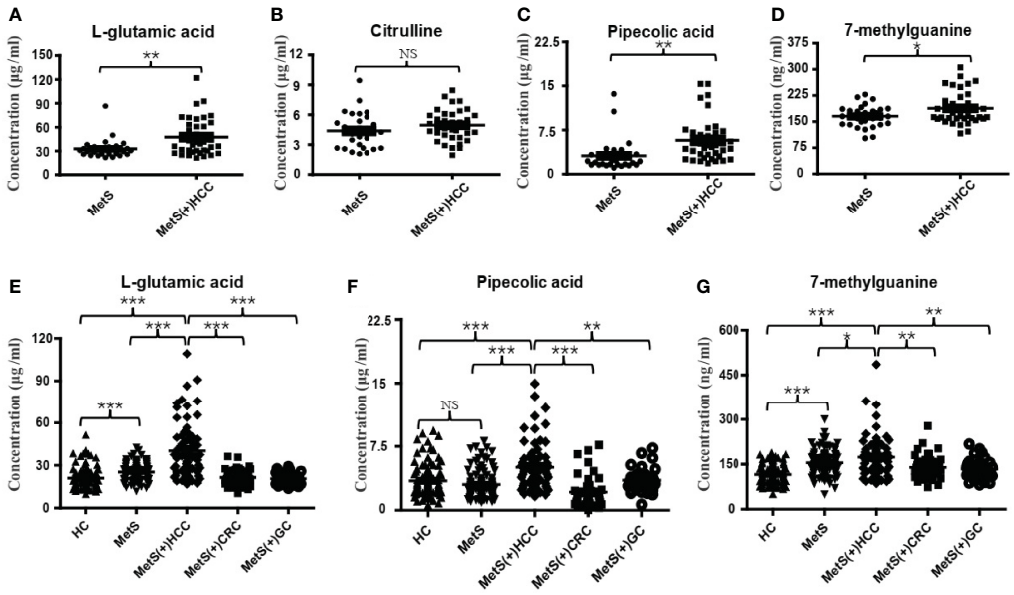

FIGURE 3 | Expression profiles of some dysregulated metabolites in the discovery and validation cohorts. **(A)** The levels of serum L-glu in the discovery cohort. **(B)** The levels of serum Citru in the discovery cohort. **(C)** The levels of serum PA in the discovery cohort. **(D)** The levels of serum 7-mG in the discovery cohort. **(E)** The levels of serum L-glu in the validation cohort. **(F)** The levels of serum PA in the validation cohort. **(G)** The levels of serum 7-mG in the validation cohort. NS, not significant. *p value < 0.05; **p value < 0.01; ***p value < 0.001.

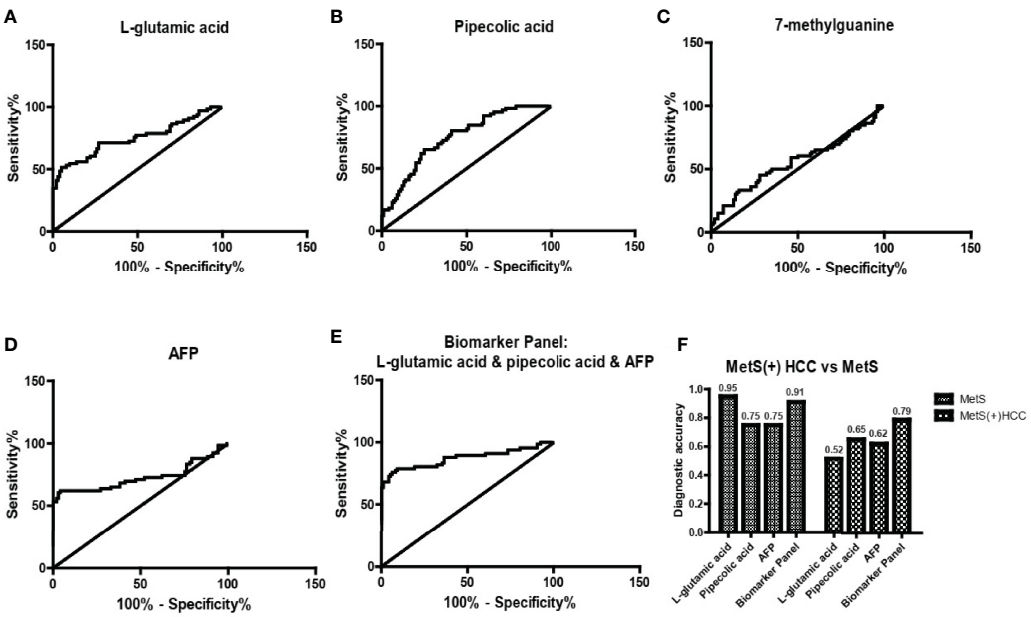

FIGURE 4 | The diagnostic performance of L-glu, PA and 7-mG. **(A)** The ROC curve of L-glu for discriminating MetS(+) HCC from MetS. **(B)** The ROC curve of PA for discriminating MetS(+) HCC from MetS. **(C)** The ROC curve of 7-mG for discriminating MetS(+) HCC from MetS. **(D)** The ROC curve of AFP for discriminating MetS(+) HCC from MetS. **(E)** The ROC curve of the biomarker panel including L-glu, PA and AFP for discriminating MetS(+) HCC from MetS. **(F)** The diagnostic accuracy of L-glu, PA, AFP and the biomarker panel for the diagnosis of MetS and MetS(+) HCC, respectively. ROC, receiver operating characteristic.

TABLE 2 | The diagnostic performance of serum metabolites, AFP or their combination for HCC detection in MetS population.

	AUC (95%CI)	Sensitivity (%)	Specificity (%)	p value
L-glu	0.75 (0.67-0.83)	51.52	95.00	<0.0001
PA	0.75 (0.68-0.82)	65.15	75.00	<0.0001
7-mG	0.56 (0.47-0.65)	45.45	72.00	0.2005
AFP	0.73 (0.64-0.82)	62.12	76.00	<0.0001
L-glu & PA & AFP	0.87 (0.81-0.94)	78.79	91.00	<0.0001

TABLE 3 | Correlation of the score of the biomarker panel with clinical variables in MetS(+) HCC patients in the validation cohort.

Variables	N	Biomarker Panel Score		P value
		Low (n = 33)	High (n = 33)	
Age				0.45
≤60 y	40	18	22	
>60 y	26	15	11	
Gender				0.22
Male	53	29	24	
Female	13	4	9	
FG (mmol/L)				0.42
		7.23 ± 2.48	6.65 ± 2.91	
TG (mmol/L)				0.20
		1.33 ± 0.57	1.56 ± 0.81	
HDL-C (mmol/L)				0.77
		0.95 ± 0.23	0.93 ± 0.26	
Central obesity				0.80
Yes	40	21	19	
No	26	12	14	
Hypertension				0.79
Yes	44	21	23	
No	22	12	10	
HBV				0.61
Positive	43	20	23	
Negative	23	13	10	
HCV				1.00
Positive	1	1	0	
Negative	65	32	33	
Cirrhosis				1.00
Yes	38	19	19	
No	28	14	14	
Alcohol Consumption				0.30
Yes	10	3	7	
No	56	30	26	
Child-Pugh Classification				0.62
A	35	19	16	
B-C	31	14	17	
Tumor Size				0.13
>5 cm	27	10	17	
≤5 cm	39	23	16	
Tumor Number				0.01*
=1		29	19	
>1		4	14	
Clinical Stage				0.08
I-II	26	17	9	
III-IV	40	16	24	
Differentiation				0.43
High-Moderate	44	24	20	
Low	22	9	13	
Vascular invasion				0.32
Yes	35	15	20	
No	31	18	13	

**P value < 0.05.*

biomarker panel exhibited an AUC of 0.82 in discriminating small MetS(+) HCC from MetS, and the optimal sensitivity and specificity were 69.23% and 91.00%, respectively. However, AFP showed much poorer diagnostic performance than the biomarker panel in discriminating small MetS(+) HCC from MetS, and the AUC, sensitivity and specificity were 0.67, 54.55% and 76.00%, respectively (**Figure 5B** and **Table 4**). More importantly, the diagnostic accuracy of the biomarker panel was 0.91 for MetS patients and 0.69 for small MetS(+) HCC patients, which was much higher than that of AFP(**Figure 5C**).

In addition, the biomarker panel exhibited an AUC of 0.78 in discriminating early-stage (stage I-II) MetS(+) HCC from MetS, and the optimal sensitivity and specificity were 65.38% and 91.00%, respectively (**Figure 5D** and **Table 4**). Consistently, AFP showed much poorer diagnostic performance than the biomarker panel in discriminating early-stage MetS(+) HCC from MetS, and the AUC, sensitivity and specificity were 0.63, 50.00% and 76.00%, respectively (**Figure 5E** and **Table 4**). The diagnostic accuracy of the biomarker panel was 0.91 for MetS patients and 0.65 for early-stage MetS(+) HCC patients, which were much higher than that of AFP(**Figure 5F**), indicating that the results with early-stage MetS(+) HCC were similar to the results with small MetS(+) HCC. Collectively, these findings indicated the importance of the biomarker panel in the diagnosis of small and early-stage MetS(+) HCC.

The Specificity of the Biomarker Panel for MetS(+) HCC

As L-glu and PA were specifically upregulated in MetS(+) HCC, but not MetS(+) CRC and MetS(+) GC, we then evaluated the specificity of biomarker panel for MetS(+) HCC. As shown in **Figure 6A** and **Table 5**, the biomarker panel exhibited an AUC of 0.93 in discriminating MetS(+) HCC from MetS(+) CRC & GC, and the optimal sensitivity and specificity were 84.85% and 91.67%, respectively. It showed better diagnostic performance than AFP alone, the AUC, sensitivity and specificity of which were 0.85, 62.12% and 87.50%, respectively (**Figure 6B** and **Table 5**). The diagnostic accuracy of the biomarker panel was 0.85 for MetS(+) HCC patients and 0.92 for MetS(+) CRC & GC patients, which were higher than that of AFP as well (**Figure 6C**). These data clearly suggested the high specificity of the biomarker panel for the diagnosis of MetS(+) HCC.

DISCUSSION

In this study, serum L-glu and PA were found to be upregulated in MetS(+) HCC patients compared to MetS(+) individuals. Dysregulated L-glu and PA showed adequate diagnostic performance in differentiating MetS(+) HCC from MetS(+) individuals, and the combination of L-glu, PA and AFP exhibited much better diagnostic performance than AFP alone. The biomarker panel also offered high diagnostic accuracy in the

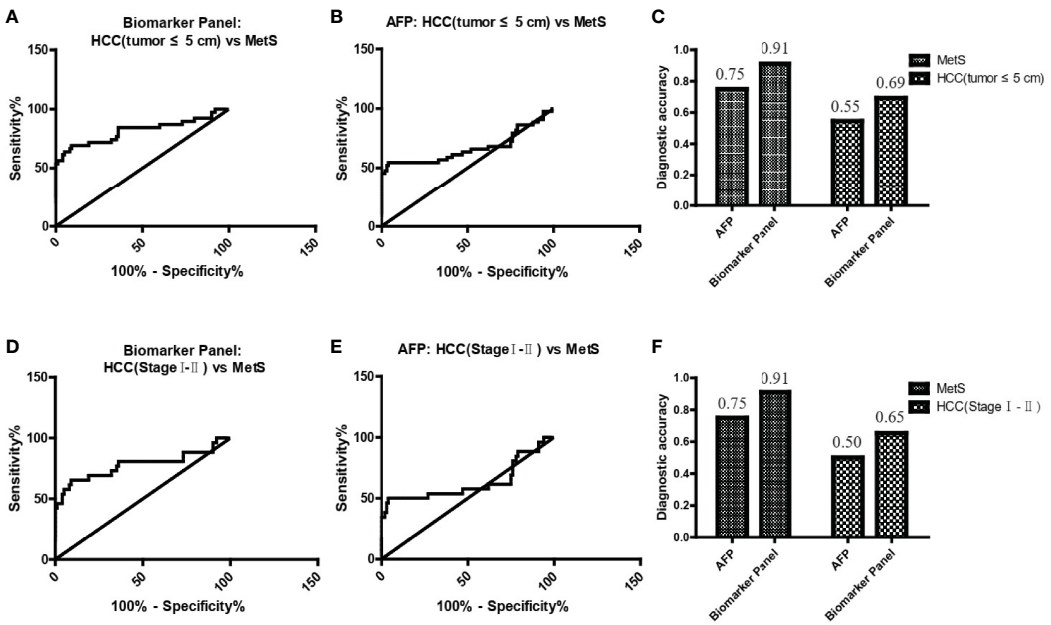

FIGURE 5 | The role of the biomarker panel in the diagnosis of small and early-stage HCC patients. **(A)** The ROC curve of the biomarker panel for discriminating small (tumor ≤ 5 cm) MetS(+) HCC patients from MetS individuals. **(B)** The ROC curve of AFP for discriminating small (tumor ≤ 5 cm) MetS(+) HCC patients from MetS individuals. **(C)** The diagnostic accuracy of AFP and the biomarker panel for the diagnosis of MetS and small (tumor ≤ 5 cm) MetS(+) HCC, respectively. **(D)** The ROC curve of the biomarker panel for discriminating early-stage (stage I-II) MetS(+) HCC patients from MetS individuals. **(E)** The ROC curve of AFP for discriminating early-stage (stage I-II) MetS(+) HCC patients from MetS individuals. **(F)** The diagnostic accuracy of AFP and the biomarker panel for the diagnosis of MetS and early-stage (stage I-II) MetS(+) HCC, respectively. ROC, receiver operating characteristic.

TABLE 4 | The diagnostic performance of the biomarker panel for the detection of small and early-stage HCC in MetS population.

Groups	AUC (95%CI)	Sensitivity (%)	Specificity (%)	p value
AFP				
HCC (tumor ≤ 5 cm) vs MetS	0.67 (0.55-0.78)	54.55	76.00	0.001319
HCC (Stage I-II) vs MetS	0.63 (0.48-0.78)	50.00	76.00	0.03986
Biomarker Panel				
HCC (tumor ≤ 5 cm) vs MetS	0.82 (0.72-0.91)	69.23	91.00	<0.0001
HCC (Stage I-II) vs MetS	0.78 (0.65-0.91)	65.38	91.00	<0.0001

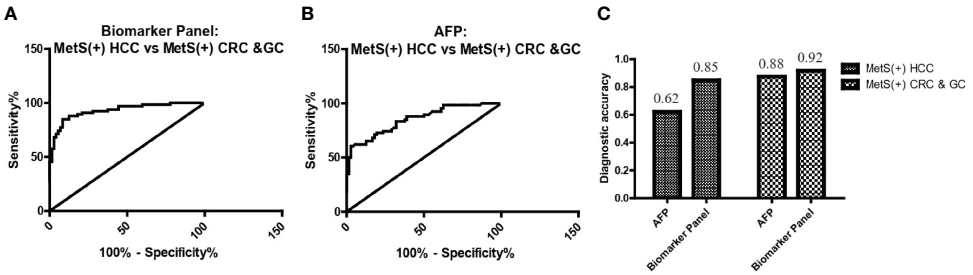

FIGURE 6 | The specificity of the biomarker panel in the diagnosis of MetS(+) HCC patients. **(A)** The ROC curve of the biomarker panel for discriminating MetS(+) HCC patients from MetS(+) CRC & GC patients. **(B)** The ROC curve of AFP for discriminating MetS(+) HCC patients from MetS(+) CRC & GC patients. **(C)** The diagnostic accuracy of AFP and the biomarker panel for the diagnosis of MetS(+) HCC and MetS(+) CRC & GC, respectively. ROC, receiver operating characteristic.

TABLE 5 | The diagnostic performance of the biomarker panel for discriminating MetS(+) HCC from MetS(+) CRC & GC.

	AUC (95%CI)	Sensitivity (%)	Specificity (%)	p value
AFP	0.85(0.79-0.92)	62.12	87.50	<0.0001
Biomarker Panel	0.93(0.89-0.97)	84.85	91.67	<0.0001

detection of small and early-stage MetS(+) HCC. The specificity of the biomarker panel was high for MetS(+) HCC as it distinguished patients with MetS(+) HCC from patients with MetS(+) CRC & GC accurately.

It is essential to explore potential biomarkers for HCC surveillance in MetS population because of the high prevalence of MetS worldwide and the close association of MetS with HCC (4, 35). Currently, there is no effective diagnostic marker for MetS(+) HCC in clinic, and the screening of small and early-stage tumors remains a challenge. In the present study, we found that L-glu, PA and 7-mG were upregulated in MetS(+) HCC. However, they were not uniformly higher in MetS(+) HCC patients compared to MetS individuals, and no single marker would be sufficient to identify patients with tumors. Therefore, we constructed a biomarker panel including L-glu, PA and AFP, which could effectively discriminate patients with MetS(+) HCC from the high-risk MetS population. In addition, it was able to detect small and early-stage MetS(+) HCC with high sensitivity and specificity. This study highlights the early diagnostic potential of this biomarker panel. It will help avoid delays in treatment and progression of the disease, and exert an important impact on prognosis improvement of MetS(+) HCC patients.

A growing number of studies have described the important role of serum metabolites in the diagnosis of HCC. For example, the specific changes in serum concentrations of several amino acids and lipids, including glycine, aspartic acid, sphingomyelin (42:3), and sphingomyelin (43:2), are useful for the early diagnosis of HCC (36). In addition, it has been reported by another group that the serum metabolite panel including phenylalanyl-tryptophan and glycocholate, as well as the combination of betaine and propionylcarnitine, conferred good diagnostic potential to discriminate HCC from chronic hepatitis and cirrhosis (18, 37). Moreover, the combination of retinol and retinal, and the serum metabolite panel including chenodeoxycholic acid, lysophosphatidylcholine (20:5), succinyladenosine and uridine were identified as potential diagnostic tools for HCC as well (20, 38). The results of these metabolomic studies were inconsistent, which might be due to the unreliability of untargeted metabolomics and the differences in sample selection. In this study, we verified the results of untargeted metabolomics with targeted LC-MS/MS analyses to ensure the analytical accuracy. In addition, as the aim of this study was to explore novel diagnostic markers for MetS(+) HCC, all included HCC patients had MetS. In this study, we found that serum L-glu and PA was dysregulated in MetS(+) HCC compared to MetS group, and might be specific for the diagnosis of MetS(+) HCC individuals.

The molecular mechanism by which MetS induced the development of HCC remains intriguing. It is well established

that insulin resistance exerts a critical role in the pathogenesis of HCC by increasing insulin growth factor-1 (IGF-1), which has important proliferative, antiapoptotic and angiogenesis effects (39). In addition, obesity promotes liver inflammation and tumorigenesis by enhancing the expression of interleukin-6 (IL-6) and tumor necrosis factor (TNF), which further activates several pro-oncogenic pathways (40, 41). Previous studies have also demonstrated that small molecule metabolites were important for MetS(+) HCC tumorigenesis. For example, MetS played an important role in HBV-associated HCC tumorigenesis, and the dysregulation of lipid metabolic genes and lipid (triglycerides, cholesterol, and fatty acids) profiles might promote the occurrence of HCC in chronic hepatitis B patients (42). In addition, 8-hydroxydeoxyguanosine, L-arginine and glucose metabolites were found to be upregulated in MetS and non-alcoholic steatohepatitis-associated hepatocarcinogenesis, and might take part in various tumor-associated processes, including the activation of oxidative stress resistance, mTOR pathways and cell proliferation (43). However, these studies were mainly conducted in mice model, and the dysregulation in MetS(+) HCC compared to MetS patients is still largely unclear at present. In this study, we compared the serum metabolite profiles in MetS patients and MetS(+) HCC patients, and found that some metabolites and pathways were disturbed significantly in MetS(+) HCC patients (**Figure 2**), indicating that they might influence the HCC tumorigenesis in MetS population.

Amino acids and their derivatives are usually aberrantly regulated in cancer, and play a key role in the diagnosis of various cancers (44, 45). However, their dysregulation in HCC is still controversial. For example, L-glu participated in several metabolic pathways, including arginine biosynthesis, histidine metabolism and D-glutamine and D-glutamate metabolism (**Figure 2C**), and several studies reported that L-glu was significantly increased in HCC compared with cirrhosis (46, 47), but some other studies indicated that it was downregulated (20) or had no significant change (18, 48) in HCC. PA, which is a metabolite of lysine degradation, was also found significantly differed between HCC and the other two cohorts of health and cirrhosis group (49). However, it showed no significant difference in other studies (18, 20). The inconsistency of these studies might be due to different included HCC patients. In this study, we recruited MetS(+) HCC patients specifically to explore the metabolite features in this type of HCC. Both L-glu and PA were upregulated in MetS(+) HCC compared to MetS individuals, indicating the alterations in particular metabolic pathways, such as arginine biosynthesis, histidine metabolism, D-glutamine and D-glutamate metabolism and lysine degradation. Our results further support the potential of amino acids and their derivatives as cancer biomarkers.

In conclusion, the present study is the first to demonstrate that serum L-glu and PA are upregulated in MetS(+) HCC patients, and biomarker panel including L-glu, PA and AFP exhibits good diagnostic performance for discriminating MetS (+) HCC from MetS patients. In addition, the biomarker panel is specific for MetS(+) HCC, but not MetS(+) CRC or MetS(+) GC. Therefore, this biomarker panel has great promise for clinical application in MetS(+) HCC diagnosis. In the future, large-scale, multicenter prospective studies will be needed to further confirm our findings.

DATA AVAILABILITY STATEMENT

The original contributions presented in the study are included in the article/**Supplementary Material**. Further inquiries can be directed to the corresponding author.

ETHICS STATEMENT

The studies involving human participants were reviewed and approved by The Ethics Committee of Peking University People's Hospital. The patients/participants provided their written informed consent to participate in this study.

AUTHOR CONTRIBUTIONS

L-LC conceived and designed the experiments. YH, YW, LP, and LQ collected the clinical samples. L-LC, YH, BL, and JC performed the experiments. ZY, MJ, and L-LC analyzed the data. L-LC and HW wrote the manuscript. ZY, MJ, and HW revised the manuscript. All authors contributed to the article and approved the submitted version.

FUNDING

This work was supported by the National Natural Science Foundation of China grant 81702788.

ACKNOWLEDGMENTS

The authors thank Yikun Li (Calibra Diagnostics) and Sha Chen (Biotree Biomedical Technology) for technical support.

SUPPLEMENTARY MATERIAL

The Supplementary Material for this article can be found online at: https://www.frontiersin.org/articles/10.3389/fendo.2021.816748/full#supplementary-material

Supplementary Figure 1 | Representative base peak chromatograms under the ESI+ **(A)** and ESI- **(B)** mode.

Supplementary Figure 2 | The correlation coefficients of the QC samples under the ESI+ **(A)** and ESI- **(B)** mode.

Supplementary Figure 3 | The diagnostic performance of L-glu **(A)** and PA **(B)** for discriminating AFP(-) MetS(+) HCC from MetS.

REFERENCES

1. Bray F, Ferlay J, Soerjomataram I, Siegel RL, Torre LA, Jemal A. Global Cancer Statistics 2018: GLOBOCAN Estimates of Incidence and Mortality Worldwide for 36 Cancers in 185 Countries. *CA Cancer J Clin* (2018) 68 (6):394–424. doi: 10.3322/caac.21492
2. Yang JD, Hainaut P, Gores GJ, Amadou A, Plymoth A, Roberts LR. A Global View of Hepatocellular Carcinoma: Trends, Risk, Prevention and Management. *Nat Rev Gastroenterol Hepatol* (2019) 16(10):589–604. doi: 10.1038/s41575-019-0186-y
3. Llovet JM, Zucman-Rossi J, Pikarsky E, Sangro B, Schwartz M, Sherman M, et al. Hepatocellular Carcinoma. *Nat Rev Dis Primers* (2016) 2:16018. doi: 10.1038/nrdp.2016.18
4. McGlynn KA, Petrick JL, El-Serag HB. Epidemiology of Hepatocellular Carcinoma. *Hepatology* (2021) 73(Suppl;1):4–13. doi: 10.1002/hep.31288
5. Welzel TM, Graubard BI, Zeuzem S, El-Serag HB, Davila JA, McGlynn KA. Metabolic Syndrome Increases the Risk of Primary Liver Cancer in the United States: A Study in the SEER-Medicare Database. *Hepatology* (2011) 54 (2):463–71. doi: 10.1002/hep.24397
6. Borena W, Strohmaier S, Lukanova A, Bjorge T, Lindkvist B, Hallmans G, et al. Metabolic Risk Factors and Primary Liver Cancer in a Prospective Study of 578,700 Adults. *Int J Cancer* (2012) 131(1):193–200. doi: 10.1002/ijc.26338
7. Kasmari AJ, Welch A, Liu G, Leslie D, McGarrity T, Riley T. Independent of Cirrhosis, Hepatocellular Carcinoma Risk Is Increased With Diabetes and Metabolic Syndrome. *Am J Med* (2017) 130(6):746.e741–746.e747. doi: 10.1016/j.amjmed.2016.12.029
8. Jinjuvadia R, Patel S, Liangpunsakul S. The Association Between Metabolic Syndrome and Hepatocellular Carcinoma: Systemic Review and Meta-Analysis. *J Clin Gastroenterol* (2014) 48(2):172–7. doi: 10.1097/MCG.0b013e3182a030c4
9. Lin XJ, Chong Y, Guo ZW, Xie C, Yang XJ, Zhang Q, et al. A Serum microRNA Classifier for Early Detection of Hepatocellular Carcinoma: A Multicentre, Retrospective, Longitudinal Biomarker Identification Study With a Nested Case-Control Study. *Lancet Oncol* (2015) 16(7):804–15. doi: 10.1016/S1470-2045(15)00048-0
10. Shang S, Plymoth A, Ge S, Feng Z, Rosen HR, Sangrajrang S, et al. Identification of Osteopontin as a Novel Marker for Early Hepatocellular Carcinoma. *Hepatology* (2012) 55(2):483–90. doi: 10.1002/hep.24703
11. Tsai TH, Song E, Zhu R, Di Poto C, Wang M, Luo Y, et al. LC-MS/MS-Based Serum Proteomics for Identification of Candidate Biomarkers for Hepatocellular Carcinoma. *Proteomics* (2015) 15(13):2369–81. doi: 10.1002/pmic.201400364
12. Zhao Y, Xue F, Sun J, Guo S, Zhang H, Qiu B, et al. Genome-Wide Methylation Profiling of the Different Stages of Hepatitis B Virus-Related Hepatocellular Carcinoma Development in Plasma Cell-Free DNA Reveals Potential Biomarkers for Early Detection and High-Risk Monitoring of Hepatocellular Carcinoma. *Clin Epigenet* (2014) 6(1):30. doi: 10.1186/1868-7083-6-30
13. Kisiel JB, Dukek BA, Kanipakam R, V.S.R., Ghoz HM, Yab TC, Berger CK, et al. Hepatocellular Carcinoma Detection by Plasma Methylated DNA: Discovery, Phase I Pilot, and Phase II Clinical Validation. *Hepatology* (2019) 69(3):1180–92. doi: 10.1002/hep.30244
14. Newgard CB. Metabolomics and Metabolic Diseases: Where Do We Stand? *Cell Metab* (2017) 25(1):43–56. doi: 10.1016/j.cmet.2016.09.018
15. Kimhofer T, Fye H, Taylor-Robinson S, Thursz M, Holmes E. Proteomic and Metabonomic Biomarkers for Hepatocellular Carcinoma: A Comprehensive Review. *Br J Cancer* (2015) 112(7):1141–56. doi: 10.1038/bjc.2015.38
16. Chen T, Xie G, Wang X, Fan J, Qiu Y, Zheng X, et al. Serum and Urine Metabolite Profiling Reveals Potential Biomarkers of Human Hepatocellular Carcinoma. *Mol Cell Proteomics* (2011) 10(7):M110 004945. doi: 10.1074/mcp.M110.004945
17. Shao Y, Zhu B, Zheng R, Zhao X, Yin P, Lu X, et al. Development of Urinary Pseudotargeted LC-MS-Based Metabolomics Method and Its Application in Hepatocellular Carcinoma Biomarker Discovery. *J Proteome Res* (2015) 14 (2):906–16. doi: 10.1021/pr500973d
18. Luo P, Yin P, Hua R, Tan Y, Li Z, Qiu G, et al. A Large-Scale, Multicenter Serum Metabolite Biomarker Identification Study for the Early Detection of Hepatocellular Carcinoma. *Hepatology* (2018) 67(2):662–75. doi: 10.1002/hep.29561
19. Ferrarini A, Di Poto C, He S, Tu C, Varghese RS, Kara Balla A, et al. Metabolomic Analysis of Liver Tissues for Characterization of Hepatocellular Carcinoma. *J Proteome Res* (2019) 18(8):3067–76. doi: 10.1021/acs.jproteome.9b00185
20. Han J, Han ML, Xing H, Li ZL, Yuan DY, Wu H, et al. Tissue and Serum Metabolomic Phenotyping for Diagnosis and Prognosis of Hepatocellular Carcinoma. *Int J Cancer* (2020) 146(6):1741–53. doi: 10.1002/ijc.32599
21. Zhou PC, Sun LQ, Shao L, Yi LZ, Li N, Fan XG. Establishment of a Pattern Recognition Metabolomics Model for the Diagnosis of Hepatocellular Carcinoma. *World J Gastroenterol* (2020) 26(31):4607–23. doi: 10.3748/wjg.v26.i31.4607
22. Jia W, Weng J, Zhu D, Ji L, Lu J, Zhou Z, et al. Standards of Medical Care for Type 2 Diabetes in China 2019. *Diabetes Metab Res Rev* (2019) 35(6):e3158. doi: 10.1002/dmrr.3158
23. Topp H, Sander G, Heller-Schoch G, Schoch G. Determination of 7-Methylguanine, N2,N2-Dimethylguanosine, and Pseudouridine in Ultrafiltrated Serum of Healthy Adults by High-Performance Liquid Chromatography. *Anal Biochem* (1987) 161(1):49–56. doi: 10.1016/0003-2697(87)90650-6
24. Lai X, Kline JA, Wang M. Development, Validation, and Comparison of Four Methods to Simultaneously Quantify L-Arginine, Citrulline, and Ornithine in Human Plasma Using Hydrophilic Interaction Liquid Chromatography and Electrospray Tandem Mass Spectrometry. *J Chromatogr B Analyt Technol BioMed Life Sci* (2015) 1005:47–55. doi: 10.1016/j.jchromb.2015.10.001
25. Semeraro M, Muraca M, Catesini G, Inglese R, Iacovone F, Barraco GM, et al. Determination of Plasma Pipecolic Acid by an Easy and Rapid Liquid Chromatography-Tandem Mass Spectrometry Method. *Clin Chim Acta* (2015) 440:108–12. doi: 10.1016/j.cca.2014.11.014
26. de Bie TH, Witkamp RF, Jongsma MA, Balvers MGJ. Development and Validation of a UPLC-MS/MS Method for the Simultaneous Determination of Gamma-Aminobutyric Acid and Glutamic Acid in Human Plasma. *J Chromatogr B Analyt Technol BioMed Life Sci* (2021) 1164:122519. doi: 10.1016/j.jchromb.2020.122519
27. Chambers MC, Maclean B, Burke R, Amodei D, Ruderman DL, Neumann S, et al. A Cross-Platform Toolkit for Mass Spectrometry and Proteomics. *Nat Biotechnol* (2012) 30(10):918–20. doi: 10.1038/nbt.2377
28. Wu L, Li L, Meng S, Qi R, Mao Z, Lin M. Expression of Argininosuccinate Synthetase in Patients With Hepatocellular Carcinoma. *J Gastroenterol Hepatol* (2013) 28(2):365–8. doi: 10.1111/jgh.12043
29. Sanabria JR, Kombu RS, Zhang GF, Sandlers Y, Ai J, Ibarra RA, et al. Glutathione Species and Metabolomic Prints in Subjects With Liver Disease as Biological Markers for the Detection of Hepatocellular Carcinoma. *HPB (Oxford)* (2016) 18(12):979–90. doi: 10.1016/j.hpb.2016.09.007
30. Nilsson A, Haanstra JR, Engqvist M, Gerding A, Bakker BM, Klingmuller U, et al. Quantitative Analysis of Amino Acid Metabolism in Liver Cancer Links Glutamate Excretion to Nucleotide Synthesis. *Proc Natl Acad Sci USA* (2020) 117(19):10294–304. doi: 10.1073/pnas.1919250117
31. Stepien M, Keski-Rahkonen P, Kiss A, Robinot N, Duarte-Salles T, Murphy N, et al. Metabolic Perturbations Prior to Hepatocellular Carcinoma Diagnosis: Findings From a Prospective Observational Cohort Study. *Int J Cancer* (2021) 148(3):609–25. doi: 10.1002/ijc.33236
32. Esposito K, Chiodini P, Capuano A, Bellastella G, Maiorino MI, Rafaniello C, et al. Colorectal Cancer Association With Metabolic Syndrome and Its Components: A Systematic Review With Meta-Analysis. *Endocrine* (2013) 44(3):634–47. doi: 10.1007/s12020-013-9939-5
33. Li F, Du H, Li S, Liu J. The Association Between Metabolic Syndrome and Gastric Cancer in Chinese. *Front Oncol* (2018) 8:326. doi: 10.3389/fonc.2018.00326
34. Wang T, Zhang KH. New Blood Biomarkers for the Diagnosis of AFP-Negative Hepatocellular Carcinoma. *Front Oncol* (2020) 10:1316. doi: 10.3389/fonc.2020.01316
35. O'Neill S, O'Driscoll L. Metabolic Syndrome: A Closer Look at the Growing Epidemic and its Associated Pathologies. *Obes Rev* (2015) 16(1):1–12. doi: 10.1111/obr.12229
36. Banales JM, Inarrairaegui M, Arbelaiz A, Milkiewicz P, Muntane J, Munoz-Bellvis L, et al. Serum Metabolites as Diagnostic Biomarkers for Cholangiocarcinoma, Hepatocellular Carcinoma, and Primary Sclerosing Cholangitis. *Hepatology* (2019) 70(2):547–62. doi: 10.1002/hep.30319

37. Huang Q, Tan Y, Yin P, Ye G, Gao P, Lu X, et al. Metabolic Characterization of Hepatocellular Carcinoma Using Nontargeted Tissue Metabolomics. *Cancer Res* (2013) 73(16):4992–5002. doi: 10.1158/0008-5472.CAN-13-0308
38. Han J, Qin WX, Li ZL, Xu AJ, Xing H, Wu H, et al. Tissue and Serum Metabolite Profiling Reveals Potential Biomarkers of Human Hepatocellular Carcinoma. *Clin Chim Acta* (2019) 488:68–75. doi: 10.1016/j.cca.2018.10.039
39. Rahman R, Hammoud GM, Almashhrawi AA, Ahmed KT, Ibdah JA. Primary Hepatocellular Carcinoma and Metabolic Syndrome: An Update. *World J Gastrointest Oncol* (2013) 5(9):186–94. doi: 10.4251/wjgo.v5.i9.186
40. Park EJ, Lee JH, Yu GY, He G, Ali SR, Holzer RG, et al. Dietary and Genetic Obesity Promote Liver Inflammation and Tumorigenesis by Enhancing IL-6 and TNF Expression. *Cell* (2010) 140(2):197–208. doi: 10.1016/j.cell.2009.12.052
41. Uzunlulu M, Telci Caklili O, Oguz A. Association Between Metabolic Syndrome and Cancer. *Ann Nutr Metab* (2016) 68(3):173–9. doi: 10.1159/000443743
42. Teng CF, Hsieh WC, Yang CW, Su HM, Tsai TF, Sung WC, et al. A Biphasic Response Pattern of Lipid Metabolomics in the Stage Progression of Hepatitis B Virus X Tumorigenesis. *Mol Carcinog* (2016) 55(1):105–14. doi: 10.1002/mc.22266
43. Kakehashi A, Suzuki S, Ishii N, Okuno T, Kuwae Y, Fujioka M, et al. Accumulation of 8-Hydroxydeoxyguanosine, L-Arginine and Glucose Metabolites by Liver Tumor Cells Are the Important Characteristic Features of Metabolic Syndrome and Non-Alcoholic Steatohepatitis-Associated Hepatocarcinogenesis. *Int J Mol Sci* (2020) 21(20):7746. doi: 10.3390/ijms21207746
44. Lieu EL, Nguyen T, Rhyne S, Kim J. Amino Acids in Cancer. *Exp Mol Med* (2020) 52(1):15–30. doi: 10.1038/s12276-020-0375-3
45. Wei Z, Liu X, Cheng C, Yu W, Yi P. Metabolism of Amino Acids in Cancer. *Front Cell Dev Biol* (2020) 8:603837. doi: 10.3389/fcell.2020.603837
46. Gao R, Cheng J, Fan C, Shi X, Cao Y, Sun B, et al. Serum Metabolomics to Identify the Liver Disease-Specific Biomarkers for the Progression of Hepatitis to Hepatocellular Carcinoma. *Sci Rep* (2015) 5:18175. doi: 10.1038/srep18175
47. Nezami Ranjbar MR, Luo Y, Di Poto C, Varghese RS, Ferrarini A, Zhang C, et al. GC-MS Based Plasma Metabolomics for Identification of Candidate Biomarkers for Hepatocellular Carcinoma in Egyptian Cohort. *PloS One* (2015) 10(6):e0127299. doi: 10.1371/journal.pone.0127299
48. Liu Z, Tu MJ, Zhang C, Jilek JL, Zhang QY, Yu AM. A Reliable LC-MS/MS Method for the Quantification of Natural Amino Acids in Mouse Plasma: Method Validation and Application to a Study on Amino Acid Dynamics During Hepatocellular Carcinoma Progression. *J Chromatogr B Analyt Technol BioMed Life Sci* (2019) 1124:72–81. doi: 10.1016/j.jchromb.2019.05.039
49. Zeng J, Yin P, Tan Y, Dong L, Hu C, Huang Q, et al. Metabolomics Study of Hepatocellular Carcinoma: Discovery and Validation of Serum Potential Biomarkers by Using Capillary Electrophoresis-Mass Spectrometry. *J Proteome Res* (2014) 13(7):3420–31. doi: 10.1021/pr500390y

Conflict of Interest: JC was employed by SCIEX Analytical Instrument Trading Co., Shanghai, China.

The remaining authors declare that the research was conducted in the absence of any commecial or financial relationships that could be construed as a potential conflict of interest.

Publisher's Note: All claims expressed in this article are solely those of the authors and do not necessarily represent those of their affiliated organizations, or those of the publisher, the editors and the reviewers. Any product that may be evaluated in this article, or claim that may be made by its manufacturer, is not guaranteed or endorsed by the publisher.

frontiers in Endocrinology

MINI REVIEW
published: 15 March 2022
doi: 10.3389/fendo.2022.852382

Connecting the Dots Between the Gut–IGF-1–Prostate Axis: A Role of IGF-1 in Prostate Carcinogenesis

Makoto Matsushita[1], *Kazutoshi Fujita*[1,2*], *Koji Hatano*[1], *Marco A. De Velasco*[2,3], *Hirotsugu Uemura*[2] *and Norio Nonomura*[1]

[1] Department of Urology, Graduate School of Medicine, Osaka University, Suita, Japan, [2] Department of Urology, Faculty of Medicine, Kindai University, Osakasayama, Japan, [3] Department of Genome Biology, Faculty of Medicine, Kindai University, Osakasayama, Japan

Prostate cancer (PCa) is the most common malignancy in men worldwide, thus developing effective prevention strategies remain a critical challenge. Insulin-like growth factor 1 (IGF-1) is produced mainly in the liver by growth hormone signaling and is necessary for normal physical growth. However, several studies have shown an association between increased levels of circulating IGF-1 and the risk of developing solid malignancies, including PCa. Because the IGF-1 receptor is overexpressed in PCa, IGF-1 can accelerate PCa growth by activating phosphoinositide 3-kinase and mitogen-activated protein kinase, or increasing sex hormone sensitivity. Short-chain fatty acids (SCFAs) are beneficial gut microbial metabolites, mainly because of their anti-inflammatory effects. However, we have demonstrated that gut microbiota-derived SCFAs increase the production of IGF-1 in the liver and prostate. This promotes the progression of PCa by the activation of IGF-1 receptor downstream signaling. In addition, the relative abundance of SCFA-producing bacteria, such as *Alistipes*, are increased in gut microbiomes of patients with high-grade PCa. IGF-1 production is therefore affected by the gut microbiome, dietary habits, and genetic background, and may play a central role in prostate carcinogenesis. The pro-tumor effects of bacteria and diet-derived metabolites might be potentially countered through dietary regimens and supplements. The specific diets or supplements that are effective are unclear. Further research into the "Gut–IGF-1–Prostate Axis" may help discover optimal diets and nutritional supplements that could be implemented for prevention of PCa.

Keywords: prostate cancer, IGF-1, short-chain fatty acids, gut microbiome, bacteria

OPEN ACCESS

Edited by:
Conghui Yao,
Harvard Medical School, United States

Reviewed by:
Yahui Wang,
Washington University in St. Louis, United States

****Correspondence:***
Kazutoshi Fujita
kazufujita2@gmail.com

Specialty section:
This article was submitted to Cancer Endocrinology, a section of the journal Frontiers in Endocrinology

Received: *11 January 2022*
Accepted: *21 February 2022*
Published: *15 March 2022*

Citation:
Matsushita M, Fujita K, Hatano K, De Velasco MA, Uemura H and Nonomura N (2022) Connecting the Dots Between the Gut–IGF-1–Prostate Axis: A Role of IGF-1 in Prostate Carcinogenesis. Front. Endocrinol. 13:852382. doi: 10.3389/fendo.2022.852382

INTRODUCTION

Prostate cancer (PCa) is the most common malignancy in men worldwide and the fifth most common cause of cancer-related death with as many as 360,000 men dying of PCa annually (1). PCa morbidity varies somewhat by region and race, and has consistently been increasing in recent years (2, 3). Although androgen deprivation therapy is very effective for PCa, high-grade PCa becomes

androgen resistant, which makes subsequent treatment challenging. Therefore, it is important to find new targets for the prevention and treatment of high-risk PCa.

The age-adjusted prevalence of latent PCa at autopsy in Japanese migrants in Hawaii >50 years old was higher than that of Japanese men living in Japan (25.6% vs. 20.5%), suggesting that PCa risk is not only altered by genetic factors but also by various environmental factors, such as diet (4). Many studies have reported that excessive intake of animal fat, carbohydrate, and dairy products increases PCa risk. However, different cohorts have yielded different results, and no consensus has been reached (5). This is because diet affects PCa development and progression through multiple mechanisms (6). The relationship between the diet and PCa is complex and not fully understood and as a result has hindered PCa prevention and treatment strategies *via* dietary interventions.

We recently identified a novel mechanism by which specific intestinal bacteria promote PCa through insulin-like growth factor I (IGF-1) signaling (7). Various studies have shown that diet can disrupt gut microbial composition resulting in dysbiosis and loss of homeostasis, affecting local intestinal disease as well as diseases and disorders in distant organs, such as the liver and brain (8–13). These relationships have been referred to as gut–liver axis and gut–brain axis, respectively. In cancer biology, the relationships between gut microbiota and various types of cancer, such as colorectal, hepatocellular, and breast cancer, have been well studied. In contrast, little is known about the influence of the gut microbiota on PCa (14). IGF-1 is implicated in the pathogenesis of PCa and may be the key player that links diet to prostate carcinogenesis and progression that is mediated by gut microbes. This review summarizes the present knowledge of the functions of IGF-1 in PCa progression, especially its relationship to diet and gut microbiota.

MECHANISM OF IGF-1 SIGNALING

IGF-1 is a growth factor that plays a crucial role in cell proliferation and physical growth. IGF-1 signal transduction is mediated through the IGF-1 receptor (IGF1R) and insulin receptor (INSR). The structures of IGF1R and INSR are highly homologous (15). These receptors stimulated by IGF-1 activate tyrosine kinase activity directed at the β subunit, resulting in substrate phosphorylation, such as insulin receptor substrate (IRS) 1, IRS2, and Src homology collagen. The phosphorylated residues are recognized by the signaling molecules p85 and Grb2, which stimulate the phosphoinositide 3-kinase (PI3K) and mitogen-activated protein kinase (MAPK) signaling cascades. These signaling cascades mediate crucial biological functions of IGF-1 (15).

IGF-1 production in the healthy liver is mainly positively regulated by growth hormone (GH) signaling through the GH receptor pathway (16, 17). IGF-1 is released into circulation. IGF-1 is produced in other organs by various other cells that express IGF1R and is activated *via* autocrine signaling, although hepatocytes do not express enough IGF1R (18). Therefore, in liver-specific IGF-1-deficient mouse models, circulating IGF-1 levels are reduced to <20% of control mice and GH levels are elevated, but physical growth is normal (19). The bioavailability of circulating IGF-1 is regulated by the IGF-binding protein (IGFBP) family that blocks access to its receptor (20). In particular, IGFBP3 produced by Kupffer cells in the liver is important in IGF-1 homeostasis (21).

EFFECTS OF IGF-1 ON ORGANS

IGF-1 has tissue-specific roles through IGF1R and INSR. Muscle-specific IGF1R knockout mice display disrupted muscle fiber formation and reduced muscle weight early in development (22). However, muscle weight of differentiated muscles is not affected in mice with IGF1R knockout (23). IGF-1 has a significant effect on physical growth, but not on adult physiology. IGF-1 is also critical in bone growth and maintenance during postnatal life. IGF-1 can directly affect chondrocytes and osteoblasts and increase ephrin ligand-receptor signaling, leading to the differentiation of each cell. IGF-1 signaling also inhibits the formation of differentiated osteoclasts, contributing to bone growth (24). In the pancreas, IGF-1 signaling retains normal β-cell function, which is necessary to maintain glucose tolerance *in vivo* (25, 26). *In vitro*, IGF-1 stimulates expression of cellular communication network factor 5 (CCN5) and promotes β-cell proliferation (27). The phenotype of diabetes by blocking IGF-1 signaling is more obvious in mouse models lacking both IGF1R and INSR in β-cells (28). IGF-1 signaling is required for adipocyte development and function in adipose tissue, which is a major nutrient storage site. Mice lacking IGF1R and INSR in adipocytes contain almost no adipose tissue and develop significant diabetes, dyslipidemia, and fatty liver (29). IGF-1 is involved in myeloid cell function. IGF-1 activates M2 macrophages. Secretion of IGF-1 by the macrophages in turn leads to insulin resistance in mice fed a high-fat diet (30). A very important role of IGF-1 is its effect on the endocrine system. IGF-1 can directly support thyroid hormone production, and organ-specific IGF-1 signal loss reduces thyroid hormone and significantly increases thyroid stimulating hormone (TSH) levels (31). IGF1R and INSR knockout inhibit the development of the adrenal cortex and testes, and reduce testosterone levels. How IGF-1 signaling affects adrenal and testes function remains unknown (32). The role of IGF-1 signaling in prostate development and normal prostate physiology has not been established *in vivo*, however, silencing IGF-1 in not only the WPMY-1 prostate stroma cell line, and but also BPH-1, a prostate epithelium cell line, decreased cell proliferation and increased apoptosis rate *in vitro* (33). In human, *IGF1R* is located on the long arm of chromosome 15, and 36 different probable mutations have been reported (34). Most patients are heterozygous carriers, and all show pre- and postnatal growth retardation and dysmorphic features, such as a triangular face. The collective findings reveal that IGF-1 is an essential hormone for normal growth and maintain homeostasis.

CANCERS AND IGF-1 SIGNALING

IGF-1 is involved in several diseases. It is clear that diabetes is influenced by IGF-1 because of its effect on pancreatic β-cell function. IGF-1 increases nutrient-stimulated insulin release. The increased level of insulin increases IGF-1 production by stimulating GH signaling (35). Impaired insulin secretion due to type 1 diabetes lowers serum IGF-1 levels, and improves glycemic control in patients with type 2 diabetes leads to increased IGF-1 levels (36–38). Obese individuals have lower serum IGF-1 levels than normal-weight individuals, although over nourishment is associated with high insulin and IGF-1 levels (39). Several large studies found that serum IGF-1 levels are highest in both men and women with a body mass index of 24–27 kg/m^2 (40, 41). A possible reason why serum IGF-1 levels are decreased in obese patients is that increased free IGF-1 fraction by reduction in IGFBP production enhances negative feedback on GH secretion by the pituitary gland (42). Therefore, IGF-1 bioactivity may not be decreased, even in obese patients. In a study of 27 samples of benign prostatic hyperplasia (BPH) patients, there was no significant relationship between serum IGF-1 levels and prostate volume (P = 0.91). However, the gene expression of IGF-1 in prostate tissue was significantly increased (P = 0.001) and the expression of IGFBP3 was significantly decreased (P = 0.003) in patients with larger prostate size (>30 mL) (43). Local IGF-1 was reportedly upregulated in hyperplastic prostate tissues (33). Patients with acromegaly characterized by GH hypersecretion display high IGF-1 levels, and acromegaly patients are highly susceptible to IGF-1 related diseases including diabetes mellitus and BPH, suggesting IGF-1 regulation of various diseases. Acromegaly patients <40 years of age were found to have significantly larger prostate than healthy men (18.2 vs. 28.5 mL, P < 0.001), and suppression of GH and IGF-1 using octreotide caused prostate shrinkage (44).

IGF-1 has been associated with the development and progression of some cancer types due to its function in activating the MAPK and PI3K signaling pathways (15). A positive association was observed between serum IGF-1 level and overall cancer risk in men in the United Kingdom (hazard ratio [HR] = 1.03 per 5-nmol/L increment in IGF-1) and specific cancer risk, such as prostate, melanoma, kidney, and thyroid (HR = 1.09, 1.08, 1.10, and 1.22, respectively) (45). In these cancer types, basic studies have also shown an association with IGF-1 signaling (46–48). Although melanoma cells do not produce IGF-1, activation of the MAPK and PI3K signaling pathway by paracrine stimulation of IGF-1 from stromal fibroblasts enhanced survival, migration, and growth of melanoma cells only from biologically early tumors (46). A cell line derived from metastatic clear cell renal cell carcinoma highly expresses IGFBP3 and IGF-1 compared to normal proximal tubule cell, and the autocrine actions of IGF-1 and IGFBP3 promote and inhibit cell proliferation, respectively (47). IGF-1 secreted by M2-like tumor–associated macrophages promote the invasion and stemness of C643 cells, an anaplastic thyroid carcinoma cell line, by activating PI3K signaling (48). Furthermore, IGF-1 is involved in bone metastasis biology, such as in homing, dormancy, colonization, and expansion (49). In an *in vivo* study, the presence of high IGF-1 levels in the primary tumor environment tended to induce cancer cells to metastasize to bone, and cancer cell lines that highly expressed IGF1R were prone to display enlarged bone mass (50, 51). IGF1R is highly expressed in PCa cells. Therefore, PCa may be susceptible to IGF-1 signaling (52). The relationship between IGF-1 and PCa is detailed in the next section.

ROLE OF IGF-1 SIGNALING IN PROSTATE CANCER BIOLOGY

IGF-1 promotes the proliferation of 22RV1 and DU145 PCa cell lines *in vitro* (7). In these cell lines, protein kinase B (AKT) in the PI3K pathway and extracellular signal-regulated kinase (ERK) in the MAPK pathway were phosphorylated in an IGF-1 dose dependent manner, suggesting that IGF-1 directly influences PCa proliferation (7). *In vivo*, IGF-1 expression was reportedly reduced in xenografts of Los Angeles PCa-4 (LAPC-4) in mice fed a low-fat diet, and tumor volume was suppressed (53). IGF-1 decreased miR-143 expression and increased IGF1R expression in PC-3 and DU145 cells, and made these cell lines more resistant to docetaxel treatment, suggesting that IGF-1 levels are also involved in resistance to treatment in PCa (54). IGF-1 is also implicated in castration-resistant PCa and has been shown to activate androgen receptor (AR) signaling in prostate cancer cells *via* the IGF-1R-forkhead box protein O1 (FOXO1) signaling axis (**Figure 1**) (55–57).

Elevated blood IGF-1 levels increase the future risk of PCa in healthy men (45). Acromegaly patients with systemically high GH and IGF-1 levels also have significantly higher incidence of PCa and risk of PCa-related mortality (HR = 1.33 and 1.44, respectively), suggesting that IGF-1 has a positive effect on PCa development and progression, even in humans (58). Several studies reported that blood IGF-1 levels in elderly men with suspected PCa on screening tests are not associated with cancer positivity (59, 60). Serum IGF-1 levels in 94 men who required prostate biopsy showed no significant difference between positive and negative cancer (26.4 vs. 23.7 nmol/L; P = 0.08) (59). This discrepancy suggests that prostate epithelial cells may be at an increased risk of cancer development or progression only after prolonged exposure to high concentrations of IGF-1. Suppression of IGF-1 signaling is a potential therapeutic approach, because the IGF1R inhibitor in combination with castration inhibited PCa growth in rodent models of bone metastasis and subcutaneous xenografts (61, 62). However, in a phase 2 study, limsitinib, the most extensively evaluated IGF1R inhibitor, failed to significantly improve levels of prostate-specific antigen after 12 weeks of treatment and did not improve overall survival in men with metastatic castrate-resistant PCa (63). In the future, as a more potent treatment strategy, a combination of novel IGF1R inhibitors and existing prostate cancer therapies is expected to be effective.

SCFAs AS MAJOR METABOLITES OF INTESTINAL BACTERIA

In recent years, studies investigating the interactions between gut microbiota and its host has focused on recognizing an essential

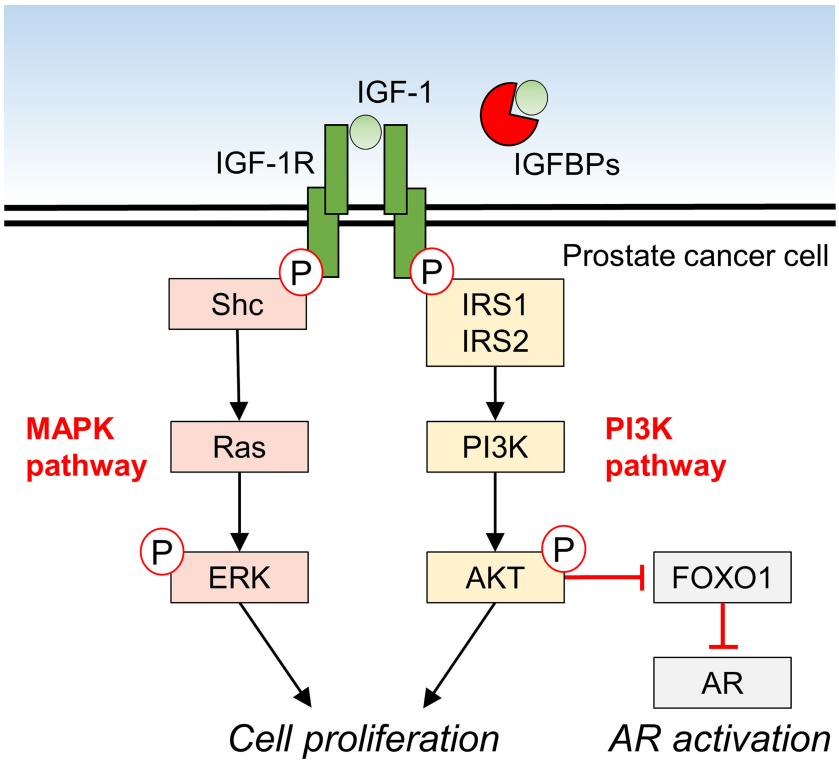

FIGURE 1 | Molecular mechanism of IGF-1 signaling and downstream effects in prostate cancer cells.

factor that influences homeostasis. One of the mechanisms by which intestinal bacteria affect humans is through bacterial structural components and their metabolites. Short-chain fatty acids (SCFAs) are major bacterial metabolites that play an important role in physiology. SCFAs include fatty acids with six or fewer carbon atoms. Of these, acetate (C2), propionate (C3), and butyrate (C4) are mainly produced by fermentation of dietary fiber by intestinal bacteria (64). Bacterial-derived SCFAs affect not only locally the gut but also distant organs in various ways. The anti-inflammatory effect is one of the major characteristics of SCFAs. Bacterial-derived butyrate promotes the differentiation of colonic regulatory T cells, suppresses inappropriate mucosal immunity, and improves local colitis and distant arthritis (65, 66). Propionic acids that reach the liver *via* the portal circulation increase glycogen synthesis and storage, improve insulin sensitivity, and repress lipogenesis in hepatocytes, resulting in the maintenance of energy homeostasis (67, 68). In the central nervous system (CNS), bacterial-derived SCFAs contribute to normal maturation of microglia *via* the free fatty acid receptor 2 (FFAR2) as a SCFA receptor (69). SCFAs also have some effects on several brain functions involved in circadian rhythm and appetite control (70).

SCFAs are also involved in the development and progression of cancer (71). In colorectal cancer, SCFAs, especially butyrate, function as anti-inflammatory metabolites and histone deacetylate (HDAC) inhibitors, resulting in the suppression of cancer progression (72). HDAC is a very important enzyme that modulates the expression of genes involved in signaling pathways, such as MAPK and Wnt (72). Therefore, accumulation of butyrate in some types of cancer cells that abundantly express a variety of HDACs, could inhibit their proliferation and promote apoptosis. In PCa, HDAC1, 2, and 3 are highly expressed (73). *In vitro*, sodium butyrate can directly decrease androgen receptor gene expression in LNCaP and C4-2 PCa cells, and can decrease the viability of these cells at concentrations >2.5 mM (74). However, it was demonstrated that high concentrations of butyrate were needed to inhibit colorectal cancer growth as an HDAC inhibitor, while <5 mM butyrate promoted cancer growth (75). SCFAs metabolized by intestinal bacteria are absorbed into the portal circulation and reach the liver, where most of the SCFAs are consumed (76). Therefore, only a small amount of bacteria-derived SCFAs can reach the prostate *via* systemic circulation. *In vivo*, bacteria-derived butyrate is not likely to work as an HDAC inhibitor in PCa due to this low concentration.

IGF-1 MEDIATED EFFECT OF SCFAs ON PROSTATE CANCER PROLIFERATION

In young mice, gut microbiota-derived SCFAs are likely to induce IGF-1 production, suggesting that SCFAs modulate the bone and physical growth (77). The authors also described that germ-free mice and mice orally administered antibiotics showed

lower cecal SCFA concentrations and IGF-1 production, resulting in decreased bone growth (77). SCFAs play a positive role in bone formation *via* an IGF-1-mediated mechanism. Unfortunately, the pathway by which SCFAs result in the elevation of IGF-1 is still not well understood.

We have reported that SCFAs metabolized by intestinal bacteria contribute to PCa growth by increasing systemic and prostate local IGF-1 productions, and revealed the "gut–prostate axis" involving bacterial metabolites (7). Prostate-specific phosphatase and tensin homolog (*PTEN*)-knockout mice [*Pb*-Cre+; *Pten*$^{fl/fl}$] were used as a PCa model. In these mice, a western-style high-fat diet (HFD) containing mainly lard accelerated PCa growth (78). This diet-induced PCa growth was inhibited by oral administration of metformin or celecoxib, as well as by an antibiotic mixture (ampicillin, vancomycin, neomycin, and metronidazole) (7, 78, 79). Antibiotics cause substantial changes in the composition of the gut microbiota of HFD-fed mice. Fecal SCFAs in the mice were reportedly reduced by 75%, resulting in decreased production of IGF-1 in the liver and prostate. In addition, phosphorylation of IGF-1R, ERK, and AKT was reduced in PCa cells of mice fed a HFD who received antibiotic, suggesting that decreased IGF-1 might suppress the activity of MAPK and PI3K signaling cascades. Oral supplementation of SCFAs to mice fed a HFD who received antibiotic resulted in increased serum IGF-1 levels and promoted prostate cancer growth. These results suggest that SCFAs derived from intestinal bacteria promote PCa growth through IGF-1 signaling, although butyrate in SCFAs may inhibit cancer cell proliferation as an HDAC inhibitor.

The examination of mice treated with antibiotics has revealed the absence of members of the family Rikenellaceae, order Clostridiales in the gut microbiota. Examination of the gut microbiota of men with a high-risk of PCa has revealed the increased abundance of genus *Alistipes* belonging to Rikenellaceae and the genus *Lachnospira* compared to men at low risk of PCa and those who are PCa-free (80). These bacterial taxa are associated with SCFA content in the stool and are SCFA-producing bacteria (81–86). These results suggest that SCFAs and their producing bacteria in the gut may be risk factors for PCa in humans and mice. Consumption of milk and other dairy products increase the dietary intake of SCFAs, thus resulting in the increase of serum IGF-1 levels and that is because these are the among the few foods that contain butyrate (87, 88). Many epidemiological studies have indicated that consumption of milk and dairy products increases the risk of PCa (5). This increased risk may be due to the butyrate contained in these foods (88). While dairy products are essential for nutrition and may a preventive effect in various diseases, including colorectal cancer (89), the roles are complex and most likely context-dependent. For example, low-fat milk containing no SCFAs does not increase the risk of PCa, unlike whole milk (90). Additional studies have reinforced this notion. In the NIH-AACR Diet and Health Study, during 7 years of follow-up, the highest quintile of dairy food intake had a significantly lower risk of colorectal cancer (relative risk [RR] = 0.85, P = 0.01) and a higher risk of prostate cancer (RR = 1.06, P = 0.01) compared to the lowest quintile (91). We hypothesize that the regulation of IGF-1 signaling contributing to prostate cancer risk in a real-world setting is increased by intestinal factors.

There are still some questions that need to be clarified regarding the gut–prostate axis involving SCFAs and IGF-1 signaling. It has been also reported that butyrate and propionate may have inhibitory effects on prostate cancer (74, 92). In our animal study, we found that a mixture of SCFAs (acetate, propionate, and butyrate) promoted prostate cancer growth (7), but we have not been able to determine which types of SCFAs are responsible for this promotive effect and at what concentration. Perhaps these may act cooperatively. Furthermore, although several G protein-coupled receptors, such as GPR41 and GPR43, are known as SCFA receptors, neither the receptor nor the signaling pathway(s) involved in the regulation of IGF-1 by SCFAs have been established (93, 94). Finally, the impact of interventions on the gut–prostate axis in human using fecal microbiota transplantation (FMT) or pro/

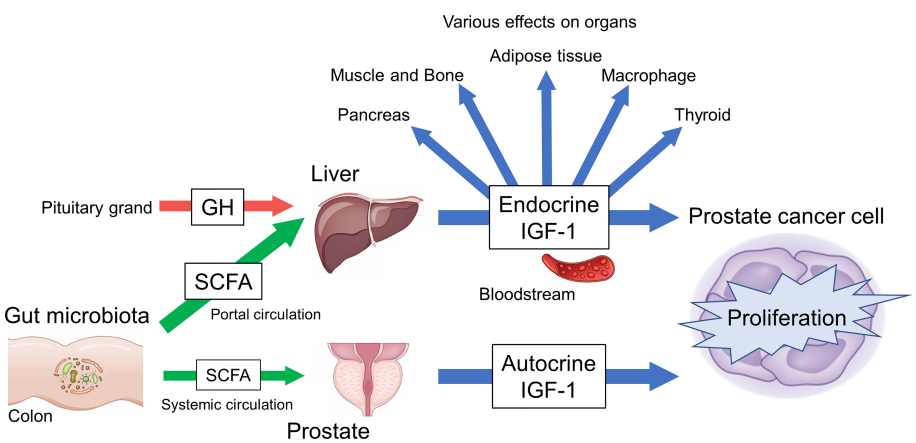

FIGURE 2 | Overview of gut–IGF-1–prostate axis mediated by gut microbiota-derived SCFAs.

prebiotics has not been studied. There are however several basic studies that have reported that FMT derived from prostate cancer individuals altered prostate cancer progression in mouse (95, 96), and we think that this axis may be a promising therapeutic target.

CONCLUSION

IGF-1 is an essential hormone for physical growth and has various effects in several diseases, especially prostate cancer, where it functions as an exacerbating factor. *In vivo*, local and systemic IGF-1 production might be regulated by SCFAs, which is in turn influenced by gut factors, such as gut microbiota and diet. The data thus far indicate that the gut–IGF-1–prostate axis is connected by SCFAs (**Figure 2**). This axis could provide a new direction for effective PCa treatment and prevention strategies. However, there are factors that remain unclear such as detailed mechanisms of IGF-1 regulation by SCFAs and the continuous control of SCFA levels in humans. Further study of the gut–IGF-1–prostate axis is needed to provide additional answers.

AUTHOR CONTRIBUTIONS

MM: writing—original draft preparation. KF, KH, and MV: conceptualization and writing—review and editing. HU and NN: supervision. All authors have read and agreed to the published version of the manuscript.

FUNDING

This work was supported by JSPS KAKENHI Grant Number JP21K09421.

REFERENCES

1. Bray F, Ferlay J, Soerjomataram I, Siegel RL, Torre LA, Jemal A. Global Cancer Statistics 2018: GLOBOCAN Estimates of Incidence and Mortality Worldwide for 36 Cancers in 185 Countries. *CA Cancer J Clin* (2018) 68:394–424. doi: 10.3322/caac.21492
2. Marima R, Hull R, Mathabe K, Setlai B, Batra J, Sartor O, et al. Prostate Cancer Racial, Socioeconomic, Geographic Disparities: Targeting the Genomic Landscape and Splicing Events in Search for Diagnostic, Prognostic and Therapeutic Targets. *Am J Cancer Res* (2021) 11:1012–30.
3. Lloyd T, Hounsome L, Mehay A, Mee S, Verne J, Cooper A. Lifetime Risk of Being Diagnosed With, or Dying From, Prostate Cancer by Major Ethnic Group in England 2008-2010. *BMC Med* (2015) 13:171. doi: 10.1186/s12916-015-0405-5
4. Yatani R, Chigusa I, Akazaki K, Stemmermann GN, Welsh RA, Correa P. Geographic Pathology of Latent Prostatic Carcinoma. *Int J cancer* (1982) 29:611–6. doi: 10.1002/ijc.2910290602
5. Matsushita M, Fujita K, Nonomura N. Influence of Diet and Nutrition on Prostate Cancer. *Int J Mol Sci* (2020) 21:1447. doi: 10.3390/ijms21041447
6. Narita S, Nara T, Sato H, Koizumi A, Huang M, Inoue T. Research Evidence on High-Fat Diet-Induced Prostate Cancer Development and Progression. *J Clin Med* (2019) 8:597. doi: 10.3390/jcm8050597
7. Matsushita M, Fujita K, Hayashi T, Kayama H, Motooka D, Hase H, et al. Gut Microbiota-Derived Short-Chain Fatty Acids Promote Prostate Cancer Growth *via* IGF1 Signaling. *Cancer Res* (2021) 81:4014–26. doi: 10.1158/0008-5472.CAN-20-4090
8. Stange EF, Schroeder BO. Microbiota and Mucosal Defense in IBD: An Update. *Expert Rev Gastroenterol Hepatol* (2019) 13:963–76. doi: 10.1080/17474124.2019.1671822
9. Nishida A, Inoue R, Inatomi O, Bamba S, Naito Y, Andoh A. Gut Microbiota in the Pathogenesis of Inflammatory Bowel Disease. *Clin J Gastroenterol* (2018) 11:1–10. doi: 10.1007/s12328-017-0813-5
10. Yu LX, Schwabe RF. The Gut Microbiome and Liver Cancer: Mechanisms and Clinical Translation. *Nat Rev Gastroenterol Hepatol* (2017) 14:527–39. doi: 10.1038/nrgastro.2017.72
11. Usami M, Miyoshi M, Yamashita H. Gut Microbiota and Host Metabolism in Liver Cirrhosis. *World J Gastroenterol* (2015) 21:11597–608. doi: 10.3748/wjg.v21.i41.11597
12. Doifode T, Giridharan VV, Generoso JS, Bhatti G, Collodel A, Schulz PE. The Impact of the Microbiota-Gut-Brain Axis on Alzheimer's Disease Pathophysiology. *Pharmacol Res* (2021) 164:105314. doi: 10.1016/j.phrs.2020.105314
13. Rutsch A, Kantsjö JB, Ronchi F. The Gut-Brain Axis: How Microbiota and Host Inflammasome Influence Brain Physiology and Pathology. *Front Immunol* (2020) 11:604179. doi: 10.3389/fimmu.2020.604179
14. Dzutsev A, Badger JH, Perez-Chanona E, Roy S, Salcedo R, Smith CK, et al. Microbes and Cancer. *Annu Rev Immunol* (2017) 35:199–228. doi: 10.1146/annurev-immunol-051116-052133
15. Hakuno F, Takahashi SI. IGF1 Receptor Signaling Pathways. *J Mol Endocrinol* (2018) 61:T69–86. doi: 10.1530/JME-17-0311
16. Feigerlova E, Hwa V, Derr MA, Rosenfeld RG. Current Issues on Molecular Diagnosis of GH Signaling Defects. *Endocr Dev* (2013) 24:118–27. doi: 10.1159/000342586
17. Rotwein P. Mapping the Growth Hormone–Stat5b–IGF-I Transcriptional Circuit. *Trends Endocrinol Metab* (2012) 23:186–93. doi: 10.1016/j.tem.2012.01.001
18. Kineman RD, del Rio-Moreno M, Sarmento-Cabral A. 40 YEARS of IGF1: Understanding the Tissue-Specific Roles of IGF1/IGF1R in Regulating Metabolism Using the Cre/Loxp System. *J Mol Endocrinol* (2018) 61:T187–98. doi: 10.1530/JME-18-0076
19. LeRoith D. Clinical Relevance of Systemic and Local IGF-I: Lessons From Animal Models. *Pediatr Endocrinol Rev* (2008) 5:739–43.
20. Clemmons DR. Role of IGF-Binding Proteins in Regulating IGF Responses to Changes in Metabolism. *J Mol Endocrinol* (2018) 61:T139–69. doi: 10.1530/JME-18-0016
21. Novosyadlyy R, Dargel R, Scharf JG. Expression of Insulin-Like Growth Factor-I and Insulin-Like Growth Factor Binding Proteins During Thioacetamide-Induced Liver Cirrhosis in Rats. *Growth Horm IGF Res* (2005) 15:313–23. doi: 10.1016/j.ghir.2005.06.015
22. O'Neill BT, Lauritzen HP, Hirshman MF, Smyth G, Goodyear LJ, Kahn CR. Differential Role of Insulin/IGF-1 Receptor Signaling in Muscle Growth and Glucose Homeostasis. *Cell Rep* (2015) 11:1220–35. doi: 10.1016/j.celrep.2015.04.037
23. Mavalli MD, DiGirolamo DJ, Fan Y, Riddle RC, Campbell KS, Van Groen T, et al. Distinct Growth Hormone Receptor Signaling Modes Regulate Skeletal Muscle Development and Insulin Sensitivity in Mice. *J Clin Invest* (2010) 120:4007–20. doi: 10.1172/JCI42447
24. Lindsey RC, Rundle CH, Mohan S. Role of IGF1 and EFN-EPH Signaling in Skeletal Metabolism. *J Mol Endocrinol* (2018) 61:T87–T102. doi: 10.1530/JME-17-0284
25. Xuan S, Kitamura T, Nakae J, Politi K, Kido Y, Fisher PE, et al. Defective Insulin Secretion in Pancreatic Beta Cells Lacking Type 1 IGF Receptor. *J Clin Invest* (2002) 110:1011–9. doi: 10.1172/JCI15276
26. Kulkarni RN, Holzenberger M, Shih DQ, Ozcan U, Stoffel M, Magnuson MA, et al. Beta-Cell-Specific Deletion of the Igf1 Receptor Leads to Hyperinsulinemia and Glucose Intolerance But Does Not Alter Beta-Cell Mass. *Nat Genet* (2002) 31:111–5. doi: 10.1038/ng872
27. Chowdhury S, Wang X, Srikant CB, Li Q, Fu M, Gong YJ, et al. IGF-I Stimulates CCN5/WISP2 Gene Expression in Pancreatic β-Cells, Which

Promotes Cell Proliferation and Survival Against Streptozotocin. *Endocrinology* (2014) 155:1629–42. doi: 10.1210/en.2013-1735
28. Ueki K, Okada T, Hu J, Chong WL, Assmann A, Dahlgren GM, et al. Total Insulin and IGF-I Resistance in Pancreatic Beta Cells Causes Overt Diabetes. *Nat Genet* (2006) 38:583–8. doi: 10.1038/ng1787
29. Boucher J, Softic S, El Ouaamari A, Krumpoch MT, Kleinridders A, Kulkarni RN, et al. Differential Roles of Insulin and IGF-1 Receptors in Adipose Tissue Development and Function. *Diabetes* (2016) 65:2201–13. doi: 10.2337/db16-0212
30. Spadaro O, Camell CD, Bosurgi L, Nguyen KY, Youm YH, Rothlin CV, et al. IGF1 Shapes Macrophage Activation in Response to Immunometabolic Challenge. *Cell Rep* (2017) 19:225–34. doi: 10.1016/j.celrep.2017.03.046
31. Müller K, Führer D, Mittag J, Klöting N, Blüher M, Weiss RE, et al. TSH Compensates Thyroid-Specific IGF-I Receptor Knockout and Causes Papillary Thyroid Hyperplasia. *Mol Endocrinol* (2011) 25:1867–79. doi: 10.1210/me.2011-0065
32. Neirijnck Y, Calvel P, Kilcoyne KR, Kühne F, Stévant I, Griffeth RJ, et al. Insulin and IGF1 Receptors Are Essential for the Development and Steroidogenic Function of Adult Leydig Cells. *FASEB J* (2018) 32:3321–35. doi: 10.1096/fj.201700769RR
33. Qian Q, He W, Liu D, Yin J, Ye L, Chen P, et al. M2a Macrophage can Rescue Proliferation and Gene Expression of Benign Prostate Hyperplasia Epithelial and Stroma Cells From Insulin-Like Growth Factor 1 Knockdown. *Prostate* (2021) 81:530–42. doi: 10.1002/pros.24131
34. Walenkamp MJE, Robers JML, Wit JM, Zandwijken GRJ, van Duyvenvoorde HA, Oostdijk W, et al. Phenotypic Features and Response to GH Treatment of Patients With a Molecular Defect of the IGF-1 Receptor. *J Clin Endocrinol Metab* (2019) 104:3157–71. doi: 10.1210/JC.2018-02065
35. Lewitt M, Dent M, Hall K. The Insulin-Like Growth Factor System in Obesity, Insulin Resistance and Type 2 Diabetes Mellitus. *J Clin Med* (2014) 3:1561–74. doi: 10.3390/jcm3041561
36. Suda K, Matsumoto R, Fukuoka H, Iguchi G, Hirota Y, Nishizawa H, et al. The Influence of Type 2 Diabetes on Serum GH and IGF-I Levels in Hospitalized Japanese Patients. *Growth Horm IGF Res* (2016) 29:4–10. doi: 10.1016/j.ghir.2016.03.002
37. Kanazawa I, Yamaguchi T, Sugimoto T. Effects of Intensive Glycemic Control on Serum Levels of Insulin-Like Growth Factor-I and Dehydroepiandrosterone Sulfate in Type 2 Diabetes Mellitus. *J Endocrinol Invest* (2012) 35:469–72. doi: 10.3275/8033
38. Hata S, Mori H, Yasuda T, Irie Y, Yamamoto T, Umayahara Y, et al. A Low Serum IGF-1 Is Correlated With Sarcopenia in Subjects With Type 1 Diabetes Mellitus: Findings From a *Post-Hoc* Analysis of the Idiamond Study. *Diabetes Res Clin Pract* (2021) 179:108998. doi: 10.1016/j.diabres.2021.108998
39. Kaaks R, Lukanova A. Energy Balance and Cancer: The Role of Insulin and Insulin-Like Growth Factor-I. *Proc Nutr Soc* (2001) 60:91–106. doi: 10.1079/pns200070
40. Holmes MD, Pollak MN, Hankinson SE. Lifestyle Correlates of Plasma Insulin-Like Growth Factor I and Insulin-Like Growth Factor Binding Protein 3 Concentrations. *Cancer Epidemiol Biomarkers Prev* (2002) 11:862–7.
41. Allen NE, Appleby PN, Kaaks R, Rinaldi S, Davey GK, Key TJ. Lifestyle Determinants of Serum Insulin-Like Growth-Factor-I (IGF-I), C-Peptide and Hormone Binding Protein Levels in British Women. *Cancer Causes Control* (2003) 14:65–74. doi: 10.1023/a:1022518321634
42. Calle EE, Kaaks R. Overweight, Obesity and Cancer: Epidemiological Evidence and Proposed Mechanisms. *Nat Rev Cancer* (2004) 4:579–91. doi: 10.1038/nrc1408
43. Sreenivasulu K, Nandeesha H, Dorairajan LN, Rajappa M, Vinayagam V, Cherupanakkal C. Gene Expression of Insulin Receptor, Insulin-Like Growth Factor Increases and Insulin-Like Growth Factor-Binding Protein-3 Reduces With Increase in Prostate Size in Benign Prostatic Hyperplasia. *Aging Male* (2018) 21:138–44. doi: 10.1080/13685538.2017.1401994
44. Colao A, Marzullo P, Ferone D, Spiezia S, Cerbone G, Marinò V, et al. Prostatic Hyperplasia: An Unknown Feature of Acromegaly. *J Clin Endocrinol Metab* (1998) 83:775–9. doi: 10.1210/jcem.83.3.4645
45. Qian F, Huo D. Circulating Insulin-Like Growth Factor-1 and Risk of Total and 19 Site-Specific Cancers: Cohort Study Analyses From the UK Biobank. *Cancer Epidemiol Biomarkers Prev* (2020) 29:2332–42. doi: 10.1158/1055-9965.EPI-20-0743
46. Satyamoorthy K, Li G, Vaidya B, Patel D, Herlyn M. Insulin-Like Growth Factor-1 Induces Survival and Growth of Biologically Early Melanoma Cells Through Both the Mitogen-Activated Protein Kinase and Beta-Catenin Pathways. *Cancer Res* (2001) 61:7318–24.
47. Cheung CW, Vesey DA, Nicol DL, Johnson DW. The Roles of IGF-I and IGFBP-3 in the Regulation of Proximal Tubule, and Renal Cell Carcinoma Cell Proliferation. *Kidney Int* (2004) 65:1272–9. doi: 10.1111/J.1523-1755.2004.00535.X
48. Lv J, Liu C, Chen FK, Feng ZP, Jia L, Liu PJ, et al. M2-Like Tumour-Associated Macrophage-Secreted IGF Promotes Thyroid Cancer Stemness and Metastasis by Activating the PI3K/AKT/Mtor Pathway. *Mol Med Rep* (2021) 24:604. doi: 10.3892/MMR.2021.12249
49. Rieunier G, Wu X, Macaulay VM, Lee AV, Weyer-Czernilofsky U, Bogenrieder T. Bad to the Bone: The Role of the Insulin-Like Growth Factor Axis in Osseous Metastasis. *Clin Cancer Res* (2019) 25:3479–85. doi: 10.1158/1078-0432.CCR-18-2697
50. Zhang XH, Jin X, Malladi S, Zou Y, Wen YH, Brogi E, et al. Selection of Bone Metastasis Seeds by Mesenchymal Signals in the Primary Tumor Stroma. *Cell* (2013) 154:1060–73. doi: 10.1016/j.cell.2013.07.036
51. Van Golen CM, Schwab TS, Kim B, Soules ME, Su Oh S, Fung K, et al. Insulin-Like Growth Factor-I Receptor Expression Regulates Neuroblastoma Metastasis to Bone. *Cancer Res* (2006) 66:6570–8. doi: 10.1158/0008-5472.CAN-05-1448
52. Heidegger I, Massoner P, Sampson N, Klocker H. The Insulin-Like Growth Factor (IGF) Axis as an Anticancer Target in Prostate Cancer. *Cancer Lett* (2015) 367:113–21. doi: 10.1016/j.canlet.2015.07.026
53. Ngo TH, Barnard RJ, Cohen P, Freedland S, Tran C, DeGregorio F, et al. Effect of Isocaloric Low-Fat Diet on Human LAPC-4 Prostate Cancer Xenografts in Severe Combined Immunodeficient Mice and the Insulin-Like Growth Factor Axis. *Clin Cancer Res* (2003) 9:2734–43.
54. Niu XB, Fu GB, Wang L, Ge X, Liu WT, Wen YY, et al. Insulin-Like Growth Factor-I Induces Chemoresistence to Docetaxel by Inhibiting Mir-143 in Human Prostate Cancer. *Oncotarget* (2017) 8:107157–66. doi: 10.18632/oncotarget.22362
55. Weyer-Czernilofsky U, Hofmann MH, Friedbichler K, Baumgartinger R, Adam PJ, Solca F, et al. Antitumor Activity of the IGF-1/IGF-2-Neutralizing Antibody Xentuzumab (BI 836845) in Combination With Enzalutamide in Prostate Cancer Models. *Mol Cancer Ther* (2020) 19:1059–69. doi: 10.1158/1535-7163.MCT-19-0378
56. Plymate SR, Haugk K, Coleman I, Woodke L, Vessella R, Nelson P, et al. An Antibody Targeting the Type I Insulin-Like Growth Factor Receptor Enhances the Castration-Induced Response in Androgen-Dependent Prostate Cancer. *Clin Cancer Res* (2007) 13:6429–39. doi: 10.1158/1078-0432.CCR-07-0648
57. Fan WQ, Yanase T, Morinaga H, Okabe T, Nomura M, Daitoku H, et al. Insulin-Like Growth Factor 1/Insulin Signaling Activates Androgen Signaling Through Direct Interactions of Foxo1 With Androgen Receptor. *J Biol Chem* (2007) 282:7329–38. doi: 10.1074/jbc.M610447200
58. Watts EL, Goldacre R, Key TJ, Allen NE, Travis RC, Perez-Cornago A. Hormone-Related Diseases and Prostate Cancer: An English National Record Linkage Study. *Int J cancer* (2020) 147:803–10. doi: 10.1002/ijc.32808
59. Cutting CW, Hunt C, Nisbet JA, Bland JM, Dalgleish AG, Kirby RS. Serum Insulin-Like Growth Factor-1 Is Not a Useful Marker of Prostate Cancer. *BJU Int* (1999) 83:996–9. doi: 10.1046/j.1464-410x.1999.00088.x
60. Finne P, Auvinen A, Koistinen H, Zhang WM, Määttänen L, Rannikko S, et al. Insulin-Like Growth Factor I Is Not a Useful Marker of Prostate Cancer in Men With Elevated Levels of Prostate-Specific Antigen. *J Clin Endocrinol Metab* (2000) 85:2744–7. doi: 10.1210/jcem.85.8.6725
61. Nordstrand A, Bergström SH, Thysell E, Bovinder-Ylitalo E, Lerner UH, Widmark A, et al. Inhibition of the Insulin-Like Growth Factor-1 Receptor Potentiates Acute Effects of Castration in a Rat Model for Prostate Cancer Growth in Bone. *Clin Exp Metastasis* (2017) 34:261–71. doi: 10.1007/s10585-017-9848-8
62. Fahrenholtz CD, Beltran PJ, Burnstein KL. Targeting IGF-IR With Ganitumab Inhibits Tumorigenesis and Increases Durability of Response to Androgen-Deprivation Therapy in Vcap Prostate Cancer Xenografts. *Mol Cancer Ther* (2013) 12:394–404. doi: 10.1158/1535-7163.MCT-12-0648
63. Barata P, Cooney M, Tyler A, Wright J, Dreicer R, Garcia JA. A Phase 2 Study of OSI-906 (Linsitinib, an Insulin-Like Growth Factor Receptor-1 Inhibitor) in Patients With Asymptomatic or Mildly Symptomatic (Non-Opioid

Requiring) Metastatic Castrate Resistant Prostate Cancer (CRPC). *Invest New Drugs* (2018) 36:451–7. doi: 10.1007/s10637-018-0574-0
64. Cook SI, Sellin JH. Review Article: Short Chain Fatty Acids in Health and Disease. *Aliment Pharmacol Ther* (1998) 12:499–507. doi: 10.1046/j.1365-2036.1998.00337.x
65. Takahashi D, Hoshina N, Kabumoto Y, Maeda Y, Suzuki A, Tanabe H, et al. Microbiota-Derived Butyrate Limits the Autoimmune Response by Promoting the Differentiation of Follicular Regulatory T Cells. *EBioMedicine* (2020) 58:102913. doi: 10.1016/j.ebiom.2020.102913
66. Furusawa Y, Obata Y, Fukuda S, Endo TA, Nakato G, Takahashi D, et al. Commensal Microbe-Derived Butyrate Induces the Differentiation of Colonic Regulatory T Cells. *Nature* (2013) 504:446–50. doi: 10.1038/nature12721
67. Weitkunat K, Schumann S, Nickel D, Kappo KA, Petzke KJ, Kipp AP, et al. Importance of Propionate for the Repression of Hepatic Lipogenesis and Improvement of Insulin Sensitivity in High-Fat Diet-Induced Obesity. *Mol Nutr Food Res* (2016) 60:2611–21. doi: 10.1002/mnfr.201600305
68. El Hage R, Hernandez-Sanabria E, Arroyo MC, van de Wiele T. Supplementation of a Propionate-Producing Consortium Improves Markers of Insulin Resistance in an *In Vitro* Model of Gut-Liver Axis. *Am J Physiol Endocrinol Metab* (2020) 318:E742–9. doi: 10.1152/ajpendo.00523.2019
69. Erny D, Hrabě de Angelis AL, Jaitin D, Wieghofer P, Staszewski O, David E, et al. Host Microbiota Constantly Control Maturation and Function of Microglia in the CNS. *Nat Neurosci* (2015) 18:965–77. doi: 10.1038/nn.4030
70. Silva YP, Bernardi A, Frozza RL. The Role of Short-Chain Fatty Acids From Gut Microbiota in Gut-Brain Communication. *Front Endocrinol (Lausanne)* (2020) 11:25. doi: 10.3389/fendo.2020.00025
71. Mirzaei R, Afaghi A, Babakhani S, Sohrabi MR, Hosseini-Fard SR, Babolhavaeji K, et al. Role of Microbiota-Derived Short-Chain Fatty Acids in Cancer Development and Prevention. *BioMed Pharmacother* (2021) 139:111619. doi: 10.1016/j.biopha.2021.111619
72. Wu X, Wu Y, He L, Wu L, Wang X, Liu Z. Effects of the Intestinal Microbial Metabolite Butyrate on the Development of Colorectal Cancer. *J Cancer* (2018) 9:2510–7. doi: 10.7150/jca.25324
73. Li Y, Seto E. Hdacs and HDAC Inhibitors in Cancer Development and Therapy. *Cold Spring Harb Perspect Med* (2016) 6:a026831. doi: 10.1101/cshperspect.a026831
74. Paskova L, Smesny Trtkova K, Fialova B, Benedikova A, Langova K, Kolar Z. Different Effect of Sodium Butyrate on Cancer and Normal Prostate Cells. *Toxicol In Vitro* (2013) 27:1489–95. doi: 10.1016/j.tiv.2013.03.002
75. Donohoe DR, Collins LB, Wali A, Bigler R, Sun W, Bultman SJ. The Warburg Effect Dictates the Mechanism of Butyrate-Mediated Histone Acetylation and Cell Proliferation. *Mol Cell* (2012) 48:612–26. doi: 10.1016/j.molcel.2012.08.033
76. Morrison DJ, Preston T. Formation of Short Chain Fatty Acids by the Gut Microbiota and Their Impact on Human Metabolism. *Gut Microbes* (2016) 7:189–200. doi: 10.1080/19490976.2015.1134082
77. Yan J, Herzog JW, Tsang K, Brennan CA, Bower MA, Garrett WS, et al. Gut Microbiota Induce IGF-1 and Promote Bone Formation and Growth. *Proc Natl Acad Sci USA*. (2016) 113:E7554–63. doi: 10.1073/pnas.1607235113
78. Hayashi T, Fujita K, Nojima S, Hayashi Y, Nakano K, Ishizuya Y, et al. High-Fat Diet-Induced Inflammation Accelerates Prostate Cancer Growth *via* IL6 Signaling. *Clin Cancer Res* (2018) 24:4309–18. doi: 10.1158/1078-0432.CCR-18-0106
79. Hayashi T, Fujita K, Matsushita M, Hayashi Y, Uemura M, Nonomura N. Metformin Inhibits Prostate Cancer Growth Induced by a High-Fat Diet in Pten-Deficient Model Mice. *Int J Urol* (2019) 26:307–9. doi: 10.1111/iju.13847
80. Matsushita M, Fujita K, Motooka D, Hatano K, Fukae S, Kawamura N, et al. The Gut Microbiota Associated With High-Gleason Prostate Cancer. *Cancer Sci* (2021) 112:3125–35. doi: 10.1111/cas.14998
81. Wang B, Kong Q, Li X, Zhao J, Zhang H, Chen W, et al. A High-Fat Diet Increases Gut Microbiota Biodiversity and Energy Expenditure Due to Nutrient Difference. *Nutrients* (2020) 12:1–20. doi: 10.3390/nu12103197
82. Shi H, Chang Y, Gao Y, Wang X, Chen X, Wang Y, et al. Dietary Fucoidan of Acaudina Molpadioides Alters Gut Microbiota and Mitigates Intestinal Mucosal Injury Induced by Cyclophosphamide. *Food Funct* (2017) 8:3383–93. doi: 10.1039/c7fo00932a
83. Meehan CJ, Beiko RG. A Phylogenomic View of Ecological Specialization in the Lachnospiraceae, a Family of Digestive Tract-Associated Bacteria. *Genome Biol Evol* (2014) 6:703–13. doi: 10.1093/gbe/evu050
84. Xu Y, Yu Y, Shen Y, Li Q, Lan J, Wu Y, et al. Effects of Bacillus Subtilis and Bacillus Licheniformis on Growth Performance, Immunity, Short Chain Fatty Acid Production, Antioxidant Capacity, and Cecal Microflora in Broilers. *Poult Sci* (2021) 100:101358. doi: 10.1016/j.psj.2021.101358
85. Li B, Chen H, Cao L, Hu Y, Chen D, Yin Y. Escherichia Coli Exopolysaccharides Induced by Ceftriaxone Regulated Human Gut Microbiota *In Vitro*. *Front Microbiol* (2021) 12:634204. doi: 10.3389/fmicb.2021.634204
86. Allen JM, Mailing LJ, Niemiro GM, Moore R, Cook MD, White BA, et al. Exercise Alters Gut Microbiota Composition and Function in Lean and Obese Humans. *Med Sci Sports Exerc* (2018) 50:747–57. doi: 10.1249/MSS.0000000000001495
87. Beasley JM, Gunter MJ, LaCroix AZ, Prentice RL, Neuhouser ML, Tinker LF, et al. Associations of Serum Insulin-Like Growth Factor-I and Insulin-Like Growth Factor-Binding Protein 3 Levels With Biomarker-Calibrated Protein, Dairy Product and Milk Intake in the Women's Health Initiative. *Br J Nutr* (2014) 111:847–53. doi: 10.1017/S000711451300319X
88. Harrison S, Lennon R, Holly J, Higgins JPT, Gardner M, Perks C, et al. Does Milk Intake Promote Prostate Cancer Initiation or Progression *via* Effects on Insulin-Like Growth Factors (Igfs)? A Systematic Review and Meta-Analysis. *Cancer Causes Control* (2017) 28:497–528. doi: 10.1007/S10552-017-0883-1
89. Pereira PC. Milk Nutritional Composition and Its Role in Human Health. *Nutrition* (2014) 30:619–27. doi: 10.1016/j.nut.2013.10.011
90. Downer MK, Batista JL, Mucci LA, Stampfer MJ, Epstein MM, Håkansson N, et al. Dairy Intake in Relation to Prostate Cancer Survival. *Int J cancer* (2017) 140:2060–9. doi: 10.1002/ijc.30642
91. Park Y, Leitzmann MF, Subar AF, Hollenbeck A, Schatzkin A. Dairy Food, Calcium, and Risk of Cancer in the NIH-AARP Diet and Health Study. *Arch Intern Med* (2009) 169:391–401. doi: 10.1001/archintermed.2008.578
92. Mahmud SM, Franco EL, Turner D, Platt RW, Beck P, Skarsgard D, et al. Use of Non-Steroidal Anti-Inflammatory Drugs and Prostate Cancer Risk: A Population-Based Nested Case-Control Study. *PloS One* (2011) 6:e16412. doi: 10.1371/journal.pone.0016412
93. Kimura I, Ozawa K, Inoue D, Imamura T, Kimura K, Maeda T, et al. The Gut Microbiota Suppresses Insulin-Mediated Fat Accumulation *via* the Short-Chain Fatty Acid Receptor GPR43. *Nat Commun* (2013) 4:1829. doi: 10.1038/ncomms2852
94. Kimura I, Inoue D, Maeda T, Hara T, Ichimura A, Miyauchi S, et al. Short-Chain Fatty Acids and Ketones Directly Regulate Sympathetic Nervous System *via* G Protein-Coupled Receptor 41 (GPR41). *Proc Natl Acad Sci U S A.* (2011) 108:8030–5. doi: 10.1073/pnas.1016088108
95. Pernigoni N, Zagato E, Calcinotto A, Troiani M, Mestre RP, Calì B, et al. Commensal Bacteria Promote Endocrine Resistance in Prostate Cancer Through Androgen Biosynthesis. *Science* (2021) 374:216–24. doi: 10.1126/science.abf8403
96. Liu Y, Yang C, Zhang Z, Jiang H. Gut Microbiota Dysbiosis Accelerates Prostate Cancer Progression Through Increased LPCAT1 Expression and Enhanced DNA Repair Pathways. *Front Oncol* (2021) 11:679712. doi: 10.3389/fonc.2021.679712

Conflict of Interest: The authors declare that the research was conducted in the absence of any commercial or financial relationships that could be construed as a potential conflict of interest.

frontiers in Oncology

ORIGINAL RESEARCH
published: 29 March 2022
doi: 10.3389/fonc.2022.860446

Tumor Suppressor Par-4 Regulates Complement Factor C3 and Obesity

Nathalia Araujo[1†], James Sledziona[1†], Sunil K. Noothi[2†], Ravshan Burikhanov[3†], Nikhil Hebbar[1], Saptadwipa Ganguly[1], Tripti Shrestha-Bhattarai[4], Beibei Zhu[5,6], Wendy S. Katz[6,7], Yi Zhang[8], Barry S. Taylor[4], Jinze Liu[8], Li Chen[5,9], Heidi L. Weiss[5,9], Daheng He[10], Chi Wang[9,11], Andrew J. Morris[5,9], Lisa A. Cassis[6,7], Mariana Nikolova-Karakashian[9,12], Prabhakar R. Nagareddy[13], Olle Melander[14,15], B. Mark Evers[9,16], Philip A. Kern[5,6] and Vivek M. Rangnekar[1,2,3,9]*

[1] Department of Toxicology and Cancer Biology, University of Kentucky, Lexington, KY, United States, [2] Department of Microbiology, Immunology and Molecular Genetics, University of Kentucky, Lexington, KY, United States, [3] Department of Radiation Medicine, University of Kentucky, Lexington, KY, United States, [4] Department of Epidemiology and Biostatistics, Memorial Sloan Kettering Cancer Center, New York, NY, United States, [5] Division of Internal Medicine, University of Kentucky, Lexington, KY, United States, [6] Barnstable Brown Diabetes and Obesity Center, University of Kentucky, Lexington, KY, United States, [7] Department of Pharmacology and Nutritional Sciences, University of Kentucky, Lexington, KY, United States, [8] Department of Computer Science, University of Kentucky, Lexington, KY, United States, [9] Markey Cancer Center, University of Kentucky, Lexington, KY, United States, [10] Department of Statistics, University of Kentucky, Lexington, KY, United States, [11] Department of Biostatistics, University of Kentucky, Lexington, KY, United States, [12] Department of Physiology, University of Kentucky, Lexington, KY, United States, [13] Division of Cardiac Surgery, The Ohio State University, Columbus, OH, United States, [14] Department of Clinical Sciences, Lund University, Malmö, Sweden, [15] Department of Internal Medicine, Skåne University Hospital, Malmö, Sweden, [16] Department of Surgery, University of Kentucky, Lexington, KY, United States

Prostate apoptosis response-4 (Par-4) is a tumor suppressor that induces apoptosis in cancer cells. However, the physiological function of Par-4 remains unknown. Here we show that conventional Par-4 knockout (Par-4$^{-/-}$) mice and adipocyte-specific Par-4 knockout (AKO) mice, but not hepatocyte-specific Par-4 knockout mice, are obese with standard chow diet. Par-4$^{-/-}$ and AKO mice exhibit increased absorption and storage of fat in adipocytes. Mechanistically, Par-4 loss is associated with *mdm2* downregulation and activation of p53. We identified complement factor *c3* as a p53-regulated gene linked to fat storage in adipocytes. *Par-4* re-expression in adipocytes or *c3* deletion reversed the obese mouse phenotype. Moreover, obese human subjects showed lower expression of Par-4 relative to lean subjects, and in longitudinal studies, low baseline Par-4 levels denoted an increased risk of developing obesity later in life. These findings indicate that Par-4 suppresses p53 and its target *c3* to regulate obesity.

Keywords: hypertrophic obesity, adipocyte tissue storage, fat absorption, acylation stimulating protein, C3, Par-4

OPEN ACCESS

Edited by:
Che-Pei Kung, Washington University in St. Louis, United States

Reviewed by:
Philipp E. Scherer, University of Texas Southwestern Medical Center, United States
Andreas Prokesch, Medical University of Graz, Austria
Isabel Reinisch, Medical University of Graz, in collaboration with reviewer AP

***Correspondence:**
Vivek M. Rangnekar
vmrang01@uky.edu

†These authors have contributed equally to this work and share first authorship

Specialty section:
This article was submitted to Cancer Metabolism, a section of the journal Frontiers in Oncology

Received: *23 January 2022*
Accepted: *28 February 2022*
Published: *29 March 2022*

Citation:
Araujo N, Sledziona J, Noothi SK, Burikhanov R, Hebbar N, Ganguly S, Shrestha-Bhattarai T, Zhu B, Katz WS, Zhang Y, Taylor BS, Liu J, Chen L, Weiss HL, He D, Wang C, Morris AJ, Cassis LA, Nikolova-Karakashian M, Nagareddy PR, Melander O, Evers BM, Kern PA and Rangnekar VM (2022) Tumor Suppressor Par-4 Regulates Complement Factor C3 and Obesity. Front. Oncol. 12:860446. doi: 10.3389/fonc.2022.860446

INTRODUCTION

Prostate apoptosis response-4 (Par-4, also known as PAWR) is a tumor suppressor that is ubiquitously expressed in various cell types and vertebrate tissues (1). Loss of Par-4 expression by diverse mechanisms, including methylation-dependent downregulation of the Par-4 promoter, inactivation of Par-4 protein by Akt-mediated phosphorylation, or spontaneous mutation, has been associated with diverse human cancers (2–5). Moreover, Par-4 loss in tumors is associated with increased resistance to treatment and decreased patient survival (6–8). Consistently, genetic knockout of *Par-4* in mice results in spontaneous tumors, as well as increased susceptibility to

chemically- or hormone-inducible tumors in multiple tissues (9). In addition, overexpression of Par-4 induces apoptosis in cancer cell lines but not normal cells, and Par-4 transgenic mice exhibit a normal life span and cancer-free survival (10).

Par-4 is localized in multiple intracellular compartments, such as the nucleus, endoplasmic reticulum and the cytoplasm (11). Additionally, Par-4 protein is secreted by cells and can be detected in the conditioned medium of cell cultures and in mouse and human plasma (12, 13). Secreted Par-4 binds to GRP78 expressed on the surface of cancer cells and induces apoptosis (13). Par-4 is secreted by normal cells *via* the classical endoplasmic reticulum (ER)-Golgi secretory pathway, and extracellular Par-4 binds to GRP78 on the cancer cell surface to trigger apoptosis by activation of the FADD-caspase-8-caspase-3 pathway (13). Most normal cells, however, lack cell surface GRP78 and are resistant to apoptosis by secreted Par-4 (12, 13).

The key functional domains of the Par-4 protein are conserved across human, mouse and rat species and consist of a nuclear localization sequence (NLS2), a nuclear export sequence and a leucine zipper sequence at the carboxyl-terminus (5). The NLS2 domain of Par-4 permits entry of intracellular Par-4 into the nucleus (11, 14). Nuclear Par-4 functions as a transcriptional corepressor of the pro-survival gene *Bcl2* (11). However, the physiological significance of the transcriptional regulatory function of Par-4 is not well understood. As previous studies have reported crosstalk between the tumor suppressors Par-4 and p53 in secretion of Par-4 from normal cells (12), and as p53 plays diverse roles in normal tissues (15–18), we sought to determine the physiological role of Par-4 in normal tissues using an unbiased approach by generating several Par-4 knockout mouse models. Our studies indicate that Par-4 whole-body knockout mice, as well as adipocyte-specific Par-4 knockout mice develop obesity on chow diet. As Par-4 is a tumor suppressor and as obesity is linked with an increased risk of many cancers (19–23), we interrogated the obese phenotype associated with Par-4 loss in greater depth. We present evidence that Par-4 loss in adipocytes results in obesity that is associated with increased absorption of dietary fat into circulation and its storage in adipocytes to produce hypertrophic obesity in mice. The relevance of these murine results to human obesity was demonstrated in our cohort study which indicated that baseline levels of Par-4 are associated with obesity risk in lean individuals, and that Par-4 levels are lower in obese individuals relative to lean individuals. Our findings suggest an unexpected role for adipocytes in enhancing the expression of p53 and complement factor C3/acyl stimulating protein (ASP) following loss of Par-4 leading to obesity.

MATERIALS AND METHODS

Animals

Par-4 floxed mice (Par-$4^{fl/fl}$) were generated on a C57BL/6 background by Taconic Biosciences following the strategy described on **Figure S1A**. Par-$4^{fl/fl}$ mice were crossed with Rosa26-Cre (from Taconic Biosciences) to generate Par-4 whole-body knockout (Par-$4^{-/-}$) mice. Adipocyte-specific (AKO) and hepatocyte-specific Par-4 knockout (HKO) were generated by crossing Par-$4^{fl/fl}$ mice with adiponectin-promoter-Cre mice and with albumin-promoter-Cre, respectively (in C57BL/6 background from Jackson Laboratory). Par-4/C3 double-knockout mice were generated by crossing Par-$4^{-/-}$ with C3 whole-body knockout mouse (in C57BL/6 background from Jackson Laboratory). Par-$4Ki^{tg/tg}$ mice with human Par-4 containing a Stop codon inserted in the Rosa26 locus were generated by Biocytogen LLC (Worcester, MA) using the targeting strategy described in **Figure S8A**. When Par-$4Ki^{tg/tg}$ mice were crossed with AKO mice, which contained Adipoq-Cre for adipocyte-specific expression of Cre, the Stop sequence in Par-$4Ki^{tg/tg}$ mice was removed, and expression of human Par-4 was driven in mature adipocytes.

For each mouse strain, F1 heterozygotes were crossed to each other to generate either homozygous or heterozygous offspring for the gene of interest. Both homozygous and heterozygous mice were crossed to each other to generate homozygous mice. All mice were subjected to genotyping that was performed on DNA prepared from tail snips digested with proteinase K (Sigma-Aldrich, catalog number P2308) using primer sets indicated in **Figures S1B, S3A, S6A, S8B** for Par-$4^{-/-}$, $C3^{-/-}$, Adiponectin-Cre, and primer sets described by Jackson Laboratory. Mice were fed standard chow diet that consists of 18% protein, 60% carbohydrates and 12% fat (Teklad, Envigo). Mouse phenotypes described were noted in each generation for over multiple generations.

Mouse body weight was measured weekly, and body composition was determined by Echo-MRI (EchoMRI-100, Echo Medical System, Houston, TX). The experiments performed on these mice were approved by the Institutional Animal Care and Use Committee of the University of Kentucky.

Human Specimens

Human adipose tissue samples were obtained from biopsies of normal weight and obese subjects who were recruited as part of previous studies on the effects of exercise (24) or fish oils (25). All biopsies were performed before any interventions and all participants underwent an incisional abdominal adipose biopsy, under local anesthesia, for removal of adipose tissue. The subjects had no history of coronary disease, inflammatory disease, the chronic use of any anti-inflammatory medication or other medication likely to change adipocyte metabolism. The subjects were categorized as either lean (BMI < 25 kg/m^2) or obese (BMI > 30 kg/m^2). Plasma samples from lean and obese adults of both genders were provided by the Center for Clinical and Translational Sciences Biospecimen Core and the University of Kentucky Markey Cancer Center Biospecimen Procurement and Translational Pathology Shared Resource Facility. All patient information was de-identified and adhering to HIPAA guidelines. Additional plasma samples were obtained from The Malmö Diet and Cancer study ("Minisymposium: The Malmö Diet and Cancer Study. Design, Biological Bank and Biomarker Programme. 23 October 1991, Malmo, Sweden." 1993). Fasted EDTA plasma samples at the baseline examination were available for Par-4 analyses by western blot analysis. Written informed consent was given by all participants and the study was approved by the Ethical Committee at Lund University, Lund, Sweden. All work was approved by the University of Kentucky Institutional Review Board.

Cell Culture, Constructs, and Antibodies

Wild-type, Par-4$^{-/-}$ and p53 MEFs (26) were maintained in Dulbecco's Modification of Eagle's Medium (DMEM) (Sigma #D6429) supplemented with 15% fetal bovine serum (FBS) (DMEM+15% FBS) for the first three passages and supplemented with 10% FBS onward.

The C3-luc construct was purchased from Addgene (#11358) and has been previously described (27). The p53 adenoviral constructs were obtained from Wafik el-Deiry (Brown University, Providence, RI) and have been previously described (28). Green Fluorescent Protein (GFP) adenovirus was obtained from Albert Baldwin (University of North Carolina, Chapel Hill, NC) and has also been described (14).

Antibodies for Par-4 N-terminal (R-334, sc-1807), GAPDH (G-9, sc-365062), leptin (sc-842, A-20), adiponectin (sc-17044R, N-20) and p21 (F-5, sc-6246) were from Santa Cruz Biotechnology. Two other Par-4 antibodies were used: a rabbit polyclonal (S4554-1) and a mouse monoclonal (TIAI2A9G9), both produced by Proteintech. The β-actin antibody (AC-74, A5316) was from Sigma-Aldrich. The C3a/ASP antibody (ab48581) was from Abcam; Apo48 (K23300R) was from Meridian Life Science; the LPL antibody (AF7197) was from R&D Systems; and the p53 antibody (1C12, 2524S) was from Cell Signaling Technologies. Mdm2 antibody was from Santa Cruz Biotechnology (sc-965). Secondary antibodies, anti-mouse-HRP (GENA931) and anti-rabbit-HRP (GENA934), were from Sigma-Aldrich; anti-chicken-HRP (A16054) was from Thermo Fisher Scientific; and anti-goat-HRP (HAF109) was from R&D Systems.

Luciferase Reporter Assays

Luciferase reporter assays were performed as described (12) using a Steady Lite plus reporter gene assay kit (#6066751 Perkin Elmer, Waltham, MA). Briefly, cells were co-transfected with luc reporter constructs, β-gal and test driver constructs in a 96-well plate using Lipofectamine (#18324012) and Plus reagent (#11514015) from Invitrogen. At 24 h post transfection, cell lysates were collected in appropriate lysis buffer (Radio Immuno Precipitation Assay) with protease inhibitors, combined with Steady Lite reagent and analyzed using a Perkin Elmer TopCount plate reader. The signal was normalized to β-gal expression by addition of ortho-Nitrophenyl-β-galactoside substrate and analysis at 430 nm.

Lipid Uptake in Cell Culture

Caco-2 cells (25,000 cells/300μL medium) in chamber slides were grown overnight and then treated with 50 μL of olive oil and mouse plasma (10% final concentration) for 24 h. The cells were washed three times with PBS and fixed with 10% buffered paraformaldehyde for 30 min. Slides were rinsed three times with PBS and once with sterile water. The cells were then incubated with 60% isopropanol for 5 min, the isopropanol was discarded, and the cells were then incubated with working solution of Oil Red O (ORO) for 5 min. Stock solution of ORO (Sigma) was prepared using 300 mg ORO in 100 mL of isopropanol (99%). Working solution of ORO was then prepared using 3 parts of ORO stock solution diluted in 2 parts double distilled water. After preparation, the working solution was filtrated. After ORO staining, the cells were washed with double distilled water and slides were mounted using Vectashield mounting media (Vector Labs). Pictures were taken using the NIS-Elements imaging platform at 20X magnification. For the quantitative study after ORO staining as mentioned above, cells were washed with double distilled water, the cells were dried and Oil Red O stain were extracted with 100% isopropanol for 5 min, with gentle rocking. Absorbance was read at 492 nm using Synergy HTX plate reader.

Knockdown Assays

Wild-type MEFs were transfected 24 h after seeding, with either control siRNA (Dharmacon, D-001830-10-15), siPar-4 #1 (Dharmacon, J-063180-5) or siPar-4 #2 (Dhamarcon, J-063180-6) as previously described (13). Whole-cell lysates were collected 48h after transfection for protein and RNA extraction. RNA was subjected to RT-qPCR for the detection of complement C3 and protein lysates were subjected to Western Blot for detection of p53, mdm2 and Par-4.

Next-Generation Sequencing and Data Analysis

Total RNA was extracted from visceral adipose tissue from three Par-4$^{+/+}$, three Par-4$^{-/-}$ and three AKO male mice that were 11-weeks old using the RNeasy lipid tissue mini kit (Qiagen, catalog number 74804). RNA-Seq libraries were prepared using TruSeq Stranded Total RNA Sample Prep Kit with Ribo-Zero ribosomal RNA depletion (Illumina). The manufacturer's protocols were used to sequence ribosomal RNA-depleted libraries at 2×100-bp paired-end reads on an Illumina HiSeq 2500 in high-output mode, to an average depth of 40×10^6 paired-end reads per sample.

For mapping, following data quality assessments, reads derived from residual rRNA were removed by aligning [Bowtie2 v2.1.0 (99)] against ribosomal RNA references derived from GENCODE/Ensembl v74 annotations. The RNA-Seq datasets were mapped to the target genome using STAR, which maps the reads genomically and resolves reads across splice junctions. We used the two-pass mapping method in which the reads are mapped twice. The first mapping pass used a list of known annotated junctions from Ensemble. Novel junctions found in the first pass were then added to the known junctions and a second mapping pass was done. After mapping we computed the expression count matrix from the mapped reads using HTSeq. The raw count matrix generated by HTSeq was then processed by normalizing the raw gene count based on the total reads for each sample, and the average gene count for each group was calculated for identifying up-regulated/down-regulated genes. Differentially expressed genes were identified at a threshold of log2 fold change is greater than 0.5.

Real-Time Quantitative PCR Analyses

Total RNA from MEFs was prepared using the RNeasy mini kit as described in Next-Generation Sequencing and Data Analysis. A reverse transcription polymerase chain reaction (RT-PCR) was performed using the cDNA synthesis kit purchased from BioRad (#1708891, Hercules, CA). Quantitative RT-PCR was conducted

using the SsoAdvanced Universal SYBR Green Supermix (#1725271) as the detection reagent on the BioRad CFX96 RT-PCR system according to manufacturer's instructions. Data were analyzed using the ΔΔCt methods by normalized to the internal control of 18S RNA. Primers were synthesized by Integrated DNA Technologies (IDT, Caralville, IA) and their sequences are listed below (**Table 1**). A melting curve analysis of all qPCR products was conducted to confirm a single DNA duplex.

Western Blot Analyses

Tissues were lysed in RIPA buffer plus protease inhibitor using a tissue grinder (Geno/Grinder® 2010, Spex Sample Prep) for 30 sec at 1450 rpm. The lysates were centrifuged at 14,000 rpm for 10 min at 4°C, diluted to a concentration of 2 mg/mL using Laemmli buffer and boiled for 5 min. Proteins were resolved using SDS-PAGE, transferred to PVDF membranes and subjected to Western blot analysis. Western blots were imaged using the UVP ChemiDoc-It® 810 Imager and quantified using the UVP Vision Works software.

Chromatin Immunoprecipitation Sequencing (ChIP-Seq)

ChIP was performed utilizing a ChIP-IT High Sensitivity kit (Active Motif; Carlsbad, CA) according to the manufacturer's instructions. Briefly, 3T3-L1 cultured cells (~80% confluency) were fixed in a formaldehyde-containing buffer that would also fix any DNA-binding protein complexes to the chromatin. These fixed cells were then lysed by repeated snap-freezing cycles and the chromatin sheared *via* sonication using a Bioruptor Pico device (Diagenode) until the resulting chromatin fragment size was approximately 400-500 bp. Aliquots of recovered sonicated chromatin (15-30 μg) were incubated with 4 μg of Par-4 antibody overnight at 4°C. The antibody-bound chromatin was pulled-down using G-protein agarose beads, the DNA was eluted and subjected to qPCR using the proprietary ChIP-verified negative and positive control primer sets obtained from Active Motif. Remaining DNA was subjected to ChIP-Seq at the University of Kentucky Markey Cancer Center Oncogenomics Shared Resource Facility. Library preparation was performed using the MicroPlex Library Preparation Ki v2 (Diagenode) according to manufacturer's instructions. Libraries were sequenced on an Illumina HiSeq 2500 using rapid mode run with 50-bp single-reads.

For data analysis, Bowtie2 was used to map the reads. MACS2 was used for peak assignment and peak annotation was done using HOMER.

Antibody Neutralization

To demonstrate specificity of Par-4 antibody, 2 ng of Par-4 mouse monoclonal antibody (Proteintech #TIAI2A9G9) was preincubated with either 4 ng His-Par-4 or 4 ng thioredoxin (TRX) control protein in 10 mL of nonfat dry milk for 30 minutes. Plasma of lean individuals who stayed lean (LL) or obese individuals who stayed obese (OO) individuals was subjected to SDS-PAGE, transferred to PVDF membrane and probed with Par-4 mouse monoclonal antibody + His-Par-4, Par-4 mouse monoclonal antibody + TRX control or anti-mouse secondary antibody.

Glucose Tolerance and Insulin Test

Oral glucose tolerance test was conducted on mice fasted for 6 h before the test. An oral gavage of glucose (25%, dissolved in saline) was administered to mice (at 2 g/kg body weight) and blood glucose was measured at 0 min (before gavage), 15 min, 30 min, 60 min and 120 min post gavage using glucose test strips and TRUE result glucometer (Trividia Health; Ft. Lauderdale, FL). Insulin levels in plasma were determined by using the ultrasensitive ELISA kit (Alpco; Salem, NH) according to manufacturer's instructions. ELISA plate readings of OD450 nm were obtained using a Spectramax M2 plate reader, running Softmax Pro 5.4.3 and standardized to a 5-parameter logistic curve.

Studies on Lipid Uptake in Enterocytes and TG Absorption in Blood

Olive oil administration and Oil Red O (ORO) analysis was performed as previously described (29). Briefly, mice were fasted overnight, fed commercial olive oil (17 μL/g body weight) by oral gavage and euthanized either at 0 min (before gavage), or 30 min, 60 min and 120 min after gavage. The intestine was resected and washed with cold saline. The proximal segment was processed for frozen sectioning and ORO staining. ORO staining was quantified as follows: five representative regions of villi were selected from each animal for analysis of intracellular ORO staining using Halo software's (Indica Labs) Multiplex IHC algorithm v1.2. Blood was collected in sodium citrate *via* cardiac puncture at the same time

TABLE 1 | Primers used in RT-qPCR reactions.

Gene	Forward Primer (5'-3')	Reverse Primer (5'-3')
Mouse Par-4	GCAGATCGAGAAGAGGAAGC	GTGTTTTGCTGGGTGATGG
Human Par-4	CTGCCGCAGAGTGCTTAGAT	TGCATCTTCTGCTTTCCGCT
Mouse c3	ATGCACCCGGTTCTATCATC	CCGGACATTCAGGTTGATCT
Mouse c3	AGAGGCAAGTGCTGACCAGT	CGTACTTGTGCCCCTCCTTA
Mouse factor B	ACTCGAACCTGCAGATCCAC	CCCCATTTTCAAAGTCCTG
Mouse adipsin	AAGTGAACGGCACACACG	CACCTGCACAGAGTCGTCA
Mouse p53	CCTCTGAGCCAGGAGACATT	CTTCACTTGGGCCTTCAAAA
Mouse mdm2	AGCGCAAAACGACACTTACA	ACACAATGTGCTGCTGCTTC
Human 18S	GTAACCCGTTGAACCCCATT	CCATCCAATCGGTAGTAGCG
Mouse 18S	CGCCGCTAGAGGTGAAATTCT	CGAACCTCCGACTTTCGTTCT

points and centrifuged at 10,000 rpm for 10 min and triglyceride levels were measured using a commercial kit purchased from Wako Diagnostics according to manufacturer instructions (# 992-02892 and #998-02992, Mountain View, CA). Whenever tyloxapol (Sigma Aldrich, T0307) was used to inhibit lipases, mice were fasted overnight and then injected i.p. with 15% w/v tyloxapol in saline at 500 mg/kg mouse body weight, 30 min prior to olive oil gavage. Blood was collected *via* tail-snip in sodium citrate at -0.5 h (before tyloxapol injection), 0 h (before olive oil dose), 0.5 h, 1 h, 2 h, 3 h and 4 h. Plasma was centrifuged at 10,000 rpm for 10 min and triglycerides were quantified as described above. Plasma was also subjected to Western blot analysis for ApoB48 to determine chylomicron secretion.

Behavioral and Metabolic Studies

The TSE Labmaster indirect calorimetry system (TSE-systems Inc., Chesterfield, MO) was used to quantify energy intake and locomotor activity of mice housed in metabolic cages. Whole-body composition parameters, total body fat, lean body mass, body fluids and total body water were measured using an EchoMRI-100 Body Composition Analyzer unit (EchoMRI, Houston, TX). The metabolic cages and Echo-MRI equipment are located at the University of Kentucky Center for Research in Obesity and Cardiovascular Disease.

Histologic Examination

Samples of mouse visceral adipose tissue or liver were collected and immediately fixed using 4% neutral buffered formalin for 3 days. Tissues were dehydrated and embedded in paraffin. A tissue sections were cut at 4 μm and hematoxylin and eosin staining or Par-4 immunocytochemical analysis was performed by Dana Napier in the University of Kentucky Markey Cancer Center's Biospecimen Procurement and Translational Pathology Shared Resource Facility. The adipocyte size was quantified as follows. The tissue section was viewed at 20x magnification. Three slides from each group were included in quantification and five fields were randomly selected on each slide. For each field, 10-15 adipocytes were randomly selected and quantified using the NIS-Elements imaging platform purchased from Nikon Instruments Inc. (Melville, NY). For F4/80 staining, primary antibody from Abcam (ab100790) was used at 1:100 overnight at 4°C. Sides were imaged using NIS-Elements imaging platform and quantification of crown-like structures (CLS) was done as the ratio of CLS per total number of adipocytes in the field (10x magnification). For the frozen section and ORO staining, liver samples were immediately frozen using liquid nitrogen and stored at −80°C until use; intestine samples were fixed in 4% neutral buffered formalin for 48 h and transferred to 50% sucrose solution before freezing. Liver and intestine sections were cut at 8 μm using a Cryostat. ORO staining was performed using reagents purchased from Electron Microscopy Sciences (Hatfield, PA).

Statistical Analysis

All experiments were performed independently at least three different times to verify the reproducibility of the findings. The data are expressed as mean ± SEM. Statistical analyses were carried out with GraphPad Prism, Microsoft Excel software or R software. P-values for comparing experimental groups were calculated using either the Student's *t*-test with Bonferroni correction applied when appropriate or the ANOVA with Tukey's HSD tests. The logistic regression model was used to examine the effect of Par-4 on the likelihood of being obesity-resistant adjusting for age, sex, physical activity, and energy intake.

RESULTS

Par-4 Knockout Mice Exhibit Increased Fat Accumulation

To determine the biological function of Par-4, we generated C57BL/6 Par-4 whole-body knockout (Par-$4^{-/-}$) mice. Loss of Par-4 in these mice was confirmed by genotyping and western blot analyses (**Figures S1A–C**). Both male and female Par-$4^{-/-}$ mice showed weight gain on normal chow diet beginning at 3-4 months of age when compared to age and gender-matched Par-$4^{+/+}$ controls (**Figure 1A**).

Visual observation indicated subcutaneous and visceral fat accumulation in Par-$4^{-/-}$ mice compared to Par-$4^{+/+}$ mice. Echo-MRI analyses further verified quantitative increase in total fat in the Par-$4^{-/-}$ mice (**Figure 1B**). Examination of the adipose tissues indicated adipocyte hypertrophy in Par-$4^{-/-}$ mice starting after 3 months of age (**Figure 1C**). Together, these findings indicated that Par-4 loss was associated with weight gain, hypertrophic adipocytes, and fat mass accumulation in adult mice after 3 months of age on standard chow diet.

As obesity is often associated with hepatic steatosis, we examined the liver from Par-$4^{-/-}$ mice at various age groups. Par-$4^{-/-}$ mice did not exhibit any hepatic changes at 3 months of age, but beginning at about 6 months, the livers from Par-$4^{-/-}$ mice had significantly larger weights and showed increased steatosis relative to the livers from Par-$4^{+/+}$ mice (**Figure S1D**). As obesity is a risk factor for metabolic complications, such as type 2 diabetes (30, 31), we sought to assess glucose homeostasis before and after the onset of obesity. Oral glucose tolerance tests indicated that, at 3 months, glucose and insulin levels of Par-4 knockout mice were comparable to Par-$4^{+/+}$ mice (**Figures S1E, F**). However, at 6 months, although glucose levels were controlled in Par-$4^{-/-}$ mice, insulin levels were significantly higher in Par-$4^{-/-}$ mice when compared to Par-$4^{+/+}$ control mice (**Figures S1E, F**). These data suggest that more insulin is required to maintain normal glucose excursions in the Par-$4^{-/-}$ mice after glucose challenge, suggesting insulin resistance after the mice became obese. Unlike the Par-$4^{-/-}$ mice, the control mice (i.e., Par-$4^{+/+}$ for wild-type C57BL6 mice, Par-$4^{fl/fl}$, Par-$4^{kitg/tg}$ and Par-$4^{fl/fl}$ Par-4Ki$^{tg/tg}$) did not show significant differences in body weight after 4 months (**Figure S1G**, and also see **Figure S8E**). Par-4 heterozygous knockout mice showed a trend toward obesity, but the differences were not statistically significant (**Figure S1H**). Moreover, steady-state plasma levels of triglycerides (TGs) were lower in Par-4 homozygous knockout mice relative to Par-$4^{+/+}$ mice (**Figure S1I**), consistent with increased storage of lipids in their adipocytes

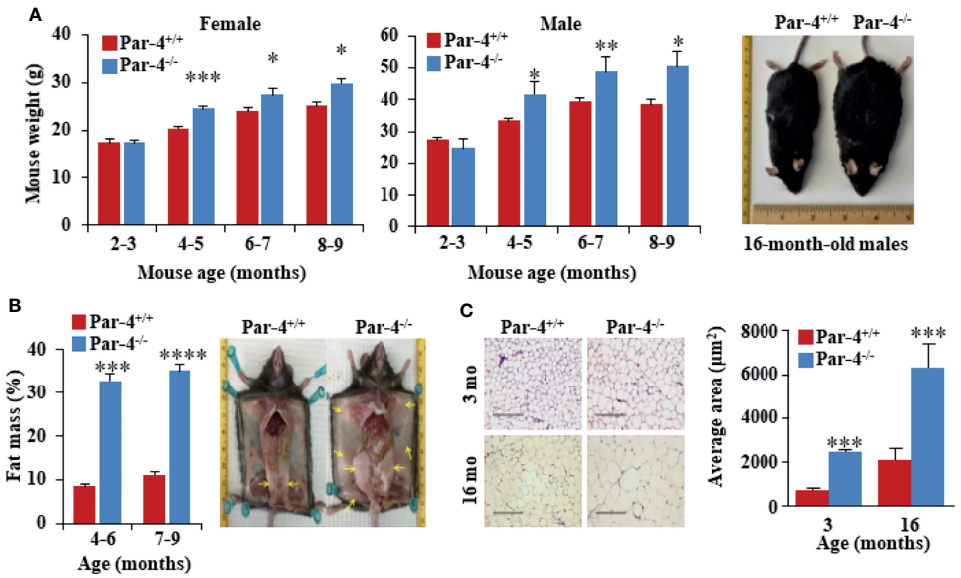

FIGURE 1 | Par-4$^{-/-}$ mice show increased fat mass and adipocyte hypertrophy. **(A)** Age- and sex-matched Par-4$^{-/-}$ mice are significantly heavier than Par-4$^{+/+}$ counterparts. Weight gain in female (n=8-13) and male mice (n=8) was determined over the indicated observation period; representative images of 16-month-old male mice are shown. **(B)** Par-4$^{-/-}$ mice show increased fat mass. Echo-MRI analyses were carried out on 4-6-month-old (n=7-10) and 7-9-month-old mice male (n=14). Subcutaneous and abdominal fat (yellow arrows) in a pair of 16-month-old male mice are shown. **(C)** Hypertrophy of adipocytes in Par-4$^{-/-}$ mice. Visceral adipose tissue from 3- or 16-month-old male mice was subjected to H&E staining and cell size was quantified (n=8 mice). Mean ± SEM, $^{*}P < 0.05$, $^{**}P < 0.01$, $^{***}P < 0.001$, $^{****}P < 0.0001$ by the Student's *t*-test or with Bonferroni method adjustment for multiple comparisons. Also see **Figure S1**.

resulting in increased fat mass. Together, these findings suggest that loss of Par-4 leads to fat accumulation, adipocyte hypertrophy, and obesity that is secondarily associated with hepatic steatosis and insulin resistance.

Par-4 Expression Is Lower in Obese Humans

As Par-4 loss in mice resulted in obesity, we determined the levels of Par-4 in visceral adipose tissues from obese (Body Mass Index [BMI]>30 kg/m^2) and lean (BMI<25 kg/m^2) individuals in Kentucky. Western blot analysis of adipose tissues and plasma levels of Par-4 indicated that obese human subjects exhibited lower tissue levels, as well as circulating plasma levels of Par-4 relative to lean human subjects (**Figure 2A**). Moreover, quantitative Polymerase Chain Reaction (qPCR) indicated that adipose tissues from obese individuals exhibited lower levels of Par-4 RNA relative to adipose tissues from non-obese individuals in Kentucky (**Figure 2B**), implying Par-4 regulation at the level of gene expression in obese individuals. These findings indicate that lower baseline levels of Par-4 are associated with obesity in human subjects.

These findings on lower Par-4 expression in obese individuals relative to lean individuals prompted us to assess the possible role of Par-4 in development of obesity in humans. Fasting levels of Par-4 in the plasma collected at baseline were analyzed in middle-aged subjects of the Malmö Diet and Cancer Study Cardiovascular Cohort (MDC-CC), a prospective population-based cohort study in Sweden with baseline exam in 1991-1994 and re-examination after an average follow-up time of 16.5 ± 1.5 years ("Minisymposium: The Malmö Diet and Cancer Study. Design, Biological Bank and Biomarker Programme. 23 October 1991, Malmo, Sweden." 1993; 29, 32). Subjects who were lean at baseline (BMI<25 kg/m^2) and developed obesity during follow-up (LO) had significantly lower baseline Par-4 protein levels than lean subjects who remained lean (LL) (**Figure 2C**). Lean subjects who remained lean during the follow-up time (LL) showed significantly higher baseline plasma levels of Par-4 compared to individuals who were obese and remained obese (OO) during the same study period (**Figure 2C**). The base population, as well as the methods of tissue collection, processing and storage was exactly the same for the cohort study participants in Sweden presented in **Figure 2C**. We further examined the association between baseline Par-4 levels and development of obesity among all lean individuals at baseline adjusting for age, sex, physical activity and energy intake. We dichotomized baseline Par-4 based on the median (Par-4-low = Par-4 < median; Par-4-high = Par-4 ≥ median) calculated from all lean individuals at baseline to evaluate the ability of Par-4 index to predict obesity. After adjusting for age, sex, physical activity and energy intake, the likelihood of being obesity-resistant was significantly higher for Par-4-high group compared to Par-4-low group (P = 0.031, odds ratio = 5.25, and 95% confidence interval = 1.16 to 23.73 based on a logistic regression model). Collectively, these studies indicate that lower Par-4 in human subjects is associated with an obese phenotype and the development of obesity.

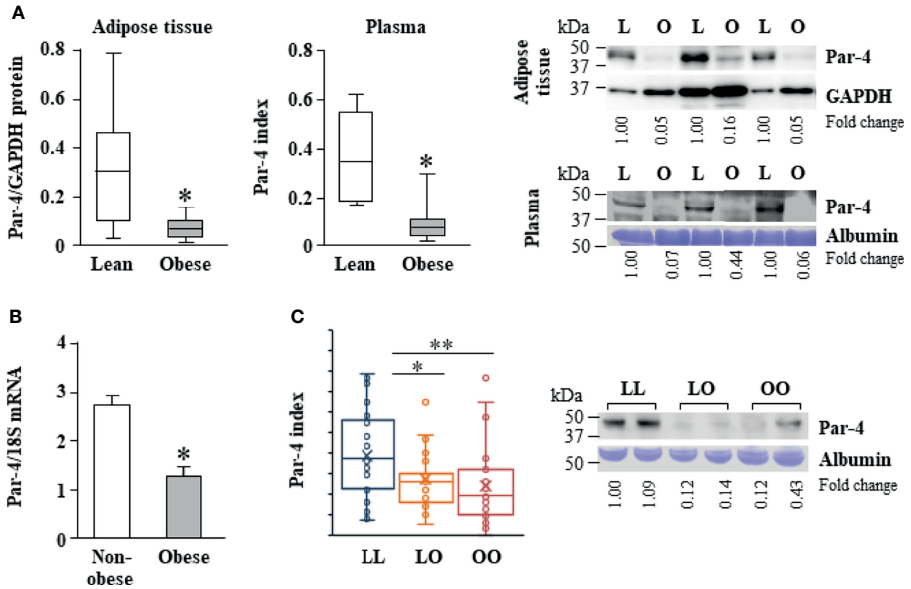

FIGURE 2 | Reduced Par-4 expression in obese humans. **(A)** Reduced Par-4 protein levels in the adipose tissue and plasma of obese individuals. Abdominal adipose tissue protein extracts or plasma from lean and obese age-matched males (n=10) was subjected to western blot analysis for Par-4. The Par-4 levels in adipose tissue were normalized to GAPDH levels. Par-4 levels in the plasma were normalized to albumin levels in Coomassie blue gels. Par-4 index was calculated as a ratio of Par-4 to albumin in each sample. Box and whiskers plots for Par-4 in lean or obese subjects and western blots representative of lower expression of Par-4 in obese (O) versus lean (L) individuals are shown. **(B)** Reduced Par-4 mRNA levels in adipose tissue of obese individuals. Abdominal adipose tissue from obese and age- and gender-matched non-obese human subjects (n=10 in each group) was subjected to qPCR analysis for Par-4 and 18S rRNA. Par-4 levels were normalized to 18S rRNA levels. **(C)** Reduced Par-4 protein levels in the plasma of lean individuals that became obese after 16.5 ± 1.5 years follow-up. Plasma from lean individuals that remained lean (LL, n=37), lean individuals that became obese (LO, n=31) and obese individuals that remained obese (OO, n=34) was subjected to western blot analysis for Par-4. Par-4 levels in the plasma were normalized to albumin levels in Coomassie blue gels (Par-4 index). Box and whiskers plots showing Par-4 and western blots representative of Par-4 levels in LL, LO and OO individuals are shown. *$P < 0.05$, **$P < 0.01$ by the Student's *t*-test with Bonferroni method for multiple comparisons adjustment. Also see **Figures S2, S10**, and **Table S1** for additional information on study participants.

Par-4 Knockout in Adipocytes, but Not in Hepatocytes, Produces Obese Mice

Given the importance of the liver and adipose tissue in lipid synthesis and storage, respectively, we sought to determine whether Par-4 loss in these tissues contributed to the obese phenotype noted in whole-body Par-4 knockout mice. We therefore generated Par-4 hepatocyte knockout (HKO) and Par-4 adipocyte knockout (AKO) mice (**Figures S3A, B**). Similar to our findings in Par-$4^{-/-}$ mice, AKO mice showed weight gain on a chow diet relative to Par-$4^{+/+}$ mice, beginning at 3-4 months after birth (**Figure 3A**), and Echo-MRI analyses indicated increased fat accumulation in AKO mice (**Figure 3B**). Moreover, adipocytes from AKO mice were significantly larger than adipocytes from control mice beginning at 3 months (**Figure 3C**). On the other hand, HKO mice did not show weight gain or fat accumulation when compared to Par-$4^{+/+}$ mice (**Figures S3C, D**). These findings indicate that Par-4 loss in adipocytes but not in the hepatocytes is sufficient to produce hypertrophic obesity in mice.

Next, we performed glucose tolerance tests to assess glucose homeostasis before and after onset of obesity. Glucose and insulin levels were similar in 3-month-old AKO and Par-$4^{+/+}$ mice but were remarkably elevated in the AKO mice at 6 months (**Figures S3E, F**). Similar to the findings in Par-$4^{-/-}$ mice, steady-state levels of TGs were lower in AKO mice relative to Par-$4^{+/+}$ mice (**Figure S3G**). These data are indicative of worse glucose tolerance and insulin resistance that occur after the onset of obesity in AKO mice.

AKO Mice Show Increased Intestinal Triglyceride Absorption

To determine the metabolic and behavioral features associated with the loss of Par-4 in both whole-body and adipocyte-specific knockout mice, we placed Par-$4^{-/-}$, AKO and Par-$4^{+/+}$ mice on a standard chow diet in metabolic chambers for indirect calorimetric measurements. When compared to Par-$4^{+/+}$ mice, neither Par-$4^{-/-}$ nor AKO mice showed any changes in food consumption, physical activity, energy expenditure or respiratory exchange ratio (RER) (**Figures S4A, C**).

As both Par-$4^{-/-}$ and AKO mice show weight gain, fat accumulation and adipocyte hypertrophy despite an unchanged metabolic chamber profile, we sought to determine whether these mice exhibited increased intestinal uptake that can lead to obesity. Oil-red O (ORO) staining of proximal intestines, performed after feeding mice with an olive oil gavage, indicated there is no detectable difference in the amount of TG that

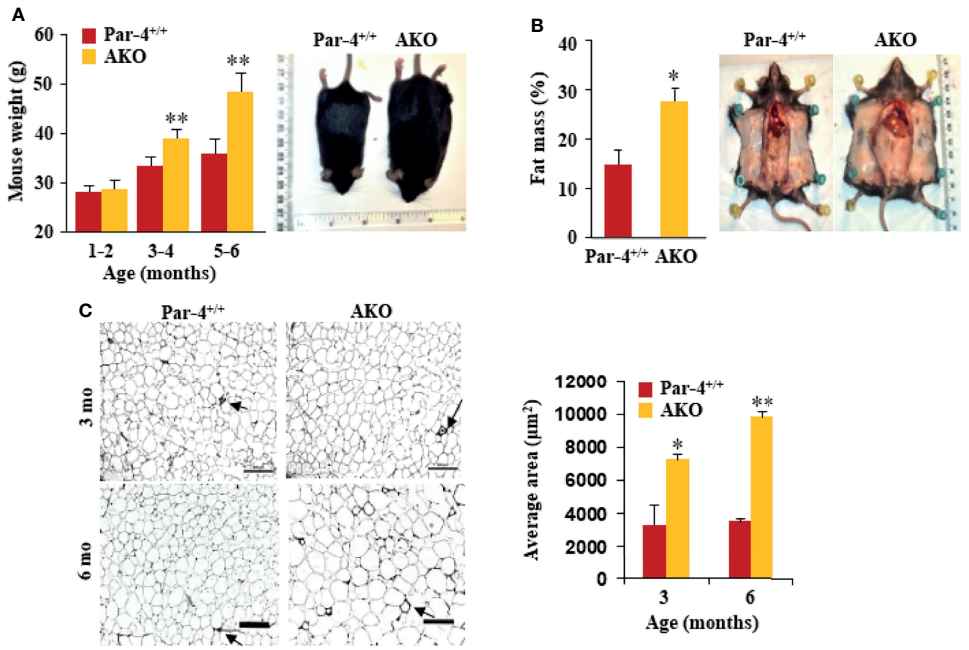

FIGURE 3 | AKO mice show fat mass accumulation and obesity. **(A)** AKO mice are significantly heavier than Par-4$^{+/+}$ mice. Body weights of age-matched male mice (1-6 months, n=6 per group) and representative images of 6-month-old male mice. **(B)** AKO mice show increased fat mass accumulation relative to Par-4$^{+/+}$ mice. Echo-MRI analyses were carried out on 6-month-old male mice (n=5-8); representative images are shown. **(C)** AKO mice show adipocyte hypertrophy relative to Par-4$^{+/+}$ mice. Visceral adipose tissue from 3-month-old or 6-month-old mice (n=3) was subjected to H&E staining and adipocyte cell size was quantified. Visceral fat from Par-4$^{+/+}$ and AKO mice was also subjected to IHC for F4/80 macrophage marker. Arrows point to crown-like structures (more details, see S9E). Mean ± SEM, $^{*}P < 0.05$, $^{**}P < 0.01$, by the Student's *t*-test or with Bonferroni method adjustment for multiple comparisons. Also see **Figure S3**.

accumulates in enterocytes in Par-4$^{-/-}$, AKO, and Par-4$^{+/+}$ mice (**Figure 4A**). As increased uptake of dietary fat may not result in increased accumulation of fat in enterocytes if the rate of absorption of fat from the enterocytes into the bloodstream is also simultaneously elevated, we tested the expression levels of chylomicrons in the plasma of Par-4$^{-/-}$, AKO, and Par-4$^{+/+}$ mice following tyloxapol pretreatment and oral gavage with olive oil. Chylomicrons are lipoprotein particles consisting of a lipid core of TG, other lipid esters, and the key monomeric protein apolipoprotein B48 (ApoB48) (33, 34). ApoB48 is expressed in an enterocyte-specific manner. Upon ingestion of fat, chylomicrons are produced by the enterocytes, then transported to the lymphatic system and released into the bloodstream. Their presence in the plasma serves as an indicator of TG and ApoB48 secretion from the intestine (35). Both TG (**Figure 4B**) and ApoB48 (**Figures 4C**, **S4D**) levels were elevated in the plasma of Par-4$^{-/-}$ and AKO mice relative to Par-4$^{+/+}$ mice. We used tyloxapol pretreatment to eliminate lipases in the mice and rule out the possibility of impaired TG clearance with reduced TG uptake by peripheral tissues, such as adipose tissues, or impaired recycling of the remnant chylomicron/ApoB48 to the liver. Accordingly, the findings can be interpreted to imply that there is greater absorption from enterocytes into circulation. These results indicate that Par-4 loss is associated with increased secretion of chylomicrons from the enterocytes.

Par-4$^{-/-}$ and AKO Mice Show Increased Expression of Acylation Stimulating Protein Associated With Fat Storage and Obesity

To determine the underlying changes in gene expression associated with Par-4 loss in Par-4$^{-/-}$ and AKO mice, we performed RNA-Seq analysis on visceral white adipose tissues collected from 11-week-old Par-4$^{+/+}$, Par-4$^{-/-}$ and AKO mice. We identified 513 genes upregulated in both Par-4$^{-/-}$ and AKO adipose tissues and 526 genes downregulated in both Par-4$^{-/-}$ and AKO tissues, and pathway analysis indicated the predominance of genes associated with fatty acid metabolism (**Figures 5A**, **S5A, B**). In particular, key genes associated with TG synthesis and storage were upregulated in both the Par-4 knockout mice (**Figure 5A**). One of the upregulated genes was Complement *c3*. C3 protein, produced by liver, macrophages and adipocytes, generates Acylation Stimulating Protein (ASP) through a series of cleavage processes requiring factor B and adipsin (also known as factor D) produced by adipocytes (36). As ASP is causally associated with obesity (37), C3/ASP was a lead candidate for further analysis as a potential mediator of obesity upon Par-4 loss. Our validation studies indicated that relative to Par-4$^{+/+}$ mice, Par-4$^{-/-}$ and AKO mice showed elevated levels of C3 expression in the adipose tissues of 3-month-old mice (**Figure 5B**). As C3 proteolytic cleavage requires factor B and adipsin to produce ASP, we tested the levels of these factors in the adipose tissues from Par-4 knockout and Par-4$^{+/+}$ mice. Both factor B and adipsin were

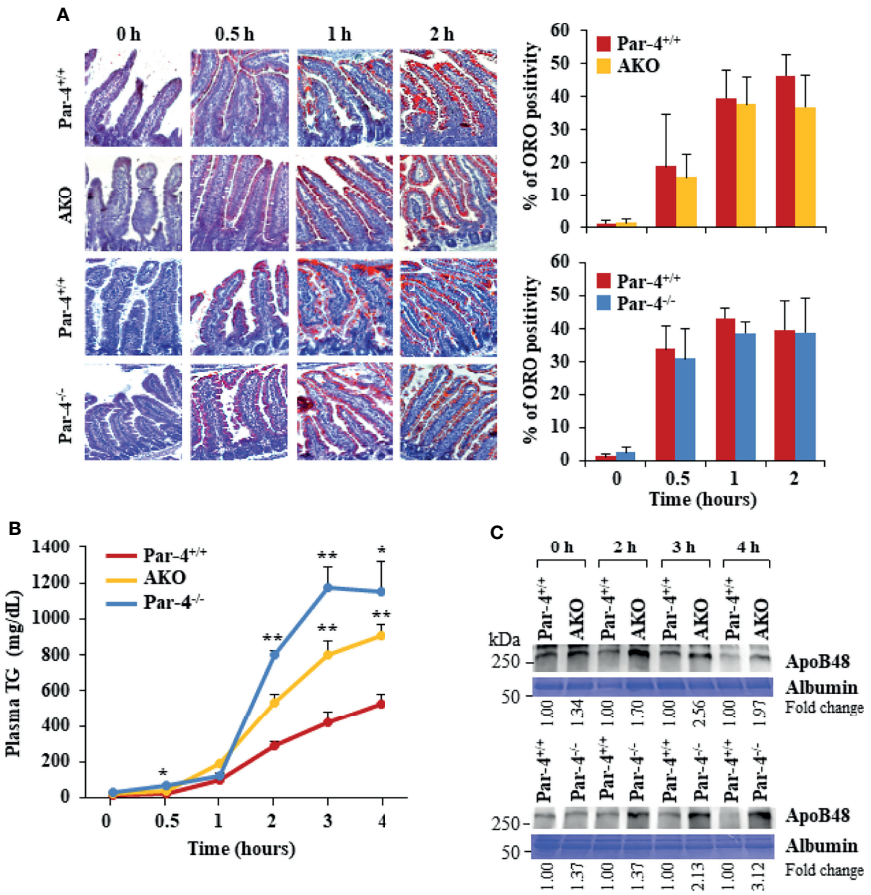

FIGURE 4 | AKO and Par-4 mice show increased intestinal triglyceride absorption after a fat load. **(A)** Intestinal triglyceride accumulation appears similar in Par-4$^{-/-}$, AKO, and Par-4$^{+/+}$ mice. After overnight fasting, Par-4$^{-/-}$, AKO and Par-4$^{+/+}$ mice (n=3) were subjected to an oral load of olive oil. Representative images of proximal intestines collected at the indicated time intervals after gavage and subjected to ORO staining (left panels). ORO staining was quantified in the enterocytes (right panels). Magnification, 10x. **(B)** Triglyceride absorption is increased in both AKO and Par-4$^{-/-}$ mice. AKO, Par-4$^{-/-}$ and Par-4$^{+/+}$ male mice (n=5-9 per group) that were 6-months old were fasted overnight and injected intraperitoneally with tyloxapol 30 min before olive oil gavage to block lipase activity. Plasma was collected at the indicated time points and subjected to triglyceride analysis. **(C)** Apolipoprotein B48 secretion is increased in both AKO and Par-4$^{-/-}$ mice. Plasma from AKO, Par-4$^{-/-}$ and Par-4$^{+/+}$ male mice was subjected to TG analysis and examined by western blot analysis for ApoB48. ApoB48 levels were normalized to albumin levels and fold change at each time point is shown. Mean ± SEM, $^{*}P < 0.05$, $^{**}P < 0.01$ by the Student's *t*-test or with Bonferroni method adjustment for multiple comparisons. Also see **Figures S4, S11**.

upregulated in the adipose tissues of 3-month-old Par-4$^{-/-}$ and AKO mice relative to Par-4$^{+/+}$ mice (**Figure 5B**). Importantly, C3 and ASP were upregulated in the plasma of 6-week-old Par-4$^{-/-}$ and AKO mice before the onset of adipocyte hypertrophy relative to Par-4$^{+/+}$ mice (**Figures 5C–E**), implying that C3/ASP were elevated before the onset of obesity at 3 months. Importantly, C3 mRNA levels were also upregulated in Par-4$^{-/-}$ mouse embryonic fibroblasts (MEFs) when compared to Par-4$^{+/+}$ MEFs (**Figure S5C**). Together, these findings indicate an inverse relationship between Par-4 and C3/ASP.

Obesity in Par-4 Knockout Mice Is Dependent on C3/ASP

To determine whether C3/ASP upregulation was functionally relevant in the obese phenotype of Par-4 knockout mice, we crossed C3$^{-/-}$ mice with Par-4$^{-/-}$ mice and tested the C3/Par-4 double knockout (DKO) mice (**Figure S6A**) for obesity on standard chow diet. DKO mice did not show weight gain, adipocyte hypertrophy or fat mass accumulation relative to Par-4$^{+/+}$ mice (**Figures 6A, B**). Moreover, chylomicron secretion measured by TG and ApoB48 levels in the plasma after olive oil gavage was not elevated in DKO mice relative to Par-4$^{+/+}$ mice (**Figure 6C**).

As elevated levels of ASP promote an increase in lipoprotein lipase (LPL) (38), we determined LPL protein levels in the adipose tissue and heart muscle of Par-4$^{+/+}$, Par-4$^{-/-}$ and AKO mice. LPL is the rate-limiting enzyme that induces the clearance of fatty acids from circulation by hydrolysis of TG-rich lipoproteins and the uptake of derived fatty acids (39). LPL is expressed by the skeletal muscles, including heart muscle, and

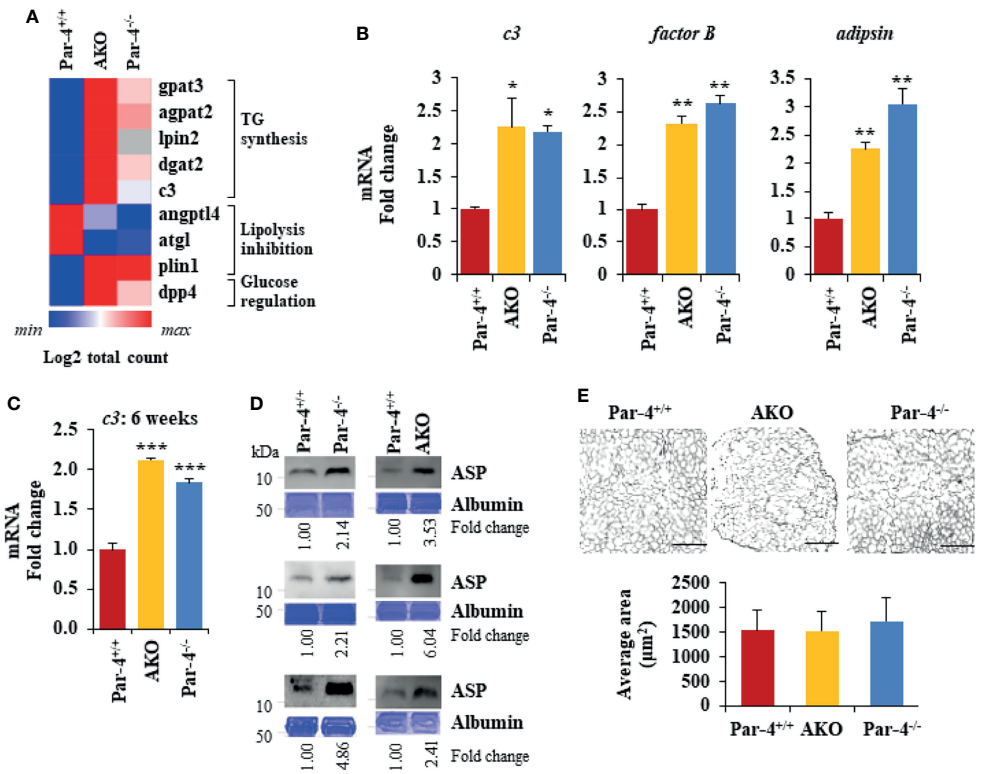

FIGURE 5 | Par-4 loss results in induction of C3/ASP. **(A)** Heatmap of key genes that were up- or downregulated in 11-week old AKO or Par-4$^{-/-}$ vs Par-4$^{+/+}$ mouse adipose tissues. We performed RNA-Seq on AKO, Par-4$^{-/-}$ and Par-4$^{+/+}$ male mouse visceral adipose tissue samples (n=3 per group). The RNA used for RNA-Seq was prepared from 11-week old mice before they were impacted by major alterations in their adipose tissue or obesity. Average gene count for each group was calculated for identifying upregulated and downregulated genes. Heatmaps were generated using Morpheus software https://software.broadinstitute.org/morpheus. **(B)** *c3*, *factor B* and *adipsin* are upregulated in 3-month-old AKO and Par-4$^{-/-}$ mice. Visceral adipose tissues from AKO, Par-4$^{-/-}$ and Par-4$^{+/+}$ male mice were subjected to qPCR analysis for *c3*, *factor B*, *adipsin*, and 18S rRNA. C3 levels were normalized to 18S rRNA and fold change was calculated. **(C)** *c3* RNA is elevated in 6-week-old AKO and Par-4$^{-/-}$ mice. Visceral adipose tissues from AKO, Par-4$^{-/-}$ and Par-4$^{+/+}$ mice were subjected to qPCR analysis for *c3*, and 18S rRNA. C3 levels were normalized to 18S rRNA and fold change was calculated. **(D)** ASP is elevated in 6-10-week-old AKO and Par-4$^{-/-}$ mice. Plasma from AKO, Par-4$^{-/-}$ and Par-4$^{+/+}$ mice was subjected to western blot analysis for ASP. ASP levels were normalized to albumin levels in parallel Coomassie blue gels and fold. **(E)** Adipocyte size is similar at 6 weeks of age. Adipose tissue from 6-week-old mice was subjected to H&E staining (scale bar, 200 μm) and adipocyte cell size was quantified. **(B, C, E)** Mean ± SEM, *P < 0.05, **P < 0.01, ***P < 0.001 by the Student's t-test with Bonferroni method. Also see **Figures S5**, **S12**.

white adipose tissue. In skeletal muscles, fatty acids are largely oxidized, whereas in the adipose tissue they are esterified and stored as TGs (40). LPL levels were elevated in the adipose tissues but not the heart of Par-4$^{-/-}$ and AKO mice relative to the corresponding tissues of Par-4$^{+/+}$ mice (**Figure 6D**). In contrast, LPL levels remained unchanged in the heart and in the adipose tissues of DKO mice relative to Par-4$^{+/+}$ mice (**Figure 6E**). As LPL in the adipose tissues is associated with clearance of TGs from circulation and storage in adipocytes, these findings are consistent with increased fat storage and hypertrophic obesity in Par-4$^{-/-}$ and AKO mice and reversal of this phenotype in DKO mice.

C3 Induction Following Par-4 Loss Is Regulated by p53

As C3 induction plays a functional role in the obese phenotype of Par-4 knockout mice, we determined the mechanism by which Par-4 regulates C3 expression. Par-4 has been previously shown to modulate gene expression by cooperating with other transcription factors as a transcriptional co-repressor (41, 42) or transcriptional co-activator (43). To identify downstream genes that are regulated by Par-4 in adipocytes, we therefore performed ChIP-Seq analysis with the Par-4 antibody using 3T3-L1 cell cultures. These experiments led to the identification of several genes, including *mdm2* encoding the ubiquitin ligase MDM2 as a potential target of Par-4 (**Table S2**). As MDM2 regulates p53 activity, and as p53 induction is associated with obesity (44–46), we validated MDM2 and p53 regulation by Par-4. As seen in **Figure 7A**, *mdm2* expression was downregulated in the adipose tissues of Par-4$^{-/-}$ and AKO mice relative to Par-4$^{+/+}$ mice. Consistently, expression of p53 (**Figure 7B**; blot with secondary antibody only is shown in **Figure S7A**), as well as its authentic target p21 (**Figure S7B**), was upregulated in Par-4$^{-/-}$ and AKO mice relative to Par-4$^{+/+}$ mice. To further examine whether p53 regulates *c3*, we tested the expression of *c3* RNA in MEFs from p53 wild type mice (p53$^{+/+}$), p53 homozygous (p53$^{-/-}$) and heterozygous (p53$^{+/-}$) knockout mice. *c3* expression was downmodulated in p53$^{-/-}$ and p53$^{+/-}$ MEFs

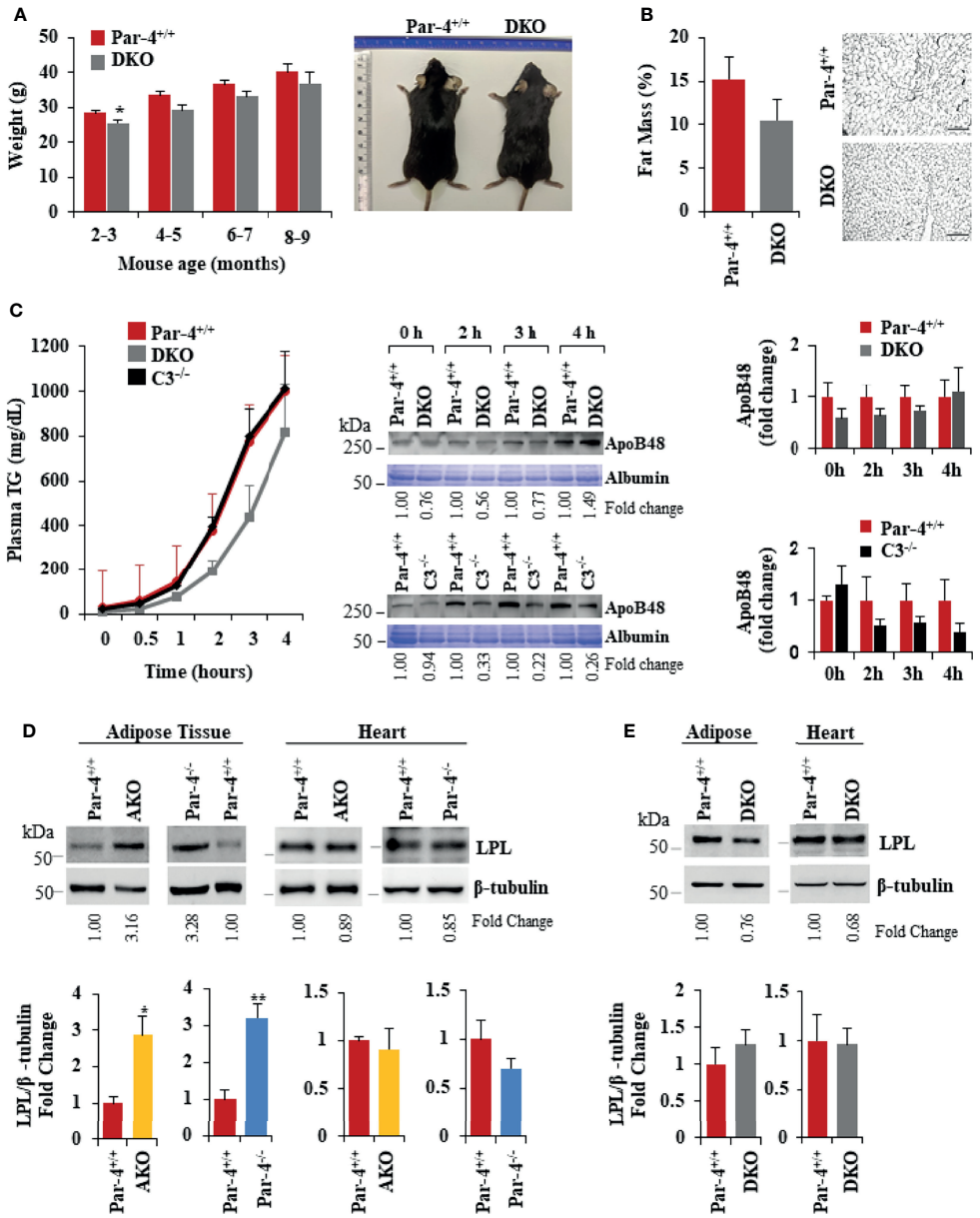

FIGURE 6 | Obesity in Par-4$^{-/-}$ mice is rescued by deletion of C3. (A) Par-4 and C3 double knockout (DKO) mice are not obese. Weight of age-matched DKO (n=13, 10, 8 and 4 for each time point respectively) and Par-4$^{+/+}$ (n=27, 16, 9, 5 for each time point respectively) male mice was determined over the course of 7 months; representative images of Par-4$^{+/+}$ and DKO at 5-6 months are shown. **(B)** DKO mice do not show increased fat accumulation. Six-month-old DKO (n=8) and Par-4$^{+/+}$ (n=7) male mice were examined for fat mass by Echo-MRI and adipocyte hypertrophy. **(C)** Triglyceride absorption is similar in DKO, C3KO and Par-4$^{+/+}$ mice. DKO (n=5-6), C3$^{-/-}$ (n=4) and Par-4$^{+/+}$ (n=11) male mice were fasted overnight and injected intraperitoneally with tyloxapol, 30 min before oral gavage of olive oil. Plasma was collected at the indicated time intervals after fat load, and triglycerides were quantified. Plasma was also subjected to western blot analysis for ApoB48. ApoB48 levels in the plasma were normalized to albumin in corresponding Coomassie blue gels, and fold change at each time point is shown (n=4). **(D)** LPL is upregulated in the adipose tissue of AKO and Par-4$^{-/-}$ mice. LPL protein levels were determined by western blot analysis in visceral adipose tissue and heart from AKO, Par-4$^{-/-}$ and Par-4$^{+/+}$ mice (n=3). **(E)** LPL is not increased in the adipose tissue of DKO mice. LPL protein levels were determined by western blot analysis in visceral adipose tissue and heart from Par-4$^{+/+}$ (n=4) and DKO (n= 4) male mice. LPL levels were normalized to β-tubulin levels and fold change was calculated. Mean ± SEM, *P < 0.05, **P < 0.01, by the Student's *t*-test. Also see **Figures S6**, **S13**.

relative to p53$^{+/+}$ MEFs (**Figure 7C**). On the other hand, reintroduction of p53 in p53$^{-/-}$ MEFs caused induction of *c3* and *p21* expression (**Figure 7D**). To determine the effects of acute Par-4 knockdown in MEFs, we used two different siRNA duplexes against Par-4. As seen in **Figure 7E** (right panel), downregulation of endogenous Par-4, resulted in inhibition of *mdm2* (**Figure S7C**), induction of p53 (**Figure 7E**, left panel) and *c3* (**Figure 7F**). Finally, we tested whether p53 regulates the expression of the C3 promoter

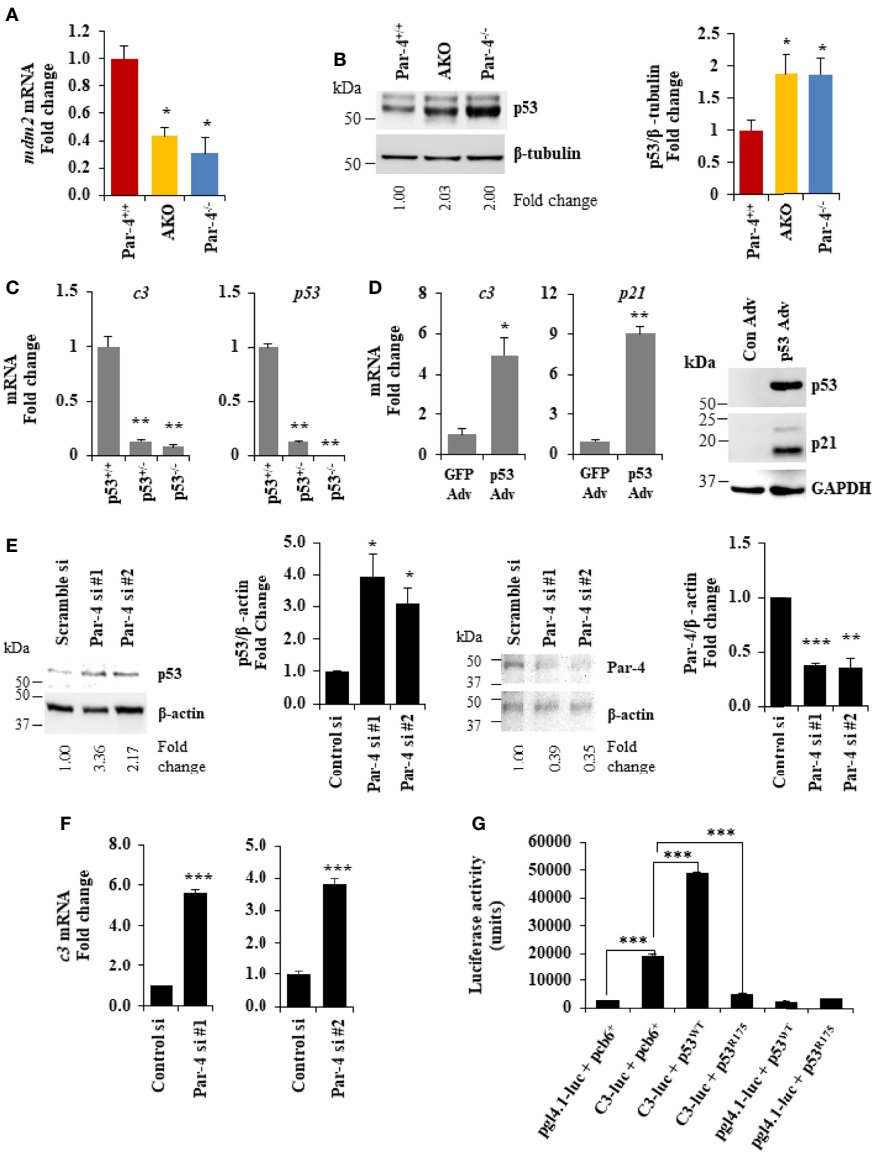

FIGURE 7 | Par-4 regulates C3 *via* p53. **(A)** *mdm2* is downregulated in the adipose tissue of AKO and Par-4$^{-/-}$ mice. RNA from visceral adipose tissues from 3-month-old AKO, Par-4$^{-/-}$ and Par-4$^{+/+}$ mice were subjected to qPCR analysis for *mdm2* and 18S rRNA. *mdm2* levels were normalized to 18S and fold change was calculated. **(B)** p53 is upregulated in the adipose tissue of AKO and Par-4$^{-/-}$ mice. Visceral adipose tissues from 6-week-old AKO, Par-4$^{-/-}$ and Par-4$^{+/+}$ mice (n=4) were subjected to western blot analysis for p53 and β-tubulin. p53 levels were normalized to β-tubulin and fold change is shown. p53 was induced in AKO and Par-4$^{-/-}$. **(C)** C3 is downregulated in the p53-null MEFs. RNA from p53$^{+/+}$, p53$^{+/-}$ and p53$^{-/-}$ MEFs was subjected to qPCR analysis for *c3*, *p53* and 18S rRNA. C3 and p53 levels were normalized to 18S rRNA and fold change was calculated (left panel). p53 status in the three MEFs lines was confirmed (right panel). **(D)** C3 is induced with p53 rescue in p53-null MEFs. p53-null (p53$^{-/-}$) MEFs were transduced with either control GFP adenovirus (Adv) or p53 adenovirus. RNA was collected 24h after infection and subjected to qPCR analysis for *c3*, *p21* and 18S rRNA (left and middle panel). Whole-cell extracts from the adenovirus infected cells were subjected to western blot analysis for p53 and p21 using GAPDH as a loading control (right panel). **(E)** p53 is upregulated in MEFs. WT MEFs were transfected with either control siRNA or two different Par-4 siRNA (#1 and #2 from Dharmacon; n=3). Whole-cell extracts from transfected cells were collected after 24h of transfection and subjected to western blot analysis for p53 (left panel) and Par-4 (right panel) using β-actin as a loading control. **(F)** *c3* RNA is upregulated in WT MEFs knocked down for Par-4. RNA from WT MEFs transfected with either scramble siRNA or two different Par-4 siRNA (si Par-4 #1, left panel; siPar-4 #2, right panel) was collected. RNA was subjected to RT-qPCR for c3 and 18S. Fold change was calculated using 18S as housekeeping control. **(G)** p53 induces the *c3* promoter. p53$^{+/+}$ MEFs were transiently co-transfected with: (1) C3-promoter reporter (TK-luc containing c3 promoter region; C3-luc), p53^{WT} and β- galactosidase expression construct; (2) C3-luc, p53^{R175} and β-galactosidase construct; (3) pgl4-1 control luciferase construct, p53^{WT} and β-galactosidase construct; and (4) C3-luc, p53^{R175} and β- galactosidase construct. Luciferase activity was determined after 24h and normalized to corresponding β-galactosidase activity. **(A–C, E, F)** Mean ± SEM, *adjusted $P < 0.05$, **$P < 0.01$, ***$P < 0.001$ by the Student's t-test or with Bonferroni method. Mean (Relative luciferase activity units) ± SEM, ***P < 0.001 by the Student's t-test or with Bonferroni method adjustment for multiple comparisons. Mean ± SEM, *$P < 0.05$, **$P < 0.01$ by the Student's *t*-test or with Bonferroni method adjustment for multiple comparisons. Also see **Figures S7**, **S14**.

in luciferase-reporter assays. As seen in **Figure 7G**, wild type p53 but not a mutant of p53, induced the *c3* promoter. Together, these findings indicate that Par-4 loss results in loss of *mdm2* that leads to p53 activation, and that p53 induces the expression of *c3* at the promoter level.

Obesity in AKO Mice Is Rescued by Par-4 Knock-In Into Adipocytes

To confirm that obesity induced by Par-4 loss in adipocytes was primarily associated with Par-4 function and was not a consequence of unrelated downstream events in mice, we tested whether obesity in AKO could be reversed by re-expression of Par-4 in adipocytes. Accordingly, Par-4Ki$^{tg/tg}$ mice were crossed with AKO mice for adipocyte specific re-expression of Par-4 as indicated in Materials and Methods section and **Figures S8A, S8B**. Induction of Par-4 in adipocytes was confirmed by Western blot analysis of adipose tissue (**Figure S8C**). Par-4 re-expressing AKO (AKO/Par-4Ki) mice showed similar weights and fat mass accumulation as Par-4$^{+/+}$ mice (**Figures 8A, B**; also see **Figure S8D, E**). Moreover, TG absorption and ApoB48 levels were similar in AKO/Par-4Ki and Par-4$^{+/+}$ mice (**Figure 8C**). Unlike AKO mice that showed increased levels of ASP and LPL in their plasma relative to Par-4$^{+/+}$ mice, AKO/Par-4Ki showed p53, p21 and ASP, as well as LPL levels similar to those of Par-4$^{+/+}$ mice (**Figures 8D**, **S8F**). AKO/Par-4Ki also showed glucose and insulin levels similar to those of Par-4$^{+/+}$ mice (**Figure S8G**). Together, these findings indicate that re-expression of Par-4 in adipocytes reverses p53 induction, ASP upregulation, LPL elevation, lipid absorption, fat mass accumulation and weight gain, as well as secondary increase in glucose and insulin levels noted in AKO mice.

DISCUSSION

The present study uncovered an unpredicted physiological function of Par-4. Conventional Par-4 knockout mice were overweight and accumulated significantly higher visceral and subcutaneous adipose tissue relative to control mice on standard chow. Adipocyte hypertrophy began at about three months after birth. Deletion of Par-4 in mouse adipocytes, but not in the mouse hepatocytes, recapitulated the obese phenotype of Par-4 whole-body knockout mice. Hepatic steatosis and hyperinsulinemia occurred as a secondary complication of obesity. Weight gain, fat mass accumulation as well as most other obesity related features of AKO mice were generally similar to that of Par-4$^{-/-}$ mice. Moreover, obesity in AKO mice was reversed by re-expression of Par-4 in adipocytes, implying that Par-4 in adipocytes regulated the obese phenotype in mice. The relevance of these observations in human obesity was substantiated by lower expression of Par-4 in the adipose tissues from obese individuals relative to lean individuals. Most importantly, our cohort study indicated that Par-4 expression in plasma was lower in lean individuals who developed obesity during an average follow-up time of 16.5 ± 1.5 years relative to those who remained lean during this time period. Obese subjects who remained obese during this follow-up time also showed significantly lower levels of Par-4 compared to lean individuals who remained lean. Both intracellular transcriptional regulatory effects and apoptotic functions of extracellular (secreted) Par-4 have been reported in literature (1). Par-4 is secreted by normal fibroblast and epithelial cell cultures, and secreted Par-4 does not induce growth inhibition in normal cells (13), but the tissue types *in vivo* that secrete Par-4 or the role of secreted Par-4 in modulating obesity is not known. Our future studies will test whether Par-4 expression in plasma is functionally involved in regulation of obesity or serves only as a biomarker to predict obesity. In view of our observation that Par-4 was lost prior to the onset of obesity in Par-4$^{-/-}$ and AKO mice, these findings imply that Par-4 loss is a predictor of future obesity.

Par-4$^{-/-}$ and AKO Mice Display Obesity on Standard Chow

Unlike most genetically engineered mouse models that develop obesity on high fat diet or due to increased food consumption and/or decreased energy expenditure (47–49), our studies indicated that Par-4$^{-/-}$ and AKO mice displayed obesity on standard chow diet. Metabolic and behavioral studies indicated that the Par-4 knockout mice did not show increased food consumption, decreased physical activity, or energy expenditure relative to control mice. Leptin levels were higher and adiponectin levels were lower in Par-4 knockout mice relative to Par-4$^{+/+}$ mice, consistent with the obese phenotype (**Figure S9A**). Lean mass was consistent with the obese phenotype in the Par-4$^{-/-}$ and AKO mice, and with reversal of obesity in the DKO and AKO/Par-4Ki mice (**Figure S9B**). Both male and female Par-4 knockout mice exhibited obesity, implying that the phenotype was not controlled by sex-specific hormonal mechanisms. This phenotype of Par-4 knockout mice is reminiscent of individuals who are unable to control obesity despite controlling their diet.

In studies to determine the underlying cause of obesity in Par-4 knockout mice, we noted that Par-4 loss is associated with increased TG levels in the plasma of mice that were fed olive oil by oral gavage. ORO staining of intestinal segments did not discern elevated levels of fat accumulation in Par-4 knockout and control mice. Increased uptake may result in increased absorption, yet increased uptake may not be discernable by ORO staining due to saturation of the enterocytes with fat. We therefore examined whether absorption of TGs from the intestine into blood circulation was enhanced by Par-4 loss. These experiments used tyloxapol pretreatment, to inhibit lipases, followed by oral gavage with olive oil to determine TG and chylomicron levels in circulation. We noted elevated levels of TG in the plasma of both Par-4$^{-/-}$ and AKO mice relative to Par-4$^{+/+}$ mice that were fed olive oil. ApoB48, which is produced in the intestine and required for chylomicron secretion, was also elevated in circulation of the Par-4$^{-/-}$ and AKO mice following tyloxapol pretreatment and olive oil gavage. As chylomicrons are comprised of TGs and ApoB48, and as ApoB48 is expressed in an enterocyte-specific manner, the presence of elevated TGs and ApoB48 in the plasma serves as an indicator of increased TG and ApoB48 absorption from the intestine (35). The use of tyloxapol

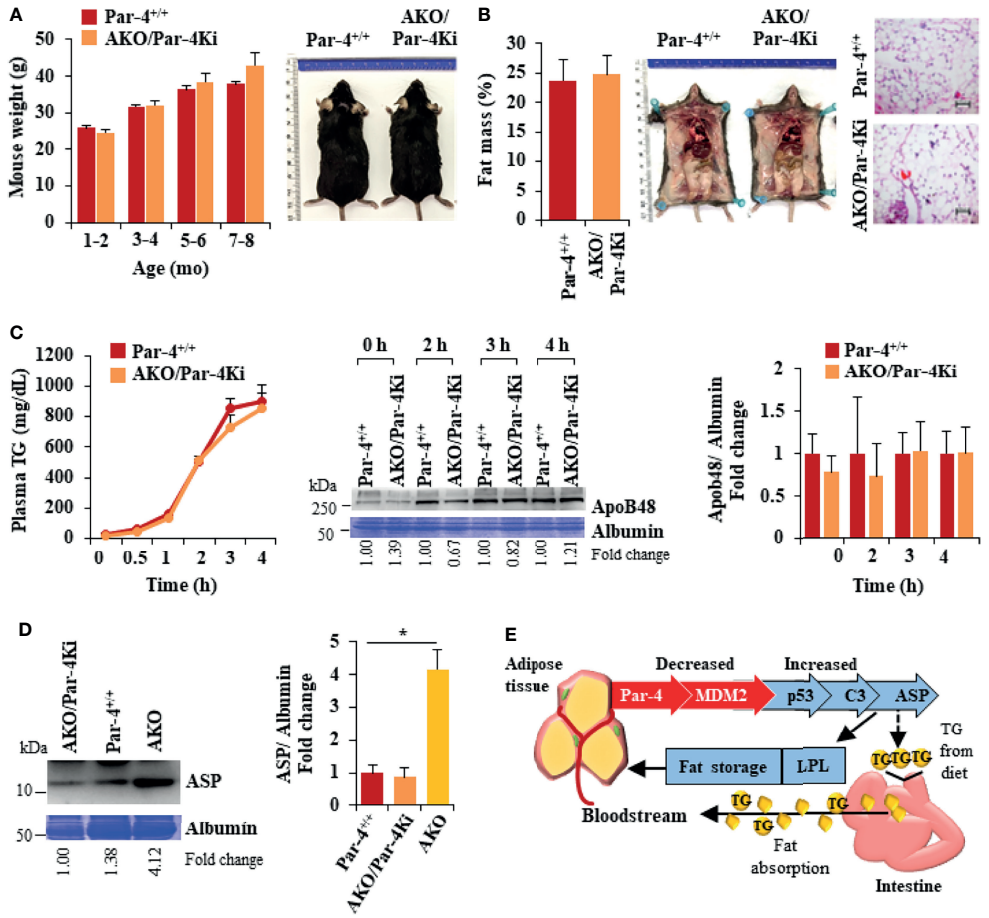

FIGURE 8 | Obesity in AKO mice is rescued by Par-4 knock-in into adipocytes. **(A)** AKO/Par-4Ki mice are not obese. Body weights of age-matched male AKO/Par-4Ki mice (n=9, 17, 11, 6) and control mice (n=6, 24, 17, 25) were collected for nine months. Representative images of 7-month-old male mice are shown. **(B)** Fat accumulation in AKO/Par-4Ki mice is comparable to controls. Echo-MRI analyses were carried out on 5-7-month-old AKO/Par-4Ki (n=7) and control (n=11) male mice; representative images of 7-month-old male mice are shown. **(C)** Triglyceride absorption is similar in AKO/Par-4Ki and Par-$4^{+/+}$ mice. AKO/Par-4Ki (n=8), and Par-$4^{+/+}$ (n=9) mice were fasted overnight and injected intraperitoneally with tyloxapol, 30 min before oral gavage of olive oil. Plasma was collected at the indicated time intervals after fat load, and triglycerides were quantified. Plasma was also subjected to western blot analysis for ApoB48. ApoB48 levels in the plasma were normalized to albumin in corresponding Coomassie blue gels, and fold change at each time point are shown (n=4). **(D)** ASP is not upregulated in AKO/Par-4Ki. Plasma from AKO/Par-4Ki (n=3), AKO (n=3) and Par-$4^{+/+}$ (n=3) male mice was subjected to western blot analysis for ASP. ASP levels in the plasma were normalized to albumin in corresponding Coomassie blue gels, and representative fold change is shown. **(E)** Par-4 loss is associated with induction of C3 and ASP, due to p53 upregulation. Par-4 loss results in downregulation of the ubiquitin ligase MDM2. This leads to p53 activation and induction of complement factor C3. Further induction of factor B and adipsin results in proteolytic cleavage of C3 protein to ASP. Elevated C3/ASP were associated with increased absorption of chylomicrons (TGs and ApoB48) from the intestine into the bloodstream and increased LPL for fat storage in the adipocytes. These latter effects of Par-4 loss were reversed by knocking out C3/ASP in Par-4 knockout mice. Thus, Par-4 loss results in fat accumulation, adipocyte hypertrophy and obesity in a C3/ASP dependent manner. Consistently, our cohort study indicated that low levels of Par-4 may predict future obesity. Mean ± SEM, *P < 0.05 by the Student's *t*-test with Bonferroni method adjustment for multiple comparisons. Also see **Figures S8**, **S15**.

pretreatment allowed us to inhibit lipases in the mice, and therefore impaired TG clearance or TG uptake by peripheral tissues, such as adipose tissues, or impaired recycling of the remnant chylomicron/ApoB48 to the liver was ruled out as a possible cause of elevated TGs and ApoB48. Our findings indicating reversal of TG absorption upon Par-4 re-expression in the adipocytes of AKO mice further suggest that elevated levels of adipose tissue fat are associated with increased intestinal TG absorption in Par-$4^{-/-}$ and AKO mice. However, as the obese phenotype in Par-$4^{-/-}$ and AKO mice was robust on chow diet, which is fat-poor and carbohydrate rich diet, it is possible that more carbohydrate is converted to fat for storage. This observation is consistent with elevated expression of genes such as *fasn* and *scd2* (see **Figure S5**) associated with *de novo* lipogenesis. Therefore, the conversion of more carbohydrates into fat and storage in adipocytes, that may be an additional reason for obesity in the chow fed animals, needs to be addressed in the future studies. Similarly, future studies will use isotope-labeled lipids to monitor lipid uptake and oxidation in adipose tissues and other metabolic tissues including heart, muscle and

liver. Moreover, it is necessary to compare food intake, energy expenditure, and lipid excretion on chow and high-fat diet in Par-4 knockout and AKO mice relative to Par-$4^{+/+}$ mice.

Par-$4^{-/-}$ and AKO Mice Display Increased C3/ASP Expression in Adipocytes That Is Causally Linked to Elevated LPL, Fat Storage and Obesity

We reasoned that, as Par-4 knockout mice show similar levels of food intake and energy expenditure as the control mice, increased fat storage in the adipose tissue and obesity must be a consequence of gene alterations in adipocytes that result in uptake of circulating TGs for storage. We therefore performed an unbiased screen for differential gene expression in adipose tissues from Par-$4^{-/-}$ or AKO mice relative to Par-$4^{+/+}$ mice. These studies identified several genes associated with TG synthesis or storage (*gpat3*, *agpat2, lpin2, dgat2, c3)*, inhibition of intracellular lipolysis in adipocytes (*angptl4, atgl*), and regulation of glucose homeostasis (*dpp4*).

In particular, C3 and its proteolytic product ASP are causally associated with fat storage and obesity (37). C3 is proteolytically processed by binding to factor B and the adipokine adipsin specifically in the adipose tissue. Importantly, ASP is upregulated in obesity and is involved in lipid clearance from circulation. The primary effect of ASP is the promotion of fat storage in adipocytes by elevating intracellular diacylglycerol acyltransferase (DGAT) activity (50), which catalyzes the formation of triglycerides from diacylglycerol and acyl-CoA, and GLUT4 translocation, which drives extracellular fatty acid and glucose uptake into cells. ASP also inhibits intracellular lipolysis, and injection of ASP increases fat storage, and neutralization of ASP with an antibody inhibits fat storage (51, 52). As expected, C3 knockout mice show ASP-deficiency, and the protective potential of ASP-deficiency against obesity was confirmed in *ob*/*ob*-$C3^{-/-}$ double knockout mice (53). Together, these observations imply that ASP is a unique factor that promotes obesity and apparently links the complement arm of the immune system to metabolism.

In adipocytes, ASP action is mediated through activation of downstream kinases (54), but the upstream signals responsible for upregulation of the C3/ASP pathway have not been delineated. Our studies indicate that C3 and ASP are expressed at higher levels at 6 weeks (**Figures 5C, D**), before the onset of adipocyte hypertrophy noted after 3 months in Par-$4^{-/-}$ and AKO mice. C3 is produced mainly by hepatocytes and adipose tissue, but C3 is converted to ASP in only the adipose tissue due to adipocyte-specific expression of adipsin. Our hepatocyte Par-4 knockout mice do not show C3 upregulation (**Figure S9C**) and are not obese. These observations implied that Par-4 regulates downstream expression of C3 in a tissue-specific manner and provided the rationale for determining whether C3/ASP elevation is functionally associated with adipocyte hypertrophy, increased visceral fat storage and obesity in Par-4 knockout mice. Remarkably, deletion of C3 in Par-$4^{-/-}$ mice resulted in reversal of adipocyte hypertrophy, fat mass accumulation and obesity. Furthermore, C3-Par-4 double knockout mice failed to show elevated absorption of TGs or ApoB48 from the intestine in response to olive oil gavage, implying a link between ASP associated adipocyte hypertrophy and enhanced TG absorption in mice lacking Par-4. Together with these observations, reversal of the obese phenotype in DKO mice is a most likely consequence of C3 loss in the adipose tissue. Given the possibility that C3 knockout may have yet unidentified pleiotropic effects that "rescue" the Par-4 phenotype through non-specific mechanisms, future studies may confirm the adipocyte-specific effects of C3 by crossing AKO mice with conditional adipocyte knockout C3 mice. To avoid confusion, we clarify that a previous publication in literature is based on protease-activated receptor 4 (also called Par-4) and complement C4a (55), and does not involve prostate apoptosis response-4 (Par-4/PAWR).

ASP elevation results in increased adipocyte LPL essential for storage of fat in adipocytes (37). LPL levels in the adipose tissues, but not the heart, were elevated in Par-$4^{-/-}$ and AKO mice relative to Par-$4^{+/+}$ mice. These findings are consistent with increased fat storage in the visceral adipose tissue of these knockout mice. On the other hand, DKO mice failed to show elevated LPL in the adipose tissue relative to Par-$4^{+/+}$ mice and failed to induce fat storage despite the lack of Par-4, implying that C3/ASP that was elevated in response to Par-4 loss was an essential downstream mediator of adipocyte hypertrophy, fat storage and obesity in Par-4 knockout mice. Together, our findings suggest that Par-4 loss in adipocytes results in obesity that is associated with adipocyte hypertrophy and fat accumulation in visceral adipose tissue caused by increased C3/ASP. Although LPL protein levels are expected to correlate with LPL activity, our future studies will measure LPL enzymatic activity. We hypothesize that high LPL levels and activity in Par-$4^{-/-}$ or AKO adipose tissue act to reduce the TG levels in circulation by increasing their storage. This creates a "sink" for TGs in circulation that stimulates fat absorption. In addition, our experiments in Caco-2 cells suggest that factors secreted by the adipocytes upon Par-4 loss in Par-$4^{-/-}$ and AKO mice may directly or indirectly regulate fat absorption (**Figure S9D**). As we were unable to detect any difference in lipid excretion in these mice, our future studies will examine whether ASP or ASP-regulated downstream factors may promote enterocyte uptake of diet-derived TGs and fatty acids in the context of Par-4 loss.

C3 Induction Following Par-4 Loss Is Regulated by p53

Par-4 is a transcriptional co-regulator that may either co-repress or co-activate gene transcription events depending on the genetic context (41–43). ChIP-Seq analysis aimed at identifying downstream mediators of C3 induction upon Par-4 loss led to the identification and validation of MDM2 as a potential target of Par-4. We focused on the MDM2-p53 axis as a potential regulator of C3 because: (a) MDM2 is the primary ubiquitin ligase responsible for degradation of the guardian of the genome p53 protein (56), (b) p53 has been previously shown to promote obesity (44, 44, 46), and (c) and several putative p53 consensus binding sites are located in the *c3* gene promoter (EPD and JASPAR databases). Our findings indicated that Par-4 loss results in downregulation of MDM2 and activation of p53 that was also

evident from p21/CDKN1A induction in mouse adipose tissues. It is noteworthy that induction of the p21/CDKN1A is associated with adipocyte hypertrophy and obesity in mice (57, 58). Moreover, p53 loss in knockout cells resulted in loss of *c3* gene expression and upregulation of p53 induced *c3* promoter and RNA expression. Together, the MDM2-p53 axis links Par-4 loss to C3 induction and obesity in Par-4 knockout mice.

Par-4$^{-/-}$ and AKO Mice Display Secondary Complications of Obesity

Our studies indicated that Par-4$^{-/-}$, AKO and Par-4$^{+/+}$ mice show similar growth characteristics, including similar weight gain in the first few months after birth. At 3 months of age, the adipose tissues from these mice did not show obvious macroscopic differences, but the adipose tissue from Par-4$^{-/-}$ and AKO mice show hypertrophy that was obvious microscopically. Unlike adipocyte hyperplasia that is associated with adipocyte proliferation and insulin sensitivity, adipocyte hypertrophy results in secondary complications such as hepatic steatosis and insulin resistance (59, 60). Infiltration of macrophages and other immune cells is often the underlying cause of these secondary complications (61). Consistent with these observations, the adipose tissues from AKO mice showed macrophage infiltration, and began developing hyperinsulinemia at 6 months but not at 3 months after birth (**Figures S3E, S3F, S9E**). Thus, adipocyte hypertrophy associated with fat storage was a primary effect that was followed subsequently by inflammatory and metabolic features that are secondarily associated with obesity, including macrophage infiltration and hyperinsulinemia. Similarly, Par-4$^{-/-}$ mice showed hepatic steatosis and hyperinsulinemia at 6 months but not at 3 months after birth (**Figures S1D–F**). We did not study the insulin resistance phenotype in more detail as high glucose or insulin levels occurred later as a secondary consequence of obesity. The phenotypic and gene expression changes noted above were similar for both male and female mice in all the experiments and were consistently observed in over multiple generations of mice. Together, these features indicate primary hypertrophic obesity in Par-4 knockout mice.

Excess body weight affects the release of inflammatory and pro-tumorigenic proteins that are produced by adipose tissue to promote the growth and metastatic properties of tumors (19–23). The precise relationship between the factors produced by adipocytes and cancer is, however, not fully understood. Moreover, not all obese individuals develop cancer, and although loss of tumor suppressors increase the risk of developing tumors, the timing of tumor development varies among individuals. As Par-4$^{-/-}$ mice exhibit obesity, high glucose and insulin levels at 6 months (this study) and are reported to develop tumors in diverse tissues later as they age (9), our findings provide the groundwork for future studies to elucidate whether specific features associated with loss of Par-4 function in adipocytes not only promote obesity, but also serve as a risk factor for cancer.

In summary, the present study revealed that Par-4 expression is lower in the adipose tissue of obese human subjects relative to lean subjects and may serve as a predictor of future obesity in lean subjects. Importantly, genetic loss of Par-4 results in hypertrophic obesity in both conventional and adipocyte-conditional Par-4 knockout mice on standard chow diet. These effects of Par-4 are functionally linked to C3/ASP upregulation, increased chylomicron secretion and LPL regulation for fat storage in adipocytes (**Figure 8E**). Thus, our findings identify Par-4 as a physiological regulator of lipid metabolism and uncover an adipocyte-intestinal axis that regulates obesity. Because obesity is a predisposing factor for cancer, and because Par-4 loss is also linked to increased tumorigenesis, Par-4 restoration may be explored to overcome obesity and thereby inhibit obesity-associated cancer.

DATA AVAILABILITY STATEMENT

The data presented in the study are deposited in the NCBI GEO repository accession number GSE159147.

ETHICS STATEMENT

The studies involving human participants were reviewed and approved by University of Kentucky IRB. Written informed consent for participation was not required for this study in accordance with the national legislation and the institutional requirements. The animal study was reviewed and approved by University of Kentucky IACUC.

AUTHOR CONTRIBUTIONS

NA and JS performed experiments and wrote the manuscript. SN, RB, NH, SG, TS-B, BZ, and WK performed experiments. DH, CW, YZ, BT, JL, LC, and HW analyzed the data. OM and PK provided reagents. AM, LAC, MN-K, PN, BME, and PK provided expertise and feedback. VR conceived and supervised the project. All authors contributed to the article and approved the submitted version.

FUNDING

This work was supported by NIH/NCI grants R01 CA165469, R01 CA187273, and R21 CA179283 (to VR), along with R01 DK071349 and DK080327, and CTSA grant UL1 TR001998 (to PK), and R01 DK112034 (to BE). NA was supported by a scholarship (ID 13137-13-1) from Coordenação de Aperfeiçoamento Superior (CAPES), Brazil. JS was supported by NCI grant T32 CA165990 (to VR).

ACKNOWLEDGMENTS

We thank Nidhi Shukla and Yanming Zhao for assistance with mouse experiments, Yuanyuan Wu for assistance with RNA-Seq analysis, and Dr. Nancy Webb, University of Kentucky, for

critical reading of the manuscript. This research was also supported by Energy Balance and Body Composition Core of the University of Kentucky Center of Research in Obesity and Cardiovascular Disease and the University of Kentucky CCTS Biospecimen Core, and the following University of Kentucky Markey Cancer Center Shared Resource Facilities (P30 CA177558): Biospecimen Procurement and Translational Pathology, Biostatistics and Bioinformatics, and Cancer Research Informatics. The University of Kentucky Markey Cancer Center's Research Communications Office assisted with preparation of the manuscript.

SUPPLEMENTARY MATERIAL

The Supplementary Material for this article can be found online at: https://www.frontiersin.org/articles/10.3389/fonc.2022.860446/full#supplementary-material

REFERENCES

1. Shrestha-Bhattarai T, Rangnekar VM. Cancer-Selective Apoptotic Effects of Extracellular and Intracellular Par-4. *Oncogene* (2010) 29(27):3873–80. doi: 10.1038/onc.2010.141
2. Cook J, Krishnan S, Ananth S, Sells SF, Shi Y, Walther MM, et al. Decreased Expression of the Pro-Apoptotic Protein Par-4 in Renal Cell Carcinoma. *Oncogene* (1999) 18(5):1205–8. doi: 10.1038/sj.onc.1202416
3. Goswami A, Burikhanov R, de Thonel A, Fujita N, Goswami M, Zhao Y, et al. Binding and Phosphorylation of Par-4 by Akt Is Essential for Cancer Cell Survival. *Mol Cell* (2005) 20(1):33–44. doi: 10.1016/j.molcel.2005.08.016
4. Moreno-Bueno G, Fernandez-Marcos PJ, Collado M, Tendero MJ, Rodriguez-Pinilla SM, Garcia-Cao I, et al. Inactivation of the Candidate Tumor Suppressor Par-4 in Endometrial Cancer. *Cancer Res* (2007) 67(5):1927–34. doi: 10.1158/0008-5472.CAN-06-2687
5. Hebbar N, Wang C, Rangnekar VM. Mechanisms of Apoptosis by the Tumor Suppressor Par-4. *J Cell Physiol* (2012) 227(12):3715–21. doi: 10.1002/jcp.24098
6. Alvarez JV, Pan T-C, Ruth J, Feng Y, Zhou A, Pant D, et al. Par-4 Downregulation Promotes Breast Cancer Recurrence by Preventing Multinucleation Following Targeted Therapy. *Cancer Cell* (2013) 24(1):30–44. doi: 10.1016/j.ccr.2013.05.007
7. Liu Y, Gilbert MR, Kyprianou N, Rangnekar VM, Horbinski C. The Tumor Suppressor Prostate Apoptosis Response-4 (Par-4) Is Regulated by Mutant IDH1 and Kills Glioma Stem Cells. *Acta Neuropathologica* (2014) 128(5):723–32. doi: 10.1007/s00401-014-1334-7
8. Jagtap JC, Parveen D, Shah RD, Desai A, Bhosale D, Chugh A, et al. Secretory Prostate Apoptosis Response (Par)-4 Sensitizes Multicellular Spheroids (MCS) of Glioblastoma Multiforme Cells to Tamoxifen-Induced Cell Death. *FEBS Open Bio* (2015) 5:8–19. doi: 10.1016/j.fob.2014.11.005
9. García-Cao I, Duran A, Collado M, Carrascosa MJ, Martín-Caballero J, Flores JM, et al. Tumour-Suppression Activity of the Proapoptotic Regulator Par4. *EMBO Rep* (2005) 6(6):577–83. doi: 10.1038/sj.embor.7400421
10. Zhao Y, Burikhanov R, Qiu S, Lele SM, Darrell Jennings C, Bondada S, et al. Cancer Resistance in Transgenic Mice Expressing the SAC Module of Par-4. *Cancer Res* (2007) 67(19):9276–85. doi: 10.1158/0008-5472.CAN-07-2124
11. El-Guendy N, Zhao Y, Gurumurthy S, Burikhanov R, Rangnekar VM. Identification of a Unique Core Domain of Par-4 Sufficient for Selective Apoptosis Induction in Cancer Cells. *Mol Cell Biol* (2003) 23(16):5516–25. doi: 10.1128/mcb.23.16.5516-5525.2003
12. Burikhanov R, Hebbar N, Noothi SK, Shukla N, Sledziona J, Araujo N, et al. Chloroquine-Inducible Par-4 Secretion Is Essential for Tumor Cell Apoptosis and Inhibition of Metastasis. *Cell Rep* (2017) 18(2):508-19. doi: 10.1016/j.celrep.2016.12.051
13. Burikhanov R, Zhao Y, Goswami A, Qiu S, Schwarze SR, Rangnekar VM. The Tumor Suppressor Par-4 Activates an Extrinsic Pathway for Apoptosis. *Cell* (2009) 138(2):377–88. doi: 10.1016/j.cell.2009.05.022
14. Chakraborty M, Qiu SG, Vasudevan KM, Rangnekar VM. Par-4 Drives Trafficking and Activation of Fas and Fasl to Induce Prostate Cancer Cell Apoptosis and Tumor Regression. *Cancer Res* (2001) 61(19):7255–63.
15. Fei P, Bernhard EJ, El-Deiry WS. Tissue-Specific Induction of P53 Targets. *Cancer Res* (2002) 62(24):7316 LP – 7327.
16. Christophorou MA, Martin-Zanca D, Soucek L, Lawlor ER, Brown-Swigart L, Verschuren EW, et al. Temporal Dissection of P53 Function *in Vitro* and *in Vivo*. *Nat Genet* (2005) 37(7):718–26. doi: 10.1038/ng1572
17. Prokesch A, Graef FA, Madl T, Kahlhofer J, Heidenreich S, Schumann A, et al. Liver P53 Is Stabilized Upon Starvation and Required for Amino Acid Catabolism and Gluconeogenesis. *FASEB Journal: Off Publ Fed Am Societies Exp Biol* (2017) 31(2):732–42. doi: 10.1096/fj.201600845R
18. Gonzalez-Rellan MJ, Fondevila MF, Fernandez U, Rodríguez A, Varela-Rey M, Veyrat-Durebex C, et al. O-GlcNAcylated P53 in the Liver Modulates Hepatic Glucose Production. *Nat Commun* (2021) 12(1):5068-88. doi: 10.1038/s41467-021-25390-0
19. Hsu IR, Kim SP, Kabir M, Bergman RN. Metabolic Syndrome, Hyperinsulinemia, and Cancer. *Am J Clin Nutr* (2007) 86(3):867S–71S. doi: 10.1093/ajcn/86.3.867S
20. Pi-Sunyer X. The Medical Risks of Obesity. *Postgraduate Med* (2009) 121 (6):21–33. doi: 10.3810/pgm.2009.11.2074
21. Khandekar MJ, Cohen P, Spiegelman BM. Molecular Mechanisms of Cancer Development in Obesity. *Nat Rev Cancer* (2011) 11(12):886–95. doi: 10.1038/nrc3174
22. Hefetz-Sela S, Scherer PE. Adipocytes: Impact on Tumor Growth and Potential Sites for Therapeutic Intervention. *Pharmacol Ther* (2013) 138 (2):197–210. doi: 10.1016/j.pharmthera.2013.01.008
23. González-Muniesa P, Mártinez-González M-A, Hu FB, Després J-P, Matsuzawa Y, Loos RJF, et al. Obesity. *Nat Rev Dis Primers* (2017) 3 (1):170345. doi: 10.1038/nrdp.2017.34
24. Walton RG, Finlin BS, Mula J, Long DE, Zhu B, Fry CS, et al. Insulin-Resistant Subjects Have Normal Angiogenic Response to Aerobic Exercise Training in Skeletal Muscle, But Not in Adipose Tissue. *Physiol Rep* (2015) 3(6):12415-29. doi: 10.14814/phy2.12415
25. Spencer M, Finlin BS, Unal R, Zhu B, Morris AJ, Shipp LR, et al. Omega-3 Fatty Acids Reduce Adipose Tissue Macrophages in Human Subjects With Insulin Resistance. *Diabetes* (2013) 62(5):1709–17. doi: 10.2337/db12-1042
26. Burikhanov R, Shrestha-Bhattarai T, Hebbar N, Qiu S, Zhao Y, Zambetti GP, et al. Paracrine Apoptotic Effect of P53 Mediated by Tumor Suppressor Par-4. *Cell Rep* (2014) 6(2):271–77. doi: 10.1016/j.celrep.2013.12.020
27. Fan JD, Wagner BL, McDonnell DP. Identification of the Sequences Within the Human Complement 3 Promoter Required for Estrogen Responsiveness Provides Insight Into the Mechanism of Tamoxifen Mixed Agonist Activity. *Mol Endocrinol (Baltimore Md)* (1996) 10(12):1605–16. doi: 10.1210/mend.10.12.8961270
28. el-Deiry WS, Tokino T, Velculescu VE, Levy DB, Parsons R, Trent JM, et al. WAF1, a Potential Mediator of P53 Tumor Suppression. *Cell* (1993) 75 (4):817–25. doi: 10.1016/0092-8674(93)90500-p
29. Li J, Song J, Zaytseva YY, Liu Y, Rychahou P, Jiang K, et al. An Obligatory Role for Neurotensin in High-Fat-Diet-Induced Obesity. *Nature* (2016) 533 (7603):411–15. doi: 10.1038/nature17662
30. Muir LA, Neeley CK, Meyer KA, Baker NA, Brosius AM, Washabaugh AR, et al. Adipose Tissue Fibrosis, Hypertrophy, and Hyperplasia: Correlations With Diabetes in Human Obesity. *Obes (Silver Spring Md.)* (2016) 24(3):597–605. doi: 10.1002/oby.21377
31. Pedersen SD. Metabolic Complications of Obesity. *Best Pract Res Clin Endocrinol Metab* (2013) 27(2):179–93. doi: 10.1016/j.beem.2013.02.004
32. Berglund G, Elmstähl S, Janzon L, Larsson SA. The Malmö Diet and Cancer Study. Design and Feasibility. *J Intern Med* (1993); 233:45– 51. doi: 10.1111/j.1365-2796.1993.tb00647.x
33. Feingold KR. *Introduction to Lipids and Lipoproteins*. In: Feingold KR, Anawalt B, Boyce A, Chrousos G, de Herder WW, Dhatariya K, et al. editors. MDText.com, Inc, South Dartmouth, MA (2020-2021).

34. Mansbach CM, Siddiqi SA. The Biogenesis of Chylomicrons. *Annu Rev Physiol* (2010) 72:315–33. doi: 10.1146/annurev-physiol-021909-135801
35. Lo C-M, Nordskog BK, Nauli AM, Zheng S, Vonlehmden SB, Yang Q, et al. Why Does the Gut Choose Apolipoprotein B48 But Not B100 for Chylomicron Formation. *Am J Physiol Gastrointestinal Liver Physiol* (2008) 294(1):G344–52. doi: 10.1152/ajpgi.00123.2007
36. Baldo A, Sniderman AD, St-Luce S, Avramoglu RK, Maslowska M, Hoang B, et al. The Adipsin-Acylation Stimulating Protein System and Regulation of Intracellular Triglyceride Synthesis. *J Clin Invest* (1993) 92(3):1543–47. doi: 10.1172/JCI116733
37. Cianflone K, Xia Z, Ying Chen L. Critical Review of Acylation-Stimulating Protein Physiology in Humans and Rodents. *Biochim Biophys Acta* (2003) 1609(2):127–43. doi: 10.1016/s0005-2736(02)00686-7
38. Faraj M, Sniderman AD, Cianflone K. Enhances in Situ Lipoprotein Lipase Activity by Increasing Fatty Acid Trapping in Adipocytes. *J Lipid Res* (2004) 45(4):657–65. doi: 10.1194/jlr.M300299-JLR200
39. Preiss-Landl K, Zimmermann R, Hämmerle G, Zechner R. Lipoprotein Lipase: The Regulation of Tissue Specific Expression and Its Role in Lipid and Energy Metabolism. *Curr Opin Lipidol* (2002) 13(5):471–81. doi: 10.1097/00041433-200210000-00002
40. Mead JR, Irvine SA, Ramji DP. Lipoprotein Lipase: Structure, Function, Regulation, and Role in Disease. *J Mol Med (Berlin Germany)* (2002) 80 (12):753–69. doi: 10.1007/s00109-002-0384-9
41. Johnstone RW, See RH, Sells SF, Wang J, Muthukkumar S, Englert C, et al. A Novel Repressor, Par-4, Modulates Transcription and Growth Suppression Functions of the Wilms' Tumor Suppressor Wt1. *Mol Cell Biol* (1996) 16 (12):6945–56. doi: 10.1128/mcb.16.12.6945
42. Cheema SK, Mishra SK, Rangnekar VM, Tari AM, Kumar R, Lopez-Berestein G. Par-4 Transcriptionally Regulates Bcl-2 Through a WT1-Binding Site on the Bcl-2 Promoter. *J Biol Chem* (2003) 278(22):19995–5. doi: 10.1074/jbc.M205865200
43. Gao S, Wang H, Lee P, Melamed J, Li CX, Zhang F, et al. Androgen Receptor and Prostate Apoptosis Response Factor-4 Target the C-FLIP Gene to Determine Survival and Apoptosis in the Prostate Gland. *J Mol Endocrinol* (2006) 36(3):463–83. doi: 10.1677/jme.1.01991
44. Kung C-P, Basu S, Murphy ME. A Link Between TP53 Polymorphisms and Metabolism. *Mol Cell Oncol* (2016) 3(4):e1173769. doi: 10.1080/23723556.2016.1173769
45. Kung C-P, Leu JI-J, Basu S, Khaku S, Anokye-Danso F, Liu Q, et al. The P72R Polymorphism of P53 Predisposes to Obesity and Metabolic Dysfunction. *Cell Rep* (2016) 14(10):2413–255. doi: 10.1016/j.celrep.2016.02.037
46. Krstic J, Reinisch I, Schupp M, Schulz TJ, Prokesch A. P53 Functions in Adipose Tissue Metabolism and Homeostasis. *Int J Mol Sci* (2018) 19(9):2622-42. doi: 10.3390/ijms19092622
47. Fan W, Boston BA, Kesterson RA, Hruby VJ, Cone RD. Role of Melanocortinergic Neurons in Feeding and the Agouti Obesity Syndrome. *Nature* (1997) 385(6612):165–68. doi: 10.1038/385165a0
48. Godlewski G, Jourdan T, Szanda G, Tam J, Cinar R, Harvey-White J, et al. Mice Lacking GPR3 Receptors Display Late-Onset Obese Phenotype Due to Impaired Thermogenic Function in Brown Adipose Tissue. *Sci Rep* (2015) 5 (October):14953. doi: 10.1038/srep14953
49. Lutz TA, Woods SC. Overview of Animal Models of Obesity. *Curr Protoc Pharmacol* (2012) Chapter 5(September):Unit5.61. doi: 10.1002/0471141755.ph0561s58
50. Yasruel Z, Cianflone K, Sniderman AD, Rosenbloom M, Walsh M, Rodriguez MA. Effect of Acylation Stimulating Protein on the Triacylglycerol Synthetic Pathway of Human Adipose Tissue. *Lipids* (1991) 26(7):495–99. doi: 10.1007/BF02536592
51. Cui W, Paglialunga S, Kalant D, Lu H, Roy C, Laplante M, et al. Acylation-Stimulating Protein/C5L2-Neutralizing Antibodies Alter Triglyceride Metabolism *in Vitro* and *in Vivo*. *Am J Physiol Endocrinol Metab* (2007) 293(6):E1482–91. doi: 10.1152/ajpendo.00565.2006
52. Paglialunga S, Fisette A, Munkonda M, Gao Y, Richard D, Cianflone K. The Effects of Acylation Stimulating Protein Supplementation VS Antibody Neutralization on Energy Expenditure in Wildtype Mice. *BMC Physiol* (2010) 10(April):4. doi: 10.1186/1472-6793-10-4
53. Xia Z, Sniderman AD, Cianflone K. Acylation-Stimulating Protein (ASP) Deficiency Induces Obesity Resistance and Increased Energy Expenditure in Ob/Ob Mice. *J Biol Chem* (2002) 277(48):45874–79. doi: 10.1074/jbc.M207281200
54. Maslowska M, Legakis H, Assadi F, Cianflone K. Targeting the Signaling Pathway of Acylation Stimulating Protein. *J Lipid Res* (2006) 47(3):643–52. doi: 10.1194/jlr.M500500-JLR200
55. Wang HB, Ricklin D, Lambris JD. Complement-Activation Fragment C4a Mediates Effector Functions by Binding as Untethered Agonist to Protease-Activated Receptors 1 and 4. *Proc Natl Acad Sci* (2017) 114(41):10948–53. doi: 10.1073/pnas.1707364114
56. Manfredi JJ. The Mdm2-P53 Relationship Evolves: Mdm2 Swings Both Ways as an Oncogene and a Tumor Suppressor. *Genes Dev* (2010) 24(15):1580–89. doi: 10.1101/gad.1941710
57. Naaz A, Holsberger DR, Iwamoto GA, Nelson A, Kiyokawa H, Cooke PS. Loss of Cyclin-Dependent Kinase Inhibitors Produces Adipocyte Hyperplasia and Obesity. *FASEB J: Off Publ Fed Am Societies Exp Biol* (2004) 18(15):1925–27. doi: 10.1096/fj.04-2631fje
58. Inoue N, Yahagi N, Yamamoto T, Ishikawa M, Watanabe K, Matsuzaka T, et al. Cyclin-Dependent Kinase Inhibitor, P21WAF1/CIP1, Is Involved in Adipocyte Differentiation and Hypertrophy, Linking to Obesity, and Insulin Resistance. *J Biol Chem* (2008) 283(30):21220–29. doi: 10.1074/jbc.M801824200
59. Kim SM, Lun M, Wang M, Senyo SE, Guillermier C, Patwari P, et al. Loss of White Adipose Hyperplastic Potential Is Associated With Enhanced Susceptibility to Insulin Resistance. *Cell Metab* (2014) 20(6):1049–58. doi: 10.1016/j.cmet.2014.10.010
60. Rydén M, Andersson DP, Bergström IB, Arner P. Adipose Tissue and Metabolic Alterations: Regional Differences in Fat Cell Size and Number Matter, But Differently: A Cross-Sectional Study. *J Clin Endocrinol Metab* (2014) 99(10):E1870–6. doi: 10.1210/jc.2014-1526
61. Xu H, Barnes GT, Yang Q, Tan G, Yang D, Chou CJ, et al. Chronic Inflammation in Fat Plays a Crucial Role in the Development of Obesity-Related Insulin Resistance. *J Clin Invest* (2003) 112(12):1821–30. doi: 10.1172/JCI19451

Conflict of Interest: Authors TS-B and BT are employed by Loxo Oncology. VR is owner of a start-up company Parcure, LLC, in Lexington, KY, USA.

The remaining authors declare that the research was conducted in the absence of any commercial or financial relationships that could be construed as a potential conflict of interest.

Publisher's Note: All claims expressed in this article are solely those of the authors and do not necessarily represent those of their affiliated organizations, or those of the publisher, the editors and the reviewers. Any product that may be evaluated in this article, or claim that may be made by its manufacturer, is not guaranteed or endorsed by the publisher.

frontiers | Frontiers in Oncology

ORIGINAL RESEARCH
published: 08 April 2022
doi: 10.3389/fonc.2022.860339

Lapatinib Suppresses HER2-Overexpressed Cholangiocarcinoma and Overcomes ABCB1– Mediated Gemcitabine Chemoresistance

Zhiqing Bai[1†], Zhiying Guo[2†], Jiaxing Liu[3], Yu-Ann Chen[2], Qian Lu[2], Ping Zhang[1], Lili Hong[4], Yunfang Wang[2] and Jiahong Dong[1,2*]*

[1] Department of Hepatobiliary and Pancreatic Surgery, The First Hospital of Jilin University, Changchun, China, [2] Hepatopancreatobiliary Center, Beijing Tsinghua Changgung Hospital, School of Clinical Medicine, Tsinghua University, Beijing, China, [3] State Key Laboratory of Bioactive Substance and Function of Natural Medicines, Institute of Materia Medica, Chinese Academy of Medical Sciences and Peking Union Medical College, Beijing, China, [4] Institute of Materia Medica, Chinese Academy of Medical Sciences & Peking Union Medical College (State Key Laboratory of Bioactive Substance and Function of Natural Medicines & NHC Key Laboratory of Biosynthesis of Natural Products), Beijing, China

OPEN ACCESS

Edited by:
Conghui Yao,
Harvard Medical School, United States

Reviewed by:
Joan Garrett,
University of Cincinnati, United States
Jun Ren,
Shanghai Pudong Hospital, China

***Correspondence:**
Jiahong Dong
dongjiahong@mail.tsinghua.edu.cn
Yunfang Wang
wangyf2011126@126.com

[†]These authors have contributed equally to this work

Specialty section:
This article was submitted to Cancer Metabolism, a section of the journal Frontiers in Oncology

Received: *22 January 2022*
Accepted: *22 March 2022*
Published: *08 April 2022*

Citation:
Bai Z, Guo Z, Liu J, Chen Y-A, Lu Q, Zhang P, Hong L, Wang Y and Dong J (2022) Lapatinib Suppresses HER2-Overexpressed Cholangiocarcinoma and Overcomes ABCB1– Mediated Gemcitabine Chemoresistance. Front. Oncol. 12:860339. doi: 10.3389/fonc.2022.860339

Background: Recent breakthroughs in cholangiocarcinoma (CCA) genomics have led to the discovery of many unique identifying mutations, of which HER2 has been found to be overexpressed specifically in cases of extrahepatic CCA. However, whether or not lapatinib (an oral tyrosine kinase inhibitor selective for inhibition of HER2), or a combination of lapatinib and gemcitabine, exerts inhibitory effects on HER2-overexpressed CCA is still unclear.

Methods: The effect of lapatinib and a lapatinib-gemcitabine combination treatment on CCA was determined using organoid and cell line models. Cell cycle arrest, apoptosis and proteins involving HER2-dependent downstream signaling pathways were analyzed to assess the effect of lapatinib on $HER2^+$ CCA. The synergistic effect of lapatinib and gemcitabine was interpreted by docking analysis, ABCB1-associated ATPase assay, rhodamine transport assay and LC-MS/MS analyses.

Results: dFdCTP, the active metabolite of gemcitabine, is proved to be the substrate of ABCB1 by docking analysis and ATPase assay. The upregulation of ABCB1 after gemcitabine treatment accounts for the resistance of gemcitabine. Lapatinib exerts a dual effect on HER2-overexpressed CCA, suppressing the growth of CCA cells by inhibiting HER2 and HER2-dependent downstream signaling pathways while inhibiting ABCB1 transporter function, allowing for the accumulation of active gemcitabine metabolites within cells.

Conclusions: Our data demonstrates that lapatinib can not only inhibit growth of CCA overexpressing HER2, but can also circumvent ABCB1-mediated chemoresistance after gemcitabine treatment. As such, this provides a preclinical rationale basis for further clinical investigation into the effectiveness of a combination treatment of lapatinib with gemcitabine in HER2-overexpressed CCA.

Keywords: lapatinib, cholangiocarcinoma, HER2, ABCB1, gemcitabine, chemoresistance

INTRODUCTION

Cholangiocarcinoma (CCA) is the second most commonly occurring hepatobiliary malignancy after hepatocellular carcinoma (HCC) (1). Because most patients with early stage CCA are asymptomatic and often only diagnosed at advanced stages, this results in an overall dismal prognosis (2, 3). CCA can be categorized into two main types: intrahepatic CCA (iCCA), originating within the hepatic parenchyma, and pCCA/dCCA, which can be further classified into either perihilar or distal tumors (4).2',2'-difluoro-2'-deoxycytidine (gemcitabine), is a fundamental component of the chemotherapeutic agents used in the treatment of CCA. However, gemcitabine-based chemotherapies are limited in their ability to provide therapeutic effects for patients due in part to the presence of complex mechanisms of chemoresistance (MOC) (5–7). ATP-binding cassette (ABC) transporters are one the mechanisms of MOC, actively helping tumor cells export intracellularly active agents across the cell membrane, greatly impairing the cytotoxic effects. Furthermore, the ATP-binding cassette subfamily B member 1 (ABCB1) gene encoded protein ABCB1 (also known as P-glycoprotein or MDR1), has been previously reported to be highly expressed in CCA, is a potential key contributing factor to the degree of drug refractory (8, 9). As such, better strategies for improving the clinical outcomes of gemcitabine treatments and the discovery of novel targeted molecular therapy still urgently need to be developed.

The independent characterization of CCA at the genomic, epigenetic and molecular level helped to ascertain pathogenesis mechanisms, while shedding new light on novel therapeutic options and assisting with precision medicine innovation. One of the most clinically significant breakthroughs of cholangiocarcinoma genomics is the discovery of frequent IDH and FGFR2 mutations in iCCA, the inhibitors of which are currently being evaluated with promising results in clinical trials (10–12). Unlike iCCA, eCCA is found to be more likely to harbor either mutations or amplifications in TP53, HER2/3, ARID1B, etc. (13, 14). When considering all the results from the different studies (**Table S1**), the frequency of HER2 amplification is found to account for approximately 1.3%-23% of all biliary tract carcinoma patient populations. Recent developments in CCA molecular biology has brought more attention to using HER2 as a potential target. An article by Javle et al. (15)reported that a HER2 blockade might be a promising treatment strategy for CCA patients with HER2-overexpression. In the NCT02091141 ("My Pathway") phase 2 prospective study, 2 of 7 patients with $HER2^+$ pCCA/dCCA achieved a partial response after treatment with trastuzumab and pertuzumab (16).

Lapatinib, an oral tyrosine kinase inhibitor selective for inhibition of HER1, HER2, and HER1/HER2-dependent downstream signaling pathways (17), has been widely applied in successfully treating HER2-positive breast, colorectal, and non-small-cell lung cancers (18, 19). Current data from several studies examining the effectiveness of HER2 directed therapy in advanced CCA cases are contradictory and thus, inconclusive. Several of the early phase-2 clinical studies involving use of lapatinib (20) or afatinib (21) have had disappointing results, but these experimental therapies focused mainly on patients harboring EGFR mutations rather than those of HER2. Upon further assessment using immunohistochemical staining, fluorescence *in situ* hybridization and sequencing found that none of the previous cases were those of HER2-overexpression, and therefore it cannot be definitively concluded that lapatinib is ineffective at treating $HER2^+$ CCA. We therefore needed to assess whether or not lapatinib can inhibit the growth of $HER2^+$ CCA. Moreover, as emerging evidence suggests that many TKIs, including lapatinib have been found to be able to interact with ABCB1 and behave as an ABCB1 inhibitor (22, 23), we believed that TKIs may have important implications in inhibiting ABC transporters and overcoming drug resistance, providing a new opportunity for use in combination with conventional chemotherapies (24). As a result, we investigated the potential synergistic repressive influences lapatinib has on the viability of $HER2^+$ CCA cells when combined with gemcitabine.

In this article, we show that gemcitabine upregulates ABCB1 while dFdCTP, an active metabolite of gemcitabine, is the main substrate of ABCB1 and can be expelled from tumor cells. Increasing levels of ABCB1 expression reduce the intracellular drug concentration, resulting in gemcitabine-resistance. Because lapatinib exerts anti-tumor effects on HER2-overexpressed CCA cells while simultaneously overcoming ABCB1–mediated chemoresistance, this proves that a lapatinib-gemcitabine combination-based therapy can be significantly more effective at treating HER2-positive CCA cases.

MATERIALS AND METHODS

Establishment of Organoids Using CCA Specimens Obtained From Patients

For organoid cultures, primary tumor tissues were obtained from patients who underwent radical resection of cholangiocarcinoma, as confirmed by pathological examination at the Beijing Tsinghua Changgung Hospital (Beijing, China). This study was approved by the Ethics Committee of the Beijing Tsinghua Changgung Hospital, and informed consent was obtained prior to surgery. Information about the tumor tissue specimens obtained from patients is stated in **Table S2**.

Fresh tissue samples (not exceeding 4 hours from isolation) were minced into indistinguishable pieces using a surgical scalpel and then incubated in a prewarmed digestion solution at 37°C. The digestion solution is composed of Collagenase IV (Sigma-Aldrich C5138), at the concentration of 1 mg/ml. The overall digestion time lasted no longer than 90 minutes, with extra care being taken not to overdigest the sample. After incubation, cells were filtered through a 70-μm filter and resuspended in Matrigel (Corning 354230) or BME-002 (R&D Biotech) and then carefully administered one droplet at a time on a prewarmed ultra-low attachment cell culture plate (Corning). The culture medium is composed of Advanced DMEM/F12 (Gibco) supplemented with 0.1% Bovine Serum Albumin (Sigma) 1×Glutamax, 10 mM HEPES, 1×penicillin/streptomycin, 1×N2 supplement, 1×B27 supplement, 50 ng/mL recombinant human EGF (all from Life Technologies), 1.25 mM N-acetylcysteine, 10 nM [Leu15]-

gastrin I human, 10 mM nicotinamide (all from Sigma), 500 ng/ml R-Spondin 1, 100 ng/ml Wnt3a (all from R&D), 5 μM A83-01, 10 μM forskolin (all from Tocris), 100 ng/ml recombinant human FGF10, 25 ng/ml recombinant human HGF, 25 ng/ml Noggin(all from PeproTech). For the first six days of culture, 10 μM ROCK inhibitor Y-27632 (Tocris) was included. The medium was changed every 2-3 days and cells were then passaged either through mechanical disruption or TrypLE digestion every 10–14 days with a 1:5 split ratio.

HER2 Expression Evaluated Using Immunohistochemistry and FISH

Immunohistochemical overexpression of HER-2 was evaluated using the Vectastain ABC kit (Vector Labs) following the manufacturer's protocol and HER2 antibodies (4290, Cell Signaling Technology). Results were interpreted according to current criteria used for gastric cancer (25).Briefly, HER2+++ represents strong complete, basolateral or lateral membranous reactivity in ≥10% of tumor cells; HER2 amplification was evaluated by fluorescence *in situ* hybridization (FISH) probe sets (LBP medicine science and technology) and FISH positivity was defined by the HER2:CEP17 ratio≥2.0 (26).

cBioPortal

The cBioPortal for Cancer Genomics (http://www.cbioportal.org) provides multidimensional resource of cancer genomics data (27). We investigated the copy number alterations (CNA) in 334 cases with copy number alternation data diagnosed as bile tract carcinoma.

Cell Lines and Cell Cultures

Three cholangiocarcinoma cell lines (RBE, HUCCT-1 and FRH-0201) were purchased from Yaji Co (Shanghai, China). Breast cancer cell lines were purchased from American Type Culture Collection (ATCC). These cell lines were maintained in Dulbecco's modified Eagle's medium supplemented with 10% fetal bovine serum, streptomycin (100 μg/mL) and penicillin (100 U/mL).

Cell Viability Assay and Drug Combination Study

The cytotoxicity of the drug treatments was evaluated using the CellTiter-Glo Luminescent Cell Viability Assay (Promega) according to manufacturer guidelines. Briefly, cells were seeded in 96-well plates at the appropriate density per well. Cell viability was assessed after being treated with DMSO, lapatinib, gemcitabine, or both drugs in combination for two days. Before the experiment, equilibrate the plate, its contents and celltiter reagent to room temperature. Mix the CellTiter-Glo Buffer with CellTiter-Glo Substrate, Add a volume of it equal to the volume of cell culture medium in each well. Mix, stabilize and record the luminescence. Organoid viability was determined by following a drug-screening method previously established by Hans Clevers (28). Split organoids into single cells 2 days before the start of the screening. Initiate the experiment by filter the organoid using a 70-μm cell strain. Count and resuspend them in organoid medium containing 5% (vol/vol) BME. Dispense these organoids into drug-screening plates and add chemotherapeutics into the culture plate. Organoids will be exposed to drugs for 4 days. The fraction affected by the dose (FA) is defined as the fraction affected by the dose, and combination index CI value was computed using Chou–Talalay means (29), where CI <1, = 1, and >1 indicated synergism, additivity, and antagonism, respectively.

Establishment of Gemcitabine-Resistant Cells

Initially, FRH-0201 cells were cultured in a 1×IC50 gemcitabine supplemented medium for the duration of 3 days. Once the surviving cells reached an 80% confluency and exhibited stable proliferation after passaging, they were exposed to an increasing gemcitabine concentration gradient of 2 μM, 4 μM, 6 μM, 8 μM until a final concentration 20μM. Gemcitabine-resistant CCA cell line FRH0201-GEM was achieved when cells displayed stable growth and continued passaging in the presence of the drug at 20 μM.

Western Blotting Analysis

Total protein was obtained by lysing cells with Laemmli Sample Buffer (Biorad) and the membrane protein was extracted according to the manufacturer's instructions from the Membrane Protein Extraction Kit (Beyotime). Cleared lysates were resolved by SDS-PAGE, transferred to PVDF membrane and probed with specified antibodies. The following primary antibodies were purchased from Cell Signaling Technology: phospho-Akt(4060), Akt(4691), phosphop-p44/42 MAPK(4370), p44/42 MAPK(4695), HER2 (4290), phospho-HER2(2249), Cyclin D1(55506), p27 ^{Kip1}(3686), c-myc(5605), ABCB1(13978), Na,K-ATPase α1 (23565, control for membrane proteins), and GAPDH(5174, control for total proteins).

Immunocytofluorescense and Multiplex Immunofluorescence

Tissues and organoids were formalin-fixed, paraffin-embedded and sectioned (4 μm) for histological examination. Sections were first stained with hematoxylin–eosin (H&E). Multiplex immunofluorescence was performed with TSA-dendron-fluorophores (NEON 5-color Allround Discovery Kit for FFPE, Histova Biotechnology, NEFP5100) according to the manufacturer's protocol. The 4 μm paraffin sections were first deparaffinized, rehydrated, and then the endogenous peroxidase was quenched followed by the addition of a blocking reagent. Then sections were incubated with primary antibodies and corresponding secondary antibodies (Zhongshan Golden Bridge) and stained with TSA-dendron-fluorophores. The primary and secondary antibodies were thoroughly eliminated by microwaving the slides in retrieval/elution buffer. With regard to immunocytofluorescense, cells were fixed after treatment in a 4% formaldehyde and blocked with horse serum. After that, cells were incubated with primary antibody followed by Alexa Fluor 488 conjugated secondary antibody (Thermo Fisher Scientific). Slices were counterstained with DAPI. The following primary antibodies were used: MUC-1 (ab109185), CK7(ab68459) (from Abcam), HER-2 (4290, CST).

Real-Time Quantitative PCR

The total RNA was extracted from organoids or cell lines using the Trizol® reagent (Invitrogen) and cDNA was synthesized using the ReverTra Ace® qPCR RT Master Mix with gDNA Remover (Toyobo life science). Real-time qPCR was performed using the THUNDERBIRD® SYBR® qPCR Mix (Toyobo life science). Relative gene-expression levels were calculated using the delta–delta CT method. A total of three biological replicates were performed. The primer sequences are as follows: 5'-TTGCT GCTTACATTCAGGTTTCA-3' and 5'-AGCCTATCTCCT GTCGCATTA-3' for the ABCB1 gene, 5'-TGTGGGCATC AATGGATTTGG-3' and 5'-ACACCATGTATTCCGGG TCAAT-3' for the GAPDH gene.

Docking Analysis

All docking analyses were performed using MOE software (Molecular Operating Environment, Chemical Computing Group, Montreal, Canada). The ABCB1 protein model was retrieved from the DeepMind algorithm AlphaFold (entry: P08183), based on deep neural network learning (30). The ABCB1 model was then refined through energy minimization, under the parameters set to AMBER10: EHT force field and the active sites of the ABCB1 protein were predicted using the "Site Finder" feature. The structure of dFdC, dFdU, dFdCTP, lapatinib and verapamil were downloaded from the ZINC database (31) and structural refinement and energy minimization were executed. The drugs were docked into the active site of protein using the DOCK module of the MOE algorithm separately (32). Finally, "Triangle Matcher, London dG" and "Induced fit algorithm, GBVI-WSA dG" parameters were chosen respectively as the placement and refinement methods for the docking (33).

Cell Cycle and Apoptosis Analysis

FRH-0201 cells were seeded at 2×10^5 cells in a 6 cm cell culture dish and cultured overnight, after which the cells were exposed to one of three different treatments: varying concentrations of lapatinib(0, 1, 5, 20 μM) at 48 hours, constant concentration exposure (20 μM) for different time durations (0, 12, 24, 48 hours) and a combination of a varying concentrations of lapatinib(0, 1, 5, 10 μM) and a constant concentration of gemcitabine(0.5 μM) over a duration of 48 hours. The cell cycle distribution was detected by staining DNA with propidium iodide (C1052 Beyotime), while apoptosis and necrosis were detected using an Annexin V-FITC staining kit (C1062 Beyotime). The cell cycle distribution and apoptosis were determined through flow cytometry (Beckman CytoFLEX).

Rhodamine Transport Assay

The organoids or cell lines were incubated with 2 μM Rhodamine 123 (MedChemExpress) at 37°C for 5 minutes and washed three times with the culture medium. Afterwards, cells were incubated in the culture medium with varying lapatinib concentrations at 37°C for 30 minutes. The cell lines were then analyzed by flow cytometry (Beckman CytoFLEX). The immunofluorescence of organoids was visualized using a confocal microscope (Olympus FV3000).

ATPase Assay

The ABCB1-associated ATPase activity was measured using the Pgp-Glo™ Assay Systems (Promega). Briefly, ABCB1 membranes were incubated with gradient concentrations of verapamil, lapatinib or dFdCTP on the 37°C heat block for 5 minutes. Then 10 μl of 25 mM MgATP were added into each well and incubated at 37°C for 100 minutes. Then the reaction was terminated by adding 50 μl ATP Detection Reagent into all wells. Luminescence was then read on a multi-detection microplate reader (Biotek).

LC-MS/MS Analysis

FRH-0201 and FRH0201-Gem cells were treated with a combination of a varying concentrations of lapatinib (0, 1, 5, 20 μM) and a constant concentration of gemcitabine (1 μM). Cells treated with 1 μM Gem + 5 μM Verapamil were set as the positive control. Cells were exposed to these drugs for 6 hours. To determine the concentration of intracellular dFdCTP, we employed LC-MS/MS. The cells were collected with 0.05% Trypsin-EDTA, and washed three times with cold PBS. Then the cells were counted and collected into 1.5 ml centrifuge tubes. Intracellular fluid was extracted by using a MeOH/H_2O (4:1) solvent. The standard linear calibration curve was established by diluting a 10 μg/mL standard stock solution into a concentration gradient. We performed LC-MS/MS analysis using AB Sciex Exion LCTMAD chromatography coupled with an electrospray ion source and AB Sciex QTRAP 6500 + mass spectrometry (AB SCIEX, USA). Samples were loaded onto an ACQUITY UPLC HSS T3 column (2.1×100mm, 1.7μm, Waters, USA) and eluted using a solution of 30 mM formic acid (phase A)/ acetonitrile containing 0.1% formic acid (phase B). The LC parameters were set as follows: column temperature, 50°C; flow rate, 0.35mL/min; injection volume, 2 μL. The dFdCTP was gradient eluted with phase A/phase B. Mass spectrometry data was acquired on the multiple reaction monitoring (MRM) positive mode, with the ion source temperature set at 550°C, ion source voltage at 4500, curtain gas as 35 psi, gas1 as 60 psi, gas2 as 60 psi, MRM transition as 504.2/326.4, declustering potential (DP) as 63V and collision energy as 31eV. Peak processing and integration were completed using SCIEX OS software (AB SCIEX).

Statistical Analysis

All statistic data were presented as the mean ± standard deviation (SD) of at least three independent experiments, and statistical analyses were performed with GraphPad Prism version 7.0. Significance was denoted as n.s. not significant, $^*p < 0.05$, $^{**}p < 0.01$, and $^{***}p < 0.001$.

RESULTS

HER2 Amplification Is Related to Dismal Prognosis in Biliary Tract Carcinoma

In order to investigate the amplification status of HER2 in patients with biliary tract carcinoma, HER2 copy number alternations (CNAs) in biliary tract cancer populations were analyzed, including a total of 329 patients CNA data using the cBioPortal tools from 3 studies:

Gallbladder Cancer (MSK, Cancer 2018), Cholangiocarcinoma (MSK, Clin Cancer Res 2018) and Cholangiocarcinoma (TCGA, Firehose Legacy) (**Figure S1A**). HER2 amplification was found in 14 out of 329 patients, accounting for 4% of total sample size and patients with HER2 amplification were found to have markedly shorter survival times than those with lower levels using a Kaplan-Meier plotter analysis (**Figure S1B**).

Patient-Derived CCA Organoids With HER2 Overexpression Are More Sensitive to Lapatinib

We obtained CCA tissue from patients who underwent radical resection of cholangiocarcinoma with informed consent. We acquired isolated CCA cells from tissue through mechanical disruption and collagenase digestion. Isolated cells were then embedded in Matrigel or BME drops and overlaid with CCA organoid culture medium (reference Methods for more detailed information). We successfully established 3 patient-derived organoid lines of CCA for stable, long-term proliferation (**Figure 1A**). Tissue of CC6062 was proved to be HER2-overexpressed (**Figures S1C, D**), while CC2196 and CC9630 was proved to be HER2-negative (**Figure 1C**). All the H&E-stained primary tissues were found to be that of adenocarcinoma with glandular and tubular structures surrounded by mesenchymal and inflammatory cells, while the organoids established from these tissues were found to be exclusively epithelial tissues with remarkably well-preserved tumor cell organization (**Figure 1B**). MUC-1 and CK7 were the classical molecular markers of CCA (34, 35). The primary tissue and organoids showed similar MUC-1 and CK7 staining patterns (**Figure 1C**), demonstrating that CCA organoids are able adequately to retain their primary tissue histopathological features. Additionally, we found that the original HER2 status of CCA was well maintained in organoid culture, as determined through immunofluorescence staining (**Figure 1C**). Because HER2 status was well retained in the patient-derived tumor organoids, we decided to further examine whether or not lapatinib exerts its growth inhibitory effects on HER2-overexpressed organoids. As shown in **Figure 2A**, both numbers and sizes of CC6062 organoids were drastically reduced after being treated by lapatinib. In contrast, treatment with lapatinib did not result in significant changes in CC2196 and CC9630 (**Figures 2B, C** and **Videos S1A, B, E-H**). Since it has been previously established that lapatinib inhibits both EGFR and HER2, we next examined the EGFR status of these 3 organoid lines. As shown in **Figure S4A**, both the tissue and organoid samples of the lapatinib-sensitive CC6062 were found to be EGFR negative, while those of CC2196 was proved to be EGFR-positive. This proves that lapatinib suppresses the growth of CCA organoids, most likely due to the blockade of the HER2 pathway.

CCA Cell Line With HER2 Overexpression Is More Sensitive to Lapatinib

Next, we examined the expression level of HER2 proteins in 3 different CCA cell lines. Two breast cancer cells (BCRA) whose HER2 protein expression levels have already been well investigated were set as the positive and negative controls: SK-BR-3 was used as the HER2 overexpression control and MCF-7 was set as the negative control. Both western blotting and immunofluorescence results suggest that the HER2 protein expression in FRH-0201 is very similar to that of SK-BR-3, but RBE and HUCCT-1 are not (**Figures 3A, B**). We examined the inhibitory effect of lapatinib on these five cell lines and the results show that lapatinib was able to suppress cell growth in a concentration-dependent manner more effectively in HER2-overexpressed CCA cell line FRH-0201, than in RBE and HUCCT-1 (**Figure 3C**). In addition, IC50 values of lapatinib in FRH-0201 were found to be on the same level as those in SK-BR-3 ($p > 0.05$). However, in RBE and HUCCT-1 these were significantly higher ($p < 0.001$), suggesting that HER2-overexpressed CCA cells are more sensitive to lapatinib (**Figure 3D**). At the same time, we assessed the EGFR status of FRH-0201, RBE and HUCCT-1 (**Figure S4B**). Both FRH-0201 and HUCCT-1 has higher EGFR expression. We used cetuximab (CTX), an EGFR inhibitor, in a side by side comparison. As shown in **Figure S4C**, 1μM CTX can inhibit the phosphorylation level of EGFR, however, this concentration of CTX has no inhibitory effect on FRH-0201(**Figure S4D**). This suggests that the inhibitory effect of lapatinib on FRH-0201, a cell line overexpressing both EGFR and HER2, is mainly achieved by inhibiting the HER2 pathway rather than the EGFR pathway.

Lapatinib Induces Cell Cycle Arrest and Apoptosis in FRH-0201 in a Concentration and Time- Dependent Manner

Having determined that lapatinib has a robust inhibitory effect on HER2-overexpressed organoids and cells lines, we analyzed its effects on the cell cycle and apoptosis in order to identify the underlying mechanism responsible for this inhibition. FRH-0201 was treated with lapatinib at the previously indicated concentration gradient (0, 1, 5 and 20μM) during a set period of 48 hours and at 20 μM in varying time durations (0,12, 24 and 48 hours). The percentage of FRH-0201 cells arrested in the G1 phase was significantly increased after being treated with lapatinib in a time and concentration-dependent manner (**Figures 3E, F** and **Figures S2A, C**). A down-regulation of c-myc was observed, consistent with the suppression of cyclin D1 and the induction of $p27^{Kip1}$ as determined by Western blot analysis (**Figures 3I, J**). Meanwhile, apoptotic cells increased drastically after being treated with lapatinib with increasing dose and time (**Figures 3G, H** and **Figures S2A, C**). HER2 and HER2-dependent downstream signaling pathways were inhibited after the treatment with lapatinib, as shown by a decreased level of phosphorylation of HER2 and its downstream proteins (**Figures 3K, L**). In conclusion, lapatinib results in definite reduction of p-HER2, p-ERK and p-Akt in HER2-overexpressed cholangiocarcinoma, and thus induces the G1 cell cycle arrest and apoptosis in a concentration and time-dependent manner (**Figure 3M**).

Lapatinib and Gemcitabine Synergistically Inhibit the Proliferation of $HER2^+$ CCA Cells *In- Vitro*

Because gemcitabine is one of the most significant first-line chemotherapeutic agents of CCA, we considered whether or not lapatinib has a synergistic repressive influence on the viability of $HER2^+$ CCA cells when combined with gemcitabine. The efficacy of

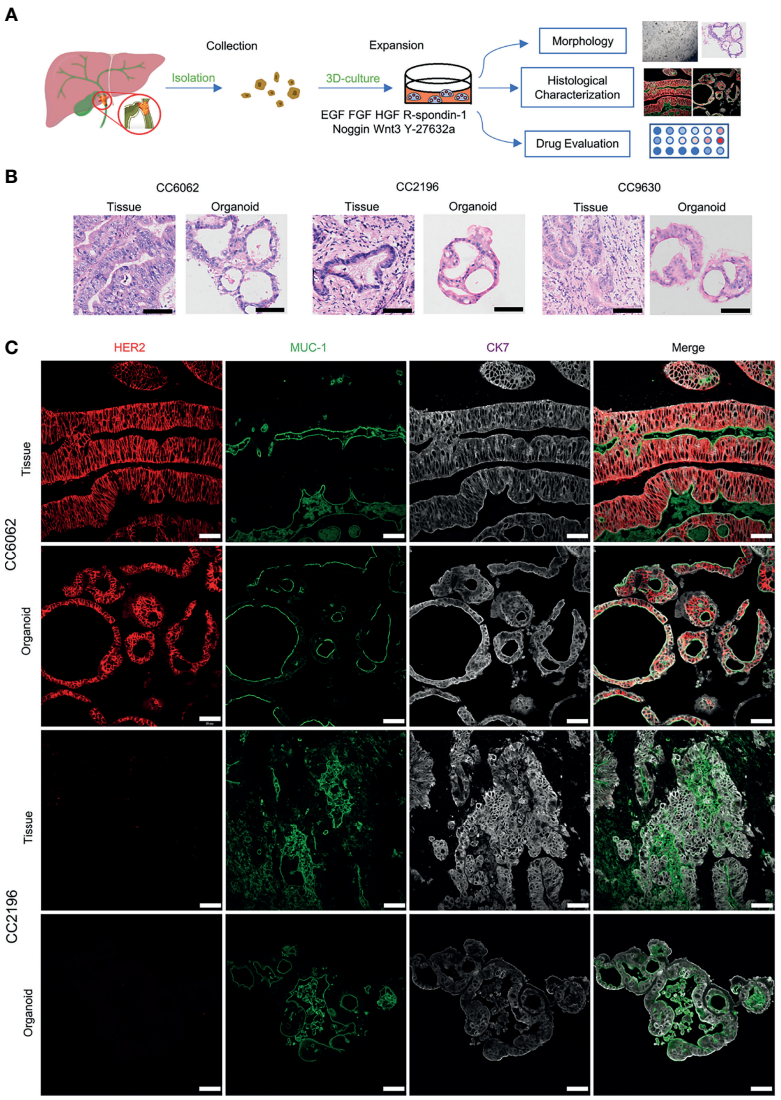

FIGURE 1 | Patient-derived CCA organoids recapitulate the histopathological features of the primary tumors. **(A)** A schematic representation of CCA organoids collection, processing and experimental designs. **(B)** H&E staining images of the CCA tissue specimens CC6062, CC2196, CC9630 and the derived organoids. Scale bar, 50 μm. **(C)** Multiplex immunofluorescence co-staining images of HER2 (red), MUC-1 (green), CK7 (grey) of primary clinical tissue (top row of each group) and organoids (bottom row of each group). Scale bar, 50 μm.

various concentrations of the combination of lapatinib and gemcitabine was assessed by determining the combination index (CI) which was calculated using the Chou -Talalay method. We observed that lapatinib and gemcitabine dual treatment resulted in stronger growth inhibition in FRH-0201 and CC6062 cells, and that the resulting CI values were consistently less than 1, suggesting that the combination of Lapa and Gem had an overall synergistic effect (**Figures 4A, C**). As shown in **Figure 4B** and **Videos S1A-D**, combination therapy led to higher inhibition of cell growth in CC6062. Further analysis revealed that the percentage of apoptotic and G1 arrested FRH-0201 cells were significantly increased in response to the combined treatments when compared with individual treatments with an increasing lapatinib concentration gradients. In particular, the proportion of apoptotic and G1 arrested cells treated with 10.0μM Lapa +0.5μM Gem 0.5μM corresponded the most to that of cells treated with 20μM Lapa (**Figures 4D, E** and **Figures S2A, B**). In other words, the lapatinib-gemcitabine combined treatment demonstrated a more robust anti-tumor effect in comparison with that of separate treatments.

Upregulation of ABCB1 Results in Chemoresistance in CCA After Gemcitabine Treatment

Next, we investigated the mechanism by which lapatinib synergistically inhibits the growth of CCA cells when combined

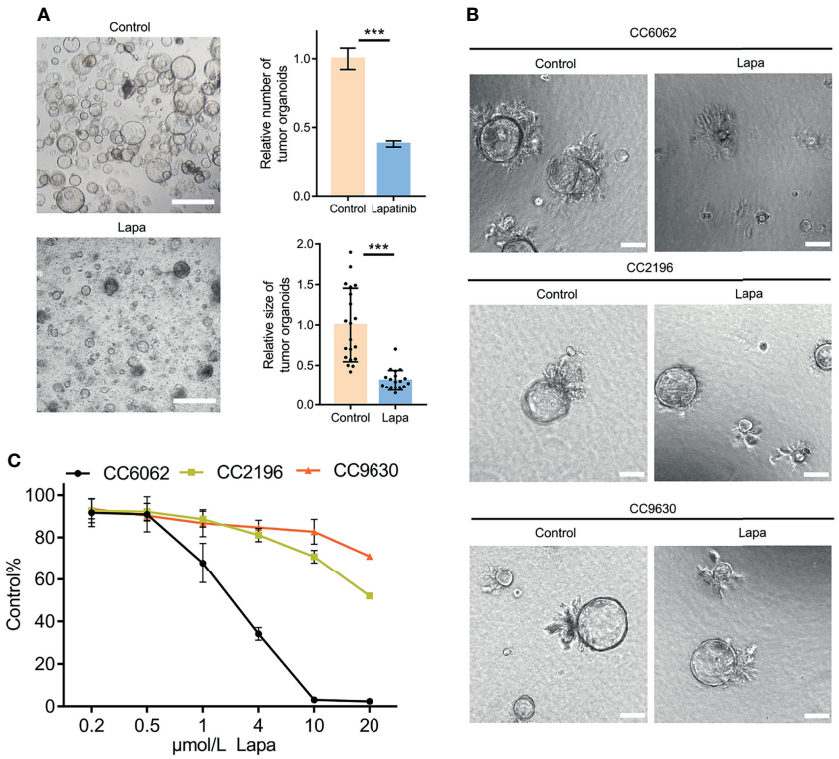

FIGURE 2 | Lapatinib exhibits a stronger inhibitory effect on the growth of HER2-overexpressed CCA patient-derived organoids. **(A)** Bright-field images of HER2-overexpressed CCA organoids treated with 5 μM lapatinib. Relative numbers (n = 3 biologically independent samples per group) and sizes (n =20 biologically independent organoids per group) of organoids were quantified as fold-change compared to control. Scale bar = 200 μm. **(B)** Bright-field images of CC6062, CC2196 and CC9630 treated with 5μM lapatinib (Lapa) compared to control. Scale bar, 20μm. **(C)** Growth inhibitory effect curves of lapatinib (Lapa) in patient-derived CCA organoids proved that CC6062 is more sensitive to lapatinib when compared to other CCA organoids. The data is expressed as the mean ± S.D., two-sided Student's t-test, ***$p < 0.001$.

with gemcitabine. Given that ABCB1 is one of the most important, complex mechanisms of chemoresistance (MOC), and many other chemotherapeutics have been proved to increase the expression of ABCB1 (36–41), we considered whether or not gemcitabine could cause the upregulation of ABCB1 and what specific effects lapatinib exerts on ABCB1. We initially established the gemcitabine-resistant CCA cell line, FRH0201-Gem. When we tested the cytotoxicity of gemcitabine comparing the primary and resistant cell lines, higher cellular viability was confirmed in FRH0201-Gem (**Figure 5A**). We can observe the different morphology between FRH-0201 and FRH0201-Gem (**Figure S5A**). Additionally, in the colony-forming assay, after treatment of 5μM gemcitabine, the colony sizes and number of colonies of FRH0201-Gem were larger in comparison with that of the parental FRH-0201, thus demonstrating that FRH0201-Gem cells possess the ability to proliferate for long periods while under continuous exposure to gemcitabine (**Figures S5B, C**). Both western blot and immunofluorescence images suggest that ABCB1 expression was conspicuously elevated in the gemcitabine-resistant CCA cells (**Figures 5B–D**). Even after being treated with gemcitabine, the RNA and protein levels of ABCB1 also significantly increased in HUCCT-1 cells, while gemcitabine-only -treated RBE cells experienced only slight changes (**Figures 5E, F**). This suggests that the upregulation of ABCB1 mediated by gemcitabine might be a commonly occurring phenomenon in CCA.

It is possible that lapatinib's synergistic effect with gemcitabine can either be achieved through decreasing ABCB1 expression or inhibiting ABCB1 function. Therefore, we first evaluated the effect of lapatinib on the expression of ABCB1. Lapatinib did not decrease the expression level of ABCB1 in FRH0201-Gem as shown in **Figure 5C**. At the same time, in both HUCCT-1 and RBE cells, co-incubation with gemcitabine and lapatinib for a duration of 48 hours resulted in a slight downregulation of ABCB1 at the RNA level, but resulted in no significant changes at the protein level. This proves that the synergistic effect of lapatinib and gemcitabine is not related to the inhibition of ABCB1 protein expression by lapatinib, but instead may be related to the inhibition of ABCB1 function by lapatinib (**Figures 5C–F**).

Lapatinib Inhibits the Function of ABCB1 Transporters

Since the gemcitabine-only treatment was found to increase the expression of ABCB1 while lapatinib on its own did not influence it significantly, we considered the possibility of whether or not

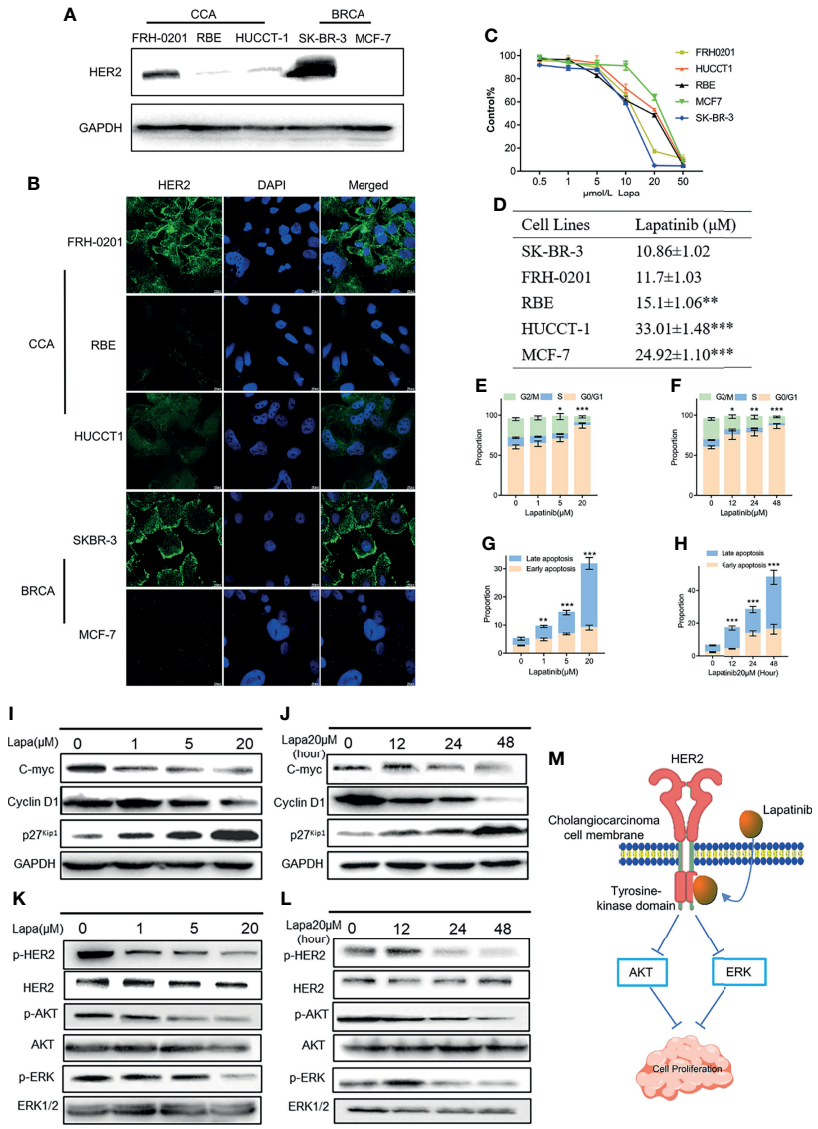

FIGURE 3 | The underlying mechanisms by which lapatinib (Lapa) induces FRH-0201 cell cycle arrest and apoptosis in a concentration- and time-dependent manner. **(A, B)** HER2 protein expression in CCA cell lines was detected by Western blotting and immunofluorescence. **(C, D)** Growth inhibitory effects of lapatinib (Lapa) in HER2^{+} and HER2^{-} cell lines. **(E, F)** Lapatinib dramatically induced G1 cell cycle arrest in HER2-positive CCA cells in both time and dose-dependent manners. **(G, H)** Apoptosis of FRH-0201 was induced post-exposure to varying treatment concentrations of lapatinib or a constant concentration exposure over different time durations. **(I, J)** Down-regulation of c-myc was observed with induction of p27^{Kip1} and down-regulation of Cyclin D1 after lapatinib treatment **(K, L)** HER2 and HER2-dependent downstream signaling pathways were suppressed by lapatinib in FRH-0201 cells. **(M)** A Schematic representation of the mechanisms with which lapatinib inhibits the growth of HER2^{+} CCA cells. The data is expressed as the mean ± S.D., two-sided Student's t-test, $^{*}p < 0.05$, $^{**}p < 0.01$, $^{***}p < 0.001$.

gemcitabine or its metabolites were the substrate of ABCB1 and lapatinib could functionally inhibit ABCB1. As shown in **Figure 6E**, gemcitabine undergoes complex intracellular conversion to nucleotides gemcitabine triphosphate (dFdCTP) (mainly responsible for its cytotoxic actions) and its deaminated metabolite, 2',2'-difluorodeoxyuridine (dFdU). Initially, we performed a docking simulation analysis in order to predict and evaluate the binding affinities of metabolites of gemcitabine and lapatinib with an ABCB1 model. Verapamil, a classic ABCB1 substrate and inhibitor, with the docking score of –8.41 kcal/mol was used as a positive control. As shown in **Table S3**, the scores of dFdCTP and lapatinib was closest to that of verapamil. The panoramic and detailed interactions between the ABCB1 model and the binding site of lapatinib and dFdCTP were shown in **Figure 5G**. A two-dimensional interactive map is depicted in **Figures S3A, B**. As revealed in **Table S4** and **Figures S3C, D**, comparative analysis of common amino acids involved at the substrate-binding sites between dFdCTP and lapatinib suggests that 8 out of the 16 are the same amino acid residues as those involved in dFdCTP interaction. Overall, these results indicate

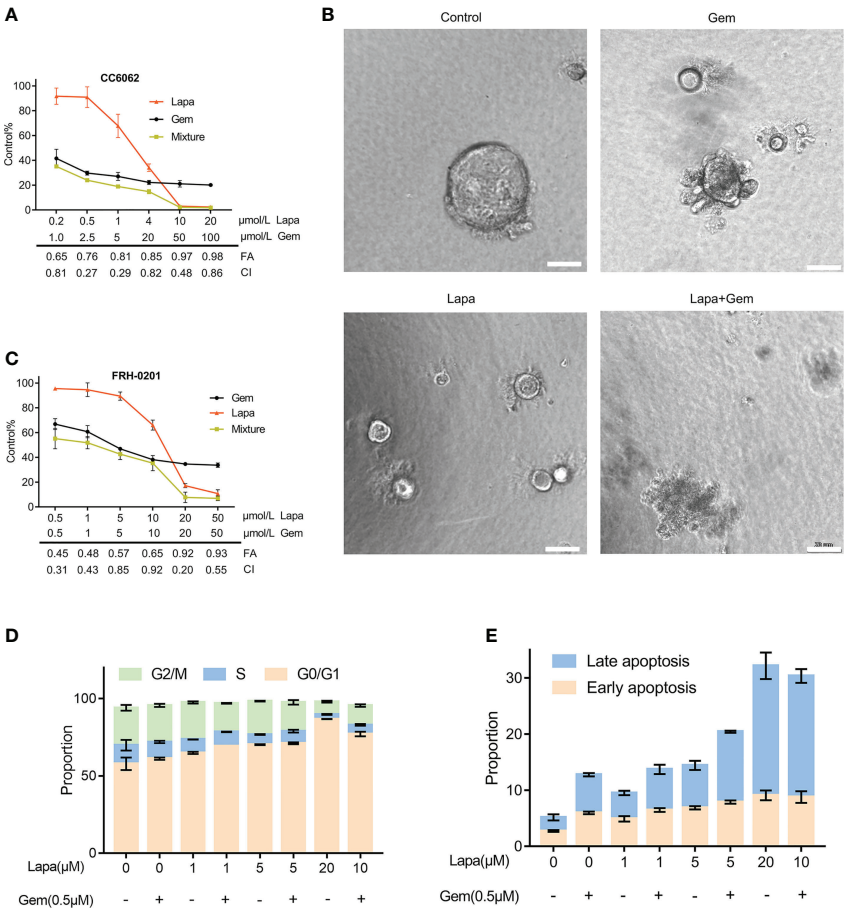

FIGURE 4 | Lapatinib exerts synergistic growth inhibitory effects on HER2-overpressed CCA organoid and cell line when combined with gemcitabine. **(A)** Synergistic growth inhibitory effects of a lapatinib (Lapa) - gemcitabine (Gem) combination treatment of HER2-overexpressed organoids. **(B)** Bright-field images of HER2-overexpressed tumor organoids treated with DMSO, gemcitabine (5 μM Gem), lapatinib (5 μM Lapa) and gemcitabine+lapatinib(5 μM Gem +5 μM Lapa) for 4 days. Scale bar, 20 μm. **(C)** Synergistic growth inhibitory effects of lapatinib (Lapa) combined with gemcitabine (Gem) in FRH-0201. **(D, E)** The lapatinib-gemcitabine combined treatment induced G1 arrest and apoptosis in FRH-0201. Data is expressed as the mean ± S.D. based on three independent experiments.

that dFdCTP is potentially the substrate of ABCB1.Since dFdCTP is the most critical agent for gemcitabine-induced apoptosis (42), it may be the reason that the upregulation of ABCB1 induces the drug resistance of tumor cells. Lapatinib interacts with the binding site of ABCB1 with a score of −8.93 kcal/mol, a score that is even higher than that of verapamil, suggesting that lapatinib possesses excellent affinities to ABCB1 and similarly may also bind competitively with the amino acid residues involved in dFdCTP interactions.

The ABCB1 transporter function has previously been reported to rely on energy from ATP catalyzed by the ABCB1-associated ATPase (43), which can be either stimulated or inhibited by ABCB1 substrates. We subsequently determined the effect of various concentrations of dFdCTP and lapatinib based on ABCB1 ATPase activity. Verapamil was set as the positive control. As exemplified in **Figures 5H–I**, both dFdCTP and lapatinib can stimulate the activity of the ABCB1, while the ability of lapatinib to produce ABCB1 activity is much stronger and more comparable to that of verapamil. This further confirms that both dFdCTP and lapatinib were substrates of ABCB1. Compared with dFdCTP, lapatinib is better at activating ABCB1 ATPases and similarly to verapamil, may bind with ABCB1 competitively.

We further investigated ability of lapatinib to decrease the efflux of ABCB1 substrates. After incubating with Rhodamine 123, one of the classical fluorescent substrates of ABCB1, FRH0201-Gem was then treated with various concentrations of lapatinib. Compared with cells stained with rhodamine without being treated with lapatinib (0 μM lapatinib),various concentrations of lapatinib were found to increase the mean fluorescence intensity of rhodamine in FRH0201-Gem cells in a concentration-dependent manner (**Figure 5J**). Additionally, incubating CC6062 with lapatinib for 30 minutes blocked ABCB1 activity and caused the accumulation of Rhodamine 123 within the cell, while Rhodamine 123 was ejected into the lumen of organoids in the control group (**Figure 5K**).

Lapatinib Decreases the Efflux of dFdCTP From Cells by LC-MS/MS Analysis

After previously confirming dFdCTP as the substrate of ABCB1 and its ability to block the transportation of substrate of ABCB1, we further determined the direct effect of lapatinib on the efflux of dFdCTP, the results of which can confirm the synergistic effects of a combined lapatinib and gemcitabine treatment. FRH-0201 and FRH0201-Gem were treated with 1μM gemcitabine combined with various concentrations of lapatinib for 6 hours and then cells were collected for LC-MS/MS analysis and verapamil was set as the positive control. From the MS/MS spectrum of dFdCTP standards sample, we chose 504.2→326.4 as MRM ion pair and the peak appeared at a retention time of 0.68 min (**Figure 6A**). Then we assessed linearity using serially diluted working solutions with different concentrations, and the linearity of the calibration curve was well accepted with the correlation coefficients (R^2) equal to 0.9971 and the range was from 10 to 1000 ng/mL (**Figure 6B**). The method accuracy (recovery rate) and precision (QC RSD) were all acceptable for the precise assessment of intracellular dFdCTP (**Figure 6C**). As shown in **Figure 6D**, the initial amount of dFdCTP found within FRH0201-Gem cells was less than that of FRH-0201 cells. This supports the idea that gemcitabine chemoresistant cells have a higher intracellular efflux due to the upregulation of ABCB1. We set verapamil as positive control and verapamil is proved to be able to inhibit the efflux of dFdCTP (**Figure 6D**). After a treatment with varying concentrations of lapatinib between 1 to 20μM, we detected that lapatinib promotes an accumulation of dFdCTP in both FRH-0201 and FRH0201-Gem comparable to that of not being treated with lapatinib (0μM Lapa) in a dose-dependent manner. This confirms the suppression of intracellular dFdCTP expulsion by lapatinib (**Figure 6D**).

DISCUSSION

As mentioned previously, a gemcitabine-based chemotherapy is considered to be the standard first-line treatment for advanced CCA cases, as supported by the results from several phase two and three clinical studies (6, 44, 45). However, because only a small portion of patients with CCA exhibit sensitivity and the median progression-free survival (PFS) is only about 5.3-7.7 months for those receiving gemcitabine-based chemotherapy (46, 47); initial and acquired drug resistance often results in recurrence, ultimately preventing it from being used extensively. One of the most common mechanisms found in the multi-drug resistance of CCA is the induction of drug efflux through ABC pumps (8, 48).

Our study suggests that dFdCTP, the active metabolite of gemcitabine, is the substrate of ABCB1, having proven to be capable of interacting with the binding pocket of ABCB1 and stimulating ABCB1-associated ATPase activity. It acts as the substrate of ABCB1-like topotecan and 5-fluorouracil. We have found that an increase in ABCB1 expression results in a parallel increase in efflux of dFdCTP which accounts for the prolific instances of drug resistance occurring after gemcitabine treatment. As such, new developments of targeted therapies and chemosensitizers, such as those targeting ABCB1 efflux pumps are crucial for improving future treatment options for cholangiocarcinoma patients.

The "Precision Medicine" revolution in the treatment of CCA is in the midst of rapid development due to improved knowledge in the molecular biology of these neoplasms. HER2 amplifications are among the most frequently targetable genetic variation found in eCCA, and can potentially be targeted with tyrosine kinase inhibitors (TKIs), such as lapatinib (49). Recent studies demonstrate that HER2 overexpression represents an independent prognostic factor for disease recurrence in CCA (26). Similarly, our research also suggests that HER2-overexpression positively correlates with poor prognosis in certain patients. Since HER2 overexpression represents an independent prognostic factor for prognosis in CCA and can be a therapeutic target, it is worthy of further investigation. A thorough perusal of scientific literature led us to find out about the efficacy of trastuzumab and pertuzumab in patients with HER2-positive CCA. Furthermore, we also found that HER2-targeted therapy includes not only monoclonal antibodies such as trastuzumab, but also tyrosine kinase inhibitors. In this study, we selected lapatinib (a type of TKI) for investigation. Our study demonstrates that HER2-overexpressed CCA is sensitive to lapatinib treatment *in vitro*. Lapatinib is the earliest developed TKI, a reversible inhibitor against both EGFR and HER2 targets. The further studies evaluating the efficacy of new generations of TKIs such as neratinib and tucatinib in HER2-positive cholangiocarcinoma is also something worth looking forward to. In addition, in our study while the cell lines FRH0201 and CC6062 were both found to be HER2 overexpressed, their IC50 values very different, the lapatinib IC50 value of FRH0201 was higher than the maximum plasma concentration (Cmax) achieved by the clinical dose (50). We believe that this may be caused by the presence of heterogeneity in CCA, which suggests that the responsiveness of HER2-overexpressing CCA to lapatinib may also be different, which is worth exploring further.

Organoids derived from primary tumor tissue make it possible to test and develop therapeutic approaches in a pre-clinical setting. It has been previously reported that the HER2 status can be maintained in organoids derived from breast cancer tumors. These HER2-positive breast cancer organoids were confirmed to be sensitive to drugs that inhibit the HER signaling pathway (51). Based on this, we established the first organoid model used to evaluate the inhibitory effects of lapatinib on HER2-overexpressed cholangiocarcinoma. As confirmed through our research, HER2 positive patient-derived tumor resections were similarly able to retain HER2 expression when cultured as organoids. Lapatinib was found to significantly suppress the growth of HER2- overexpressed CCA organoids. Since *in-vitro* cultured organoids often accurately correspond with responses found *in-vivo* (52–56), we hypothesized that lapatinib could potentially also be effective when used in treating HER2- overexpressed CCA patients. This hypothesis still needs to be thoroughly examined through further testing with animal and patient-based clinical research.

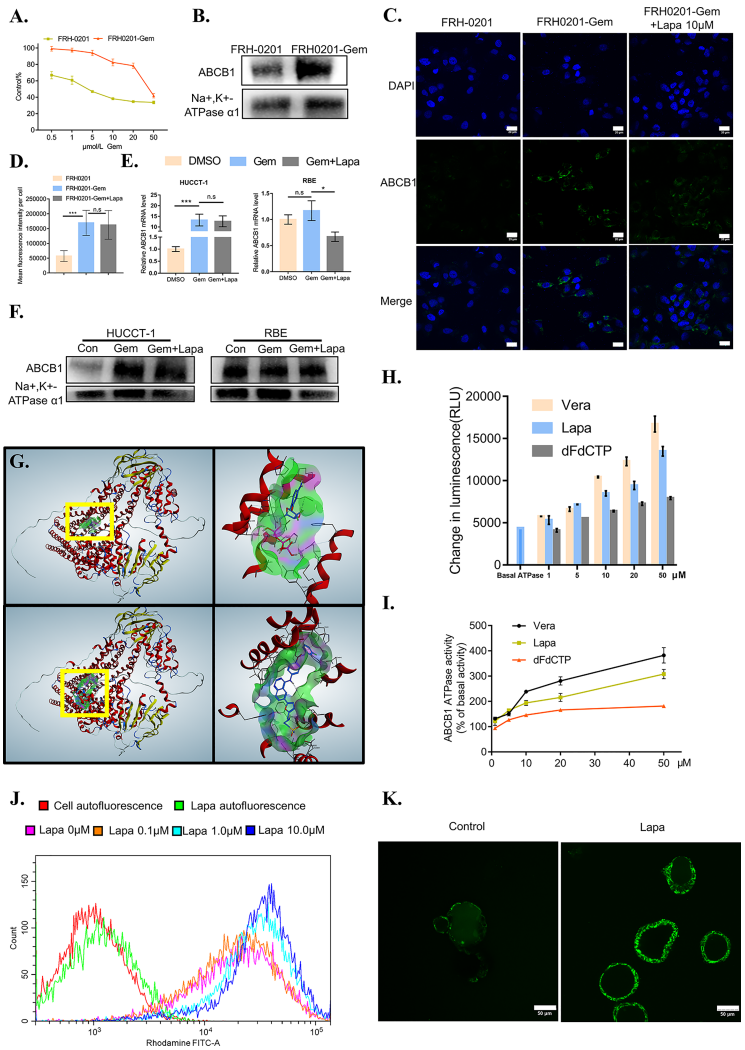

FIGURE 5 | Lapatinib suppresses the function of elevated ABCB1 after being treated with gemcitabine in CCA cells. **(A)** The growth inhibitory effects of gemcitabine (Gem) on FRH-0201 and FRH0201-Gem. **(B, C)** ABCB1 protein expression in FRH-0201 and FRH0201-Gem was detected with Western blotting and immunofluorescence. Scale bar: 20 μm. **(D)** Quantification of fluorescence intensity for ABCB1 in FRH-0201, FRH0201-Gem and FRH0201-Gem incubated with 10μM lapatinib (Lapa) **(E, F)** Relative mRNA levels and protein levels of ABCB1 in various CCA cell lines after treatment with gemcitabine (10 μM Gem) or a combination of gemcitabine and lapatinib (10μM Gem +5μM Lapa) for 48 h. **(G)** Upper left: The panoramic structure of ABCB1 and dFdCTP binding site. Upper right: A detailed three-dimensional plot of the interaction of dFdCTP and ABCB1. Bottom left: The panoramic structure of ABCB1 and lapatinib binding site. Bottom right: A detailed three-dimension plot of the interaction between lapatinib and ABCB1. The ABCB1 protein is depicted in red. H-bondings are shown in purple, hydrophobic bonds are shown in green, and mild polar bonds are shown in blue. Lapatinib and dFdCTP are depicted with the following color codes: carbon (blue), oxygen (red), nitrogen (dark blue), sulfur (yellow), fluoride (green), hydrogen (grey), chlorine (dark green), phosphorus (purple). **(H)** The luminescence increases in a dose-dependent manner following the incubation of verapamil (positive control), lapatinib or dFdCTP with P-glycoprotein-containing membranes. **(I)** ABCB1 ATPase activity increases in a dose-dependent manner with varying concentrations of verapamil, lapatinib, and dFdCTP. **(J)** The fluorescence intensity changes in rhodamine-dyed FRH0201-Gem after treatment with previously indicated concentrations of lapatinib. **(K)** Confocal images of CC6062 dyed with rhodamine after being treated with or without lapatinib. The data is expressed as the mean ± S.D., two-sided Student's t-test, n.s. not significant, $*p < 0.05$, $***p < 0.001$.

Our research found that a combination of lapatinib and gemcitabine has a robust synergistic effect, having obtained CI values of less than 1 in both drug combination assays conducted on HER2-positive organoids and cell lines. Lapatinib has an affinity with ABCB1 that is comparable with that of verapamil, a well-known ABCB1 inhibitor. The ability of ABCB1 to expel its substrates relies on ATP hydrolysis by ATPases (57, 58). Based on this, we conducted an ABCB1-associated ATPase assay and found that lapatinib could stimulate ATPase activity in a concentration dependent manner. Additionally, lapatinib was also able to significantly increase the intracellular accumulation of Rhodamine 123, a fluorescent substrate of ABCB1. A LC-MS/MS analysis of dFdCTP in the presence of a concentration gradient of lapatinib provided evidence that lapatinib

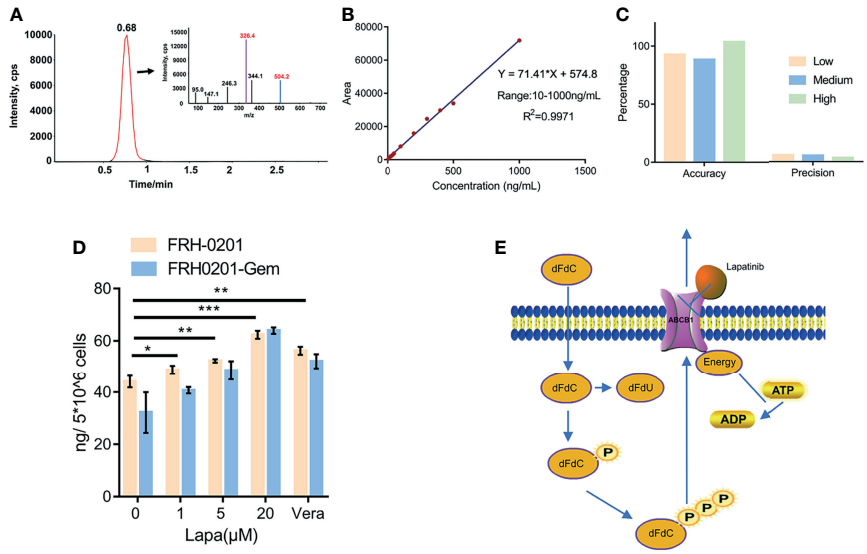

FIGURE 6 | Lapatinib promotes the accumulation of dFdCTP within CCA cells. **(A)** Extracted ion chromatography (XIC) and MS/MS spectrum of dFdCTP. **(B)** Linearity and range of the calibration curve **(C)** Accuracy and precision of the qualitative method under low, medium and high concentrations. **(D)** The concentration of intracellular dFdCTP is positively correlated with increasing concentrations of lapatinib. FRH-0201, FRH0201-Gem were treated with a combination of a varying concentrations of lapatinib (0, 1, 5, 20 μM) and a constant concentration of gemcitabine (1 μM). Cells treated with 1 μM Gem + 5 μM Verapamil were set as the positive control. **(E)** A Schematic representation of the mechanisms with which lapatinib inhibits the efflux of dFdCTP within CCA cells. The data is expressed as the mean ± S.D., two-sided Student's t-test, $^{*}p < 0.05$, $^{**}p < 0.01$, $^{***}p < 0.001$.

suppresses the efflux of dFdCTP and thus increases the cytoxic effect dFdCTP has on CCA cells. Our results indicate that lapatinib exerts a dual effect on HER2-overexpressed CCA, suppressing the growth of CCA cells by inhibiting HER2 and HER2-dependent downstream signaling pathways. Lapatinib is also found to be able to bind to ABCB1 competitively, increasing gemcitabine efficacy by blocking the efflux of dFdCTP from tumor cells, and promoting its accumulation within cells. A combination of lapatinib and chemotherapy has previously been proven to be safe and efficient for HER2-overexpressed gastroesophageal adenocarcinoma and breast cancer (59, 60). As such our study provides clear evidence that lapatinib can be substantially coordinated with gemcitabine as a first line treatment for HER2-overexpressed CCA cases. We have provided an excellent preclinical evaluation of the efficacy of a lapatinib-gemcitabine combination-based therapy which can be applied to future treatments of HER2-overexpressed cholangiocarcinoma, while simultaneously shedding new light on the potential of molecular targeted CCA therapies.

CONCLUSION

Lapatinib inhibits tumor growth in organoids and cell lines overexpressing HER2 and circumvents ABCB1-mediated chemoresistance after gemcitabine treatment. We believe that this is a precursor for further clinical investigation of the effectiveness of a lapatinib-gemcitabine combined treatment in HER2-overexpressed cholangiocarcinoma.

DATA AVAILABILITY STATEMENT

The original contributions presented in the study are included in the article/**Supplementary Material**. Further inquiries can be directed to the corresponding authors.

ETHICS STATEMENT

The studies involving human participants were reviewed and approved by Ethics Committee of Beijing Tsinghua Changgung Hospital. The patients/participants provided their written informed consent to participate in this study.

AUTHOR CONTRIBUTIONS

ZB and ZG contributed equally to conception and design of the study. JL, LH, and QL performed the statistical analysis. ZB and Y-AC wrote the first draft of the manuscript. PZ, Y-AC, ZG, and JL wrote sections of the manuscript. JD and YW designed and supervised the entire project. All authors contributed to the article and approved the submitted version.

FUNDING

This work was supported by CAMS Innovation Fund for Medical Sciences (2019-I2M-5-056), National Natural Science

Foundation of China (No. 81930119, 82090050), Beijing Hospitals Authority' Ascent Plan (DFL20190901), and Tsinghua University Spring Breeze Fund (2021Z99CFZ008).

ACKNOWLEDGMENTS

We thank the c-bioPortal for high-quality data. L M. Reid edited the manuscript for English.

SUPPLEMENTARY MATERIAL

The Supplementary Material for this article can be found online at: https://www.frontiersin.org/articles/10.3389/fonc.2022.860339/full#supplementary-material

Supplementary Figure 1 | HER2 amplification/overexpression profiles within CCA patient populations. **(A)** HER2 amplification profiles in biliary tract carcinoma as analyzed by cBioPortal. **(B)** Overall survival (OS) curve analysis of patients diagnosed as either HER2 positive or HER2 negative. **(C)** Images of HER2 immunohistochemistry in CCA tissue CC6062. **(D)** Images of HER2 FISH in CCA tissue CC6062.

Supplementary Figure 2 | A detailed distribution of G1 cycle arrested and apoptotic cells induced by lapatinib (Lapa), gemcitabine (Gem) or a combination (Lapa+Gem) treatment in FRH-0201. **(A)** Cell cycle arrest was induced by lapatinib, gemcitabine or a combination of both compounds for a duration of 48 h. **(B)** Apoptosis was induced by lapatinib,gemcitabine or combination of both compounds for a duration of 48 h. **(C)** Apoptosis and cell cycle arrest in FRH-0201 was measured after being treated with lapatinib (Lapa) for the above indicated time periods.

Supplementary Figure 3 | Lapatinib and gemcitabine show a strong binding affinity towards ABCB1. **(A)** A two-dimensional diagram of the binding of lapatinib with ABCB1. **(B)** A two-dimensional diagram of the binding of dFdCTP with ABCB1. In both **(A, B)** aromatic residues are colored in green, whereas polar amino acids are shown in magenta. **(C)** A Venn diagrammatic representation of amino acid residues shared by dFdCTP, verapamil, and lapatinib at the substrate-binding domain of ABCB1. **(D)** Detailed depiction of dFdCTP and lapatinib interactions with ABCB1 binding pockets. The dFdCTP molecule is represented using a sphere and pole model and covered with a solid-gray pocket, while the lapatinib molecule is represented using a pole model and covered with a dotted-green pocket.

Supplementary Figure 4 | EGFR status of cells and the inhibitory effect of Cetuximab (CTX) on FRH0201. **(A)** EGFR IHC staining of tissue and organoid revealed that both CC6062 and CC9630 were EGFR-negative, while CC2196 was positive. Scale bar= 100 μm **(B)** EGFR protein expression in CCA cell lines was detected by Western blotting. **(C)** Both cetuximab (CTX) and lapatinib (Lapa) were able to suppress p-EGFR of FRH-0201. **(D)** Growth inhibitory effect curves of cetuximab (CTX) in FRH-0201 proved that FRH-0201 is resistant to cetuximab (CTX).

Supplementary Figure 5 | Establishment of Gemcitabine-resistant FRH0201-Gem. **(A)** Bright-field image of FRH-0201 and FRH0201-Gem. Scale bar= 500 μm. **(B)** Parental FRH-0201 and gemcitabine-resistant FRH0201-Gem were plated in six well plates and cells were allowed 48 h to initiate colonies. Then cells were incubated at 5 μM gemcitabine for an additional 12 days to assess the drug resistance of FRH0201-Gem using colony-forming assay. **(C)** Colony assay results for FRH-0201 and FRH0201-Gem treated with gemcitabine treatments.

Supplementary Video 1 | Time-lapse movie of organoids treated with DMSO (Control), 5 μM gemcitabine (Gem), 5 μM lapatinib (Lapa), and 5 μM gemcitabine+5 μM lapatinib (Gem+Lapa). The movie was initiated as the drug was added into the medium and continued for 4 days. Each picture was taken at an interval of 1 hour using the Live Cell Imaging System (Etaluma, Ameirica). **(A–D)** CC6062 treated with DMSO, Lapa, Gem and Gem+Lapa. **(E, F)** CC2196 treated with DMSO and Lapa. **(G, H)** CC9630 treated with DMSO and Lapa.

REFERENCES

1. Welzel TM, McGlynn KA, Hsing AW, O'Brien TR, Pfeiffer RM. Impact of Classification of Hilar Cholangiocarcinomas (Klatskin Tumors) on the Incidence of Intra- and Extrahepatic Cholangiocarcinoma in the United States. *J Natl Cancer Inst* (2006) 98(12):873–5. doi: 10.1093/jnci/djj234
2. Banales JM, Marin JJG, Lamarca A, Rodrigues PM, Khan SA, Roberts LR, et al. Cholangiocarcinoma 2020: The Next Horizon in Mechanisms and Management. *Nat Rev Gastroenterol Hepatol* (2020) 17(9):557–88. doi: 10.1038/s41575-020-0310-z
3. Jarnagin WR, Fong Y, DeMatteo RP, Gonen M, Burke EC, Bodniewicz BJ, et al. Staging, Resectability, and Outcome in 225 Patients With Hilar Cholangiocarcinoma. *Ann Surg* (2001) 234(4):507–17; discussion 517-9. doi: 10.1097/00000658-200110000-00010
4. Kendall T, Verheij J, Gaudio E, Evert M, Guido M, Goeppert B, et al. Anatomical, Histomorphological and Molecular Classification of Cholangiocarcinoma. *Liver Int: Off J Int Assoc Study Liver* (2019) 39 Suppl 1:7–18. doi: 10.1111/liv.14093
5. Fouassier L, Marzioni M, Afonso MB, Dooley S, Gaston K, Giannelli G, et al. Signalling Networks in Cholangiocarcinoma: Molecular Pathogenesis, Targeted Therapies and Drug Resistance. *Liver Int: Off J Int Assoc Study Liver* (2019) 39 Suppl 1:43–62. doi: 10.1111/liv.14102
6. Valle J, Wasan H, Palmer DH, Cunningham D, Anthoney A, Maraveyas A, et al. Cisplatin Plus Gemcitabine Versus Gemcitabine for Biliary Tract Cancer. *New Engl J Med* (2010) 362(14):1273–81. doi: 10.1056/NEJMoa0908721
7. Marin JJG, Lozano E, Herraez E, Asensio M, Di Giacomo S, Romero MR, et al. Chemoresistance and Chemosensitization in Cholangiocarcinoma. *Biochim Biophys Acta Mol Basis Dis* (2018) 1864(4 Pt B):1444–53. doi: 10.1016/j.bbadis.2017.06.005
8. Naus PJ, Henson R, Bleeker G, Wehbe H, Meng F, Patel T. Tannic Acid Synergizes the Cytotoxicity of Chemotherapeutic Drugs in Human Cholangiocarcinoma by Modulating Drug Efflux Pathways. *J Hepatol* (2007) 46(2):222–9. doi: 10.1016/j.jhep.2006.08.012
9. Marin JJG, Macias RIR, Cives-Losada C, Peleteiro-Vigil A, Herraez E, Lozano E. Plasma Membrane Transporters as Biomarkers and Molecular Targets in Cholangiocarcinoma. *Cells* (2020) 9(2):498–510. doi: 10.3390/cells9020498
10. Abou-Alfa GK, Sahai V, Hollebecque A, Vaccaro G, Melisi D, Al-Rajabi R, et al. Pemigatinib for Previously Treated, Locally Advanced or Metastatic Cholangiocarcinoma: A Multicentre, Open-Label, Phase 2 Study. *Lancet Oncol* (2020) 21(5):671–84. doi: 10.1016/s1470-2045(20)30109-1
11. Goyal L, Shi L, Liu LY, Fece de la Cruz F, Lennerz JK, Raghavan S, et al. TAS-120 Overcomes Resistance to ATP-Competitive FGFR Inhibitors in Patients With FGFR2 Fusion-Positive Intrahepatic Cholangiocarcinoma. *Cancer Discovery* (2019) 9(8):1064–79. doi: 10.1158/2159-8290.Cd-19-0182
12. Abou-Alfa GK, Macarulla T, Javle MM, Kelley RK, Lubner SJ, Adeva J, et al. Ivosidenib in IDH1-Mutant, Chemotherapy-Refractory Cholangiocarcinoma (ClarIDHy): A Multicentre, Randomised, Double-Blind, Placebo-Controlled, Phase 3 Study. *Lancet Oncol* (2020) 21(6):796–807. doi: 10.1016/s1470-2045(20)30157-1
13. Nakamura H, Arai Y, Totoki Y, Shirota T, Elzawahry A, Kato M, et al. Genomic Spectra of Biliary Tract Cancer. *Nat Genet* (2015) 47(9):1003–10. doi: 10.1038/ng.3375
14. Jusakul A, Cutcutache I, Yong CH, Lim JQ, Huang MN, Padmanabhan N, et al. Whole-Genome and Epigenomic Landscapes of Etiologically Distinct Subtypes of Cholangiocarcinoma. *Cancer Discovery* (2017) 7(10):1116–35. doi: 10.1158/2159-8290.Cd-17-0368
15. Javle M, Churi C, Kang HC, Shroff R, Janku F, Surapaneni R, et al. HER2/neu-Directed Therapy for Biliary Tract Cancer. *J Hematol Oncol* (2015) 8:58. doi: 10.1186/s13045-015-0155-z

16. Javle M, Borad MJ, Azad NS, Kurzrock R, Abou-Alfa GK, George B, et al. Pertuzumab and Trastuzumab for HER2-Positive, Metastatic Biliary Tract Cancer (MyPathway): A Multicentre, Open-Label, Phase 2a, Multiple Basket Study. *Lancet Oncol* (2021) 22(9):1290–300. doi: 10.1016/s1470-2045(21)00336-3
17. Geyer CE, Forster J, Lindquist D, Chan S, Romieu CG, Pienkowski T, et al. Lapatinib Plus Capecitabine for HER2-Positive Advanced Breast Cancer. *New Engl J Med* (2006) 355(26):2733–43. doi: 10.1056/NEJMoa064320
18. Bilancia D, Rosati G, Dinota A, Germano D, Romano R, Manzione L. Lapatinib in Breast Cancer. *Ann Oncol: Off J Eur Soc Med Oncol* (2007) 18 Suppl 6:vi26–30. doi: 10.1093/annonc/mdm220
19. Oh DY, Bang YJ. HER2-Targeted Therapies - a Role Beyond Breast Cancer. *Nat Rev Clin Oncol* (2020) 17(1):33–48. doi: 10.1038/s41571-019-0268-3
20. Peck J, Wei L, Zalupski M, O'Neil B, Villalona Calero M, Bekaii-Saab T. HER2/neu may Not be an Interesting Target in Biliary Cancers: Results of an Early Phase II Study With Lapatinib. *Oncology* (2012) 82(3):175–9. doi: 10.1159/000336488
21. El-Khoueiry AB, Rankin C, Siegel AB, Iqbal S, Gong IY, Micetich KC, et al. S0941: A Phase 2 SWOG Study of Sorafenib and Erlotinib in Patients With Advanced Gallbladder Carcinoma or Cholangiocarcinoma. *Br J Cancer* (2014) 110(4):882–7. doi: 10.1038/bjc.2013.801
22. Wang YJ, Zhang YK, Kathawala RJ, Chen ZS. Repositioning of Tyrosine Kinase Inhibitors as Antagonists of ATP-Binding Cassette Transporters in Anticancer Drug Resistance. *Cancers* (2014) 6(4):1925–52. doi: 10.3390/cancers6041925
23. Fletcher JI, Haber M, Henderson MJ, Norris MD. ABC Transporters in Cancer: More Than Just Drug Efflux Pumps. *Nat Rev Cancer* (2010) 10(2):147–56. doi: 10.1038/nrc2789
24. Beretta GL, Cassinelli G, Pennati M, Zuco V, Gatti L. Overcoming ABC Transporter-Mediated Multidrug Resistance: The Dual Role of Tyrosine Kinase Inhibitors as Multitargeting Agents. *Eur J Med Chem* (2017) 142:271–89. doi: 10.1016/j.ejmech.2017.07.062
25. Rosenbaum MW, Gonzalez RS. Targeted Therapy for Upper Gastrointestinal Tract Cancer: Current and Future Prospects. *Histopathology* (2021) 78(1):148–61. doi: 10.1111/his.14244
26. Vivaldi C, Fornaro L, Ugolini C, Niccoli C, Musettini G, Pecora I, et al. HER2 Overexpression as a Poor Prognostic Determinant in Resected Biliary Tract Cancer. *Oncol* (2020) 25(10):886–93. doi: 10.1634/theoncologist.2019-0922
27. Cerami E, Gao J, Dogrusoz U, Gross BE, Sumer SO, Aksoy BA, et al. The Cbio Cancer Genomics Portal: An Open Platform for Exploring Multidimensional Cancer Genomics Data. *Cancer Discovery* (2012) 2(5):401–4. doi: 10.1158/2159-8290.Cd-12-0095
28. Driehuis E, Kretzschmar K, Clevers H. Establishment of Patient-Derived Cancer Organoids for Drug-Screening Applications. *Nat Protoc* (2020) 15(10):3380–409. doi: 10.1038/s41596-020-0379-4
29. Chou. Drug combination studies TC. And Their Synergy Quantification Using the Chou-Talalay Method. *Cancer Res* (2010) 70(2):440–6. doi: 10.1158/0008-5472.Can-09-1947
30. Jumper J, Evans R, Pritzel A, Green T, Figurnov M, Ronneberger O, et al. Highly Accurate Protein Structure Prediction With AlphaFold. *Nature* (2021) 596(7873):583–9. doi: 10.1038/s41586-021-03819-2
31. Irwin JJ, Shoichet BK. ZINC–a Free Database of Commercially Available Compounds for Virtual Screening. *J Chem Inf Model* (2005) 45(1):177–82. doi: 10.1021/ci049714+
32. Zaman Z, Khan S, Nouroz F, Farooq U, Urooj A. Targeting Protein Tyrosine Phosphatase to Unravel Possible Inhibitors for Streptococcus Pneumoniae Using Molecular Docking, Molecular Dynamics Simulations Coupled With Free Energy Calculations. *Life Sci* (2021) 264:118621. doi: 10.1016/j.lfs.2020.118621
33. Hong LL, Kong JQ. Altering the Regioselectivity of Cytochrome P450 BM3 Variant M13 Toward Genistein Through Protein Engineering and Variation of Reaction Conditions. *ACS Omega* (2020) 5(49):32059–66. doi: 10.1021/acsomega.0c05088
34. Balitzer D, Joseph NM, Ferrell L, Shafizadeh N, Jain D, Zhang X, et al. Immunohistochemical and Molecular Features of Cholangiolocellular Carcinoma are Similar to Well-Differentiated Intrahepatic Cholangiocarcinoma. *Mod Pathol* (2019) 32(10):1486–94. doi: 10.1038/s41379-019-0290-0
35. Maeno S, Kondo F, Sano K, Takada T, Asano T. Morphometric and Immunohistochemical Study of Cholangiolocellular Carcinoma: Comparison With non-Neoplastic Cholangiole, Interlobular Duct and Septal Duct. *J Hepatobiliary Pancreat Sci* (2012) 19(3):289–96. doi: 10.1007/s00534-011-0483-5
36. Robey RW, Pluchino KM, Hall MD, Fojo AT, Bates SE, Gottesman MM. Revisiting the Role of ABC Transporters in Multidrug-Resistant Cancer. *Nat Rev Cancer* (2018) 18(7):452–64. doi: 10.1038/s41568-018-0005-8
37. Vagiannis D, Yu Z, Novotna E, Morell A, Hofman J. Entrectinib Reverses Cytostatic Resistance Through the Inhibition of ABCB1 Efflux Transporter, But Not the CYP3A4 Drug-Metabolizing Enzyme. *Biochem Pharmacol* (2020) 178:114061. doi: 10.1016/j.bcp.2020.114061
38. Wang F, Li D, Zheng Z, Kin Wah To K, Chen Z, Zhong M, et al. Reversal of ABCB1-Related Multidrug Resistance by ERK5-IN-1. *J Exp Clin Cancer Res: CR* (2020) 39(1):50. doi: 10.1186/s13046-020-1537-9
39. Liu T, Li Z, Zhang Q, De Amorim Bernstein K, Lozano-Calderon S, Choy E, et al. Targeting ABCB1 (MDR1) in Multi-Drug Resistant Osteosarcoma Cells Using the CRISPR-Cas9 System to Reverse Drug Resistance. *Oncotarget* (2016) 7(50):83502–13. doi: 10.18632/oncotarget.13148
40. Vaidyanathan A, Sawers L, Gannon AL, Chakravarty P, Scott AL, Bray SE, et al. ABCB1 (MDR1) Induction Defines a Common Resistance Mechanism in Paclitaxel- and Olaparib-Resistant Ovarian Cancer Cells. *Br J Cancer* (2016) 115(4):431–41. doi: 10.1038/bjc.2016.203
41. Luo X, Teng QX, Dong JY, Yang DH, Wang M, Dessie W, et al. Antimicrobial Peptide Reverses ABCB1-Mediated Chemotherapeutic Drug Resistance. *Front Pharmacol* (2020) 11:1208. doi: 10.3389/fphar.2020.01208
42. Mini E, Nobili S, Caciagli B, Landini I, Mazzei T. Cellular Pharmacology of Gemcitabine. *Ann Oncol: Off J Eur Soc Med Oncol* (2006) 17 Suppl 5:v7–12. doi: 10.1093/annonc/mdj941
43. Wu CP, Hung TH, Hsiao SH, Huang YH, Hung LC, Yu YJ, et al. Erdafitinib Resensitizes ABCB1-Overexpressing Multidrug-Resistant Cancer Cells to Cytotoxic Anticancer Drugs. *Cancers* (2020) 12(6):1366–86. doi: 10.3390/cancers12061366
44. Lee J, Park SH, Chang HM, Kim JS, Choi HJ, Lee MA, et al. Gemcitabine and Oxaliplatin With or Without Erlotinib in Advanced Biliary-Tract Cancer: A Multicentre, Open-Label, Randomised, Phase 3 Study. *Lancet Oncol* (2012) 13(2):181–8. doi: 10.1016/s1470-2045(11)70301-1
45. Valle JW, Wasan H, Johnson P, Jones E, Dixon L, Swindell R, et al. Gemcitabine Alone or in Combination With Cisplatin in Patients With Advanced or Metastatic Cholangiocarcinomas or Other Biliary Tract Tumours: A Multicentre Randomised Phase II Study - The UK ABC-01 Study. *Br J Cancer* (2009) 101(4):621–7. doi: 10.1038/sj.bjc.6605211
46. Sahai V, Catalano PJ, Zalupski MM, Lubner SJ, Menge MR, Nimeiri HS, et al. Nab-Paclitaxel and Gemcitabine as First-Line Treatment of Advanced or Metastatic Cholangiocarcinoma: A Phase 2 Clinical Trial. *JAMA Oncol* (2018) 4(12):1707–12. doi: 10.1001/jamaoncol.2018.3277
47. Kim ST, Kang JH, Lee J, Lee HW, Oh SY, Jang JS, et al. Capecitabine Plus Oxaliplatin Versus Gemcitabine Plus Oxaliplatin as First-Line Therapy for Advanced Biliary Tract Cancers: A Multicenter, Open-Label, Randomized, Phase III, Noninferiority Trial. *Ann Oncol: Off J Eur Soc Med Oncol* (2019) 30(5):788–95. doi: 10.1093/annonc/mdz058
48. Lozano E, Asensio M, Perez-Silva L, Banales JM, Briz O, Marin JJG. MRP3-Mediated Chemoresistance in Cholangiocarcinoma: Target for Chemosensitization Through Restoring SOX17 Expression. *Hepatol (Baltimore Md.)* (2020) 72(3):949–64. doi: 10.1002/hep.31088
49. Hyman DM, Piha-Paul SA, Won H, Rodon J, Saura C, Shapiro GI, et al. HER Kinase Inhibition in Patients With HER2- and HER3-Mutant Cancers. *Nature* (2018) 554(7691):189–94. doi: 10.1038/nature25475
50. Liston DR, Davis M. Clinically Relevant Concentrations of Anticancer Drugs: A Guide for Nonclinical Studies. *Clin Cancer Res: Off J Am Assoc Cancer Res* (2017) 23(14):3489–98. doi: 10.1158/1078-0432.Ccr-16-3083
51. Sachs N, de Ligt J, Kopper O, Gogola E, Bounova G, Weeber F, et al. A Living Biobank of Breast Cancer Organoids Captures Disease Heterogeneity. *Cell* (2018) 172(1-2):373–386.e10. doi: 10.1016/j.cell.2017.11.010
52. Pasch CA, Favreau PF, Yueh AE, Babiarz CP, Gillette AA, Sharick JT, et al. Patient-Derived Cancer Organoid Cultures to Predict Sensitivity to Chemotherapy and Radiation. *Clin Cancer Res: Off J Am Assoc Cancer Res* (2019) 25(17):5376–87. doi: 10.1158/1078-0432.Ccr-18-3590

53. Kim SY, Kim SM, Lim S, Lee JY, Choi SJ, Yang SD, et al. Modeling Clinical Responses to Targeted Therapies by Patient-Derived Organoids of Advanced Lung Adenocarcinoma. *Clin Cancer Res: Off J Am Assoc Cancer Res* (2021) 27 (15):4397–409. doi: 10.1158/1078-0432.Ccr-20-5026
54. de Witte CJ, Espejo Valle-Inclan J, Hami N, Lõhmussaar K, Kopper O, Vreuls CPH, et al. Patient-Derived Ovarian Cancer Organoids Mimic Clinical Response and Exhibit Heterogeneous Inter- and Intrapatient Drug Responses. *Cell Rep* (2020) 31(11):107762. doi: 10.1016/j.celrep.2020.107762
55. Wang T, Pan W, Zheng H, Zheng H, Wang Z, Li JJ, et al. Accuracy of Using a Patient-Derived Tumor Organoid Culture Model to Predict the Response to Chemotherapy Regimens In Stage IV Colorectal Cancer: A Blinded Study. *Dis Colon Rectum* (2021) 64(7):833–50. doi: 10.1097/dcr.0000000000001971
56. Steele NG, Chakrabarti J, Wang J, Biesiada J, Holokai L, Chang J, et al. An Organoid-Based Preclinical Model of Human Gastric Cancer. *Cell Mol Gastroenterol Hepatol* (2019) 7(1):161–84. doi: 10.1016/j.jcmgh.2018.09.008
57. Wang JQ, Teng QX, Lei ZN, Ji N, Cui Q, Fu H, et al. Reversal of Cancer Multidrug Resistance (MDR) Mediated by ATP-Binding Cassette Transporter G2 (ABCG2) by AZ-628, a RAF Kinase Inhibitor. *Front Cell Dev Biol* (2020) 8:601400. doi: 10.3389/fcell.2020.601400
58. Yang Y, Ji N, Cai CY, Wang JQ, Lei ZN, Teng QX, et al. Modulating the Function of ABCB1: *In Vitro* and *In Vivo* Characterization of Sitravatinib, a Tyrosine Kinase Inhibitor. *Cancer Commun (Lond Engl)* (2020) 40(7):285–300. doi: 10.1002/cac2.12040
59. Smyth EC, Rowley S, Cafferty FH, Allum W, Grabsch HI, Stenning S, et al. Safety and Efficacy of the Addition of Lapatinib to Perioperative Chemotherapy for Resectable HER2-Positive Gastroesophageal Adenocarcinoma: A Randomized Phase 2 Clinical Trial. *JAMA Oncol* (2019) 5(8):1181–7. doi: 10.1001/jamaoncol.2019.1179
60. Le Du F, Diéras V, Curigliano G. The Role of Tyrosine Kinase Inhibitors in the Treatment of HER2+ Metastatic Breast Cancer. *Eur J Cancer (Oxf Engl: 1990)* (2021) 154:175–89. doi: 10.1016/j.ejca.2021.06.026

Conflict of Interest: The authors declare that the research was conducted in the absence of any commercial or financial relationships that could be construed as a potential conflict of interest.

Publisher's Note: All claims expressed in this article are solely those of the authors and do not necessarily represent those of their affiliated organizations, or those of the publisher, the editors and the reviewers. Any product that may be evaluated in this article, or claim that may be made by its manufacturer, is not guaranteed or endorsed by the publisher.

frontiers | Frontiers in Oncology

MINI REVIEW
published: 30 May 2022
doi: 10.3389/fonc.2022.895112

p53-Mediated Indirect Regulation on Cellular Metabolism: From the Mechanism of Pathogenesis to the Development of Cancer Therapeutics

Chen-Yun Wang[1,2] *and Chi-Hong Chao*[1,2,3]*

[1] Institute of Molecular Medicine and Bioengineering, National Yang Ming Chiao Tung University, Hsinchu, Taiwan, [2] Center For Intelligent Drug Systems and Smart Bio-devices (IDS2B), National Yang Ming Chiao Tung University, Hsinchu, Taiwan, [3] Department of Biological Science and Technology, National Yang Ming Chiao Tung University, Hsinchu, Taiwan

The transcription factor p53 is the most well-characterized tumor suppressor involved in multiple cellular processes, which has expanded to the regulation of metabolism in recent decades. Accumulating evidence reinforces the link between the disturbance of p53-relevant metabolic activities and tumor development. However, a full-fledged understanding of the metabolic roles of p53 and the underlying detailed molecular mechanisms in human normal and cancer cells remain elusive, and persistent endeavor is required to foster the entry of drugs targeting p53 into clinical use. This mini-review summarizes the indirect regulation of cellular metabolism by wild-type p53 as well as mutant p53, in which mechanisms are categorized into three major groups: through modulating downstream transcriptional targets, protein-protein interaction with other transcription factors, and affecting signaling pathways. Indirect mechanisms expand the p53 regulatory networks of cellular metabolism, making p53 a master regulator of metabolism and a key metabolic sensor. Moreover, we provide a brief overview of recent achievements and potential developments in the therapeutic strategies targeting mutant p53, emphasizing synthetic lethal methods targeting mutant p53 with metabolism. Then, we delineate synthetic lethality targeting mutant p53 with its indirect regulation on metabolism, which expands the synthetic lethal networks of mutant p53 and broadens the horizon of developing novel therapeutic strategies for p53 mutated cancers, providing more opportunities for cancer patients with mutant p53. Finally, the limitations and current research gaps in studies of metabolic networks controlled by p53 and challenges of research on p53-mediated indirect regulation on metabolism are further discussed.

Keywords: wild-type p53, mutant p53, indirect regulation, metabolism, cancer treatment, synthetic lethality

OPEN ACCESS

Edited by:
Thibaut Barnoud, Medical University of South Carolina, United States

Reviewed by:
Eytan Ruppin, Tel Aviv University, Israel

***Correspondence:**
Chi-Hong Chao
chao7@nycu.edu.tw

Specialty section:
This article was submitted to Cancer Metabolism, a section of the journal Frontiers in Oncology

Received: *13 March 2022*
Accepted: *28 April 2022*
Published: *30 May 2022*

Citation:
Wang C-Y and Chao C-H (2022) p53-Mediated Indirect Regulation on Cellular Metabolism: From the Mechanism of Pathogenesis to the Development of Cancer Therapeutics. Front. Oncol. 12:895112. doi: 10.3389/fonc.2022.895112

INTRODUCTION

During the 40 years of discovery, *TP53*, encoding a transcription factor known as the guardian of the genome, has been well characterized as a pivotal tumor suppressor. Upon various stress signals, including DNA damage, metabolic stress, and induction of oncogenes, p53 is released from its core negative regulator MDM2 and activated through multiple post-translational modifications (PTMs),

which subsequently results in the upregulation or downregulation of genes involved in DNA repair, cell-cycle arrest, senescence, and apoptosis. Furthermore, p53 has been identified as an important regulator of stemness, autophagy, redox homeostasis, cellular metabolism, as well as tumor microenvironments (TMEs) (1–3).

Being the most frequently mutated tumor suppressor gene in human cancers, *TP53* mutation exists in more than 50% of human cancers. *TP53* mutates variably in different types or subtypes of cancer (4), and the majority of *TP53* mutations are missense mutations, a single-base substitution located in the DNA-binding domain (DBD), giving rise to a full-length p53 protein (5). The existence of hotspot mutations, which account for almost 30% of all the missense mutations in *TP53*, may confer maximal benefits on tumor cells (6). These mutations are classified into two main categories: DNA-contact mutations abrogate residues directly involved in DNA binding, such as R273H, while structural or conformational mutations disrupt the structure of the DBD, such as R175H (3). Typically, oncogenic effects of *TP53* mutations might be exerted through loss of function (LOF) of wild-type p53 (WTp53), dominant-negative effect (DNE) over WTp53, and gain-of-function (GOF) independent of WTp53, which are not mutually exclusive (7, 8). Despite losing sequence-specific DNA binding (SSDB) activity, mutant p53 (MTp53) can regulate gene expression through both direct and indirect mechanisms (7, 9, 10). Direct binding of MTp53 to DNA can be achieved by DNA structure-selective binding (DSSB), in which MTp53 recognizes its target genes by selective binding to DNA secondary structures. On the other hand, MTp53 associates with various transcription factors to act as a transcriptional repressor or transcription cofactor. Moreover, cooperation between MTp53 and the SWI/SNF chromatin remodeling complex contributes to over 40% of MTp53-regulated gene expression (11). MTp53 also exerts its oncogenic functions *via* modulating non-coding RNAs (ncRNAs) (12). Taken together, all these facts reveal a significant contribution of the indirect mechanisms to MTp53-mediated biological effects.

As previously mentioned, p53 has emerged as a critical modulator of cellular metabolism. Actually, p53-mediated metabolic activities have been reported to involve in the development of several human diseases, including diabetes, ischemia, neurodegeneration, as well as cancer (13), which we will focus on in this review. In addition to inducing or repressing the expression of transcriptional target genes associated with p53-mediated metabolic pathways and directly interacting with metabolic enzymes to activate or inhibit their activities, p53 also regulates metabolism *via* indirect mechanisms. The indirect mechanisms which we define here are categorized into three groups. First, p53 regulates metabolic genes through modulating its direct targets, such as microRNAs (miRNAs) and long non-coding RNAs (lncRNAs). Second, p53 activates or suppresses the expression of metabolic genes through interacting with other transcription factors. Third, p53 controls metabolism by affecting signaling pathways. These indirect mechanisms scale up the number of metabolism-associated genes regulated by p53, extend the influence of p53 to a wide variety of metabolic pathways, and expand the p53 regulatory networks of metabolism, further highlighting p53 as a master regulator of metabolism. The critical role of p53-mediated indirect regulation on metabolism in tumorigenesis and tumor progression is evident, for example, in our previous study that in spite of several direct transcriptional targets of p53 involved in mitochondrial respiration, restoration of the decreased oxidative phosphorylation (OXPHOS) caused by MTp53 could be achieved through ectopic expression of miR-200c, a downstream direct transcriptional target of p53, which enhances phosphoenolpyruvate carboxykinase 2 (PCK2) expression *via* downregulating ZEB1/BMI1 (14). Moreover, restoring miR-200c expression leads to suppression of tumor growth, whereas interference of PCK2, the key enzyme linking the TCA cycle and glycolysis (15), counteracts the miR-200c-mediated tumor-suppressing effect, which accentuates the vital role of the indirect mechanisms accounting for p53-regulated cellular metabolism, and provides a functional link between p53-regulated metabolism and p53-mediated biological functions. Furthermore, p53 is generally considered an important metabolic sensor by positioning at the center of several signaling pathways coordinating cellular metabolism (16). Notably, direct and indirect regulation of metabolism by p53 are not mutually exclusive but overlapped to some extent. This is exemplified by hexokinase 2 (HK2), the first rate-limiting enzyme of glycolysis, which is both a direct transcriptional target of p53 (17) and an indirect metabolic target of p53 through miR-34a (18) and miR-143 (19). Interestingly, glucose transporter 1 (GLUT1), transcriptionally repressed by p53 (20) is an indirect target of MTp53 through modulation of the RhoA/ROCK signaling pathway (21), indicating the flexibility of indirect mechanisms underlying p53-mediated metabolic activities.

Transcriptional targets of p53 in regulating metabolism have been delineated in widespread literature, especially in a review article that gives a clear summary of direct target genes activated or repressed by p53 in every aspect of metabolic pathways (16). Considering that the indirect mechanisms seem to play a critical role in contributing to p53-mediated control of cellular metabolisms and other biological functions, and a growing number of metabolic-associated genes and proteins have been reported to be indirectly modulated by p53, in the present work, we will briefly summarize the indirect regulation of cellular metabolism by WTp53 (**Figure 1** and **Table 1**) and MTp53 (**Figure 2** and **Table 2**), respectively.

WILD-TYPE P53-MEDIATED INDIRECT REGULATION ON METABOLISM

As illustrated in **Figure 1** and summarized in **Table 1**, mechanisms accounting for WTp53-mediated indirect regulation of metabolism can be categorized into three major types: through transcriptionally regulating downstream target genes (**Figure 1A** and **Table 1A**), through protein-protein

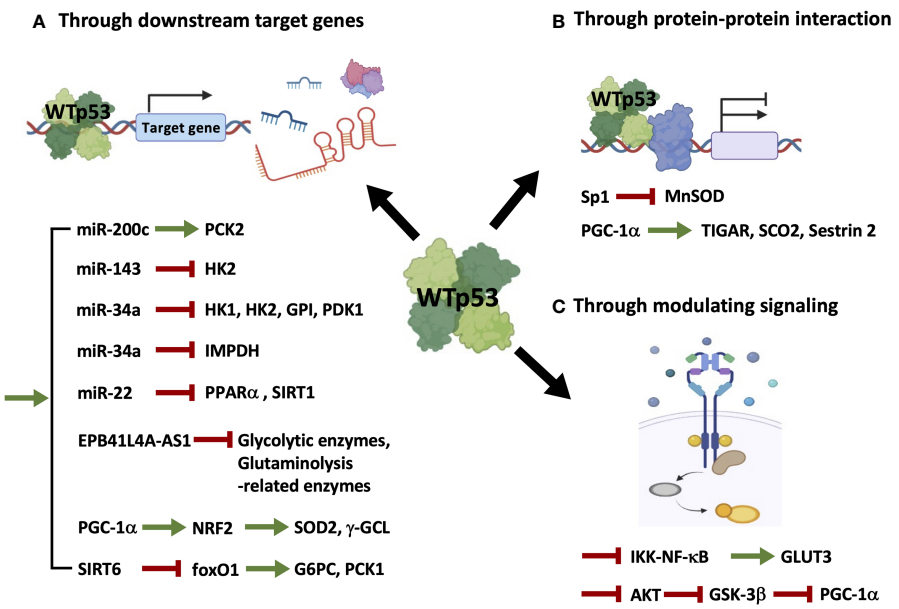

FIGURE 1 | Wild-type p53 regulates cellular metabolism through indirect mechanisms. WTp53 indirectly regulates metabolism through inducing its direct targets, including miRNAs, lncRNAs, and proteins **(A)**, associating with other transcription factors **(B)**, or modulating signaling pathways **(C)**.

interactions (**Figure 1B** and **Table 1B**), and through modulating signaling pathways (**Figure 1C** and **Table 1C**).

(A). WTp53 indirectly regulates the expression of metabolism-related genes by modulating its direct targets (**Figure 1A** and **Table 1A**). In our previous study (14), we demonstrate that miR-200c, a WTp53 target negatively regulating epithelial-mesenchymal transition (EMT) and stemness (39), promotes OXPHOS in basal-like breast cancer (BLBC) cells by inhibiting the downstream targets, ZEB1 and BMI1, which subsequently activates PCK2 expression. In prostate cancers, loss of p53 compromises p53-induced miR-143, facilitating degradation of HK2 mRNA, which is required for *Pten/p53*-deficiency-driven aerobic glycolysis, proliferation, transformation, and *in vivo* tumor growth (19). In another study, induction of miR-34a by p53 downregulates hexokinase 1 (HK1), HK2, glucose-6-phosphate isomerase (GPI), and pyruvate dehydrogenase kinase 1 (PDK1), potentiating mitochondrial respiration and decreasing glycolysis (18). In addition to regulating glucose metabolism, p53-induced miR-34a also represses the expression of inosine 5'-monophosphate dehydrogenase (IMPDH), the rate-limiting enzyme of GTP biosynthesis, leading to decreased Ras signaling (22). In the mouse model of diet-induced obesity (DIO)-related hepatic steatosis, activation of the hepatic cannabinoid-1 receptor (CB_1R) induces expression of miR-22 through modulating the transcriptional activity of p53, which disturbs peroxisome proliferator-activated receptor-α (PPARα) and NAD^+-dependent histone deacetylase sirtuin 1 (SIRT1), leading to decreased fatty acid oxidation (FAO) and increased fat accumulation in the liver (23). The lncRNA EPB41L4A-AS1, a transcriptional target of WTp53, decreases glycolysis and glutaminolysis *via* interacting with histone deacetylase 2 (HDAC2), in which interference of EPB41L4A-AS1 sensitizes tumor cells to glutaminase inhibitor (24). Aside from modulating non-coding RNAs, p53 transactivates peroxisome proliferator-activated receptor γ coactivator-1α (PGC-1α), the master regulator of mitochondrial biogenesis and function (40), upon glutathione (GSH) depletion, which induces antioxidant response through nuclear factor E2-related factor 2 (NRF2)-mediated expression of manganese superoxide dismutase (MnSOD or SOD2) and γ-glutamylcysteine ligase (γ-GCL) (25). Furthermore, p53 inhibits the expression of the rate-limiting enzymes of gluconeogenesis, glucose-6-phosphatase (G6PC) and phosphoenolpyruvate carboxykinase 1 (PCK1), through transactivating NAD^+-dependent histone deacetylase sirtuin 6 (SIRT6), which subsequently causes deacetylation and nuclear exclusion of forkhead box protein O1 (foxO1), the inducer of G6PC and PCK1 (26).

(B). WTp53 indirectly regulates metabolism through a protein-protein interaction with other transcription factors (**Figure 1B** and **Table 1B**). For example, p53 associates with the transcription factor, specificity protein 1 (Sp1), to repress transcription of MnSOD (27), an antioxidant enzyme differentially expressed in cancers (41). Interestingly, in addition to transcriptional control, p53 recruits PGC-1α to modulate its transactivation activity at early periods of metabolic stress, as indicated by upregulation of the proarrest and metabolic genes, including TP53-induced glycolysis regulatory phosphatase (TIGAR), synthesis of

TABLE 1 | Metabolic targets indirectly regulated by wild-type p53.

p53 Status	Targets	Mechanism of Regulation	Metabolic Effect	Biological Consequence	Ref.
(A) Through transcriptionally regulating downstream target genes					
WTp53	Phosphoenolpyruvate carboxykinase 2 (PCK2)	Induce miR-200c to upregulate expression.	Increased OXPHOS.	p53 mutation facilitates cancer stemness.	(14)
WTp53	Hexokinase 2 (HK2)	Induce miR-143, which facilitates degradation of HK2 mRNA.	Decreased aerobic glycolysis.	Loss of p53 leads to *Pten/p53*-deficiency-driven proliferation, transformation, and *in vivo* tumor growth.	(19)
WTp53	Hexokinase 1 (HK1), HK2, Glucose-6-phosphate isomerase (GPI), Pyruvate dehydrogenase kinase 1 (PDK1)	Induce miR-34a to downregulate expression.	Decreased glycolysis and increased mitochondrial respiration.	Not applicable.	(18)
WTp53	Inosine 5'-monophosphate dehydrogenase (IMPDH)	Induce miR-34a to downregulate expression.	Decreased GTP biosynthesis (purine synthesis).	p53 represses GTP-dependent Ras signaling pathway.	(22)
WTp53	Peroxisome proliferator-activated receptor-α (PPARα), NAD^+-dependent histone deacetylase sirtuin 1 (SIRT1)	Induce miR-22 to downregulate expression.	Decreased FAO.	Blockade of this signaling pathway ameliorates high-fat diet (HFD)-induced hepatic steatosis.	(23)
WTp53	Glycolytic enzymes such as HK1 and pyruvate kinase M2 (PKM2); Glutaminolysis-related enzymes such as alanine-serine-cysteine transporter type 2 (ASCT2) and Glutaminase 2 (GLS2)	Induce the lncRNA EPB41L4A-AS1 to downregulate expression through modulating the VHL/HIF-1α pathway and the VDAC1/ATF4 pathway, respectively	Decreased glucose uptake, glycolysis, and lactate production. Decreased glutaminolysis.	Depletion of EPB41L4A-AS1 largely increases the anti-tumor effect of glutaminase inhibitors.	(24)
WTp53	Manganese superoxide dismutase (MnSOD or SOD2), γ-glutamylcysteine ligase (γ-GCL)	Transactivate PGC-1α to upregulate expression through NRF2.	Decreased ROS.	Blockade of the p53-PGC-1α-NRF2 pathway increases ROS and cell death.	(25)
WTp53	Glucose-6-phosphatase (G6PC), Phosphoenolpyruvate carboxykinase 1 (PCK1)	Transactivate SIRT6 to cause deacetylation and nuclear exclusion of foxO1, which is the inducer of G6PC and PCK1.	Decreased gluconeogenesis.	p53 decreases the recovery of murine blood glucose levels induced by pyruvate.	(26)
(B) Through protein-protein interaction					
WTp53	Manganese superoxide dismutase (MnSOD or SOD2)	Associate with Sp1 to inhibit transcription.	Not applicable.	Not applicable.	(27)
WTp53	TP53-induced glycolysis regulatory phosphatase (TIGAR), Synthesis of cytochrome C oxidase 2 (SCO2), Sestrin 2	Recruit PGC-1α to upregulate expression.	Decreased ROS.	p53 binds to PGC-1α to promote cell-cycle arrest and ROS clearance at early periods of glucose starvation.	(28)
(C) Through modulating signaling pathways					
WTp53	Glucose transporter 3 (GLUT3)	Inhibit the IKK-NF-κB pathway, which activates GLUT3.	Decreased glycolysis and lactate production.	p53 deficiency leads to oncogene-induced cell transformation.	(29)
WTp53	Peroxisome proliferator-activated receptor γ coactivator-1α (PGC-1α)	Inhibit AKT and activate GSK-3β to promote degradation through the ubiquitin-proteasome system.	Decreased mitochondrial function.	Knockdown of PGC-1α synergizes with cisplatin to promote apoptosis and inhibit tumor growth.	(30)

cytochrome C oxidase 2 (SCO2), and sestrin 2, which induces cell-cycle arrest and reactive oxygen species (ROS) clearance (28).

(C). WTp53 modulates signaling pathways to affect cellular metabolism (**Figure 1C** and **Table 1C**). An example of this is the study from Kawauchi et al. in which p53 deficiency in mouse embryonic fibroblasts (MEFs) leads to activation of the IKK-NF-κB pathway, which transactivates the *Glut3* gene, and increases aerobic glycolysis and lactate production, contributing to oncogene-induced cell transformation (29). In contrast to transactivating or recruiting PGC-1α to serve as a coactivator, p53 destabilizes PGC-1α through activating the ubiquitin-proteasome system, mediated by AKT/GSK-3β-dependent phosphorylation of PGC-1α, which impairs mitochondrial function and increases chemosensitivity of non-small cell lung cancer (NSCLC) (30).

MUTANT P53-MEDIATED INDIRECT REGULATION ON METABOLISM

As illustrated in **Figure 2** and summarized in **Table 2**, MTp53 indirectly regulates metabolism either by disturbing WTp53 function (**Figure 2A** and **Table 2A**) or by exerting its gain-of-function properties (**Figures 2B, C** and **Tables 2B, C**).

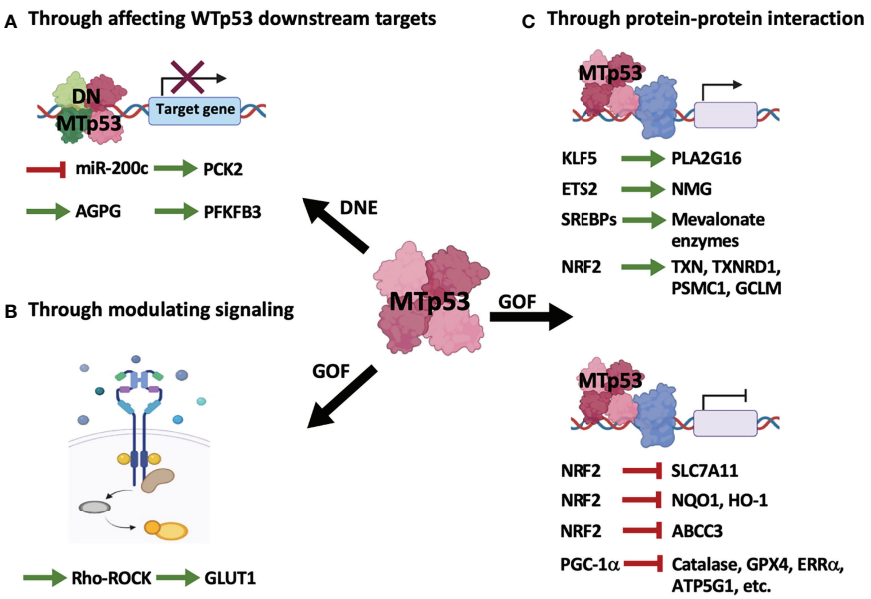

FIGURE 2 | Mutant p53 regulates cellular metabolism through indirect mechanisms. MTp53 indirectly regulates metabolism by its dominant-negative effect (DNE) over WTp53 **(A)**, and the gain-of-function (GOF) properties encompassing modulation of signaling pathways **(B)** or interaction with other transcription factors **(C)**.

(A). MTp53-mediated metabolic reprogramming from perturbation of WTp53 downstream targets (**Figure 2A** and **Table 2A**) can be exemplified by our previous research that MTp53 attenuates OXPHOS through downregulating miR-200c, the positive regulator of PCK2, which facilitates cancer stemness in BLBC (14). In our study, the MTp53-exerted dominant-negative effect impedes the expression of miR-200c, which upregulates ZEB1 and BMI1 and subsequent downregulates PCK2. PCK2 deficiency not only leads to decreased OXPHOS in normal mammary epithelial cells but also compromises the increased OXPHOS by restoration of miR-200c in BLBC cells (14). Another example is a recent study that upregulation of the lncRNA Actin Gamma 1 Pseudogene (AGPG) by p53 deficiency leads to stabilization of fructose-2,6-biphosphatase 3 (PFKFB3), contributing to enhanced glycolysis, proliferation, and tumor growth (31).

(B). Independent of WTp53, the gain-of-function of MTp53 has a profound effect on various metabolic pathways. Similar to WTp53, MTp53 also regulates metabolism by affecting signaling pathways (**Figure 2B** and **Table 2B**). This is evidenced in a study that MTp53-boosted glycolysis promotes tumorigenesis through activation of the RhoA/ROCK signaling, subsequently inducing actin polymerization and translocation of GLUT1 to the plasma membrane (PM) (21).

(C). Distinct from WTp53-mediated indirect regulation on metabolism which is mainly mediated by its downstream target genes (**Figure 1A** and **Table 1A**), MTp53 gains novel abilities to interact with a variety of proteins, particularly transcription factors, to drive tumor-associated metabolic alterations (**Figure 2C** and **Table 2C**). Examples of metabolic genes activated by MTp53 encompass *PLA2G16*, encoding a phospholipase catalyzing the formation of free fatty acids and lysophospholipids. The association of MTp53 with Kruppel-like factor 5 (KLF5) transactivates *PLA2G16*, which leads to increased glycolytic rate and accelerates tumor growth (32). Besides, enhanced expression of nucleotide metabolism genes (NMG) can be induced by cooperation between MTp53 and ETS proto-oncogene 2 transcription factor (ETS2), which is associated with poor prognosis in breast cancer patients (33). Gain-of-function of MTp53 also confers its ability to interact with the sterol regulatory element binding proteins (SREBPs) and be recruited to the sterol regulatory elements (SRE-1), which then induces genes encoding enzymes in the mevalonate pathway, contributing to the disrupted acinar formation in breast cancer cells (34). Later research further demonstrates that MTp53 exerts a differential regulation on NRF2 targets regardless of whether cells are under unstressed or oxidative stress conditions, where expression of genes upregulated by MTp53, including thioredoxin (TXN), thioredoxin reductase 1 (TXNRD1), proteasome 26S subunit ATPase 1 (PSMC1), and glutamate-cysteine ligase modifier subunit (GCLM), correlates with worse overall survival in breast cancer patients (35).

On the other hand, accumulated MTp53 proteins interfere with NRF2 activity, resulting in decreased expression of SLC7A11, a cystine/glutamate antiporter. Downregulation of SLC7A11 leads to GSH depletion and increased ROS, which sensitizes cancer cells to APR-246, a MTp53 reactivator (36). In another study, MTp53 is found to protect cancer cells confronted

TABLE 2 | Metabolic targets indirectly regulated by mutant p53.

p53 Status	Targets	Mechanism of Regulation	Metabolic Effect	Biological Consequence	Ref.
(A) Dominant-negative effect: Through affecting WTp53 downstream targets					
MTp53 (R175H, R249S, R273H, R280K)	PCK2	Downregulate WTp53-induced miRNA miR-200c, which increases PCK2 expression through inhibiting ZEB1 and BMI1.	Decreased OXPHOS.	Downregulation of PCK2 by MTp53 through the miR-200c-ZEB1/BMI1 axis facilitates cancer stemness.	(14)
MTp53 (V272M, R110L + E326K)	Fructose-2,6-biphosphatase 3 (PFKFB3)	Rescue WTp53-repressed lncRNA AGPG to prevent ubiquitination and stabilize PFKFB3.	Enhanced glycolysis.	Upregulation of AGPG by MTp53 promotes cell proliferation and *in vivo* tumor growth.	(31)
(B) Gain-of-function: Through modulating signaling pathways					
MTp53 (R175H, R248Q, R273H)	Glucose transporter 1 (GLUT1)	Activate the RhoA/ROCK signaling, which induces GLUT1 translocation to the plasma membrane.	Enhanced glycolysis.	Knocking down GLUT1 abolishes MTp53-promoted anchorage-independent growth and xenograft tumor growth.	(21)
(C) Gain-of-function: Through protein-protein interaction					
MTp53 (R273H, R248W)	Phospholipase A2, group XVI (PLA2G16)	Associate with KLF5 to activate transcription.	Increased glycolysis.	High PLA2G16 predicts a poor prognosis. Knockdown of PLA2G16 impairs proliferation, anchorage-independent growth, and tumor growth.	(32)
MTp53 (R249S, R273L, R280K, R248W)	Nucleotide metabolism genes (NMG)	Associate with ETS2 to activate transcription.	Increased dNTP and rNTP pools.	NMG expression contributes to invasion and metastatic potential.	(33)
MTp53 (R175H, R248Q, R273H, R248W, G245S, R280K)	Mevalonate pathway enzymes such as HMG-CoA reductase (HMGCR)	Associate with SREBPs to activate transcription.	Elevated activity of the mevalonate pathway.	Supplementing metabolites produced by the mevalonate pathway reverses the phenotypic reversion of disrupted acinar formation caused by the KD of MTp53.	(34)
MTp53 (R175H, R280K)	NRF2 target genes Activated: Thioredoxin (TXN), Thioredoxin reductase 1 (TXNRD1), Proteasome 26S subunit ATPase 1 (PSMC1), Glutamate-cysteine ligase modifier subunit (GCLM) Inhibited: Heme oxygenase 1 (HO-1), Solute carrier family 7 member 11 (SLC7A11), ATP binding cassette subfamily C member 3 (ABCC3)	Associate with NRF2 to activate or inhibit transcription.	Not applicable.	Differential regulation of NRF2 targets by MTp53 contributes to cell survival and migration under oxidative stress. MTp53-activated NRF2 targets are correlated with poor prognosis.	(35)
MTp53 (C277F, R248Q, R248W, G266E, R175H, R273H)	SLC7A11	Bind to and interfere with NRF2 to inhibit transcription.	Depleted glutathione and increased ROS.	A low level of SLC7A11 sensitizes cancer cells with MTp53 to APR-246, which induces oxidative stress.	(36)
MTp53 (R273H)	NAD(P)H quinone dehydrogenase (NQO1), HO-1	Interfere with NRF2 to inhibit transcription.	Increased ROS.	MTp53-mediated reduction of phase 2 detoxifying enzymes promotes cell survival following oxidative damage.	(37)
MTp53 (R175H, R273H)	PGC-1α target genes such as Catalase, Glutathione peroxidase 4 (GPX4), Estrogen-related receptor α (ERRα), ATP synthase lipid-binding protein (ATP5G1)	Associate with PGC-1α to inhibit its function.	R72-MTp53 shows increased OXPHOS.	Tumor cells with R72-MTp53 have greater migration, invasion, and metastatic ability than tumor cells with P72-MTp53.	(38)

with oxidative stress from death through diminishing NRF2-mediated phase 2 ROS detoxifying enzymes, NAD(P)H quinone dehydrogenase (NQO1) and heme oxygenase 1 (HO-1) (37). Like the aforementioned, MTp53 differentially regulates NRF2 targets, in which metabolic genes are suppressed by MTp53 including HO-1, SLC7A11, and ATP binding cassette subfamily C member 3 (ABCC3) (35). Surprisingly, not only WTp53 binds to PGC-1α, MTp53 also interacts with PGC-1α; though this association exerts an inhibitory effect on PGC-1α. Basu et al. demonstrate that the codon 72 polymorphism in *TP53* impacts the binding and regulation of MTp53 to PGC-1α. The arginine 72 variant (R72) of MTp53, instead of the proline 72 variant

(P72), shows decreased association with PGC-1α, resulting in increased PGC-1α function, enhanced OXPHOS, invasion, and metastasis (38).

TARGETING MUTANT P53: RECENT ADVANCES AND FUTURE PERSPECTIVES

Direct or Indirect?

Therapeutic strategies against tumors with p53 mutation are classified into direct and indirect approaches (42, 43). Direct targeting of MTp53 is attained by either restoring WTp53 function to MTp53 or depleting MTp53. Several MTp53 reactivators have been developed to refold MTp53 into the conformation of WTp53, prevent aggregation of MTp53 proteins, and restore DNA binding and transcriptional activity. In contrast, MTp53 destabilizers promote the degeneration of MTp53 and thus limit its expression, mainly through ubiquitin-proteasome degradation or autophagy-lysosome degradation pathways (44). Afterward, immunotherapies have emerged as promising strategies targeting tumors bearing MTp53 (45), including adoptive T cell therapy, the usage of antibody-drug conjugate (ADC) (46), and more recently, the development of the innovative bispecific antibody (BsAb) (47).

On the contrary, indirect approaches aim to disrupt connections between MTp53 and its synthetic lethal partners. Synthetic lethality is the concept that the simultaneous disturbance of two genes leads to cell death. In contrast, perturbation of an individual gene is tolerable, in which disruption of the two genes can be achieved by double mutations or single mutation of one gene combined with pharmacological inhibition of the other (48, 49). Due to the extensive influence of MTp53 on a variety of cellular processes and tumor development, synthetic lethality for cancer therapeutics against MTp53 is prospectively applicable to a wide range of cancers with *TP53* mutation, and thus, the identification of synthetic lethal genes to MTp53 becomes attractive. The development of synthetic lethal strategies targeting MTp53 provides more opportunities and therapeutic options for cancer patients with *TP53* mutation, which has advantages over approaches directly targeting MTp53, which are listed below.

(1). Synthetic lethality-based drugs are promising to broaden the strategies against cancers by their potential to overcome the major limitation of genetically targeted therapies. Not all cancer mutations are druggable, especially loss-of-function mutations (50, 51).

(2). It is quite challenging to develop MTp53 reactivators or inhibitors because of the diverse nature of MTp53 proteins. The structural diversity and the consequent distinct functional properties of every MTp53 make it practically infeasible to target all MTp53 with a single compound (42, 52). Synthetic lethal methods are more flexible because of the high dependency on MTp53-induced oncogenic effects rather than on MTp53 itself.

(3). MTp53 reactivators or inhibitors may induce severe toxicities and intolerable adverse effects. For example, MIRA-1, a MTp53 reactivator, could cause acute cytotoxicity to normal cells through induction of caspase-9-mediated apoptosis independent of p53 (53). APR-246 and COTI-2 are the only two drugs in clinical trials (42). Moreover, the relatively low-specificity inhibitors promoting degradation of MTp53, such as histone deacetylase inhibitors (HDACis), may elicit unfavorable adverse effects due to their widespread influence on normal cells (54).

(4). Restoration of WTp53 function to MTp53 might backfire because WTp53 has been paradoxically reported to favor tumor progression, particularly through metabolic regulation, which we highlight in this article. This notion is evident in a study that WTp53 potentiates glycolysis and decreases pyruvate uptake and thus OXPHOS in hepatocarcinoma (HCC) through inducing PUMA inhibition on mitochondrial pyruvate carrier (MPC) (55). Another study also substantiates that a low dosage of sulforaphane, the inducer of NRF2, could prevent apoptosis, promote proliferation, and enhance mitochondrial respiration in colorectal cancer (CRC) cells with WTp53 but not in p53-knockout CRC cells, suggesting a tumor-promoting role of WTp53 (56). Because of the potentially bi-faceted role of WTp53 in cancer, it is indispensable to ascertain the WTp53-mediated metabolic regulation and biological effects in different types of cancer.

Synthetic Lethality With Metabolism

Several candidate synthetic lethal genes to p53 involved in various cellular processes, such as DNA repair, cell-cycle control, cell growth and proliferation, and metabolism, have been identified (57). Among these, we suggest that synthetic lethality targeting MTp53 with metabolism is the most potentially feasible for clinical application for the reasons stated below.

(1). In comparison to targeting MTp53 with metabolism, synthetic lethality with other cellular processes like DNA damage response and cell-cycle arrest may not only kill tumor cells but also damage normal cells, which could lead to severe adverse effects. For example, UCN01, an inhibitor of checkpoint kinase 1 (Chk1), the critical regulator of intra-S and G2/M checkpoints (58), has been halted for further clinical development due to the worse efficacy and the induction of unacceptable toxicities (59). Similarly, BI 2536, an inhibitor of polo-like kinase 1 (Plk1), which plays a crucial role in mitosis (60), exhibited a poor response rate and short half-life and could induce severe adverse events, leading to discontinued clinical progress (61).

(2). The highly intertwined relationships among different biomolecular processes contribute to the formation of metabolic networks, which interact with each other to form the complex construct of metabolism (62). Perturbations of the connected molecules could lead to disconnection of these pathways and breakdown of the metabolic networks,

consequently destroying the resilience, which could cause cellular dysfunction and diseases (62). For tumor cells displaying high metabolic plasticity, the above features make it a potential treatment strategy to disrupt the crosstalk between the interconnected metabolic pathways by dual inhibition of these pathways with metabolic drugs or targeting compensatory mechanisms with a combination of drugs inhibiting global regulators and the respective compensatory bioenergetic pathways (63). Dual targeting of metabolic pathways as a therapeutic strategy has been demonstrated in the case of Lewis lung carcinoma (LLA), in which 2-deoxy-D-glucose (2-DG), a non-metabolizable analog of glucose that competitively binds to hexokinase and inhibits glycolysis (64), significantly enhances the antitumor activity of dichloroacetate (DCA), an inhibitor of pyruvate dehydrogenase kinase (PDK) that activates pyruvate dehydrogenase (PDH) and boosts OXPHOS activity (65, 66), accompanied with inhibition of glycolysis and increased cytotoxicity of tumor-infiltrating monocytes (67). In the case of p53 mutated breast cancer cells, 2-DG increases the sensitivity of tumor cells to metformin, which indirectly activates AMP-activated protein kinase (AMPK) by inhibiting complex I of the mitochondrial electron transport chain (68), indicating co-treatment of 2-DG and metformin may be an effective therapeutic strategy (69). Alternatively, a combination of phenformin, an AMPK activator, and 2-DG induces metabolic stress, suppresses tumor growth, and promotes degradation of MTp53 proteins (70), foreshadowing the promising future of inhibiting compensatory mechanisms accounting for the metabolic flexibility of tumor cells.

(3). Nowadays, there have been various metabolic drugs approved for clinical use in cancers and other diseases, such as 5-fluorouracil (5-FU) targeting nucleotide metabolism and metformin inhibiting mitochondrial function. Besides, several metabolic inhibitors are currently in cancer clinical trials (71), which are prospectively applicable in cancer treatments in the imminent future. Uncovering the MTp53-induced metabolic alterations in cancers would assist the utilization of these metabolic drugs in combination therapies or adjuvant therapies.

Targeting p53-Mediated Indirect Regulation on Metabolism

In addition to targeting MTp53 with metabolism, mediators of MTp53-driven metabolic alterations are extremely potential synthetic lethal partners to MTp53. Specifically, the human genome comprises about 2% of protein-coding genes, leaving the vast majority to be non-coding RNAs (72). ncRNAs are critical regulators of many cellular processes, which indispensably coordinate the functional operation of complex networks in cells. Dysregulation of ncRNAs is detrimental, leading to pathological development like cancer (73). In viewing that p53 plays a pivotal role in regulating ncRNAs (12, 74), and that disturbance of ncRNAs contributes to cancer-associated metabolic reprogramming (75, 76), ncRNAs are expected to expand the synthetic lethal networks of MTp53 with metabolism. The examples below illustrate this point in detail.

As demonstrated in our previous work, MTp53 attenuates OXPHOS through disturbing the miR-200c-PCK2 axis, in which restoration of miR-200c rescues the decreased OXPHOS by MTp53 (14), implying therapeutic delivery of miR-200c through viral vectors or non-viral approaches, such as nanoparticles and liposomes (77), is a potential treatment strategy for intractable BLBC. It is noteworthy that restoring miR-200c expression not only boosts OXPHOS, but further nullifies MTp53-induced EMT and stemness, which may result from simultaneous activation of OXPHOS and direct inhibition of its downstream targets, ZEB1 and BMI1 (14). Likewise, miR-149-3p has been revealed to restore chemosensitivity of colorectal cancer cells through decreasing glycolytic activity *via* downregulating pyruvate dehydrogenase kinase 2 (PDK2), suggesting CRC patients with MTp53, in which the frequency of *TP53* mutation is around 40-50%, might benefit from combined employment of chemotherapy and miR-149-3p-based therapy (78). In addition to miRNAs, targeting lncRNAs synthetic lethal to MTp53 is also a potential therapeutic intervention. In the case aforementioned in the section of MTp53-mediated indirect regulation on metabolism, the lncRNA AGPG is upregulated by MTp53, which enhances glycolysis through preventing PFKFB3 from degradation (31). Interference of AGPG shows significantly inhibitory effects on tumor cells, providing implications for developing an RNA interference-based strategy.

For the same reason, the concept of expanding the synthetic lethality to MTp53 through targeting its indirect regulation on metabolism can apply to other mechanisms, like the signaling pathways modulated by MTp53 (**Figure 2B** and **Table 2B**), or the transcription factors associated with MTp53 (**Figure 2C** and **Table 2C**). Furthermore, in addition to metabolic drugs, numerous small-molecule targeted drugs and therapeutic monoclonal antibodies are FDA-approved for cancer treatment (79–81). Consequently, further investigation of molecular mechanisms accounting for MTp53-mediated metabolic reprogramming offers opportunities for patients with MTp53 tumors, in which these targeted drugs might be available in medical treatments.

Together, this evidence unequivocally indicates that targeting MTp53-mediated indirect regulation rather than directly targeting MTp53-driven metabolic alteration may elicit more powerful tumoricidal effects.

CHALLENGES ON THE JOURNEY

Despite the accumulated myriad of research on p53 during the past four decades, a thorough understanding of the p53 regulatory network of cellular metabolism is still lacking. The progress of targeting MTp53 according to its regulation on cancer metabolism in practical clinical approaches remains stagnant, which could arise from the complexity of p53 and research limitations as following described.

(1). p53 regulation of metabolism is highly cell type-specific. A growing body of evidence has revealed that it is inappropriate to apply the general assumption of p53-regulated metabolism to all the types of cells, which is firmly supported by Kim et al. that WTp53 promotes glycolysis instead of OXPHOS in HCC (55). Furthermore, p53 regulates metabolism distinctly under stressed or unstressed conditions. For instance, p53 is demonstrated to increase OXPHOS in normoxia while decreasing OXPHOS in hypoxia in the cervix and breast cancer cells (82). As a result, the regulatory networks of p53 on cellular metabolism in different cells need to be more clearly defined.

(2). The exceedingly diverse nature of MTp53 proteins makes it a hurdle to precisely delineate MTp53-regulated metabolism in cancer cells. As shown in our previous study (14), stable expression of different MTp53 variants in normal mammary epithelial cells promotes glycolysis and suppresses mitochondrial respiration to varying extents. Erikson et al. also demonstrate that different hotspot mutations of p53 could have differential impacts on cellular metabolism like glycolysis and that endogenous and exogenous expression of even the same type of p53 mutation could exert opposite effects on OXPHOS (83).

(3). Murine cells and mouse models are frequently utilized in research exploring p53-regulated metabolism and the underlying molecular mechanisms; nevertheless, substantial differences in gene expression patterns and transcriptional regulatory programs have been observed between mice and humans (84). A more recent study corroborates that the p53 gene regulatory network (GRN) in mice differs from that in humans, in which the meta-analysis reveals extensive variation in p53-regulated gene expression profiles and high species-specificity of p53 transcriptional targets (85). This distinction can be exemplified by CPT1C, the brain isoform of the rate-limiting enzyme of FAO. CPT1C is generalized as a direct target of p53 (16, 86, 87); though, CPT1C is upregulated by p53 in mice but not in humans, reflecting the lack of p53 binding sites on human *CPT1C* promoter (85). In response to the differences in p53 GRN between mice and humans, more efforts are in need to confirm the metabolic roles of p53.

(4). Despite synthetic lethality targeting the mediators of MTp53-associated cancer metabolism portends a bright future for innumerable cancer patients with *TP53* mutation, the diverse nature of MTp53, the intracellular intricate regulatory networks accounting for the modulation of metabolism, and the extrinsic environmental factors determine together with the specific synthetic lethal partners to a specific type of MTp53, making identifying the synthetic lethal partners a quite challenging work. Once a synthetic lethal partner has been identified, the following concern is whether there are drugs specific for this synthetic lethal partner, or whether this synthetic lethal partner could be delivered to tumor sites or transported into tumor cells. The challenges of research on p53-mediated indirect regulation of metabolism are summarized below.

(a). The mechanism accounting for MTp53 indirect regulation of metabolism by dominant-negative effect over WTp53 (**Figure 2A** and **Table 2A**) may conform to multiple forms of MTp53, whereas the mechanisms underlying MTp53 indirect regulation of metabolism by gain-of-function (**Figures 2B, C** and **Tables 2B, C**) may not. Different types of MTp53 proteins might have distinct synthetic lethal partners; therefore, more efforts are required to identify the particular synthetic lethal relationship between the mediators involved in MTp53-regulated cancer metabolism and the specific types of MTp53.

(b). The synthetic lethal partner in a cell type could cause distinct, even opposite effects in another. PGC-1α illustrates this point clearly. In ERBB2$^+$ breast cancers, high expression of PGC-1α predicts poorer prognosis and is correlated with high expression of glutamine cluster, reflecting the increased expression of PGC-1α in ERBB2$^+$ breast cancer cells potentiates glutamine metabolism and facilitates proliferation under low glucose and hypoxia (88). On the contrary, elevated expression of PGC-1α leads to increased FAO and TCA cycle, decreased glycolysis, and suppression of tumor growth and metastasis in prostate cancers (89).

(c). There might be no targeted drug for a specific synthetic lethal partner, or it is tricky to develop it. For example, to our knowledge, there is no specific inhibitor for PGC-1α currently, which is activated by decreased binding to R72-MTp53, contributing to migration, invasion, and metastasis (38).

(d). Although successes in miRNA-based anti-cancer therapy have been reported (90), such as the significantly reduced tumor burden and improved survival rate in *Kras*;*Trp53* mutant NSCLC mice administered combinatorial treatment of miR-34a and let-7b using NOV340 liposomal nanoparticles (91), there are still challenges remained to be overcome in the clinical development of miRNA therapeutics. Maintaining stability and integrity of miRNA mimics or antagonists in the circulation, determining suitable dosages, delivering systems, and administration routes, increasing specificity and efficient penetration into tumors, as well as minimizing immunotoxicity and off-target effects all are issues needed to be concerned (90, 92).

In addition to the existing limitations to research on p53 regulatory networks of cellular metabolism, the links between p53-mediated cellular metabolism and p53-induced biological functions remain largely unknown since few studies have comprehensively deciphered the contribution of p53-regulated metabolic phenotype to tumor progression or tumor suppression. Deregulated metabolism has been designated as an emerging hallmark of cancer in the last decade (93), which implies uncovering the biological effects of metabolic alterations induced by p53 and the underlying molecular mechanisms is of great importance for designing the optimized treatment strategies. Like those mentioned above, our previous study reveals that MTp53 facilitates cancer stemness through attenuating OXPHOS by disturbance of the miR-200c-PCK2

axis (14), which fully addresses the molecular mechanism accounting for the connection between MTp53-induced metabolic alteration and traits of cancer. Notably, restoring miR-200c expression either in normal mammary epithelial cells overexpressing p53 mutants or in BLBC cells harboring endogenous MTp53 not only counteracts MTp53-induced EMT and stemness, but also recovers the decreased OXPHOS activity, foretelling the promising future of treating cancers with p53 mutation by modulating the mediators of metabolic reprogramming indirectly driven by MTp53. Moreover, metabostemness, describing cellular metabotypes as the driver to redirect normal cancer cells to less-differentiated cancer stem cell (CSC) states (94), interprets the significance of connecting metabolic features to traits of cancer cells, which opens a brand new way to cure cancer patients by circumventing resistance to therapies, metastasis, and tumor recurrence caused by CSCs (95) based on their metabolic dependencies.

SUMMARY

Overall, in addition to activating or repressing target genes transcriptionally, p53 regulates metabolism-related gene expression through indirect mechanisms as well, either by regulating direct transcriptional targets, associating with other transcription factors, or modulating signaling pathways. The notion that perturbations of p53 regulatory networks of cellular metabolism are in relation to tumor initiation and progression accentuates the crucial role of p53 in shaping cancer-associated metabolic phenotypes. Besides, *TP53*, as the most frequently mutated tumor suppressor gene in cancers, renders MTp53 promising for treatments of p53 mutated tumors. The diversity of MTp53 proteins and the unfavorable non-specific toxicities of MTp53 reactivators or inhibitors to normal tissues not only make it challenging to develop drugs directly targeting MTp53, but also impede the entrance of these drugs into clinical trials. Focusing on the synthetic lethal partners to MTp53 with metabolism, especially targeting the mediators involved in MTp53-driven metabolic reprogramming, might help broaden the synthetic lethal networks of MTp53. This would provide more opportunities and treatment options for cancer patients with MTp53, avoid or alleviate the off-target effects or severe adverse events, and forge the clinical application due to the existence of various metabolic and targeted drugs with FDA approval. Regardless of the substantial literature on p53 and its regulation of cellular metabolism, the metabolic roles of p53 and the mechanistic relationships between p53 and p53-mediated metabotypes are still ambiguous. Several limitations should be taken into consideration when we devote ourselves to investigating the metabolic networks of p53: (1) cell type-specificity of p53; (2) the highly diverse nature of MTp53; (3) differences in p53 GRN between mice and humans. Furthermore, challenges of research concentrating on p53-mediated indirect regulation on metabolism, include: (1) different MTp53 proteins might have distinct synthetic lethal partners; (2) synthetic lethal partner-exerted effects might be cell type-specific; (3) there might be no targeted drugs for a specific synthetic lethal partner; and (4) difficulties in the clinical development of ncRNA-based therapies, should be considered and kept in mind. Further research is also desired to unveil the biological effects of p53-associated metabolic activities, which is particularly essential for elucidating the contribution of p53-induced metabolic changes to the onset and malignancy of cancers, providing important implications for the development of prevention and treatment strategies.

AUTHOR CONTRIBUTIONS

C-YW and C-HC wrote the manuscript. All authors contributed to the article and approved the submitted version.

FUNDING

This work was financially supported in part by the following: Ministry of Science and Technology (109-2628-B-009-004 to C-HC). The "Smart Platform of Dynamic Systems Biology for Therapeutic Development" and "Center for Intelligent Drug Systems and Smart Bio-devices (IDS^{2}B) from The Featured Areas Research Center Program" within the framework of the Higher Education Sprout Project of the Ministry of Education (MOE) in Taiwan.

REFERENCES

1. Boutelle AM, Attardi LD. P53 and Tumor Suppression: It Takes a Network. *Trends Cell Biol* (2021) 31(4):298–310. doi: 10.1016/j.tcb.2020.12.011
2. Levine AJ. P53: 800 Million Years of Evolution and 40 Years of Discovery. *Nat Rev Cancer* (2020) 20(8):471–80. doi: 10.1038/s41568-020-0262-1
3. Joerger AC, Fersht AR. The P53 Pathway: Origins, Inactivation in Cancer, and Emerging Therapeutic Approaches. *Annu Rev Biochem* (2016) 85:375–404. doi: 10.1146/annurev-biochem-060815-014710
4. Leroy B, Anderson M, Soussi T. TP53 Mutations in Human Cancer: Database Reassessment and Prospects for the Next Decade. *Hum Mutat* (2014) 35 (6):672–88. doi: 10.1002/humu.22552
5. Brosh R, Rotter V. When Mutants Gain New Powers: News From the Mutant P53 Field. *Nat Rev Cancer* (2009) 9(10):701–13. doi: 10.1038/nrc2693
6. Baugh EH, Ke H, Levine AJ, Bonneau RA, Chan CS. Why Are There Hotspot Mutations in the TP53 Gene in Human Cancers? *Cell Death Differ* (2018) 25 (1):154–60. doi: 10.1038/cdd.2017.180
7. Weisz L, Oren M, Rotter V. Transcription Regulation by Mutant P53. *Oncogene* (2007) 26(15):2202–11. doi: 10.1038/sj.onc.1210294
8. Soussi T. P53 Alterations in Human Cancer: More Questions Than Answers. *Oncogene* (2007) 26(15):2145–56. doi: 10.1038/sj.onc.1210280
9. Kim E, Deppert W. Interactions of Mutant P53 With DNA: Guilt by Association. *Oncogene* (2007) 26(15):2185–90. doi: 10.1038/sj.onc.1210312
10. Alvarado-Ortiz E, de la Cruz-López K, Becerril-Rico J, Sarabia-Sánchez M, Ortiz-Sánchez E, García-Carrancá A. Mutant P53 Gain-Of-Function: Role in Cancer Development, Progression, and Therapeutic Approaches. *Front Cell Dev Biol* (2020) 8:607670–0. doi: 10.3389/fcell.2020.607670

11. Pfister NT, Fomin V, Regunath K, Zhou JY, Zhou W, Silwal-Pandit L, et al. Mutant P53 Cooperates With the SWI/SNF Chromatin Remodeling Complex to Regulate VEGFR2 in Breast Cancer Cells. *Genes Dev* (2015) 29(12):1298–315. doi: 10.1101/gad.263202.115
12. Di Agostino S. The Impact of Mutant P53 in the Non-Coding RNA World. *Biomolecules* (2020) 10(3):472. doi: 10.3390/biom10030472
13. Vousden KH, Ryan KM. P53 and Metabolism. *Nat Rev Cancer* (2009) 9 (10):691–700. doi: 10.1038/nrc2715
14. Chao C-H, Wang C-Y, Wang C-H, Chen T-W, Hsu H-Y, Huang H-W, et al. Mutant P53 Attenuates Oxidative Phosphorylation and Facilitates Cancer Stemness Through Downregulating miR-200c–PCK2 Axis in Basal-Like Breast Cancer. *Mol Cancer Res* (2021) 19(11):1900–16. doi: 10.1158/1541-7786.MCR-21-0098
15. Yu S, Meng S, Xiang M, Ma H. Phosphoenolpyruvate Carboxykinase in Cell Metabolism: Roles and Mechanisms Beyond Gluconeogenesis. *Mol Metab* (2021) 53:101257–7. doi: 10.1016/j.molmet.2021.101257
16. Lacroix M, Riscal R, Arena G, Linares LK, Le Cam L. Metabolic Functions of the Tumor Suppressor P53: Implications in Normal Physiology, Metabolic Disorders, and Cancer. *Mol Metab* (2020) 33:2–22. doi: 10.1016/j.molmet.2019.10.002
17. Mathupala SP, Heese C, Pedersen PL. Glucose Catabolism in Cancer Cells: The Type II Hexokinase Promoter Contains Functionally Active Response Elements for the Tumor Suppressor P53. *J Biol Chem* (1997) 272(36):22776–80. doi: 10.1074/jbc.272.36.22776
18. Kim H-R, Roe J-S, Lee J-E, Cho E-J, Youn H-D. P53 Regulates Glucose Metabolism by miR-34a. *Biochem Biophysl Res Commun* (2013) 437(2):225–31. doi: 10.1016/j.bbrc.2013.06.043
19. Wang L, Xiong H, Wu F, Zhang Y, Wang J, Zhao L, et al. Hexokinase 2-Mediated Warburg Effect Is Required for PTEN-And P53-Deficiency-Driven Prostate Cancer Growth. *Cell Rep* (2014) 8(5):1461–74. doi: 10.1016/j.celrep.2014.07.053
20. Schwartzenberg-Bar-Yoseph F, Armoni M, Karnieli E. The Tumor Suppressor P53 Down-Regulates Glucose Transporters GLUT1 and GLUT4 Gene Expression. *Cancer Res* (2004) 64(7):2627–33. doi: 10.1158/0008-5472.CAN-03-0846
21. Zhang C, Liu J, Liang Y, Wu R, Zhao Y, Hong X, et al. Tumour-Associated Mutant P53 Drives the Warburg Effect. *Nat Commun* (2013) 4(1):1–15. doi: 10.1038/ncomms3935
22. Kim H-R, Roe J-S, Lee J-E, Hwang I-Y, Cho E-J, Youn H-D. A P53-Inducible microRNA-34a Downregulates Ras Signaling by Targeting IMPDH. *Biochem Biophys Res Commun* (2012) 418(4):682–8. doi: 10.1016/j.bbrc.2012.01.077
23. Azar S, Udi S, Drori A, Hadar R, Nemirovski A, Vemuri KV, et al. Reversal of Diet-Induced Hepatic Steatosis by Peripheral CB1 Receptor Blockade in Mice Is P53/miRNA-22/Sirt1/Pparα Dependent. *Mol Metab* (2020) 42:101087–7. doi: 10.1016/j.molmet.2020.101087
24. Liao M, Liao W, Xu N, Li B, Liu F, Zhang S, et al. LncRNA EPB41L4A-AS1 Regulates Glycolysis and Glutaminolysis by Mediating Nucleolar Translocation of HDAC2. *EBioMedicine* (2019) 41:200–13. doi: 10.1016/j.ebiom.2019.01.035
25. Aquilano K, Baldelli S, Pagliei B, Cannata SM, Rotilio G, Ciriolo MR. P53 Orchestrates the PGC-1α-Mediated Antioxidant Response Upon Mild Redox and Metabolic Imbalance. *Antioxid Redox Signal* (2013) 18(4):386–99. doi: 10.1089/ars.2012.4615
26. Zhang P, Tu B, Wang H, Cao Z, Tang M, Zhang C, et al. Tumor Suppressor P53 Cooperates With SIRT6 to Regulate Gluconeogenesis by Promoting FoxO1 Nuclear Exclusion. *Proc Natl Acad Sci* (2014) 111(29):10684–9. doi: 10.1073/pnas.1411026111
27. Dhar SK, Xu Y, Chen Y, Clair DKS. Specificity Protein 1-Dependent P53-Mediated Suppression of Human Manganese Superoxide Dismutase Gene Expression. *J Biol Chem* (2006) 281(31):21698–709. doi: 10.1074/jbc.M601083200
28. Sen N, Satija YK, Das S. PGC-1α, a Key Modulator of P53, Promotes Cell Survival Upon Metabolic Stress. *Mol Cell* (2011) 44(4):621–34. doi: 10.1016/j.molcel.2011.08.044
29. Kawauchi K, Araki K, Tobiume K, Tanaka N. P53 Regulates Glucose Metabolism Through an IKK-NF-κB Pathway and Inhibits Cell Transformation. *Nat Cell Biol* (2008) 10(5):611–8. doi: 10.1038/ncb1724
30. Deng X, Li Y, Gu S, Chen Y, Yu B, Su J, et al. P53 Affects PGC-1α Stability Through AKT/GSK-3β to Enhance Cisplatin Sensitivity in Non-Small Cell Lung Cancer. *Front Oncol* (2020) 10:1252–2. doi: 10.3389/fonc.2020.01252
31. Liu J, Liu Z-X, Wu Q-N, Lu Y-X, Wong C-W, Miao L, et al. Long Noncoding RNA AGPG Regulates PFKFB3-Mediated Tumor Glycolytic Reprogramming. *Nat Commun* (2020) 11(1):1–16. doi: 10.1038/s41467-020-15112-3
32. Xia W, Bai H, Deng Y, Yang Y. PLA2G16 Is a Mutant P53/KLF5 Transcriptional Target and Promotes Glycolysis of Pancreatic Cancer. *J Cell Mol Med* (2020) 24(21):12642–55. doi: 10.1111/jcmm.15832
33. Kollareddy M, Dimitrova E, Vallabhaneni KC, Chan A, Le T, Chauhan KM, et al. Regulation of Nucleotide Metabolism by Mutant P53 Contributes to Its Gain-Of-Function Activities. *Nat Commun* (2015) 6(1):1–13. doi: 10.1038/ncomms8389
34. Moon RR-B, Barsotti A, Chicas A, Li W, Polotskaia10 A, Bissell11 MJ, et al. Mutant P53 Disrupts Mammary Acinar Morphogenesis *Via* the Mevalonate Pathway. *Cell* (2012) 148(1-2):244–58. doi: 10.1016/j.cell.2011.12.017
35. Lisek K, Campaner E, Ciani Y, Walerych D, Del Sal G. Mutant P53 Tunes the NRF2-Dependent Antioxidant Response to Support Survival of Cancer Cells. *Oncotarget* (2018) 9(29):20508–23. doi: 10.18632/oncotarget.24974
36. Liu DS, Duong CP, Haupt S, Montgomery KG, House CM, Azar WJ, et al. Inhibiting the System Xc^-/Glutathione Axis Selectively Targets Cancers With Mutant-P53 Accumulation. *Nat Commun* (2017) 8(1):1–14. doi: 10.1038/ncomms14844
37. Kalo E, Kogan-Sakin I, Solomon H, Bar-Nathan E, Shay M, Shetzer Y, et al. Mutant $P53^{R273H}$ Attenuates the Expression of Phase 2 Detoxifying Enzymes and Promotes the Survival of Cells With High Levels of Reactive Oxygen Species. *J Cell Sci* (2012) 125(22):5578–86. doi: 10.1242/jcs.106815
38. Basu S, Gnanapradeepan K, Barnoud T, Kung C-P, Tavecchio M, Scott J, et al. Mutant P53 Controls Tumor Metabolism and Metastasis by Regulating PGC-1α. *Genes Dev* (2018) 32(3-4):230–43. doi: 10.1101/gad.309062.117
39. Chang C-J, Chao C-H, Xia W, Yang J-Y, Xiong Y, Li C-W, et al. P53 Regulates Epithelial–Mesenchymal Transition and Stem Cell Properties Through Modulating miRNAs. *Nat Cell Biol* (2011) 13(3):317–23. doi: 10.1038/ncb2173
40. Jeninga EH, Schoonjans K, Auwerx J. Reversible Acetylation of PGC-1: Connecting Energy Sensors and Effectors to Guarantee Metabolic Flexibility. *Oncogene* (2010) 29(33):4617–24. doi: 10.1038/onc.2010.206
41. Dhar SK, Clair DKS. Manganese Superoxide Dismutase Regulation and Cancer. *Free Radic Biol Med* (2012) 52(11-12):2209–22. doi: 10.1016/j.freeradbiomed.2012.03.009
42. Hu J, Cao J, Topatana W, Juengpanich S, Li S, Zhang B, et al. Targeting Mutant P53 for Cancer Therapy: Direct and Indirect Strategies. *J Hematol Oncol* (2021) 14(1):1–19. doi: 10.1186/s13045-021-01169-0
43. Zhang C, Liu J, Xu D, Zhang T, Hu W, Feng Z. Gain-Of-Function Mutant P53 in Cancer Progression and Therapy. *J Mol Cell Biol* (2020) 12(9):674–87. doi: 10.1093/jmcb/mjaa040
44. Xu Z, Wu W, Yan H, Hu Y, He Q, Luo P. Regulation of P53 Stability as a Therapeutic Strategy for Cancer. *Biochem Pharmacol* (2021) 185:114407–04407. doi: 10.1016/j.bcp.2021.114407
45. Chasov V, Zaripov M, Mirgayazova R, Khadiullina R, Zmievskaya E, Ganeeva I, et al. Promising New Tools for Targeting P53 Mutant Cancers: Humoral and Cell-Based Immunotherapies. *Front Immunol* (2021) 12:707734–4. doi: 10.3389/fimmu.2021.707734
46. Low L, Goh A, Koh J, Lim S, Wang C-I. Targeting Mutant P53-Expressing Tumours With a T Cell Receptor-Like Antibody Specific for a Wild-Type Antigen. *Nat Commun* (2019) 10(1):1–14. doi: 10.1038/s41467-019-13305-z
47. Yang C, Lou G, Jin W. The Arsenal of TP53 Mutants Therapies: Neoantigens and Bispecific Antibodies. *Signal Transduct Target Ther* (2021) 6(1):1–2. doi: 10.1038/s41392-021-00635-y
48. O'Neil NJ, Bailey ML, Hieter P. Synthetic Lethality and Cancer. *Nat Rev Genet* (2017) 18(10):613–23. doi: 10.1038/nrg.2017.47
49. Topatana W, Juengpanich S, Li S, Cao J, Hu J, Lee J, et al. Advances in Synthetic Lethality for Cancer Therapy: Cellular Mechanism and Clinical Translation. *J Hematol Oncol* (2020) 13(1):1–22. doi: 10.1186/s13045-020-00956-5
50. Huang A, Garraway LA, Ashworth A, Weber B. Synthetic Lethality as an Engine for Cancer Drug Target Discovery. *Nat Rev Drug Discovery* (2020) 19 (1):23–38. doi: 10.1038/s41573-019-0046-z

51. Li S, Topatana W, Juengpanich S, Cao J, Hu J, Zhang B, et al. Development of Synthetic Lethality in Cancer: Molecular and Cellular Classification. *Signal Transduct Target Ther* (2020) 5(1):1–14. doi: 10.1038/s41392-020-00358-6
52. Sabapathy K, Lane DP. Therapeutic Targeting of P53: All Mutants Are Equal, But Some Mutants Are More Equal Than Others. *Nat Rev Clin Oncol* (2018) 15(1):13–30. doi: 10.1038/nrclinonc.2017.151
53. Bou-Hanna C, Jarry A, Lode L, Schmitz I, Schulze-Osthoff K, Kury S, et al. Acute Cytotoxicity of MIRA-1/NSC19630, a Mutant P53-Reactivating Small Molecule, Against Human Normal and Cancer Cells *Via* a Caspase-9-Dependent Apoptosis. *Cancer Lett* (2015) 359(2):211–7. doi: 10.1016/j.canlet.2015.01.014
54. Borrero LJH, El-Deiry WS. Tumor Suppressor P53: Biology, Signaling Pathways, and Therapeutic Targeting. *Biochim Biophys Acta Rev Cancer* (2021) 1876(1):188556. doi: 10.1016/j.bbcan.2021.188556
55. Kim J, Yu L, Chen W, Xu Y, Wu M, Todorova D, et al. Wild-Type P53 Promotes Cancer Metabolic Switch by Inducing PUMA-Dependent Suppression of Oxidative Phosphorylation. *Cancer Cell* (2019) 35(2):191–203. doi: 10.1016/j.ccell.2018.12.012
56. Gwon Y, Oh J, Kim J-S. Sulforaphane Induces Colorectal Cancer Cell Proliferation Through Nrf2 Activation in a P53-Dependent Manner. *Appl Biol Chem* (2020) 63(1):1–11. doi: 10.1186/s13765-020-00578-y
57. Wang X, Simon R. Identification of Potential Synthetic Lethal Genes to P53 Using a Computational Biology Approach. *BMC Med Genomics* (2013) 6 (1):1–10. doi: 10.1186/1755-8794-6-30
58. Neizer-Ashun F, Bhattacharya R. Reality CHEK: Understanding the Biology and Clinical Potential of CHK1. *Cancer Lett* (2021) 497:202–11. doi: 10.1016/j.canlet.2020.09.016
59. Morandell S, Yaffe MB. Exploiting Synthetic Lethal Interactions Between DNA Damage Signaling, Checkpoint Control, and P53 for Targeted Cancer Therapy. *Prog Mol Biol Transl Sci* (2012) 110:289–314. doi: 10.1016/B978-0-12-387665-2.00011-0
60. Lee S-Y, Jang C, Lee K-A. Polo-Like Kinases (Plks), a Key Regulator of Cell Cycle and New Potential Target for Cancer Therapy. *Dev Reprod* (2014) 18 (1):65–71. doi: 10.12717/DR.2014.18.1.065
61. Vose JM, Friedberg JW, Waller EK, Cheson BD, Juvvigunta V, Fritsch H, et al. The Plk1 Inhibitor BI 2536 in Patients With Refractory or Relapsed Non-Hodgkin Lymphoma: A Phase I, Open-Label, Single Dose-Escalation Study. *Leuk Lymphoma* (2013) 54(4):708–13. doi: 10.3109/10428194.2012.729833
62. Gómez-Romero L, López-Reyes K, Hernández-Lemus E. The Large Scale Structure of Human Metabolism Reveals Resilience *Via* Extensive Signaling Crosstalk. *Front Physiol* (2020) 11:588012–2. doi: 10.3389/fphys.2020.588012
63. McGuirk S, Audet-Delage Y, St-Pierre J. Metabolic Fitness and Plasticity in Cancer Progression. *Trends Cancer* (2020) 6(1):49–61. doi: 10.1016/j.trecan.2019.11.009
64. Bere J, Jonnalagadda ND, Kappari L, Karangula J, Boggula N, Kappari V. 2-Deoxy-D-Glucose: An Update Review. *J Innov Dev Pharm Tech Sci(JIDPTS)* (2021) 4(5):68–78.
65. Michelakis E, Webster L, Mackey J. Dichloroacetate (DCA) as a Potential Metabolic-Targeting Therapy for Cancer. *Br J Cancer* (2008) 99(7):989–94. doi: 10.1038/sj.bjc.6604554
66. Tataranni T, Piccoli C. Dichloroacetate (DCA) and Cancer: An Overview Towards Clinical Applications. *Oxid Med Cell Longev* (2019) 2019:8201079–8201079. doi: 10.1155/2019/8201079
67. Pyaskovskaya O, Kolesnik D, Fedorchuk A, Prochorova I, Solyanik G. 2-Deoxy-D-Glucose Enhances Dichloroacetate Antitumor Action Against Lewis Lung Carcinoma. *Exp Oncol* (2016) 38(3):176–80. doi: 10.31768/2312-8852.2016.38(3):176-180
68. Pernicova I, Korbonits M. Metformin—Mode of Action and Clinical Implications for Diabetes and Cancer. *Nat Rev Endocrinol* (2014) 10 (3):143–56. doi: 10.1038/nrendo.2013.256
69. Rajh M, Dolinar K, Miš K, Pavlin M, Pirkmajer S. Medium Renewal Blocks Anti-Proliferative Effects of Metformin in Cultured MDA-MB-231 Breast Cancer Cells. *PloS One* (2016) 11(5):e0154747–e0154747. doi: 10.1371/journal.pone.0154747
70. Jung CL, Mun H, Jo S-Y, Oh J-H, Lee C, Choi E-K, et al. Suppression of Gain-Of-Function Mutant P53 With Metabolic Inhibitors Reduces Tumor Growth *In Vivo*. *Oncotarget* (2016) 7(47):77664–682. doi: 10.18632/oncotarget.12758
71. Stine ZE, Schug ZT, Salvino JM, Dang CV. Targeting Cancer Metabolism in the Era of Precision Oncology. *Nat Rev Drug Discovery* (2022) 21(2):141–62. doi: 10.1038/s41573-021-00339-6
72. Wright MW, Bruford EA. Naming'junk': Human Non-Protein Coding RNA (ncRNA) Gene Nomenclature. *Hum Genomics* (2011) 5(2):1–9. doi: 10.1186/1479-7364-5-2-90
73. Anastasiadou E, Jacob LS, Slack FJ. Non-Coding RNA Networks in Cancer. *Nat Rev Cancer* (2018) 18(1):5–18. doi: 10.1038/nrc.2017.99
74. Chen S, Thorne RF, Zhang XD, Wu M, Liu L. Non-Coding RNAs, Guardians of the P53 Galaxy. *Semin Cancer Biol* (2021) 75:72–83. doi: 10.1016/j.semcancer.2020.09.002
75. Beltrán-Anaya FO, Cedro-Tanda A, Hidalgo-Miranda A, Romero-Cordoba SL. Insights Into the Regulatory Role of Non-Coding RNAs in Cancer Metabolism. *Front Physiol* (2016) 7:342–2. doi: 10.3389/fphys.2016.00342
76. Lin X, Wu Z, Hu H, Luo M-L, Song E. Non-Coding RNAs Rewire Cancer Metabolism Networks. *Semin Cancer Biol* (2021) 75:116–26. doi: 10.1016/j.semcancer.2020.12.019
77. Forterre A, Komuro H, Aminova S, Harada M. A Comprehensive Review of Cancer MicroRNA Therapeutic Delivery Strategies. *Cancers* (2020) 12 (7):1852. doi: 10.3390/cancers12071852
78. Liang Y, Hou L, Li L, Li L, Zhu L, Wang Y, et al. Dichloroacetate Restores Colorectal Cancer Chemosensitivity Through the P53/Mir-149-3p/PDK2-Mediated Glucose Metabolic Pathway. *Oncogene* (2020) 39(2):469–85. doi: 10.1038/s41388-019-1035-8
79. Zhong L, Li Y, Xiong L, Wang W, Wu M, Yuan T, et al. Small Molecules in Targeted Cancer Therapy: Advances, Challenges, and Future Perspectives. *Signal Transduct Target Ther* (2021) 6(1):1–48. doi: 10.1038/s41392-021-00572-w
80. Lu R-M, Hwang Y-C, Liu I-J, Lee C-C, Tsai H-Z, Li H-J, et al. Development of Therapeutic Antibodies for the Treatment of Diseases. *J BioMed Sci* (2020) 27 (1):1–30. doi: 10.1186/s12929-019-0592-z
81. Ke X, Shen L. Molecular Targeted Therapy of Cancer: The Progress and Future Prospect. *Front Lab Med* (2017) 1(2):69–75. doi: 10.1016/j.flm.2017.06.001
82. Hernández-Reséndiz I, Román-Rosales A, García-Villa E, López-Macay A, Pineda E, Saavedra E, et al. Dual Regulation of Energy Metabolism by P53 in Human Cervix and Breast Cancer Cells. *Biochim Biophys Acta Mol Cell Res* (2015) 1853(12):3266–78. doi: 10.1016/j.bbamcr.2015.09.033
83. Eriksson M, Ambroise G, Ouchida AT, Lima Queiroz A, Smith D, Gimenez-Cassina A, et al. Effect of Mutant P53 Proteins on Glycolysis and Mitochondrial Metabolism. *Mol Cell Biol* (2017) 37(24):e00328–17. doi: 10.1128/MCB.00328-17
84. Yue F, Cheng Y, Breschi A, Vierstra J, Wu W, Ryba T, et al. A Comparative Encyclopedia of DNA Elements in the Mouse Genome. *Nature* (2014) 515 (7527):355–64. doi: 10.1038/nature13992
85. Fischer M. Conservation and Divergence of the P53 Gene Regulatory Network Between Mice and Humans. *Oncogene* (2019) 38(21):4095–109. doi: 10.1038/s41388-019-0706-9
86. Reilly PT, Mak TW. Molecular Pathways: Tumor Cells Co-Opt the Brain-Specific Metabolism Gene CPT1C to Promote Survival. *Clin Cancer Res* (2012) 18(21):5850–5. doi: 10.1158/1078-0432.CCR-11-3281
87. Goldstein I, Rotter V. Regulation of Lipid Metabolism by P53–Fighting Two Villains With One Sword. *Trends Endocrinol Metab* (2012) 23(11):567–75. doi: 10.1016/j.tem.2012.06.007
88. McGuirk S, Gravel S-P, Deblois G, Papadopoli DJ, Faubert B, Wegner A, et al. PGC-1α Supports Glutamine Metabolism in Breast Cancer. *Cancer Metab* (2013) 1(1):1–11. doi: 10.1186/2049-3002-1-22
89. Torrano V, Valcarcel-Jimenez L, Cortazar AR, Liu X, Urosevic J, Castillo-Martin M, et al. The Metabolic Co-Regulator PGC-1α Suppresses Prostate Cancer Metastasis. *Nat Cell Biol* (2016) 18(6):645–56. doi: 10.1038/ncb3357
90. Reda El Sayed S, Cristante J, Guyon L, Denis J, Chabre O, Cherradi N. MicroRNA Therapeutics in Cancer: Current Advances and Challenges. *Cancers* (2021) 13(11):2680. doi: 10.3390/cancers13112680
91. Kasinski AL, Kelnar K, Stahlhut C, Orellana E, Zhao J, Shimer E, et al. A Combinatorial MicroRNA Therapeutics Approach to Suppressing Non-Small Cell Lung Cancer. *Oncogene* (2015) 34(27):3547–55. doi: 10.1038/onc.2014.282

92. Chen Y, Gao D-Y, Huang L. *In Vivo* Delivery of miRNAs for Cancer Therapy: Challenges and Strategies. *Adv Drug Del Rev* (2015) 81:128–41. doi: 10.1016/j.addr.2014.05.009
93. Hanahan D, Weinberg RA. Hallmarks of Cancer: The Next Generation. *Cell* (2011) 144(5):646–74. doi: 10.1016/j.cell.2011.02.013
94. Menendez JA, Alarcón T. Metabostemness: A New Cancer Hallmark. *Front Oncol* (2014) 4:262–2. doi: 10.3389/fonc.2014.00262
95. Yang L, Shi P, Zhao G, Xu J, Peng W, Zhang J, et al. Targeting Cancer Stem Cell Pathways for Cancer Therapy. *Signal Transduct Target Ther* (2020) 5 (1):1–35. doi: 10.1038/s41392-020-0110-5

Conflict of Interest: The authors declare that the research was conducted in the absence of any commercial or financial relationships that could be construed as a potential conflict of interest.

frontiers | Frontiers in Oncology

ORIGINAL RESEARCH
published: 21 July 2022
doi: 10.3389/fonc.2022.940402

Mutant p53-microRNA-200c-ZEB2-Axis-Induced CPT1C Elevation Contributes to Metabolic Reprogramming and Tumor Progression in Basal-Like Breast Cancers

Chen-Yun Wang[1,2†], *Cing-Hong Wang*[1,2†], *Ru-Tsun Mai*[1,2,3†], *Ting-Wen Chen*[1,2,4], *Chia-Wei Li*[5] *and Chi-Hong Chao*[1,2,3*]

[1] Institute of Molecular Medicine and Bioengineering, National Yang Ming Chiao Tung University, Hsinchu, Taiwan, [2] Center For Intelligent Drug Systems and Smart Bio-devices (IDS^{2}B), National Yang Ming Chiao Tung University, Hsinchu, Taiwan, [3] Department of Biological Science and Technology, National Yang Ming Chiao Tung University, Hsinchu, Taiwan, [4] Institute of Bioinformatics and Systems Biology, National Yang Ming Chiao Tung University, Hsinchu, Taiwan, [5] Institute of Biomedical Sciences, Academia Sinica, Taipei, Taiwan

TP53 is mutated in more than 80% of basal-like breast cancers (BLBCs). BLBCs with *TP53* mutation are usually high-grade and have worse responses to chemotherapy, leading to poor clinical outcomes. Wild-type p53 (WTp53) is well-accepted to promote fatty acid oxidation (FAO); however, in this study, we demonstrate that mutant p53 (Mutp53) enhances FAO activity through constitutively upregulating CPT1C *via* dysregulating the miR-200c-ZEB2 axis. Sustained CPT1C expression contributes to the metabolic preference of FAO, epithelial-mesenchymal transition (EMT) phenotypes, migration, invasion, and cancer stemness in BLBC, which is mediated by modulating the redox status. Furthermore, interference of CPT1C expression impairs tumor growth and pulmonary colonization of BLBC cells *in vivo*, and even postpones the occurrence of spontaneous metastasis, resulting in a prolonged disease-specific survival (DSS). Consistently, clinical validation reveals that high CPT1C is observed in breast cancer patients with metastasis and is correlated with poor overall, disease-free, progression-free, and disease-specific survival in BLBC patients. Together, unlike WTp53 which transiently transactivates CPT1C, Mutp53 provides long-term benefits through sustaining CPT1C expression by disturbing the miR-200c-ZEB2 axis, which potentiates FAO and facilitates tumor progression in BLBC, suggesting that targeting Mutp53-CPT1C-driven metabolic reprogramming is promising to serve as novel therapeutic strategies for BLBC in the future.

Keywords: mutant p53, tumor progression, CPT1C, FAO, basal-like breast cancer

OPEN ACCESS

Edited by:
Che-Pei Kung,
Washington University in St. Louis, United States

Reviewed by:
Mukhi Dhanunjay,
University of Pennsylvania, United States
Aleksandra Jankovic,
University of Belgrade, Serbia

****Correspondence:***
Chi-Hong Chao
chao7@nycu.edu.tw

†These authors have contributed equally to this work and share first authorship

Specialty section:
This article was submitted to Cancer Metabolism, a section of the journal Frontiers in Oncology

Received: *10 May 2022*
Accepted: *08 June 2022*
Published: *21 July 2022*

Citation:
Wang C-Y, Wang C-H, Mai R-T, Chen T-W, Li C-W and Chao C-H (2022) Mutant p53-microRNA-200c-ZEB2-Axis-Induced CPT1C Elevation Contributes to Metabolic Reprogramming and Tumor Progression in Basal-Like Breast Cancers. Front. Oncol. 12:940402. doi: 10.3389/fonc.2022.940402

INTRODUCTION

TP53 gene, the most frequently mutated tumor suppressor gene (1), is mutated in more than 50% of human cancers (2). Unlike other tumor suppressor genes, over 70% of cancer-associated *TP53* mutations are missense mutations mainly located in the DNA-binding domain (3), causing single amino acid substitutions and consequently DNA-contact or structural mutations (4). *TP53* mutations not only result in loss of function and dominant-negative effect over wild-type p53 (WTp53) but also endow mutant p53 (Mutp53) with gain-of-function properties, which have high relevance to tumorigenesis (5). In breast cancers, the frequency of *TP53* mutation ranges from 12% in luminal A to over 80% in basal-like breast cancers (BLBCs) (2). BLBC comprises 15-20% of breast cancers but harbors the worst clinical outcome as well as high metastasis and tumor recurrence rate (6) due to the lack of targeted therapies. BLBCs with *TP53* mutation are highly invasive, poorly differentiated, usually high-grade, and have a poor response to chemotherapy (7), reflecting the unusually high frequency of *TP53* mutation and the indispensable role of Mutp53 in BLBC.

Beyond the guardian of the genome, p53 has emerged as an important regulator of multiple metabolic pathways in the past decades. p53 is known to suppress the Warburg effect, which is the metabolic alteration favored by a majority of cancer cells, by directly inhibiting the transcription of glucose transporters and several key enzymes involved in glycolysis (8), whereas p53 mutation stimulates the Warburg effect (9). Additionally, p53 regulates glucose metabolism indirectly through microRNAs (miRNAs). For example, p53 downregulates glycolytic enzymes by transactivating miR-34a (10). Recent evidence further indicates that Mutp53 decreases oxidative phosphorylation (OXPHOS) and increases cancer stemness by downregulating the miR-200c-PCK2 axis in BLBCs (11).

In addition to the regulation of glucose metabolism, p53 has been shown to modulate lipid metabolism. Evidence indicates that WTp53 suppresses fatty acid synthesis (FAS) and promotes fatty acid oxidation (FAO) (12). WTp53 could enhance FAO by directly transactivating *carnitine palmitoyltransferase 1C* (*CPT1C*), the brain isoform of the rate-limiting enzyme of FAO, to promote the survival of murine embryonic fibroblasts under metabolic stress (13). However, the positive role of WTp53 in FAO seems contradictory to the extremely high mutation rate of *TP53* and the metabolic preference of FAO in BLBC, as FAO contributes to tumorigenesis (14, 15), metastasis (16–18), cancer stem cell properties (19), chemo-resistance (19) and tumor recurrence (20) in BLBCs. Therefore, the regulatory role of Mutp53 in FAO and the underlying molecular mechanisms require further investigation.

Here, we demonstrate that, instead of suppressing fatty acid degradation, Mutp53 upregulates CPT1C and potentiates FAO by interfering with the miR-200c-ZEB2 axis. Overexpression of CPT1C not only contributes to increased FAO activity but also induces EMT, enhances migration, invasion, and stemness in mammary epithelial cells. On the contrary, knockdown of CPT1C attenuates migration, invasion, and cancer stemness in Mutp53-overexpressing mammary epithelial cells and human BLBC cells harboring endogenous Mutp53. CPT1C mediates Mutp53-exerted oncogenic events by reducing reactive oxygen species (ROS), which might be modulated by the enhanced FAO activity. Furthermore, our *in vivo* study reveals that interference of CPT1C expression leads to impaired tumor growth, attenuated pulmonary colonization, and postponed occurrence of spontaneous metastasis, conferring a better disease-specific survival, which is coincident with clinical validation that high CPT1C expression is associated with metastasis and poor outcomes in BLBC patients. Overall, the robust evidence presented in this study clarifies the controversial role of Mutp53 in lipid metabolism and clearly elucidates the mechanistic relationship between Mutp53 and Mutp53-driven metabolic reprogramming. More importantly, we uncover novel oncogenic roles of CPT1C contributing to the progression of BLBC, which not only is a breakthrough for establishing the p53 regulatory network of cellular metabolism but also accentuates CPT1C as an extraordinarily potential therapeutic target in tumors overexpressing CPT1C, providing crucial implications for developing urgently needed novel treatment strategies for BLBC.

MATERIALS AND METHODS

Cell Lines and Culture

Human normal mammary epithelial cell line, MCF12A (ATCC Cat# CRL-10782, RRID : CVCL_3744), human basal-like breast cancer cell lines, BT549 (ATCC Cat# HTB-122, RRID : CVCL_1092), MDA-MB-231 (ATCC Cat# HTB-26, RRID : CVCL_0062), and murine breast cancer cell line, 4T1(ATCC Cat# CRL-2539, RRID : CVCL_0125), were purchased from American Type Culture Collection (ATCC) during 2016-2017. Mutp53-expressing MCF12A cells (MCF12A-p53R175H, MCF12A-p53R249S, MCF12A-p53R273H and MCF12A-p53R280K), miR-200c-KO MCF12A (MCF12A-miR-200c-Sg1 and MCF12A-miR-200c-Sg2), cells (MCF12A- p53R273H, MDA-MB-231 and BT549) with ZEB-1, ZEB-2, Bmi1 or Slug knockdown were described in our previous study (11). Cells have been cultured for 1-3 months were discarded, and new cells were recovered from cryopreserved stocks to ensure authentication and avoid possible mycoplasma contamination; therefore, cell authentication and contamination of mycoplasma were not re-examined in our laboratory.

Plasmid Construction

To construct pCDH/CPT1C, CPT1C cDNA fragments amplified from reverse transcription-PCR were cloned into the pCDH-CMV-MCS-EF1-Puro lentiviral vector. Lentiviral shRNA constructs for knockdown CPT1C were provided by the National RNAi Core Facility services at Academia Sinica in Taiwan. Mutp53-expressing constructs (pLenti6/V5-p53_R175H, RRID : Addgene_22936; pLenti6/V5-p53_R249S, RRID : Addgene_22935; pLenti6/V5-p53_R273H, RRID : Addgene_22934; and pLenti6/V5-p53_R280K, RRID : Addgene_22933) and their control vectors were purchased

from Addgene (21). To obtain pLenti6/V5-Luc2, the p53 cDNA fragment in pLenti6/V5-p53_R273H was replaced with a PCR-amplified *Luc2* cDNA fragment. Cloning strategies, sequences of cloning primer sets, and plasmid maps will be provided upon request.

Generation of Stable Expressed, Knocked-Down, or Knocked-Out Cell Lines

MCF12A, BT549, MDA-MB-231, and 4T1 cells were infected with lentiviral constructs for gene overexpression or knockdown. Infected cells were selected with Puromycin (2 μg/ml) or Blasticidin (10 μg/ml) for two weeks to establish stable clones.

Total RNA Extraction and Real Time-PCR

The RNA extraction and RT-PCR were performed as described before (11). The expression of CPT1C mRNA was examined by using the primer set: CPT1C-F, TGCCATGTCGTTCCATTCTCCC; CPT1C-R, GCCGACTCATAAGTCAGGCAGA. Actin gene served as an internal control for quantitation using the primer set: ACTB-F, CACCATTGGCAATGAGCGGTTC; ACTB-R, AGGTCTTT GCGGATGTCCACGT.

Antibodies

The commercial available antibodies and dilutions used in the immunoblotting analysis were listed below: anti-ZEB1 (1:1000, Cell Signaling, Danvers, MA, USA, #3369), anti-ZEB2 (1:1000, Cell Signaling, #97885), anti-p53 (1:2000, Santa Cruz, Dallas, Texas, USA, sc-126), anti-E-Cadherin (1:500, Santa Cruz, sc-8426), anti-N-Cadherin (1:250, Santa Cruz, Sc-59987), anti-CPT1C (1:500, Santa Cruz, sc-514555), and anti-Actin (1:1000, Santa Cruz, sc-47778).

Mammosphere Formation Assay, Transwell Migration/Invasion Assay, and Soft Agar Foci Formation Assay

Detailed experimental procedures were described in our previous study (11). Briefly, for mammosphere formation assay, 4-5x10^4 of MCF12A, BT549, or MDA-MB-231 cells were used, and mammosphere numbers were determined after growing in suspension culture for 6-7 days. For migration assay, cells (1x10^5 for MCF12A, 5x10^4 for MDA-MB-231, and 5x10^4 for BT549 cells/well) were seeded into the upper chamber of a transwell. For invasion Assay, cells (2x10^5 for MCF12A, 5x10^4 for MDA-MB-231, and 1x10^5 for BT549 cells/well) were seeded into the upper chamber precoated with 100 μL of 2% Matrigel (Corning, NY, USA). The migrated/invaded cells were then visualized by crystal violet staining after 16-24 hours. To perform soft-agar foci formation assay, cells (2.5x10^4 for MCF12A and 5x10^4 for MDA-MB-231 cells/well) were grown in the soft agarose layer (0.4%) on top of the hard agarose (0.8%) in six-well plates (Falcon, Chicago, Illinois, USA). The foci numbers were then determined after 3-4 weeks of incubation. All experiments were performed in triplicate.

Extracellular Metabolic Flux Analysis

FAO assay was performed by combining XF palmitate-BSA FAO substrate with XF Mito Stress kit (Agilent, Santa Clara, CA, USA). Cells (3.5x10^4 for MCF12A, and 4x10^4 for BT549 cells/well) were resuspended in 80 μL of culture medium containing palmitate-BSA conjugate (100 μmol/L) and carnitine (1 mmol/L) and seeded into Seahorse XF Cell Culture Microplates. The next day, cells were washed and the medium was replaced by XF Assay Medium Modified DMEM containing GlutaMAX™ (Billings, Montana, USA), palmitate-BSA conjugate (100 μmol/L), carnitine (1 mmol/L), and distilled water (for vehicle group) or etomoxir (2-4 μmol/L, for ETO group; Cayman Chemical, Ann Arbor, Michigan, USA). After cells were incubated for 1-2 hours at 37°C in a non-CO_2 incubator, the oxygen consumption rate was measured by Seahorse XF Extracellular Flux Analyzer. All experiments were performed in triplicate. The results were analyzed using the software XFp Wave. The basal ratio was calculated as [(vehicle basal–ETO basal respiration)/vehicle basal respiration] x 100%.

Determination of ATP Level

To determine the FAO-associated ATP production, cells were cultured in a glucose-free medium (containing carnitine and GlutaMAX™) supplemented with/without palmitate-BSA conjugate (100 μmol/L) in the absence/presence of etomoxir (2 μmol/L) for 2 hours then subjected to the measurement of ATP level. ATP level was measured by using the ATP Determination kit (Invitrogen, Waltham, MA, USA) following the manufacturer's instructions. Briefly, cell pellets were lysed by Bioruptor plus sonication device (Diagenode, Denville, NJ, USA), and sample assays were prepared (10% of sample solution mixed with 90% of reaction solution) followed by incubation in the dark for 10 minutes. The luminescence was measured by the CLARIOstar microplate reader (BMG LABTECH, Ortenberg, Germany). All experiments were performed in triplicate and normalized to respective protein concentrations.

Determination of Total Cellular ROS Level

To determine the cellular ROS level, cells grown to confluence were stained with CellROX™ Green Reagent (Invitrogen) at a final concentration of 2.5 μmol/L and incubated for 30 minutes at 37°C for MCF12A, and 10 μmol/L with 1-hour incubation at 37°C for MDA-MB-231, which were then washed with PBS, trypsinized, and subjected to FACS analysis by NovoCyte Flow Cytometer (ACEA Biosciences, San Diego, CA, USA). On the other hand, cells in suspension were stained with DCFDA/H2DCFDA (Abcam, Cambridge, UK) at a final concentration of 1 μmol/L and incubated for 15 minutes at 37°C for MCF12A, and 4 μmol/L with 15-minute incubation at 37°C for MDA-MB-231, which were then washed and subjected to FACS analysis.

Determination of NADPH/$NADP^+$ Ratio by Metabolome Analysis

Detailed information on metabolome analysis was described in our previous study (11). Briefly, the quantification of 116 metabolites including NADPH and $NADP^+$ was conducted by the C-SCOPE service of [Human Metabolome Technologies, Inc., (HMT)] using capillary electrophoresis time-of-flight mass spectrometry (CE-TOFMS, Agilent CE-TOFMS system Machine

No. 3, Agilent Technologies) for cation analysis and CE- tandem mass spectrometry (CE-QqQMS; CE system with Agilent 6460 TripleQuad LC/MS Machine No, QqQ1, Agilent Technologies) for anion analysis. To prepare the sample for metabolome analysis, cells were washed with 5% mannitol solution, and cellular metabolites were extracted by methanol. Extracts were added with internal standards and then filtered to remove macromolecules. Filtrates were then subjected to metabolomic analysis at HMT. Detailed methods will be provided upon request. NADPH/$NADP^+$ ratio was calculated as following: [NADPH]/[$NADP^+$].

In Vivo Studies

For orthotopic inoculation, female SCID mice (NOD.CB17-*Prkdc*^{scid}/JNarl; purchased from National Laboratory Animal Center, Taipei, Taiwan; 8-10 weeks old) were inoculated with $3x10^6$ of MDA-MB-231-Control and siCPT1C cells mixed with Matrigel (Matrigel: PBS=1:1) into the second and the fourth mammary fat pads. Tumor size was measured every three days with a caliper, and tumor volume was determined with the formula: ($d1x\ d2^2$)/2 (d1: larger diameter; d2: smaller diameter). For tail vein injection, female SCID mice (8-10 weeks old) were randomly divided into two groups. $1x10^6$ of MDA-MB-231-Control or siCPT1C cells expressing firefly luciferase were suspended in 100 μL of PBS and injected into tail veins. Metastasis was monitored by the *in vivo* imaging system (IVIS) followed by intraperitoneal injection (IP) of D-luciferin (150 mg/kg body weight). Briefly, the images were captured by using Auto exposure, then the raw signal was calibrated, and the measurement region of interests (ROIs) were determined. Animal experiments and animal care were handled according to the protocol approved by the Institutional Animal Care and Use Committee at National Yang Ming Chiao Tung University, Taiwan. (IACUC number: NCTU-IACUC-106030).

TCGA Data Processing and Survival Analysis

The expression levels of miRNAs/mRNA, mutation profiles, and clinical information for the TCGA Breast invasive carcinoma cohort (BRCA) were downloaded from Broad GDAC Firehose (https://gdac.broadinstitute.org). The mRNA expression values calculated with RSEM (22) were used for the PAM50 model analysis. All the breast cancer samples were classified into four breast cancer subtypes, i.e., basal-like breast tumor, HER2-enriched, Luminal A, and Luminal B (23, 24). *TP53* mutated patients are defined as those carrying non-silent mutations on *TP53*. All four synonymous (silent) mutations found on *TP53* were predicted to be likely benign by InterVar (25), hence treated as non-mutated in our analysis.

To perform survival analysis according to CPT1C expression level, all the breast cancer patients were divided into two equal-sized groups based on the expression level of CPT1C. The survival information for OS (overall survival), DFS (disease-free survival), PFS (progression-free survival), and DSS (disease-specific survival) were all downloaded from cBioPortal (26). Kaplan-Meier survival plot (KM plot) and log-rank test were used for the comparison of survival data between the high expression and low expression groups.

Data and Materials Availability

All data files supporting the findings of this study are available upon reasonable request.

RESULTS

Mutant p53 Enhances Fatty Acid β-Oxidation Activity in Immortal Mammary Epithelial Cells

To investigate whether Mutp53 involves in the regulation of FAO, a set of p53 hot-spot mutations-bearing MCF12A cell lines was used (11, 21). Consistent with previous findings, MCF-12A cells bearing p53 mutations (R175H, R249S, R273H, and R280K) showed an EMT phenotype (**Figure 1A**). Overexpression of p53 mutations also significantly enhanced stemness (**Supplementary Figures S1A, B**). and led to the transformation of mammary epithelial cells (**Supplementary Figure S1C**). To examine whether these p53 hot-spot mutant cells exhibit elevated FAO activity, we performed a non-isotopic FAO assay by measuring the FAO-associated oxygen consumption rate (OCR) with Seahorse XF Extracellular Flux Analyzer (**Figures 1B–F**) to evaluate the ability of oxidizing fatty acids (27). The basal OCR between the vehicle control and the etomoxir (ETO)-treated group in the presence of palmitate was compared to determine the FAO-mediated oxygen consumption. To quantify the FAO activity which contributes to total cellular oxygen consumption, a "basal ratio" (the ratio between FAO-mediated OCR and total OCR) was assigned by the following equation: [(basal respiration of the vehicle group–basal respiration of the ETO group)/basal respiration of the vehicle group] x 100%. As shown in **Figure 1G**, the basal ratio of control cells is around 13%, which means FAO contributes to 13% of cellular oxygen consumption, whereas it was at least doubled in Mutp53-bearing MCF12A cells. Additionally, palmitate feeding exerted a more profound effect in fueling ATP production in p53 mutant-expressing cells, as an 11.43- and 1.85-fold increase of steady-state ATP level was observed in MCF12A-$p53^{R273H}$ and control cells, respectively, and this increase was abolished by ETO-treatment (**Figure 1H**), indicating an increased FAO activity in p53 mutant-expressing cells. Together, all these results suggested that p53 mutations could upregulate cellular FAO activity in mammary epithelial cells.

Etomoxir Treatment Interferes With Mutp53-Induced Biological Effects

Since Mutp53 has been shown to affect cancer migration, invasion, and cancer stemness in addition to cell proliferation (28), to understand whether FAO is involved in Mutp53-promoted tumor properties, we suppressed cellular FAO activity with etomoxir (ETO), the pan-CPT1 inhibitor. The p53-R273H and p53-R280K MCF-12A cells were pretreated with ETO (50 and 100 μmol/L) for seven days, then subjected to migration, invasion, and

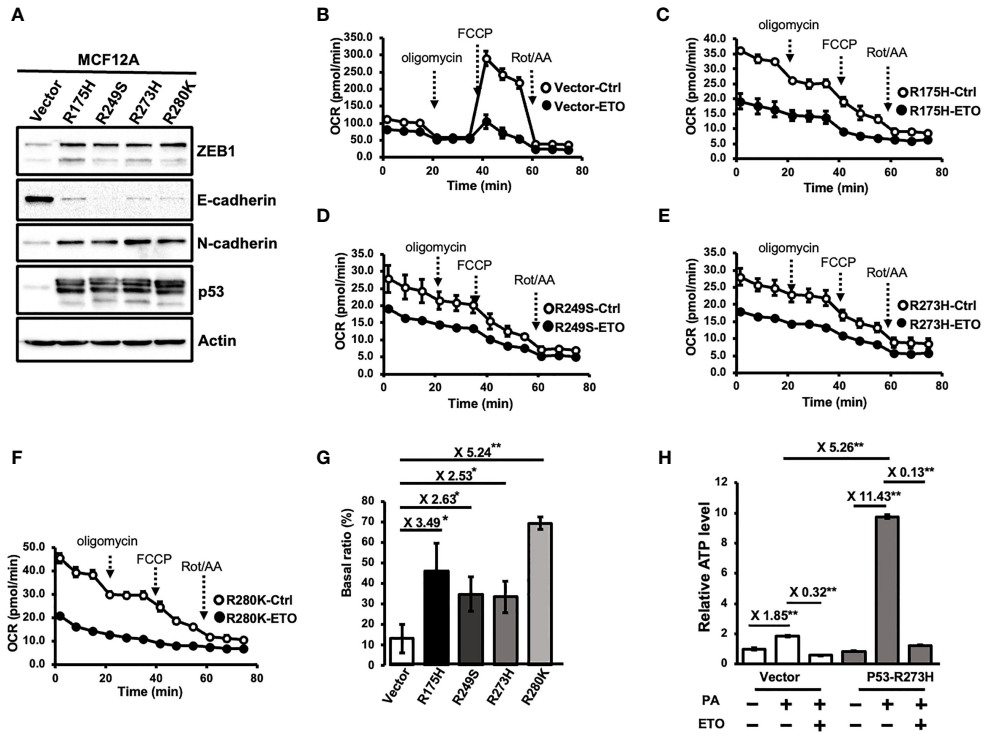

FIGURE 1 | Mutant p53 enhances fatty acid beta-oxidation (FAO) activity in immortal mammary epithelial cells. **(A)** Stable expression of p53 hot-spot mutations in MCF12A cells. The expressional levels of ZEB1, E-Cadherin, N-Cadherin, p53, and Actin were examined by Western Blotting. All of the immunoblotting analysis was performed under the same experimental conditions. Results were obtained from the same or different PAGEs using the same samples and presented as cropped images. **(B–G)** Mutant p53 enhances FAO activity. FAO activity of MCF12A-Ctrl **(B)**. MCF12A-p53^{R175H} **(C)**. MCF12A-p53^{R249S} **(D)**. MCF12A-p53^{R273H} **(E)** and MCF12A-p53^{R280K} **(F)** were measured by seahorse metabolic flux analyzer with FAO assay kit. **(G)** the FAO activity of individual cell lines was determined by averaging Basal ratios from three independent experiments (mean ± SD, n = 3). Basal ratio = (basal OCR^{Ctrl}- basal OCR^{ETO})/basal OCR^{Ctrl}. The two sides of the lines above the bars indicated the comparison of each Mutp53 to the control, and the value of fold changes with the asterisks representing significance was marked above the line. Data were analyzed by unpaired t-test. *p < 0.05; **p < 0.01. **(H)** FAO-produced ATP is increased by the expression of p53 mutant. MCF-12A-Ctrl (Vector) and MCF12A-P53-R273H cells (P53-R273H) were treated with palmitate and/or ETO (2 μM) and then subjected to the ATP assay to measure the steady-state ATP level (mean ± SD, n = 3). The relative ATP level was plotted by comparing to the ATP level of the Vector group without the treatment of PA. The two sides of the lines above the bars indicated the comparison of the two groups, and the value of fold changes with the asterisks representing significance was marked above the line. Data were analyzed by unpaired t-test. **p < 0.01.

mammosphere forming assays in the absence of ETO to examine whether interfering with Mutp53-induced FAO could compromise Mutp53-enhanced cellular motility and stemness. Pretreatment of ETO significantly decreased both migration (**Supplementary Figure S2A**) and invasion (**Supplementary Figure S2B**) ability, as well as sphere formation (**Supplementary Figure S2C**) without continuous treatment of ETO. Similar effects were also observed when ETO (50 and 200 μmol/L) was administrated during assays in p53-R273H MCF-12A and BT549 cells (**Supplementary Figures S2A–C**). Moreover, ETO treatment resulted in a dose-dependent inhibition on the foci formation of p53-R273H and p53-R280K MCF-12A cells in soft agar (**Supplementary Figure S2D**), suggesting inhibition of FAO disturbs the Mutp53-mediated anchorage-independent growth.

Taken together, these results indicated that ETO treatment interferes with Mutp53-induced migration, invasion, stemness, and cell transformation, implying a crucial role of FAO in Mutp53-mediated biological effects in BLBCs.

Mutant p53 Activates FAO Activity Through Upregulating CPT1C

To further elucidate the molecular mechanisms accounting for Mutp53-induced FAO, the mRNA expression of several FAO-associated genes was examined by Q-PCR in MCF12A-p53-R280K cells (**Figure 2A**). Among these enzymes, carnitine palmitoyltransferase 1C (CPT1C), the brain-specific isoform of the rate-limiting enzyme of FAO, was identified as one of the targets significantly upregulated by Mutp53^{R280K}. Moreover, this enhanced CPT1C expression was also found in MCF12A cells expressing other p53 hot-spot mutations in both mRNA (**Figure 2B**) and protein level (**Figure 2C**), implying a putative role of CPT1C in Mutp53-enhanced FAO.

Although the acyl-carnitine activity of CPT1C has been confirmed by *in vitro* biochemical analyses (29), whether CPT1C contributes to cellular FAO activity is still under debate (30, 31). Hence, we first overexpressed CPT1C in MCF-12A cells (**Figure 2D** left) and performed an FAO assay to address this issue. As shown in

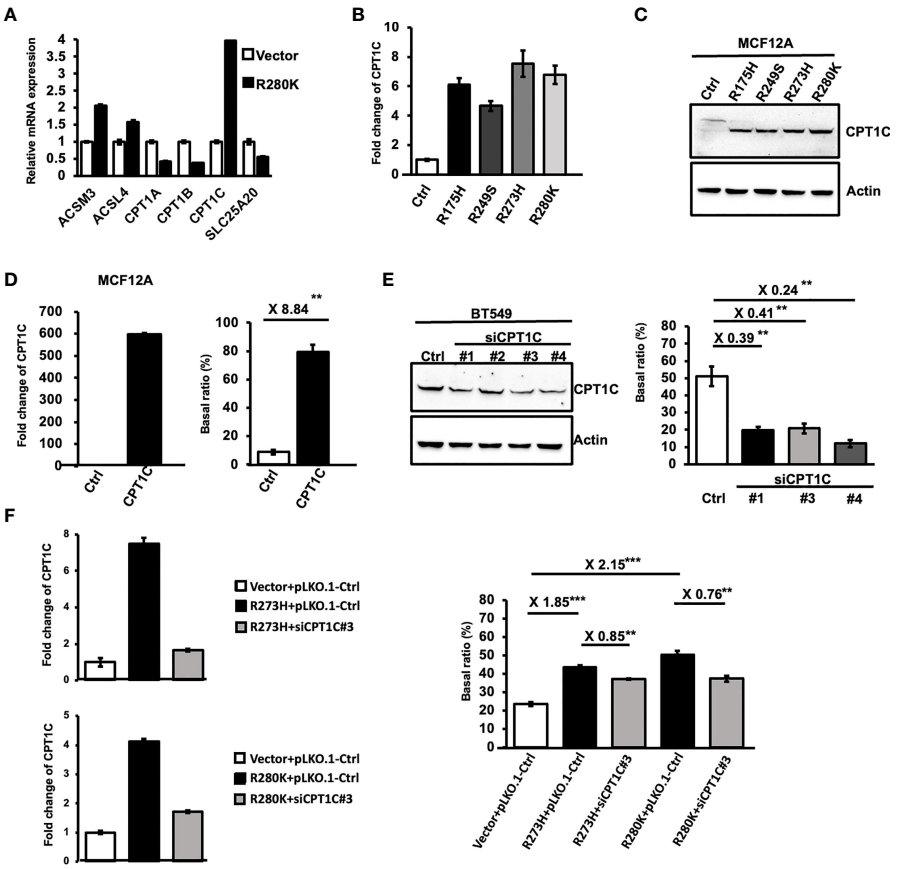

FIGURE 2 | Mutant p53 activates FAO activity through upregulating CPT1C. **(A)** The differential expression of lipid metabolism-related genes induced by mutant p53. The relative mRNA expression level of *ACSM3*, *ACSL4*, *CPT1A*, *CPT1B*, *CPT1C*, and *SLC25A20* between control and MCF12A-p53^{R280K} cells were determined by Q-PCR (mean ± SD, n = 3). **(B)** The mRNA expression of *CPT1C* is upregulated by p53 hot-spot mutants. Relative mRNA expression of *CPT1C* between control cells and p53 mutant-MCF12A cells was determined by Q-PCR (mean ± SD, n = 3). **(C)** Protein expression of CPT1C is upregulated by p53 hot-spot mutants. The expressional levels of CPT1C and Actin in control (Ctrl) and mutant p53-bearing MCF12A cells were examined by Western Blotting. **(D)** The FAO activity is upregulated by CPT1C overexpression in mammary epithelial cells. Left: The expressional levels of CPT1C and Actin in control (Ctrl) and CPT1C-overexpressing MCF12A (CPT1C) cells were examined by Western Blotting. Right: The FAO activity of Ctrl and CPT1C cells was presented as a Basal ratio and shown as a bar graph (mean ± SD, n = 3). **(E)** The FAO activity is decreased by the knockdown of CPT1C in BLBC cells. Left: The expressional levels of CPT1C and Actin in control (Ctrl) and CPT1C-KD BT549 cells (siCPT1C#1, #3, and #4) were examined by Western Blotting. Right: The FAO activity of Ctrl and CPT1C cells was presented as a Basal ratio and shown as a bar graph (mean ± SD, n = 3). The two sides of the lines above the bars indicated the comparison of each KD clone to the control, and the value of fold changes with the asterisks representing significance was marked above the line. Data were analyzed by unpaired t-test. **p < 0.01. **(F)** Downregulating CPT1C expression interferes with p53 mutant-enhanced FAO activity. Left: The mRNA expressional level of *CPT1C* in control and CPT1C-KD MCF12A-p53^{R273H} and MCF12A-p53^{R280K} cells (siCPT1C#3) were examined by Q-PCR. Right: The FAO activity of Ctrl (Vector+pLKO.1), MCF12A-p53^{R273H} (p53^{R273H}+pLKO.1), CPT1C-KD MCF12A-p53^{R273H} (p53^{R273H}+siCPT1C#3), MCF12A-p53^{R280K} (p53^{R280K}+pLKO.1), CPT1C-KD MCF12A-p53^{R280K} (p53^{R280K} +siCPT1C#3) cells were presented as Basal ratio and shown as a bar graph (mean ± SD, n = 3). The two sides of the lines above the bars indicated the comparison of the two groups, and the value of fold changes with the asterisks representing significance was marked above the line. Data were analyzed by unpaired t-test. **p < 0.01; ***p<0.001.

(**Figure 2D** right), overexpression of CPT1C led to an 8.84-fold increase in the basal ratio, indicating cellular FAO activity was enhanced by CPT1C in mammary epithelial cells. Moreover, the observation that interference of CPT1C expression attenuated FAO activity in BLBC cells (from 51.05% to 12.04%; **Figure 2E**; **Supplementary Figures S3A, B**) further supported this notion. Since our results clearly indicated that CPT1C expression contributes to the FAO activity in mammary epithelial and BLBC cells, we compromised the enhanced CPT1C expression by RNA interference in p53-R273H and p53-R280K expressing MCF-12A cells (**Figure 2F** left, **Supplementary Figures S3C, D**) to address whether CPT1C is responsible for Mutp53-enhanced FAO activity. As shown in **Figure 2F** and **Supplementary Figure S3E**, similar trends were observed in CPT1C-KD p53-R273H- and p53-R280K-MCF-12A cells. The basal ratio decreased from 43.59% to 37.2% in p53-R273H and from 50.61% to 38.35% in p53-R280K MCF-12A cells (**Figure 2F** right). All these results indicated that Mutp53 enhances FAO by upregulating the expression of CPT1C.

CPT1C Induces EMT, Enhances Migration, Invasion, and Stemness in Mammary Epithelial Cells and Contributes to Mutp53-Mediated Biological Effects in Cancer Progression

Accumulated evidence indicates that enhanced FAO not only promotes cancer cell survival under metabolic stress but also enhances tumor progression by inducing EMT and cancer stemness (32). In viewing that CPT1C plays a causal role in cell proliferation and survival (30), we further examined whether CPT1C expression also facilitates cancer progression by inducing EMT-associated phenotypes and therefore contributes to Mutp53-mediated biological effects.

To investigate the role of CPT1C in the progression of BLBC, MCF12A cells overexpressing CPT1C were subjected to a series of analyses to examine whether CPT1C contributes to EMT, migration, invasion, and stemness. As shown in **Figure 3A**, overexpression of CPT1C resulted in an increased expression of N-Cadherin and a decreased expression of E-cadherin in mammary epithelial cells. This EMT phenotype induced by CPT1C *in vitro* was further supported by an *in vivo* observation as a slight to moderate positive correlation between CPT1C and the EMT markers (CPT1C vs. E-Cadherin, R=-0.17, P<0.0001; CPT1C vs. N-Cadherin, R=0.13, P<0.0001; CPT1C vs. Vimentin, R=0.37, P<0.0001; CPT1C vs. Fibronectin, R=0.23, P<0.0001; **Figure 3B**) was found in breast cancer patients. High expression of CPT1C also led to a significant enhancement in migration (**Figure 3C**) and invasion (**Figure 3D**) potential, as well as anchorage-independent growth (**Figure 3E**). Additionally, CPT1C greatly increased mammosphere forming ability (**Figure 3F**). The mRNA level of *CPT1C* in mammospheres was highly elevated when compared with 2D culture in MCF-12A-p53^{R273H}, BT549, and MDA-MB-231 cells (**Supplementary Figure S4**). Moreover, the expression of CPT1C was positively correlated with several CSC markers (CPT1C vs. ALDH1A1, R=0.27, P<0.0001; CPT1C vs. ALDH1A2, R=0.25, P<0.0001; CPT1C vs. ALDH1A3, R=0.2, P<0.0001; CPT1C vs. PROM1, R=0.12, P<0.0001; **Figure 3G**) in breast cancer patients, further suggesting an important role of CPT1C in maintaining cancer stemness. Together, all these results indicated that CPT1C might promote BLBC progression by inducing cell transformation, strengthening stem cell properties, and enhancing cellular motility and invasiveness through the induction of EMT.

To elucidate whether CPT1C contributes to Mutp53-mediated oncogenic events, CPT1C-KD Mutp53-overexpressing MCF12A (**Supplementary Figures S3C, D**) and two human BLBC cell lines-BT549 (**Figure 2E**) and MDA-MB-231 (**Supplementary Figure S5**) with intrinsic p53 mutations were established and subjected to migration, invasion, soft-agar foci formation, and mammosphere forming assays. Downregulating CPT1C expression not only attenuated Mutp53-enhanced migration (**Figure 4A**, left) and invasion (**Figure 4B**, left) abilities but also dramatically suppressed Mutp53-induced foci formation (**Figure 4C**, left) in the Mutp53-overexpressing MCF-12A cells. Moreover, knockdown of CPT1C compromised the Mutp53-enhanced sphere formation ability (**Figure 4D**, left). Since similar effects were seen in BLBC cell lines, BT549 and MDA-MB-231 (**Figures 4A–D** right), all of our results indicated that CPT1C activated by Mutp53 not only involves in p53 mutation-enhanced FAO activity but also contributes to Mutp53-induced malignant properties. We suggested that CPT1C might play a critical role in regulating tumor cell motility, invasiveness, transformation, and maintenance of cancer stem cell properties in BLBC.

Since FAO contributes to the generation of cytosolic NADPH, which is important for cancer cells to counteract oxidative stress (33), and a previous study revealed that CPT1A-driven FAO decreases ROS levels to avoid anoikis in colorectal cancer (CRC) cells (34), we hypothesized that Mutp53-CPT1C-enhanced FAO activity is critical for maintaining redox homeostasis in BLBC. Examination of the cellular ROS levels in CPT1C-KD p53-R273H-MCF12A (**Figures 5A, B**) and MDA-MB-231 (**Figures 5C, D**) cells, respectively, by using two independent reagents, CellROX^{TM} Green Reagent (**Figures 5A, C**) and DCFDA (**Figures 5B, D**), revealed that knockdown of CPT1C led to increased ROS levels in both cell lines, whereas treatment of the antioxidant, N-acetyl cysteine (NAC), compromised the elevation of cellular ROS, which supported our previous hypothesis. To further examine whether CPT1C promotes BLBC progression by reducing ROS production, CPT1C-KD p53-R273H MCF12A, MDA-MB-231, and BT549 cells were pretreated with 5 or 10 mmol/L of NAC for 1 day and subjected to mammosphere forming assay and transwell migration assay. As shown in **Figure 5E**, treatment of NAC rescued the suppression of sphere-forming ability caused by the knockdown of CPT1C. Moreover, NAC treatment counteracted CPT1C knockdown-reduced migration ability (**Figure 5F**). Furthermore, higher NADPH/NADP$^+$ was observed in Mutp53-bearing MCF12A (MCF12A^{R280K}) cells (**Figure 5G**), suggesting CPT1C-mediated FAO might provide a NADPH pool for tumor cells, which is used to counteract oxidative stress. These results suggested that CPT1C exerts Mutp53-mediated biological effects through modulating cellular redox status.

Mutant p53 Activates CPT1C Expression Through the miR-200c-ZEB2 Axis

CPT1C is considered a direct target gene of WTp53 as WTp53 activates CPT1C expression through direct promoter binding in murine embryonic fibroblasts (13). Since p53 hot-spot mutants usually exert a dominant-negative effect by interfering with the DNA binding activity of WTp53, and the canonical p53 responsive elements were only found in the murine *Cpt1C* promoter but not in human's (35), it is possible that Mutp53 activates CPT1C expression through an indirect mechanism in human cancer cells. In our previous study, we found that Mutp53 is able to attenuate OXPHOS through an indirect downregulation of PCK2 by disturbing the expression of miR-200c (11). In this study, the genome-wide RNA sequencing analysis in miR-200c-KO MCF12A cells revealed that miR-200c KO leads to altered expression of metabolic genes in the

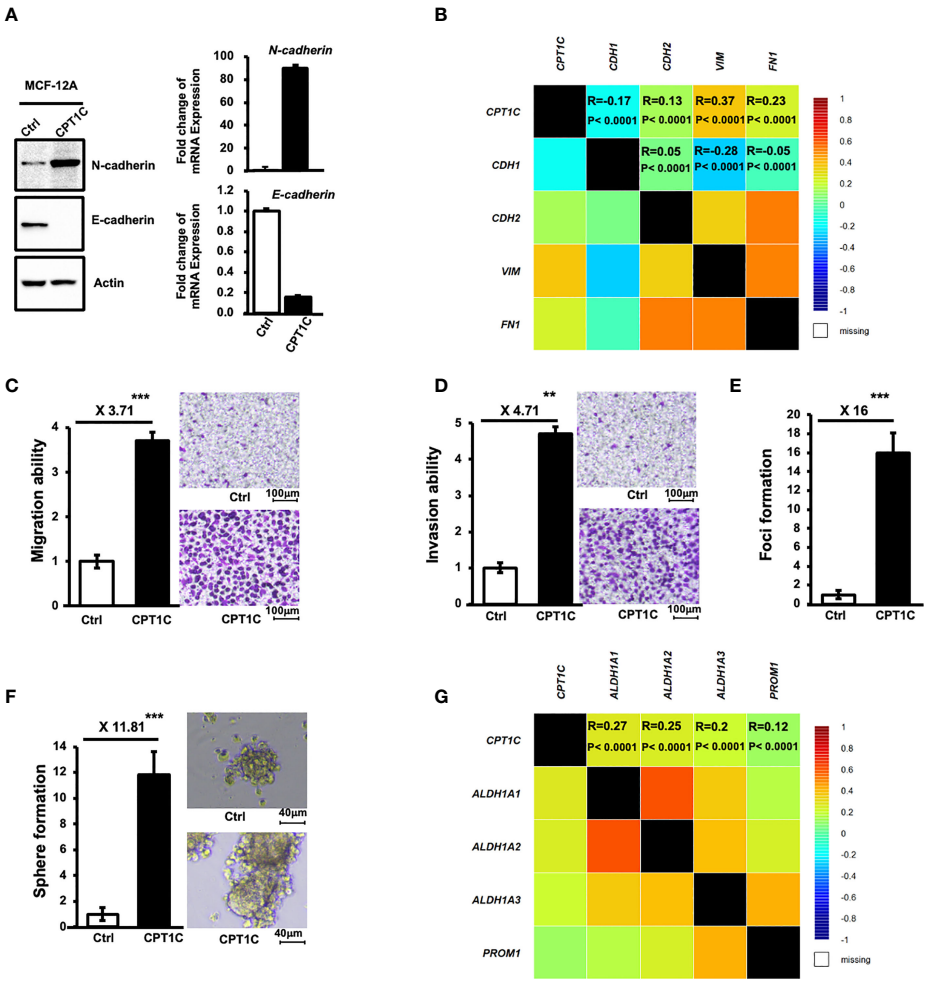

FIGURE 3 | CPT1C induces EMT and enhances migration, invasion, and stemness in mammary epithelial cells. **(A)** Ectopic expression of CPT1C induces EMT in mammary epithelial cells. The expressional levels of N-Cadherin, E-Cadherin, and Actin in control (Ctrl) and CPT1C-overexpressing (CPT1C) MCF12A cells were examined by Western Blotting. Relative mRNA expression of *N-cadherin* and *E-cadherin* between control cells and CPT1C-overexpressing (CPT1C) MCF12A cells were determined by Q-PCR (mean ± SD, n = 3). **(B)** CPT1C shows a slight to moderate positive association with EMT in breast cancer patients. Correlation map showing the Pearson's pairwise correlations among CPT1C, CDH1 (E-cadherin), CDH2 (N-cadherin), VIN (vimentin), and FN1 (fibronectin) in breast cancer patients (N = 4712). Each cell represents a statistical relation between two genes and is colored according to the value of the Pearson correlation coefficient ranging from dark blue (coefficient = -1) to dark red (coefficient = 1). R: correlation coefficient value; P: corresponding p-value. Results are derived from bc-GeneExMiner v4.5 (http://bcgenex.ico.unicancer.fr). **(C, D)** Ectopic expression of CPT1C enhances cell migration **(C)** and invasion **(D)** Migration and invasion ability of CPT1C-overexpressing MCF12A cells were analyzed by migration and invasion assay. The relative migration/invasion ability is presented as a fold change of the numbers of cells passed through trans-wells between control and CPT1C groups (mean ± SD; n=3). The two sides of the lines above the bars indicated the comparison of CPT1C-overexpressing cells to the control cells, and the value of fold changes with the asterisks representing significance was marked above the line. Data were analyzed by unpaired t-test. **p <0.01; ***p < 0.001. Representative micrographs of migrated **(C)** or invaded **(D)** cells were shown on the right. **(E)** CPT1C overexpression enhances anchorage-independent growth. A soft-agar foci formation assay was performed to determine the anchorage-independent growth ability of CPT1C-overexpressing MCF12A cells. Foci number in triplicate dishes was counted and presented as fold change between control and CPT1C groups (mean ± SD; n = 3). The two sides of the line above the bars indicated the comparison of CPT1C-overexpressing cells to the control cells, and the value of fold changes with the asterisks representing significance was marked above the line. Data were analyzed by unpaired t-test. ***: p < 0.001. **(F)** Overexpression of CPT1C enhances stemness. CPT1C-overexpressing MCF12A cells exhibit higher mammosphere forming ability. Control or CPT1C-overexpressing MCF12A cells were grown in suspension culture for 7-8 days to form mammospheres. Mammospheres with a diameter larger than 40 μm were counted and presented as fold change. Results were derived from experiments done in triplicate (mean ± SD; n = 3). The two sides of the line above the bars indicated the comparison of CPT1C-overexpressing cells to the control cells, and the value of fold changes with the asterisks representing significance was marked above the line. Data were analyzed by unpaired t-test. ***p < 0.001. Representative micrographs of mammospheres under a microscope are shown on the right. **(G)** CPT1C shows a slight to moderate positive association with stemness markers in breast cancer patients. Correlation map showing the Pearson's pairwise correlations among CPT1C and stemness markers, ALDH1A1, ALDH1A2, ALDH1A3, and CD133 (PROM1) in breast cancer patients. R: correlation coefficient value; P: corresponding p-value. Results are derived from bc-GeneExMiner v4.5 (http://bcgenex.ico.unicancer.fr).

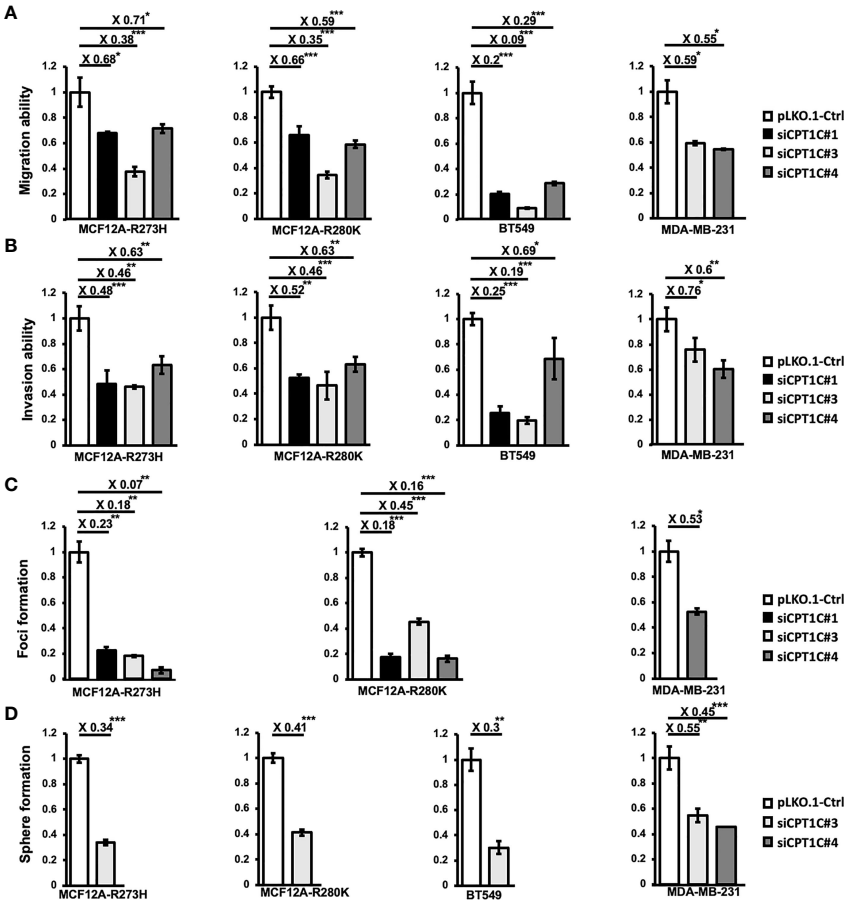

FIGURE 4 | Interference of CPT1C expression attenuates mutant p53-mediated biological effects. CPT1C expression was downregulated by RNA interference in mutant p53-overexpressing cells (MCF12A-p53^{R273H} and MCF12A-p53^{R280K}) and BLBC cell lines (BT549 and MDA-MB-231), and these cell lines were then subjected to the following analysis. **(A, B)** Downregulating CPT1C expression attenuates migration and invasion ability in mutant p53-overexpressing mammary epithelial cells and BLBCs. The migration **(A)** and invasion **(B)** ability of CPT1C-KD cells (siPCK2 #1, #3, or #4) were analyzed by migration/invasion assay done in triplicate. The relative migration/invasion ability is presented as a fold change of the numbers of cells passed through trans-wells between control and CPT1C-KD cells (mean ± SD; n = 3). The two sides of the lines above the bars indicated the comparison of each KD clone to the control, and the value of fold changes with the asterisks representing significance was marked above the line. Data were analyzed by unpaired t-test. *p <0.05; ***p < 0.001. **(C)** Downregulating CPT1C expression diminishes the anchorage-independent growth in MDA-MB-231 and mutant p53-overexpressing mammary epithelial cells. The anchorage-independent growth ability of CPT1C-KD cells was examined by soft-agar foci formation assay (mean ± SD; n = 3). The two sides of the lines above the bars indicated the comparison of each KD clone to the control, and the value of fold changes with the asterisks representing significance was marked above the line. Data were analyzed by unpaired t-test. *p <0.05; **p <0.01; ***p < 0.001. **(D)** Interference of CPT1C expression suppresses stemness/cancer stemness in mutant p53-overexpressing mammary epithelial cells and BLBCs. The stem cell/cancer stem cell properties of CPT1C KD cells were examined by mammosphere forming assay (mean ± SD; n = 3). The two sides of the lines above the bars indicated the comparison of each KD clone to the control, and the value of fold changes with the asterisks representing significance was marked above the line. Data were analyzed by unpaired t-test. **p < 0.01; ***p < 0.001.

lipid metabolism pathway, where *CPT1C* mRNA expression is highly activated in miR-200c-KO MCF12A cells (**Supplementary Figure S6**). This elevated CPT1C expression caused by miR-200c-deficiency was further confirmed as the CPT1C protein level was substantially enhanced in miR-200c-KO MCF12A cells containing *WTp53* (MCF-12A-Sg1 and -Sg2, **Figure 6A**), and the *CPT1C* mRNA expression was higher in the cohort of p53 wild-type breast cancer patients with low expression of miR-200c (**Figure 6B**), raising the possibility that Mutp53 might activate CPT1C expression through downregulating miR-200c. To examine this hypothesis, we restored miR-200c expression in p53-R249S, p53-R273H, and p53-R280K MCF-12A cells and found that the recovery of miR-200c expression compromised both the elevated mRNA (**Figure 6C**) and protein (**Figure 6D**) expression of CPT1C caused by Mutp53, suggesting Mutp53 might upregulate CPT1C expression through interfering with the expression of miR-200c. To further confirm the antagonistic relationship between Mutp53 and miR-200c on CPT1C expression, we restored miR-200c in BT549 and 4T1 cells (11). As shown in **Supplementary Figure S7**, restoration of miR-200c led to decreased expression of CPT1C in Mutp53-harboring human

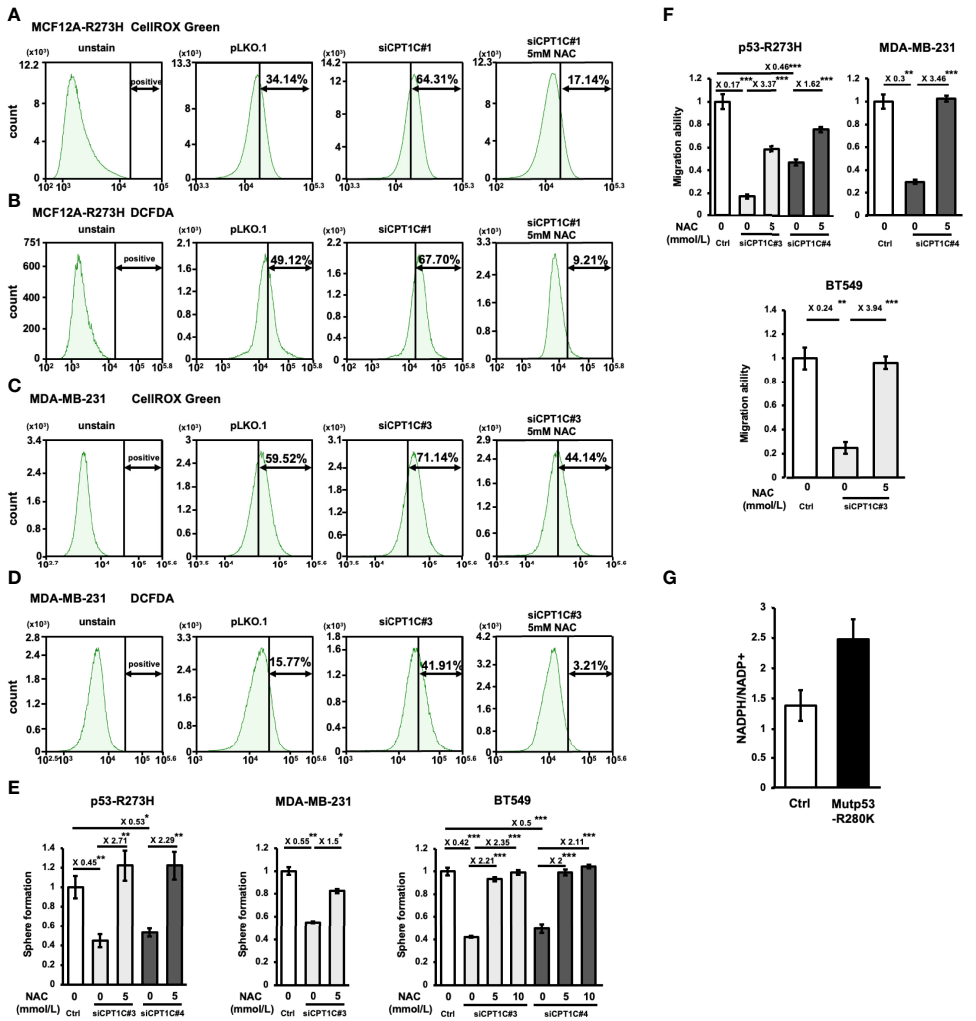

FIGURE 5 | CPT1C regulates mutant p53-mediated biological effects through modulating redox status. **(A–D)** Total cellular ROS level is elevated by knockdown of CPT1C in MCF12A^{R273H} **(A, B)** and MDA-MB-231 **(C, D)** cells and is compromised by N-acetyl cysteine (NAC) treatment. Cells were stained with CellROX^{TM} Green Reagent **(A, C)** or DCFDA **(B, D)**, then the fluorescence was measured by FACS to determine the total cellular ROS. Similar trends in the representative images were observed in three independent experiments. **(E, F)** CPT1C deficiency-mediated suppression of cancer stemness and migration ability are rescued by NAC treatment. MCF12A^{R273H} [**(E**, **F)**, left], MDA-MB-231 [**(E**, **F)** middle], and BT549 [**(E, F)** right] cells treated with NAC (0, 5, or 10 mmol/L) for 1 day and its Ctrl cells were subjected to mammosphere formation assay and transwell migration assay (mean ± SD; n = 3). The two sides of the lines above the bars indicated the comparison of the two groups, and the value of fold changes with the asterisks representing significance was marked above the line. Data were analyzed by unpaired t-test, *p < 0.05, **p < 0.01, ***p < 0.001. **(G)** The ratio of NADPH/NADP$^+$ is upregulated by mutant p53. The absolute amount of NADPH and NADP$^+$ were measured by CE-TOFMS and CE-QqQMS analysis, and the ratio of NADPH/NADP$^+$ in MCF12A-ctrl and MCF12A-p53^{R280K} were compared and shown in bar graphs (mean ± SD, n = 2).

BLBC cells and p53-null murine 4T1 cells. This *in vitro* observation could be recaptured in p53 mutated breast cancer patients, as the expression of CPT1C is lower in the cohort of miR-200c-High when compared with patients harboring low miR-200c expression (**Figure 6E**). Additionally, in total breast cancer patients, the miR-200c-Low cohort exhibits a higher expression of CPT1C (**Figure 6F**), and a moderate negative correlation between the expression of CPT1C and miR-200c was also revealed by Spearman correlation analysis (R=0.18, P<0.0001; **Figure 6G**). Based on these results, our study suggested that Mutp53 elevates CPT1C expression through disturbing miR-200c.

CPT1C is indirectly suppressed by miR-200c due to the lack of miR-200c seeding sequence in the 3'-UTR of CPT1C mRNA (analyzed by TargetScan, data not shown). Therefore, to investigate the molecular mechanism by which Mutp53 upregulates CPT1C through disturbing the miR-200c axis, we examined the CPT1C expression in MCF-12A-p53^{R273H}, BT549, and MDA-MB-231 cells knocked down with miR-200c downstream targets including ZEB1, ZEB2, Bmi-1, or Slug, which are highly induced by miR-200c deficiency (11). As shown in **Supplementary Figure S8**, downregulating the expression of ZEB1 (**Supplementary Figure S8A**), Bmi-1 (**Supplementary Figure S8B**), or Slug (**Supplementary**

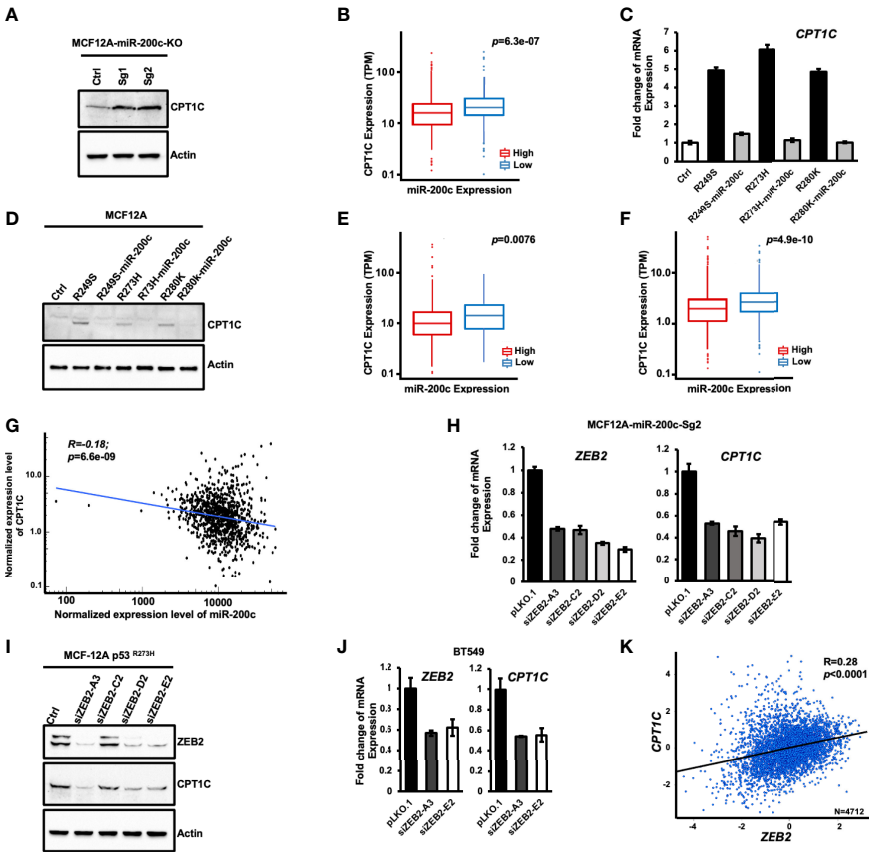

FIGURE 6 | Mutant p53 activates CPT1C expression through the miR-200c-ZEB2 axis. **(A)** miR-200c-deficiency leads to enhanced expression of CPT1C in mammary epithelial cells. The expression of CPT1C and Actin in control (Ctrl) and miR-200c-KO MCF12A cells (MCF12A-Sg1 and MCF12A-Sg2) were examined by immunoblotting. **(B)** The box and whisker plot of CPT1C expression in p53 wide-type breast cancer patients (n = 657) from TCGA with high (n = 328) or low miR-200c expression (n = 329). The statistical significance of differential CPT1C expression in miR-200c high expression and low expression groups was determined by Wilcoxon rank-sum test. p: corresponding p-value. **(C, D)** Restoring the expression of miR-200c compromises the enhanced CPT1C expression caused by mutant p53. The expression of CPT1C in control (MCF12A-Ctrl), p53 mutant cells (MCF12A-p53^{R249S}, MCF12A-p53^{R273H} and MCF12A-p53^{R280K}) and miR-200c-overexpressing p53 mutant cells (MCF12A-p53^{R249S}-miR-200c, MCF12A-p53^{R273H} -miR-200c and MCF12A-p53^{R280K}-miR-200c) were examined by Q-PCR **(C)** or immunoblotting **(D)**. **(E)** The box and whisker plot of CPT1C expression in breast cancer patients (n = 290) harboring p53 missense mutations with high (n = 145) or low miR-200c expression (n = 145). Statistic method: Wilcoxon rank-sum test. p: corresponding p-value. **(F)** The box and whisker plot of CPT1C expression in total breast cancer patients (n = 1074) from TCGA with high (n = 537) or low miR-200c expression (n = 537). Statistic method: Wilcoxon rank-sum test. p: corresponding p-value. **(G)** The Spearman correlation plot for CPT1C versus miR-200c in total breast cancer patients from the TCGA database. R: correlation coefficient value; P: corresponding p-value. **(H–J)** Knockdown of ZEB2 interferes with the enhanced expression of CPT1C in miR-200c-KO **(H)**. MCF12A-miR-200c-Sg2), p53 mutant-overexpressing **(I)**, MCF12A-p53 ^{R273H}), and BT549 **(J)** cells. **(K)** The Pearson's pairwise correlation plot for CPT1C versus ZEB2 in total breast cancer patients from TCGA. R: correlation coefficient value; P: corresponding p-value. The result is derived from bc-GeneExMiner v4.5 (http://bcgenex.ico.unicancer.fr).

Figure S8C) did not affect the expression of CPT1C in p53 mutant-expressing cells or miR-200c-deficient cells, but knockdown of ZEB2 interfered with the elevated expression of *CPT1C* caused by p53 mutation (MCF-12A-miR-200c-Sg2-siZEB2-A3, C2, D2, and E2; **Figure 6H**). Moreover, similar results were extended to ZEB2 knocked down MCF12A-p53^{R273H} (**Figure 6I**) and BT549 (**Figure 6J**) cells, and a moderate expressional correlation between CPT1C and ZEB2 was found in breast cancer patients (R=0.28; P<0.0001; **Figure 6K**). All these results together implied that Mutp53 might upregulate CPT1C through inhibiting miR-200c, subsequently compromising the suppressive effect of miR-200c on ZEB2, which in turn enhances CPT1C expression.

High CPT1C Expression Is Associated With Poor Prognosis in Basal-Like Breast Cancer Patients

To validate the biological significance and examine whether our *in vitro* observation could be recaptured *in vivo*, an orthotopic xenograft tumor mouse model was used to examine the role of CPT1C in tumor growth. CPT1C-KD (MDA-MB-231-siCPT1C#3) and its control cells were inoculated into the mammary fat pad, and the tumor size was measured every three days for five weeks. As shown in **Figure 7A**, a slow tumor growth curve was observed in CPT1C-KD cells, and knockdown of CPT1C caused a near 50% decrease both in tumor volumes and tumor weights, indicating

CPT1C contributes to the tumor growth of BLBC *in vivo*. Additionally, to address whether CPT1C involves in metastasis *in vivo*, CPT1C-KD cells expressing luciferase activity (MDA-MB-231-Luc2-siCPT1C#3) were inoculated through tail vein injection, and the metastatic lesions in the lung were visualized and quantified by an *in-vivo* imaging system (IVIS). As shown in **Figure 7B**, the control cells (MDA-MBA-231-Luc2-pLko.1-Ctrl) developed colonized tumor in the lung after five weeks. However, silencing CPT1C interfered with lung metastasis of BLBC cells, as the total metastatic burden quantified by luciferase activity was significantly decreased in MDA-MB-231-Luc2-siCPT1C#3 cells, indicating CPT1C might facilitate distal metastasis, which is in line with the clinical observation that CPT1C expression is higher in breast cancer patients with metastatic tumors ($P<0.01$; **Figure 7C**).

Furthermore, interference of CPT1C expression significantly prolonged the survival of the orthotopic tumor mouse models (**Figure 7D**, left). CPT1C-KD (MDA-MB-231-Luc2-siCPT1C#3) and the control cells (MDA-MBA-231-Luc2-pLko.1-Ctrl) were inoculated into the fourth mammary fat pads of 11 mice, respectively, in each group. The first death in control mice and CPT1C-KD mice was observed on day 56 and day 87, respectively, after inoculation, and the 50% mortality in control mice occurred within 84 days after inoculation, which was 21 days earlier than that in CPT1C-KD mice. We suggested these mice might die from metastatic burden since spontaneous metastasis from primary mammary fat pad tumors was detected by IVIS during the 112-day observation period (**Figure 7D**, right). The representative images showed that on day 75, spontaneous metastasis developed solely in control mice, which had started to die almost three weeks ago. However, on day 98, the metastatic signal was detectable on CPT1C-KD mice instead of control mice, indicating when CPT1C-KD mice began to develop metastasis, control mice had already died from metastatic disease, and those who still survived were control mice without metastatic burden. This result implied that interference of CPT1C expression hindered the spontaneous metastatic ability of BLBC cells, leading to improved disease-specific survival. The significant difference in the survival rates between control and CPT1C-KD mice not only reflected that CPT1C deficiency attenuated pulmonary colonization (**Figure 7B**), but also was in accordance with the clinical relevance of CPT1C in BLBC revealed by analyzing BLBC patients from the TCGA database. BLBC patients were divided into groups of CPT1C-High and CPT1C-Low according to the mRNA levels of *CPT1C*. As shown in **Figures 7E–H**, patients in the cohort with High CPT1C expression had much worse overall survival (OS; **Figure 7E**). Moreover, poor disease-free survival (DFS; **Figure 7F**), progression-free survival (PFS; **Figure 7G**) as well as disease-specific survival (DSS; **Figure 7H**) were observed in the CPT1C-High cohort, indicating high CPT1C expression could predict unfavorable clinical outcomes in BLBC patients, and strongly suggesting a pivotal role of CPT1C in facilitating tumor progression *in vivo*.

Since CPT1A, CPT1B, and CPT1C belong to the CPT family, we also compared the clinical relevance of CPT1A, CPT1B, and CPT1C in total breast cancer patients and patients with various subtypes of breast cancer (**Supplementary Figure S9–S12**). Differing from high expression of CPT1A that predicts a poor overall survival in total (**Supplementary Figure S9**) and luminal A (**Supplementary Figure S10**) breast cancer patients, and high expression of CPT1B that predicts a better overall survival in luminal B breast cancer patients (**Supplementary Figure S11**), high CPT1C expression specifically predicts a poor overall survival in BLBC patients, but not in total or other subtypes of breast cancers (**Supplementary Figure S12**), which further implies that targeting CPT1C, but not the other isoforms of CPT1, might be a promising treatment strategy for BLBC.

Together, the *in vivo* observation and the clinical validation revealed the critical role of CPT1C in facilitating tumor progression of BLBC and the significance of CPT1C as the prognostic indicator for patients with BLBC, reflecting our *in vitro* results that CPT1C contributes to EMT-associated phenotypes, migration, invasion, and cancer stemness in BLBC cells.

DISCUSSION

During the 40 years of discovery, p53 has been characterized as a pivotal tumor suppressor by ensuring genomic integrity, inducing cell-cycle arrest or apoptosis, controlling self-renewal and differentiation of stem cells, and preventing somatic cell reprogramming (36). In the past decade, p53 has emerged as an important regulator of cellular metabolism, in which perturbations of p53-associated metabolic networks could lead to the burden of cancers (37). Our previous study reveals that dysfunction of p53 attenuates OXPHOS by downregulating the miR-200c-PCK2 axis in BLBC (11), providing robust evidence for the causal link between Mutp53-mediated metabolic reprogramming and cancer stemness. Despite this, the complexity of p53 pathways and the cell type-specific regulation of metabolism still limit our understanding of the connection between cancer-associated metabolic rewiring and p53 deficiency-induced biological functions. Therefore, figuring out the complicated p53 networks of metabolic regulation and the underlying molecular mechanisms would be a major breakthrough in cancer metabolism, which paves the way for the development of precise metabolic therapies for specific cancers.

In response to stress conditions, such as oxidative stress and hypoxia, p53 is activated to modulate its target genes involved in DNA repair and cell survival (38). WTp53 has been reported to induce CPT1C expression under hypoxia and glucose deprivation, which promotes tumor cell survival (13). In addition, CPT1C promotes ATP production from FAO to protect tumor cells from metabolic stress (30). Although p53 directly transactivates *Cpt1c* in murine cells (13), whether *CPT1C* is a direct target gene of p53 in human is still under debate since the lack of direct interaction between WTp53 and the *CPT1C* promoter revealed by ChIP assay is reported by a recent study (35). In our study, we found that Mutp53 enhances FAO to facilitate the progression of BLBC by upregulating CPT1C through the miR-200c-ZEB2 axis. The FAO activity was measured by using Mito Stress assay with palmitate as

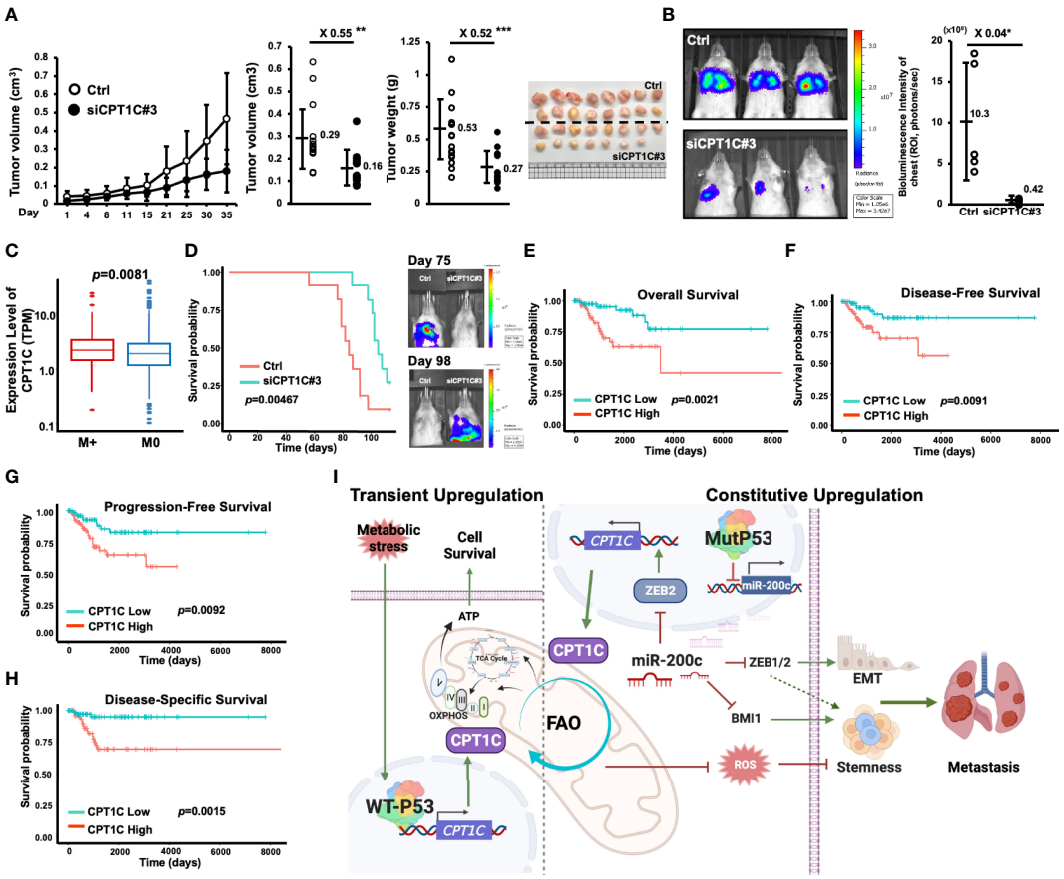

FIGURE 7 | High CPT1C expression is associated with poor prognosis in basal-like breast cancer patients. **(A)** Interfering with CPT1C expression attenuates the growth of BLBCs *in vivo*. MDA-MB-231-Ctrl (n = 16) and MDA-MB-231-siCPT1C#3 (n = 15) cells ($3x10^6$) were inoculated into the fourth mammary fat pad of SCID mice for five weeks. Tumor sizes were recorded at indicated days and plotted as a growth curve. At day 35, tumors were harvested surgically, tumor weights were measured, and tumor volumes were determined with the formula: $(d1x\ d2^2)/2$ (d1: larger diameter; d2: smaller diameter) and plotted as dot plots (mean ± SD). The two sides of the lines above the dots indicated the comparison of the CPT1C-KD group to the control group, and the value of fold changes with the asterisks representing significance was marked above the line. Data were analyzed by unpaired t-test. **p < 0.01; ***p <0.001. **(B)** Interfering with CPT1C expression suppresses the pulmonary metastasis of BLBCs *in vivo*. MDA-MB-231-Luc2-Ctrl (n = 5) and MDA-MB-231-Luc2-siCPT1C#3 (n = 5) cells ($1x10^6$) cells were inoculated into NOD-SCID mice through lateral tail-vein injection. At five weeks post-injection, an IVIS imaging was carried out to examine the pulmonary colonization of MDA-MB-231 cells. Left: Representative images of MDA-MB-231-Luc2 luciferase-mediated bioluminescence intensities in control and CPT1C-KD groups. Right: The total tumor growth was estimated based on luciferase activity detected as total bioluminescence intensity of Chest (photons/sec) and plotted as dot plot (mean ± SD). The two sides of the line above the dots indicated the comparison of the CPT1C-KD group to the control group, and the value of fold changes with the asterisks representing significance was marked above the line. Data were analyzed by unpaired t-test. *p <0.05. **(C)** The box and whisker plot of CPT1C expression in breast cancer patients with metastasis (M+, red, n = 184) or without metastasis (M0, blue, n = 909) from the TCGA database. The statistical significance was determined by Wilcoxon rank-sum test. p: corresponding p-value. **(D)** Low CPT1C expression confers better overall survival (OS) *in vivo*. MDA-MB-231-Ctrl (n = 11) and MDA-MB-231-siCPT1C#3 (n = 11) cells ($3x10^6$) were inoculated into the fourth mammary fat pad of NOD-SCID mice. Left: The Kaplan-Meier survival plot was drawn by using IBM SPSS Statistics 24 according to the time frame from the first death to the last. The statistical significance was determined with the logrank test. Right: the represented images of IVIS analysis at day 75 and day 98 post-inoculation. At day 75, only the Ctrl group exhibited lung metastasis. No metastatic lesion was found in the CPT1C-KD group. At day 98, the only survivor (1/11) of the Ctrl group showed no sign of pulmonary metastasis. Metastatic lesions were found in all of the mice (11/11) in the CPT1C-KD group, which are dead by day 112. **(E–H)** High CPT1C expression predicts poor overall survival (OS; **(E)**, disease-free survival [DFS; **(F)**], progression-free survival [PFS; **(G)**], and disease-specific survival [DSS; **(H)**] in BLBC patients. The Kaplan-Meier survival estimates of differential CPT1C expression were derived from the BLBC cohort (n = 172 for OS and PFS; n = 168 for DFS; n = 154 for DSS) of TCGA RNA-Seq data. The survival curve compared the patients with High (red, n = 86 for OS and PFS; n = 84 for DFS; n = 77 for DSS) and Low (green, n = 86 for OS and PFS; n = 84 for DFS; n = 77 for DSS) expression of CPT1C. The statistical significance was determined with the logrank test. **(I)** A proposed model of mutant p53 induces FAO and stemness through upregulating CPT1C expression *via* the miR-200c-ZEB2 axis.

substrates and presented as a basal ratio, indicating the portion of FAO-contributed OCR to the total cellular oxygen consumption (**Figures 1B–F**). As shown in **Figure 1G**, overexpressing Mutp53 in normal mammary epithelial cells led to significant increases in the basal ratio, implying Mutp53 enhances FAO activity. However, the treatment of FCCP, a mitochondrial uncoupler disrupting the proton gradient across the mitochondrial inner membrane and leading to the maximal OCR (39), resulted in a decreased OCR instead of an increased OCR in Mutp53-bearing cells (**Figures 1C–F**). The reason for this paradox might be the concentration of FCCP used in our FAO assay was the optimized concentration for that specific cell line in the Mito Stress assay, in

which cells are maintained in the medium containing glucose. In contrast, in the FAO assay, cells were starved in the glucose-free medium containing fatty acids with even micromolar concentrations of ETO that could inhibit FCCP-stimulated oxygen consumption (40). Additionally, high concentrations of FCCP can be inhibitory to the OCR rather than stimulatory due to the damaged mitochondrial and loss of membrane potential caused by the toxicity (41–43). One of the possible solutions to this issue is to perform a titration of FCCP to optimize the appropriate concentrations under the conditions of the FAO assay; though, it is not the priority in our current study because the basal ratio we used to represent the FAO activity depends on the basal OCR but not the maximal respiration or the spare respiratory capacity determined by FCCP. Therefore, the optimized concentration of FCCP for cells used in the FAO assay would be further determined in the future when only necessary.

Another important and novel observation in our present work is that Mutp53 promotes FAO activity through activating CPT1C, which seems contradictory to the current general concept that WTp53 promotes FAO *via* inducing CPT1C. In specific circumstances, Mutp53 would induce the expression of WTp53 target genes. For example, Tran et al. demonstrate that Mutp53 hyper-transactivates target genes of WTp53, including *CDKN1A*, *TIGAR*, *GLS2*, and *GADD45A*, to protect cancer cells against glutamine deprivation (44). WTp53 is activated upon acute stress stimuli, but for tumor cells confronted with various types of stress, especially the severe oxidative stress during metastasis (45), continuous activation of WTp53 is deleterious. Due to the extended half-life and thus accumulation of Mutp53 in tumors (46), we suggest that Mutp53 provides sustained beneficial effects for tumor cells than transient effects induced by WTp53. Therefore, BLBC cells are able to maintain a constitutive expression of CPT1C by Mutp53, which is critical for BLBC progression (**Figure 7I**).

During the loss of attachment to the extracellular matrix, which is the prerequisite of metastasis (47), tumor cells display inhibited glucose uptake, reduced ATP production as well as increased ROS, followed by induction of anoikis, a form of apoptosis due to loss of cell-matrix interactions (33, 48). Several lines of evidence reveal that FAO is critical for preventing detached cells from undergoing anoikis by providing extra ATP and maintaining redox homeostasis in breast cancers (49, 50), which is in line with our observations that both etomoxir treatment and CPT1C deficiency impaired migration, invasion, mammosphere formation, and anchorage-independent colony formation. Therefore, our results indicate that accumulated Mutp53 proteins lead to prolonged induction of CPT1C, potentiating FAO, which contributes to increased cellular motility and stemness in BLBC cells. CPT1C has been found by others to facilitate cancer progression by promoting proliferation, tumor growth, and survival, increasing ATP synthesis to protect against metabolic stress, contributing to chemoresistance (51), and preventing cancer cell senescence (52). To our knowledge, we first uncovered the novel roles of CPT1C in regulating EMT, cellular motility, cancer stemness, and metastasis. Furthermore, the extremely high relevance of CPT1C with clinical parameters implies that CPT1C is highly associated with tumor progression in BLBC, which is in accordance with our *in vitro* results and *in vivo* tumorigenic and metastatic mouse models.

FAO produces NADH, FADH2, and acetyl-CoA, which fuels OXPHOS directly or through the TCA cycle, hence cellular factors or signaling events could potentiate OXPHOS activity by enhancing FAO (17, 53, 54). Although OXPHOS plays a key role in regulating cellular redox status, the FAO-enhanced OXPHOS activity might not increase oxidative stress accordingly. A study by Choi et al. reveals that in spite of the increased OXPHOS in drug-resistant gastric CSCs, NADPH regeneration fueled by the enhanced FAO activity lowers the ROS level. In contrast, inhibition of FAO by ETO reduces the NADPH pool and increases mitochondrial ROS levels in CSCs (55). FAO is one of the major sources of cytosolic NADPH, which is utilized by a wide variety of cancer cells to overcome oxidative stress (33, 56). For example, inhibiting FAO by ETO decreases NADPH production, increases ROS level, leading to oxidative stress, ATP depletion, and cell death in glioblastoma cells (57). Furthermore, CPT has been reported to contribute to the generation of NADPH in several different cancer types. Wang et al. demonstrate that CPT1A-induced FAO and CPT1A-maintained NADPH/$NADP^+$ ratio are critical for redox homeostasis of detached CRC cells, in which NAC treatment increased anchorage-independent growth of detached CPT1A-KD CRC cells (34). In another study, PGC-1α, the key transcription coactivator regulating CPT1A and CPT1B, binds to the transcription factor CEBPB to promote CPT1A expression, which enhances FAO activity to maintain the high NADPH/$NADP^+$ ratio, contributing to radiation resistance of nasopharyngeal carcinoma cells (58). In addition to CPT1, elevated expression of CPT2 in gastrointestinal cancer cells is also important for fueling the NADPH pool to maintain redox homeostasis upon chemo-drug treatment (59). Together, all of these findings are consistent with ours as a higher NADPH/$NADP^+$ ratio was observed in p53-R280K MCF12A cells (**Figure 5G**), and knockdown of CPT1C in p53-R273H MCF12A cells and MDA-MB-231 cells increased oxidative stress as measured by CellROX^{TM} Green Reagent (**Figures 5A, C**) and DCFDA (**Figures 5B, D**). Moreover, CPT1C deficiency-induced oxidative stress could be rescued by NAC treatment (**Figures 5A–D**), indicating that CPT1C-driven FAO increases the generation of NADPH, which is utilized by BLBC cells to reduce oxidative stress, maintain an optimized redox equilibrium, and facilitate migration and stemness.

Paradoxically, a high NADPH/$NADP^+$ ratio can play a double-faceted role in regulating redox status by promoting both antioxidant and prooxidative pathways. As an antioxidant, NADPH is used by glutathione reductase to generate glutathione (GSH), which controls and maintains redox status by scavenging several ROS (60). However, GSH not only eliminates ROS, but also protects against nitrosative stress by buffering nitric oxide (NO), which can react with and damage cellular macromolecules like DNA, proteins, and lipids

(61). Therefore, GSH is a critical antioxidant controlling cellular redox homeostasis by neutralizing ROS and reactive nitrogen species (RNS). It is noteworthy that the DCFDA fluorogenic probe used in our study is oxidized not only by H_2O_2 but also by RNS (62, 63); hence, CPT1C-mediated control on the redox status might be through increasing GSH level by enhancing FAO to fuel the NADPH pool, which then utilized by BLBC cells to neutralize both ROS and RNS. The decreased oxidative stress was further confirmed by using another non-specific fluorogenic probe, CellROX™ Green Reagent, which is commonly used to compare total oxidative stress status.

In addition to reducing oxidative stress, CPT1C-mediated induction of EMT and enhanced stemness may be achieved by epigenetic modification since lipid serves as a major source for histone acetylation to activate gene expression (64). Whether CPT1C exerts its oncogenic functions through epigenetic control by increasing the pool of acetyl-coA from FAO for histone acetylation to activate genes involved in EMT and stemness needs further study.

Taken together, the striking consistency among our *in vitro* and *in vivo* results, as well as clinical validation strongly supports our model that Mutp53 potentiates FAO through constitutively upregulating CPT1C *via* dysregulating the miR-200c-ZEB2 axis, which in turn facilitates EMT-associated phenotypes, enhances cancer stemness, and promotes metastasis through modulating cellular redox status, leading to the progression of BLBC and the poor clinical outcomes in BLBC patients (**Figure 7I**). Our current study fully addresses the indispensable connections between Mutp53-driven metabolic reprogramming and the highly malignant characteristics of BLBC, providing a reasonable link between the extremely high frequency of p53 mutation and the reliance on FAO in BLBC. It is noteworthy that since the mediator of Mutp53-induced oncogenic events, CPT1C, is brain-specific, existing only in neurons while is overexpressed in a wide range of cancers (51), and a vast majority of small molecule drugs do not cross the blood-brain barrier (65), it is really promising to develop CPT1C inhibitors with maximal efficacy and minimal off-target effects. In conclusion, our present work unravels the previously unconfirmed function of Mutp53 in FAO, depicts the detailed molecular mechanism accounting for Mutp53-mediated metabotypes, and uncovers the novel biological roles of CPT1C in cancer progression, which is not only a milestone for the thorough understanding of the p53 regulatory network of metabolism but also an indication that targeting Mutp53-miR-200c-ZEB2-CPT1C axis might be developed into a novel and effective therapies for BLBC in the imminent future.

DATA AVAILABILITY STATEMENT

The original contributions presented in the study are included in the article/**Supplementary Materials**. Further inquiries can be directed to the corresponding author.

ETHICS STATEMENT

The animal study was reviewed and approved by Institutional Animal Care and Use Committee at National Yang Ming Chiao Tung University, Taiwan. (IACUC number: NCTU-IACUC-106030).

AUTHOR CONTRIBUTIONS

C-YW: Investigation, data curation, writing-original draft, writing-review and editing. C-HW: Investigation, data curation, methodology, visualization. R-TM: Funding acquisition, investigation, data curation, methodology. T-WC: Funding acquisition, visualization, data curation, investigation. C-WL: Funding acquisition, methodology, writing-review and editing. C-HC:Conceptualization, data curation, investigation, methodology, funding acquisition, project administration, visualization, writing-original draft, writing-review and editing. All authors contributed to the article and approved the submitted version.

FUNDING

This work was financially supported in part by the following: Ministry of Science and Technology (105-2320-B-009-004, 106-2320-B-009-002, 107-2628-B-009-002, 108-2628-B-009-002 and 109-2628-B-009-004 to Dr. C.-H. Chao; 109-2311-B-009-002 and 110-2311-B-A49-001 to Dr. T.-W. Chen; 109-2314-B-001-002 and 109-2314-B-001-008 to Dr. C.-W. Li; 107-2320-B-009-006-MY2 and 109-2320-B-009-002 to Dr. R.-T. Mai). The "Smart Platform of Dynamic Systems Biology for Therapeutic Development" and "Center for Intelligent Drug Systems and Smart Bio-devices (IDS^{2}B) from The Featured Areas Research Center Program" within the framework of the Higher Education Sprout Project of the Ministry of Education (MOE) in Taiwan. We would also like to thank the National Core Facility for Biopharmaceuticals (NCFB, MOST 106-2319-B-492-002) and the National Center for High-performance Computing (NCHC) of National Applied Research Laboratories (NARLabs) of Taiwan for providing computational resources and storage resources, and the National RNAi Core Facility at Academia Sinica in Taiwan for providing shRNA constructs.

SUPPLEMENTARY MATERIAL

The Supplementary Material for this article can be found online at: https://www.frontiersin.org/articles/10.3389/fonc.2022.940402/full#supplementary-material

REFERENCES

1. Vogelstein B, Sur S, Prives C. P53: The Most Frequently Altered Gene in Human Cancers. *Nat Educ* (2010) 3(9):6.
2. Leroy B, Anderson M, Soussi T. TP53 Mutations in Human Cancer: Database Reassessment and Prospects for the Next Decade. *Hum Mutat* (2014) 35 (6):672–88. doi: 10.1002/humu.22552
3. Olivier M, Hollstein M, Hainaut P. TP53 Mutations in Human Cancers: Origins, Consequences, and Clinical Use. *Cold Spring Harb Perspect Biol* (2010) 2(1):a001008. doi: 10.1101/cshperspect.a001008
4. Joerger A, Fersht A. Structure–Function–Rescue: The Diverse Nature of Common P53 Cancer Mutants. *Oncogene* (2007) 26(15):2226–42. doi: 10.1038/sj.onc.1210291
5. Brosh R, Rotter V. When Mutants Gain New Powers: News From the Mutant P53 Field. *Nat Rev Cancer* (2009) 9(10):701–13. doi: 10.1038/nrc2693
6. Anders CK, Carey LA. Biology, Metastatic Patterns, and Treatment of Patients With Triple-Negative Breast Cancer. *Clin Breast Cancer* (2009) 9 Suppl 2:S73–81. doi: 10.3816/CBC.2009.s.008
7. Yadav BS, Chanana P, Jhamb S. Biomarkers in Triple Negative Breast Cancer: A Review. *World J Clin Oncol* (2015) 6(6):252–63. doi: 10.5306/wjco.v6.i6.252
8. Liu J, Zhang C, Hu W, Feng Z. Tumor Suppressor P53 and Metabolism. *J Mol Cell Biol* (2019) 11(4):284–92. doi: 10.1093/jmcb/mjy070
9. Zhang C, Liu J, Liang Y, Wu R, Zhao Y, Hong X, et al. Tumour-Associated Mutant P53 Drives the Warburg Effect. *Nat Commun* (2013) 4(1):1–15. doi: 10.1038/ncomms3935
10. Kim H-R, Roe J-S, Lee J-E, Cho E-J, Youn H-D. P53 Regulates Glucose Metabolism by miR-34a. *Biochem Biophysi Res Commun* (2013) 437(2):225–31. doi: 10.1016/j.bbrc.2013.06.043
11. Chao C-H, Wang C-Y, Wang C-H, Chen T-W, Hsu H-Y, Huang H-W, et al. Mutant P53 Attenuates Oxidative Phosphorylation and Facilitates Cancer Stemness Through Downregulating miR-200c-PCK2 Axis in Basal-Like Breast Cancer. *Mol Cancer Res* (2021) 19(11):1900–16. doi: 10.1158/1541-7786.MCR-21-0098
12. Parrales A, Iwakuma T. P53 as a Regulator of Lipid Metabolism in Cancer. *Int J Mol Sci* (2016) 17(12):2074. doi: 10.3390/ijms17122074
13. Sanchez-Macedo N, Feng J, Faubert B, Chang N, Elia A, Rushing E, et al. Depletion of the Novel P53-Target Gene Carnitine Palmitoyltransferase 1c Delays Tumor Growth in the Neurofibromatosis Type I Tumor Model. *Cell Death Differ* (2013) 20(4):659–68. doi: 10.1038/cdd.2012.168
14. Camarda R, Zhou AY, Kohnz RA, Balakrishnan S, Mahieu C, Anderton B, et al. Inhibition of Fatty Acid Oxidation as a Therapy for Myc-Overexpressing Triple-Negative Breast Cancer. *Nat Med* (2016) 22(4):427–32. doi: 10.1038/nm.4055
15. Zhang C, Yue C, Herrmann A, Song J, Egelston C, Wang T, et al. STAT3 Activation-Induced Fatty Acid Oxidation in Cd8+ T Effector Cells Is Critical for Obesity-Promoted Breast Tumor Growth. *Cell Metab* (2020) 31(1):148–61. e5. doi: 10.1016/j.cmet.2019.10.013
16. Park JH, Vithayathil S, Kumar S, Sung P-L, Dobrolecki LE, Putluri V, et al. Fatty Acid Oxidation-Driven Src Links Mitochondrial Energy Reprogramming and Oncogenic Properties in Triple-Negative Breast Cancer. *Cell Rep* (2016) 14(9):2154–65. doi: 10.1016/j.celrep.2016.02.004
17. Wright HJ, Hou J, Xu B, Cortez M, Potma EO, Tromberg BJ, et al. CDCP1 Drives Triple-Negative Breast Cancer Metastasis Through Reduction of Lipid-Droplet Abundance and Stimulation of Fatty Acid Oxidation. *Proc Natl Acad Sci* (2017) 114(32):E6556–65. doi: 10.1073/pnas.1703791114
18. van Weverwijk A, Koundouros N, Iravani M, Ashenden M, Gao Q, Poulogiannis G, et al. Metabolic Adaptability in Metastatic Breast Cancer by AKR1B10-Dependent Balancing of Glycolysis and Fatty Acid Oxidation. *Nat Commun* (2019) 10(1):1–13. doi: 10.1038/s41467-019-10592-4
19. Wang T, Fahrmann JF, Lee H, Li Y-J, Tripathi SC, Yue C, et al. JAK/STAT3-Regulated Fatty Acid B-Oxidation Is Critical for Breast Cancer Stem Cell Self-Renewal and Chemoresistance. *Cell Metab* (2018) 27(1):136–50.e5. doi: 10.1016/j.cmet.2017.11.001
20. Havas KM, Milchevskaya V, Radic K, Alladin A, Kafkia E, Garcia M, et al. Metabolic Shifts in Residual Breast Cancer Drive Tumor Recurrence. *J Clin Investig* (2017) 127(6):2091–105. doi: 10.1172/JCI89914
21. Chang C-J, Chao C-H, Xia W, Yang J-Y, Xiong Y, Li C-W, et al. P53 Regulates Epithelial–Mesenchymal Transition and Stem Cell Properties Through Modulating Mirnas. *Nat Cell Biol* (2011) 13(3):317–23. doi: 10.1038/ncb2173
22. Li B, Dewey CN. Rsem: Accurate Transcript Quantification From RNA-Seq Data With or Without a Reference Genome. *BMC Bioinf* (2011) 12(1):1–16. doi: 10.1186/1471-2105-12-323
23. Parker JS, Mullins M, Cheang MC, Leung S, Voduc D, Vickery T, et al. Supervised Risk Predictor of Breast Cancer Based on Intrinsic Subtypes. *J Clin Oncol* (2009) 27:1160–7. doi: 10.1200/JCO.2008.18.1370
24. Koboldt D, Fulton R, McLellan M, Schmidt H, Kalicki-Veizer J, McMichael J, et al. Comprehensive Molecular Portraits of Human Breast Tumours. *Nature* (2012) 490(7418):61–70. doi: 10.1038/nature11412
25. Li Q, Wang K. Intervar: Clinical Interpretation of Genetic Variants by the 2015 Acmg-Amp Guidelines. *Am J Hum Genet* (2017) 100(2):267–80. doi: 10.1016/j.ajhg.2017.01.004
26. Liu J, Lichtenberg T, Hoadley KA, Poisson LM, Lazar AJ, Cherniack AD, et al. An Integrated TCGA Pan-Cancer Clinical Data Resource to Drive High-Quality Survival Outcome Analytics. *Cell* (2018) 173(2):400–16. doi: 10.1016/j.cell.2018.02.052
27. Wang D, Green MF, McDonnell E, Hirschey MD. Oxygen Flux Analysis to Understand the Biological Function of Sirtuins. *Methods Mol Biol* (2013) 1077:241–58. doi: 10.1007/978-1-62703-637-5_16
28. Alvarado-Ortiz E, de la Cruz-López K, Becerril-Rico J, Sarabia-Sánchez M, Ortiz-Sánchez E, García-Carrancá A. Mutant P53 Gain-Of-Function: Role in Cancer Development, Progression, and Therapeutic Approaches. *Front Cell Dev Biol* (2020) 8:607670–0. doi: 10.3389/fcell.2020.607670
29. Sierra AY, Gratacós E, Carrasco P, Clotet J, Ureña J, Serra D, et al. CPT1C Is Localized in Endoplasmic Reticulum of Neurons and Has Carnitine Palmitoyltransferase Activity. *J Biol Chem* (2008) 283(11):6878–85. doi: 10.1074/jbc.M707965200
30. Zaugg K, Yao Y, Reilly PT, Kannan K, Kiarash R, Mason J, et al. Carnitine Palmitoyltransferase 1c Promotes Cell Survival and Tumor Growth Under Conditions of Metabolic Stress. *Genes Dev* (2011) 25(10):1041–51. doi: 10.1101/gad.1987211
31. Wolfgang MJ, Kurama T, Dai Y, Suwa A, Asaumi M, Matsumoto S-I, et al. The Brain-Specific Carnitine Palmitoyltransferase-1c Regulates Energy Homeostasis. *Proc Natl Acad Sci* (2006) 103(19):7282–7. doi: 10.1073/pnas.0602205103
32. Ma Y, Temkin SM, Hawkridge AM, Guo C, Wang W, Wang X-Y, et al. Fatty Acid Oxidation: An Emerging Facet of Metabolic Transformation in Cancer. *Cancer Lett* (2018) 435:92–100. doi: 10.1016/j.canlet.2018.08.006
33. Carracedo A, Cantley LC, Pandolfi PP. Cancer Metabolism: Fatty Acid Oxidation in the Limelight. *Nat Rev Cancer* (2013) 13(4):227–32. doi: 10.1038/nrc3483
34. Wang Y-N, Zeng Z-L, Lu J, Wang Y, Liu Z-X, He M-M, et al. CPT1A-Mediated Fatty Acid Oxidation Promotes Colorectal Cancer Cell Metastasis by Inhibiting Anoikis. *Oncogene* (2018) 37(46):6025–40. doi: 10.1038/s41388-018-0384-z
35. Fischer M. Conservation and Divergence of the P53 Gene Regulatory Network Between Mice and Humans. *Oncogene* (2019) 38(21):4095–109. doi: 10.1038/s41388-019-0706-9
36. Boutelle AM, Attardi LD. P53 and Tumor Suppression: It Takes a Network. *Trends Cell Biol* (2021) 31(4):298–310. doi: 10.1016/j.tcb.2020.12.011
37. Lahalle A, Lacroix M, De Blasio C, Cissé MY, Linares LK, Le Cam L. The P53 Pathway and Metabolism: The Tree That Hides the Forest. *Cancers* (2021) 13 (1):133. doi: 10.3390/cancers13010133
38. Joerger AC, Fersht AR. The P53 Pathway: Origins, Inactivation in Cancer, and Emerging Therapeutic Approaches. *Annu Rev Biochem* (2016) 85:375–404. doi: 10.1146/annurev-biochem-060815-014710
39. Muller B, Lewis N, Adeniyi T, Leese HJ, Brison DR, Sturmey RG. Application of Extracellular Flux Analysis for Determining Mitochondrial Function in Mammalian Oocytes and Early Embryos. *Sci Rep* (2019) 9(1):1–14. doi: 10.1038/s41598-019-53066-9
40. Divakaruni AS, Hsieh WY, Minarrieta L, Duong TN, Kim KK, Desousa BR, et al. Etomoxir Inhibits Macrophage Polarization by Disrupting CoA Homeostasis. *Cell Metab* (2018) 28(3):490–503.e7. doi: 10.1016/j.cmet.2018.06.001
41. Dranka BP, Benavides GA, Diers AR, Giordano S, Zelickson BR, Reily C, et al. Assessing Bioenergetic Function in Response to Oxidative Stress by Metabolic

Profiling. *Free Radic Biol Med* (2011) 51(9):1621–35. doi: 10.1016/j.freeradbiomed.2011.08.005
42. Hill BG, Benavides GA, Lancaster JR, Ballinger S, Dell'Italia L, Zhang J, et al. Integration of Cellular Bioenergetics With Mitochondrial Quality Control and Autophagy. *Biol Chem* (2012) 393(12):1485–512. doi: 10.1515/hsz-2012-0198
43. Abe Y, Sakairi T, Kajiyama H, Shrivastav S, Beeson C, Kopp JB. Bioenergetic Characterization of Mouse Podocytes. *Am J Physiol Cell Physiol* (2010) 299(2): C464–C76. doi: 10.1152/ajpcell.00563.2009
44. Tran TQ, Lowman XH, Reid MA, Mendez-Dorantes C, Pan M, Yang Y, et al. Tumor-Associated Mutant P53 Promotes Cancer Cell Survival Upon Glutamine Deprivation Through P21 Induction. *Oncogene* (2017) 36 (14):1991–2001. doi: 10.1038/onc.2016.360
45. Hayes JD, Dinkova-Kostova AT, Tew KD. Oxidative Stress in Cancer. *Cancer Cell* (2020) 38(2):167–97. doi: 10.1016/j.ccell.2020.06.001
46. Bullock AN, Fersht AR. Rescuing the Function of Mutant P53. *Nat Rev Cancer* (2001) 1(1):68–76. doi: 10.1038/35094077
47. Fidler IJ. The Pathogenesis of Cancer Metastasis: The 'Seed and Soil' Hypothesis Revisited. *Nat Rev Cancer* (2003) 3(6):453–8. doi: 10.1038/nrc1098
48. Frisch SM, Francis H. Disruption of Epithelial Cell-Matrix Interactions Induces Apoptosis. *J Cell Biol* (1994) 124(4):619–26. doi: 10.1083/jcb.124.4.619
49. Schafer ZT, Grassian AR, Song L, Jiang Z, Gerhart-Hines Z, Irie HY, et al. Antioxidant and Oncogene Rescue of Metabolic Defects Caused by Loss of Matrix Attachment. *Nature* (2009) 461(7260):109–13. doi: 10.1038/nature08268
50. Carracedo A, Weiss D, Leliaert AK, Bhasin M, De Boer VC, Laurent G, et al. A Metabolic Prosurvival Role for Pml in Breast Cancer. *J Clin Investig* (2012) 122(9):3088–100. doi: 10.1172/JCI62129
51. Reilly PT, Mak TW. Molecular Pathways: Tumor Cells Co-Opt the Brain-Specific Metabolism Gene CPT1C to Promote Survival. *Clin Cancer Res* (2012) 18(21):5850–5. doi: 10.1158/1078-0432.CCR-11-3281
52. Wang Y, Chen Y, Guan L, Zhang H, Huang Y, Johnson CH, et al. Carnitine Palmitoyltransferase 1c Regulates Cancer Cell Senescence Through Mitochondria-Associated Metabolic Reprograming. *Cell Death Differ* (2018) 25(4):735–48. doi: 10.1038/s41418-017-0013-3
53. Pompura SL, Wagner A, Kitz A, LaPerche J, Yosef N, Dominguez-Villar M, et al. Oleic Acid Restores Suppressive Defects in Tissue-Resident FOXP3 Tregs From Patients With Multiple Sclerosis. *J Clin Investig* (2021) 131(2), 1–15. doi: 10.1172/JCI138519
54. Wu D, Sanin DE, Everts B, Chen Q, Qiu J, Buck MD, et al. Type 1 Interferons Induce Changes in Core Metabolism That Are Critical for Immune Function. *Immunity* (2016) 44(6):1325–36. doi: 10.1016/j.immuni.2016.06.006
55. Choi H-J, Jhe Y-L, Kim J, Lim JY, Lee JE, Shin M-K, et al. FOXM1-Dependent and Fatty Acid Oxidation-Mediated ROS Modulation Is a Cell-Intrinsic Drug Resistance Mechanism in Cancer Stem-Like Cells. *Redox Biol* (2020) 36:101589. doi: 10.1016/j.redox.2020.101589
56. Ju H-Q, Lin J-F, Tian T, Xie D, Xu R-H. NADPH Homeostasis in Cancer: Functions, Mechanisms and Therapeutic Implications. *Signal Transduct Target Ther* (2020) 5(1):1–12. doi: 10.1038/s41392-020-00326-0
57. Pike LS, Smift AL, Croteau NJ, Ferrick DA, Wu M. Inhibition of Fatty Acid Oxidation by Etomoxir Impairs NADPH Production and Increases Reactive Oxygen Species Resulting in ATP Depletion and Cell Death in Human Glioblastoma Cells. *Biochim Biophys Acta Bioenerg* (2011) 1807(6):726–34. doi: 10.1016/j.bbabio.2010.10.022
58. Du Q, Tan Z, Shi F, Tang M, Xie L, Zhao L, et al. PGC-1α/CEBPB/CPT1A Axis Promotes Radiation Resistance of Nasopharyngeal Carcinoma Through Activating Fatty Acid Oxidation. *Cancer Sci* (2019) 110(6):2050–62. doi: 10.1111/cas.14011
59. Wang Y, Lu J-H, Wang F, Wang Y-N, He M-M, Wu Q-N, et al. Inhibition of Fatty Acid Catabolism Augments the Efficacy of Oxaliplatin-Based Chemotherapy in Gastrointestinal Cancers. *Cancer Lett* (2020) 473:74–89. doi: 10.1016/j.canlet.2019.12.036
60. Baldelli S, Ciccarone F, Limongi D, Checconi P, Palamara AT, Ciriolo MR. Glutathione and Nitric Oxide: Key Team Players in Use and Disuse of Skeletal Muscle. *Nutrients* (2019) 11(10):2318. doi: 10.3390/nu11102318
61. Aquilano K, Baldelli S, Ciriolo MR. Glutathione: New Roles in Redox Signaling for an Old Antioxidant. *Front Pharmacol* (2014) 5:196. doi: 10.3389/fphar.2014.00196
62. Kalyanaraman B, Darley-Usmar V, Davies KJ, Dennery PA, Forman HJ, Grisham MB, et al. Measuring Reactive Oxygen and Nitrogen Species With Fluorescent Probes: Challenges and Limitations. *Free Radic Biol Med* (2012) 52(1):1–6. doi: 10.1016/j.freeradbiomed.2011.09.030
63. Eruslanov E, Kusmartsev S. Identification of ROS Using Oxidized DCFDA and Flow-Cytometry. *Advanced Protoc Oxid Stress Ii* (2010), 594, 57–72. doi: 10.1007/978-1-60761-411-1_4
64. McDonnell E, Crown SB, Fox DB, Kitir B, Ilkayeva OR, Olsen CA, et al. Lipids Reprogram Metabolism to Become a Major Carbon Source for Histone Acetylation. *Cell Rep* (2016) 17(6):1463–72. doi: 10.1016/j.celrep.2016.10.012
65. Pardridge W. Drug Targeting, Drug Discovery, and Brain Drug Development. *Brain Drug Target: Future Brain Drug Dev* (2001) 1:1–12. doi: 10.1017/CBO9780511549571.002

Conflict of Interest: The authors declare that the research was conducted in the absence of any commercial or financial relationships that could be construed as a potential conflict of interest.

Publisher's Note: All claims expressed in this article are solely those of the authors and do not necessarily represent those of their affiliated organizations, or those of the publisher, the editors and the reviewers. Any product that may be evaluated in this article, or claim that may be made by its manufacturer, is not guaranteed or endorsed by the publisher.

frontiers | Frontiers in Oncology

TYPE Original Research
PUBLISHED 01 August 2022
DOI 10.3389/fonc.2022.928373

OPEN ACCESS

EDITED BY
Thibaut Barnoud,
Medical University of South Carolina, United States

REVIEWED BY
Xiangming Mao,
Southern Medical University, China
Linchong Sun,
Guangdong Academy of Medical Sciences, China

*CORRESPONDENCE
Yong Wang
dryongwangfmmu@163.com
Wenqiang Yu
wenqiangyu@fudan.edu.cn
Jianlin Yuan
jianliny@fmmu.edu.cn

†These authors have contributed equally to this work and share first authorship

SPECIALTY SECTION
This article was submitted to Cancer Metabolism, a section of the journal Frontiers in Oncology

RECEIVED 25 April 2022
ACCEPTED 30 June 2022
PUBLISHED 01 August 2022

CITATION
Ju D, Liang Y, Hou G, Zheng W, Zhang G, Dun X, Wei D, Yan F, Zhang L, Lai D, Yuan J, Zheng Y, Wang F, Meng P, Wang Y, Yu W and Yuan J (2022) *FBP1*/miR-24-1/enhancer axis activation blocks renal cell carcinoma progression *via* Warburg effect.
Front. Oncol. 12:928373.
doi: 10.3389/fonc.2022.928373

FBP1/miR-24-1/enhancer axis activation blocks renal cell carcinoma progression *via* Warburg effect

Dongen Ju[1†], Ying Liang[2,3,4†], Guangdong Hou[1†], Wanxiang Zheng[1†], Geng Zhang[1], Xinlong Dun[1], Di Wei[1], Fei Yan[1], Lei Zhang[1], Dong Lai[1], Jiarui Yuan[5], Yu Zheng[1,6], Fuli Wang[1], Ping Meng[1], Yong Wang[7*], Wenqiang Yu[2,3*] and Jianlin Yuan[1*]

[1]Department of Urology, Xijing Hospital, Fourth Military Medical University, Xi'an, China, [2]Laboratory of RNA Epigenetics, Institutes of Biomedical Sciences, Shanghai Medical College, Fudan University, Shanghai, China, [3]Shanghai Public Health Clinical Center and Department of General Surgery, Huashan Hospital, Cancer Metastasis Institute, Fudan University, Shanghai, China, [4]Department of Pharmacy, Precision Pharmacy and Drug Development Center, Tangdu Hospital, Fourth Military Medical University, Xi'an, China, [5]Clinical Medicine Department, St. George's University School of Medicine, Saint George, Grenada, [6]Medical Innovation Center, Fourth Military Medical Univeristy, Xi'an, China, [7]Department of Urology, Tangdu Hospital, Fourth Military Medical University, Xi'an, China

Warburg effect is a pivotal hallmark of cancers and appears prevalently in renal cell carcinoma (RCC). FBP1 plays a negative role in Warburg effect as a rate-limiting enzyme in gluconeogenesis, yet its mechanism in RCC remains to be further characterized. Herein, we revealed that *FBP1* was downregulated in RCC tissue samples and was related to the poor survival rate of RCC. Strikingly, miR-24-1 whose DNA locus is overlapped with enhancer region chr9:95084940-95087024 was closely linked with the depletion of *FBP1* in RCC. Of note, miRNAs like miR-24-1 whose DNA loci are enriched with H3K27ac and H3K4me1 modifications are belonging to nuclear activating miRNAs (NamiRNAs), which surprisingly upregulate target genes in RCC through enhancer beyond the conventional role of repressing target gene expression. Moreover, miR-24-1 reactivated the expression of *FBP1* to suppress Warburg effect in RCC cells, and subsequently inhibited proliferation and metastasis of RCC cells. In mechanism, the activating role of miR-24-1 was dependent on enhancer integrity by dual luciferase reporter assay and CRISPR/Cas9 system. Ultimately, animal assay *in vivo* validated the suppressive function of *FBP1* on 786-O and ACHN cells. Collectively, the current study highlighted that activation of *FBP1* by enhancer-overlapped miR-24-1 is capable of contributing to Warburg effect repression through which RCC progression is robustly blocked, providing an alternative mechanism for RCC development and as well implying a potential clue for RCC treatment strategy.

KEYWORDS

***FBP1*, renal cell carcinoma, enhancer, Warburg Effect, miR-24-1**

Introduction

Renal cell carcinoma (RCC) is the most common type of kidney cancer with increasing incidence and mortality rates (1). The main subtypes of RCC include clear cell renal cell carcinoma (ccRCC), papillary renal cell carcinoma (pRCC) and chromophobe RCC (ChRCC), which account for 65–70%, 15–20%, and 5–7% of total RCC cases, respectively (2). It was highlighted that inactivation of the *VHL* tumor suppressor gene caused by biallelic mutation or promoter hypermethylation is involved in the majority of RCCs with characteristic metabolic alterations (3, 4). However, kidney-specific *VHL* deletion in mice is not sufficient to induce RCC-specific metabolic changes or tumorigenesis, indicating that alternative mechanisms are concealed (5).

Altered energy metabolism is widely recognized as a hallmark of cancer and stretches beyond adaptations to support the increased energy requirements of unrestrictedly growing and dividing cancer cells (1, 6). Typically, cancer cells take up increased amounts of glucose to produce elevated levels of the glycolytic metabolite pyruvate compared to normal cells, which is preferentially converted to lactate by lactate dehydrogenase (LDH) even in the presence of oxygen, yielding a large amount of ATP in a short-circuit pattern (7). This type of metabolism is taken as Warburg effect, characterized by drastically increased glycolytic rates and lactate production (1, 8). Of note, FBP1 plays a negative role in Warburg effect by catalyzing the hydrolysis process of fructose 1,6-bisphosphate to fructose 6-phosphate (9, 10). Given that *FBP1* is downregulated in RCC as a tumor suppressor and that its depletion enhances HIF activity to suppress kidney cancer (11), we want to investigate the underlying molecular mechanism of Warburg effect in RCC through *FBP1*.

Notably, accumulating evidence indicates that dysfunction of *FBP1* can be regulated by ectopic expression of miRNAs (9, 10, 12). To our knowledge, miRNAs post transcriptionally degrade or repress target genes *via* binding to the 3' UTR of their mRNAs, yet relatively little is known about their regulatory role in transcriptional activation. In our previous work (13), we revealed a type of miRNA whose DNA loci are overlapped with enhancer region can activate the expression of target genes through the corresponding enhancers (named NamiRNA), in particular, *FBP1* was activated by the enhancer-overlapping NamiRNA-24-1 in a manner dependent on enhancer activity in HEK293T cells. Thus, we proposed a NamiRNA-enhancer-gene activation network to better understand the miRNA activation phenomenon (14–16). Other findings also support the critical crosstalk between enhancers and their overlapping miRNAs, highlighting important tissue-specific cancer biomarkers (17, 18). Moreover, low expression of miRNAs is another feature of cancer cell. It is reported miR-24-1 can function as a tumor-suppressive miRNA in cancer development (19, 20). Therefore, we wonder whether NamiRNA-24-1 can play activating role on *FBP1* during RCC development.

Herein, we detected by bioinformatic analysis that both *FBP1* and miR-24-1 were downregulated in RCC tissue samples from the TCGA database and further verified their low expression levels in RCC tissue samples by qPCR. Furthermore, through cell-based biological assays, we clarified that overexpression of miR-24-1 can reactivate the expression level of *FBP1* in the ccRCC cell line 786-O and pRCC cell line ACHN, and thus inhibit RCC cell proliferation and migration. Moreover, we confirmed by a dual luciferase reporter assay that the enhancer region containing the miR-24-1 DNA locus can increase reporter gene activity and that its own activity can be enhanced by miR-24-1. Furthermore, we demonstrated that reactivation of *FBP1* by miR-24-1 can inhibit aerobic glycolysis in 786-O and ACHN cells and downregulate the expression of metabolism-related genes involved in the Warburg effect. Finally, overexpression of miR-24-1 suppressed tumor growth of RCC in an animal xenograft model, yet enhancer depletion led to loss of function of miR-24-1, suggesting that reactivation of *FBP1* by miR-24-1 relies on enhancer integrity and can provide a potential treatment strategy for RCC.

Materials and methods

Cell culture, and antibodies

The human kidney cancer cell lines 786-O and ACHN and the human embryonic kidney cell line HEK293T were routinely tested to confirm that they were mycoplasma-free. Cell lines were maintained in DMEM (HyClone) at 37°C with 5% CO2. Cultures were coated with 10% fetal bovine serum (FBS, HyClone) and 1% penicillin/streptomycin (HyClone). All cells used were expanded less than 6 months after resuscitation. The primary antibodies were anti-H3K27ac (ab177178, Abcam), anti-H3K4me1 (A2355, Abclonal), mouse monoclonal anti-FBP1 (DF7F25, Affinity) and anti-beta-actin (AF7018, Affinity) antibodies; secondary antibodies against mouse and rabbit IgG were purchased from Santa Cruz Biotechnology.

Plasmids and transfection

The expression plasmids of miR-24-1 were built by inserting the fragments of pre-miR-24-1 (68 bp) and pri-miR-24-1 (708 bp) amplified from genomic DNA in HEK293T cells into the multiple cloning sites in the pSUPER-retro-GFP/Neo and pCDH-CMV-MCS-EF1-copGFP vectors. The miR-24-1 mutant plasmids were generated by using a One Step Cloning Kit (C114, Vazyme). The enhancer region (chr9:95084940-95087024) containing the miR-24-1 DNA locus was cloned into the luciferase reporter gene vector pGL3-Basic (Promega)

to generate the reporter construct pGL3-enhancer. Target cells with strong GFP positivity were screened by flow cytometry (BD Biosciences). CRISPR/Cas9 vectors containing both GFP and puromycin resistance genes were obtained from Sangon. Lentivirus was produced by cotransfecting 293T cells with psPAX2, pMD2G and the pCDH-copGFP expression vector and harvested by filtration through a 0.45 μm filter (Millipore) after 72 hours of incubation. Stably transfected cells with strong GFP fluorescence were selected by flow cytometry (BD).

Tissue samples

Renal carcinoma and adjacent normal tissue sections were obtained with informed consent under the approval by the Institutional Review Board of The Fourth Military Medical University. All the patients gave informed consent. Between May 2019 and October 2020, 42 patients pathologically diagnosed with RCC at Xijing Hospital were selected. Tissue sections were collected, immediately placed and stored in liquid nitrogen.

RNA extraction and qRT-PCR

Total RNA extraction was gained by TRIzol reagent (Invitrogen, 15,596,018), purified, eluted in RNase-free water, and subsequently reverse transcribed into cDNA with a PrimeScript RT Reagent Kit with gDNA Eraser (Takara) under the instructions. A SYBR Green qRT-PCR master mix kit (TIANGEN) was utilized to perform qPCR according to the manufacturer's procedures. All primer sequences are listed in Table 1. Ct values obtained from qPCR were used to calculate the relative expression level of all reported genes *via* the $2^{-\Delta\Delta Ct}$ method.

Western blotting

Total protein from cells and tissues was extracted by using radioimmunoprecipitation assay (RIPA) buffer (TIANGEN). Protein concentrations were detected by a BCA Protein Assay Kit (TIANGEN). Protein lysates were loaded on a 4-12% gradient sodium dodecyl sulfate (SDS)-polyacrylamide gel (Life Technologies) and were then transferred onto polyvinylidene difluoride (PVDF) membranes (Millipore, Billerica). The immunoblots were probed with primary antibodies against FBP1 (1/2,000 dilution, Affinity) and beta-actin in 5% milk and were then reacted with horseradish peroxide (HRP)-conjugated donkey anti-rabbit or anti-mouse secondary antibodies (1/2,000 dilution; Amersham). Then immunoreactions were detected with an enhanced chemiluminescence (ECL) system.

CRISPR/Cas9 system

CRISPR/Cas9 vectors (Sangon) targeting the enhancer region containing the miR-24-1 DNA locus of FBP1 were transfected into 786-O and ACHN cells to delete the targeted fragment. Dual guide RNAs (5'-TGTCGATTGGACCCGCCCTC-3' and 5'-ACACACTGGCTCAGTTCAGC-3') were designed from the Zhang laboratory's public instructions (https://zlab.bio/guide-design-resources). The transfected cells were subjected to PCR to obtain the potentially deleted fragments. Then, the PCR products were sequenced by Sanger sequencing to determine the targeting efficiency of the constructed plasmids. Cells with effective deletion were separated through flow cytometry into 6 cm dishes and cultured in 5% CO2 at 37°C.

ChIP and ChIP-qPCR

The stable cells were fixed with 1% formaldehyde for 15 min at room temperature. Subsequently, the cells were coated with 0.125 M glycine solution to quench the formaldehyde crosslinking reaction for 15 min. Cold PBS was used to wash the cell for twice. The cells were transferred into 15mL Corning tubes and resuspended in lysis buffer plus protease inhibitor cocktail (Roche) to obtain nuclear extracts. Nuclear lysis buffer was added to the extracted products for sonication. After sonication, the acceptable DNA fragments were incubated with specific antibodies against H3K4me1 and H3K27ac along with Protein A Dynabeads (Invitrogen) at 4°C overnight. Immunoprecipitated DNA fragments were washed sequentially with high- and low-salt wash buffers to wash the beads. After decrosslinking at 65°C for 6 hours, DNA fragments were purified with a DNA purification kit (Qiagen) to obtain ChIP template DNA. qPCR reactions were performed in a LightCycler 96 System (Roche). The sequences of the chromatin region-specific primers are listed as in Table 1.

Dual luciferase reporter assays

The constructed pGL3-enhancer or control plasmids were cotransfected with the miR-24-1 expression vector and Renilla luciferase reporter vector pRL-SV40 into HEK293T cells. Then, the cells were harvested and lysed in lysis buffer (Promega) after transfection for 48 hours and were concentrated to obtain the supernatants. The relative luciferase units (RLU) of the supernatants were determined by using a Dual Luciferase Reporter Assay System (Promega). Renilla luciferase was applied for normalization. The ratio of firefly/Renilla luciferase units was calculated to indicate the relative enhancer activity. All luciferase assays were repeated in triplicate.

TABLE 1 The primer sequences used for plasmids construction, RT-PCR and ChIP-qPCR assays.

Primer Names	Sequence (5'→3')
pri-miR-24-1-F	GAAGATTCTAGAGCTAGCGAATTCGTCTGTCCACAGAAACATGCAC
pri-miR-24-1-R	GCAGATCCTTCGCGGCCGCGGATCCACACGCACCCACTCTAAC
pre-miR-24-1-F	ATCCGAGCTCGGTACCAAGCTTCTCCGGTGCCTACTGAGCT
pre-miR-24-1-R	AGATCGATCTCTCGAGGTCGACCTCCTGTTCCTGCTGAACTG
miR-24-1-3p-F	CGTCAGCTGTCCGAGTAGAGGtGGCTCAGTTCAGCA
miR-24-1-3p-R	TGTCAGGCAACCGTATTCACCcTGTTCC
FBP1-F	ACCCTGCCGTCACTGAGTA
FBP1-R	GCCCCATAAGGAGCTGAAT
GAPDH-F	ACCGTCAAGGCTGAGAAC
GAPDH-R	GCCTTCTCCATGGTGGTGA
GLUT1-F	GGTTGTGCCATACTCATGACC
GLUT1-R	CAGATAGGACATCCAGGGTAGC
LDHA-F	CCGTTACCTAATGGGGGAAA
LDHA-R	GCAACATTCATTCCACTCCA
miR-24-1-ChIP-F	CCGGTGCCTACTGAGCTGAT
miR-24-1-ChIP-R	TCGGGCACTTACAGACACGA

Glucose consumption and lactate production assays

Glucose (2 g) purchased from Sangon (A501991) was dissolved in 20 mL of glucose-free medium and prepared into a glucose mother solution. One milliliter of the glucose mother solution was added to 49 mL of medium to prepare 2000 mg/L glucose medium. miR-24-1 overexpressing and control 786 O and ACHN cells were seeded in 6-well plates (1×10^5 cells/well) and cultured in DMEM. After 24 hours of culture, Glucose consumption and lactate production were measured with lactate assay kit and glucose test kit (Nanjing Jiancheng Bioengineering Institute) with the manufacturer's protocol.

Seahorse glycolysis stress test

miR-24-1 overexpressing and control 786 O and ACHN cells (1.5×10^4 cells/well) were seeded into XFe24 cell culture microplates (Seahorse Bioscience) in DMEM. The cells were cultured overnight for 12 hours and were then cultured for 2 hours in the absence of glucose before Extracellular acidification rates (ECARs) were quantified using an XFe24 instrument (Seahorse Bioscience) under the protocol. After the Seahorse experiment, the BCA protein quantitation kit was used to normalize the data.

Cell proliferation, colony formation, and transwell assays

Cells were placed in 96-well plates with 5,000 cells per well in DMEM and assessed daily (24, 48, 72, and 96 hours) with a Cell Counting Kit-8 (CCK-8, Dojindo). The proliferation ability was calculated by measuring the optical density (OD) (490 nm). Besides, for the colony formation assay, a total of 500 cells were plated in each well of 6-well plates. After incubation for 14 days, the formed colonies were stained with 0.25% crystal violet, imaged, and counted, and the number of colonies was reported. For the transwell migration assay, 1×10^4 cells were transferred into each plastic insert of 24-well plates. In this two-chamber system, serum-free DMEM was added to the upper chamber, and 20% FBS-DMEM was added to the lower chamber. After 24 hours, the cells that traversed the membrane into the lower chamber were fixed with 100% methanol, stained with 0.1% crystal violet solution, imaged, and counted under a microscope. All assays were repeated in triplicate.

Animals and *in vivo* experiments

A total of 18 male nude mice in six-week-old age were purchased from the Experimental Animal Center of Fourth Military Medical University and divided randomly into three groups. All the nude mice were maintained in the Experimental Animal Center of Fourth Military Medical University under the appropriate conditions: Temperature: 22 ± 1°C; Humidity: 50 ± 10%. miR-24-1 overexpression, miR-24-1 overexpression with enhancer deletion and control ACHN cells were injected into 6 male nude mice in the left hind limb (4×10^6 cells per mouse), respectively. The tumor volume was measured every three days after 2 weeks of feeding. After another 4 weeks, tumor tissues were harvested for further analyses. The pathology of the tissues was confirmed by hematoxylin-eosin (HE) staining.

HE staining, tissue immunohistochemistry and immunofluorescence

Human and mouse tissues were soaked in 10% neutral formalin for 72 hours. Then, paraffin embedding was carried out according to the routine procedure, and HE staining analysis was carried out after the samples were dehydrated.

Tissue sections were dewaxed and washed with distilled water. Tissue sections were placed in citric acid antigen repair buffer (pH=6.0) for antigen repair in a microwave. The sections were then washed with PBS for three times after natural cooling. Then, 3% hydrogen peroxide solution was added to block endogenous peroxidase activity in the dark at room temperature for 25 min. Next, 3% bovine serum albumin (BSA) was added to cover the tissues to block nonspecific binding for 30 min. After three washes in PBS, the primary antibody was added to incubate with the tissues overnight at 4°C. Next, the slides were incubated with the secondary antibody for 50 min. For immunohistochemistry, the slides were processed with DAB solution (Wuhan Servicebio Technology) and hematoxylin solution. For immunofluorescence, the slides were processed with DAPI solution (Wuhan Servicebio Technology) and a spontaneous fluorescence quenching reagent. Finally, the cells were photographed with a fluorescence microscope (Olympus BX53).

The analysis of high throughput sequencing of human RCC samples from TCGA dataset

Tissue samples and their paired noncancerous matched tissues in current study for mRNA-seq were acquired from TCGA database. Differently expressed genes (DEGs) were identified with the R package DESeq2. Log2 (Fold change) > 1 and $p < 0.05$.

Available DNA methylation data (450k) of TSGs for RCC were downloaded from TCGA database. The difference between the mean methylation levels of paired samples >5% was considered to be of significance followed by Wilcoxon Rank Sum Test.

Statistical analysis

All results are presented as the mean standard deviation (s.d.) of triplicate experiments unless otherwise noted. Data analysis was performed with a two-tailed Student's t-test. **** means $p < 0.0001$, *** means $p < 0.001$, ** means $p < 0.01$ and * means $p < 0.05$. $p < 0.05$ was considered significant. GraphPad Prism (Version 7.0, GraphPad Software, Inc.) was utilized to perform statistical analysis.

Results

FBP1 is downregulated in RCC and related to poor prognosis

To investigate the expression patterns of *FBP1* in kidney cancer, we analyzed the mRNA-seq datasets of 611 RCC and normal renal control samples from the TCGA database. As expected, *FBP1* was downregulated in RCC, as shown in Figure 1A (blue panel, $p < 0.05$, log2FoldChange > 1). Interestingly, we discovered that genes encoding key factors in glucose metabolism involved in the Warburg effect, such as *HK2*, *HK3* and *LDHA*, were significantly upregulated in RCC compared to adjacent normal tissues (red panel, Figure 1A). This result is consistent with their positive role on Warburg effect in other cancer types (21–23). Next, KEGG pathway and gene oncology (GO) profiling for the downregulated genes in RCC revealed they are mainly related to metabolic pathways and gluconeogenesis in Figures 1B, C, respectively. It is noteworthy that 12 gluconeogenesis-associated genes like *PCK1* and *PCK2* are also lowly expressed other than *FBP1* in RCC as seen in Figure 1C (right panel), further confirming the expression of gluconeogenesis-associated genes is aberrant in RCC.

Then, to determine the mRNA expression level of *FBP1* in tissue samples, 42 paired RCC and matched adjacent tissues were utilized for qPCR detection. Consistent with our expectation, *FBP1* was obviously downregulated in RCC compared to normal tissues, as shown in Figures 1D, E. In addition, we examined the differences in protein levels between 3 paired RCC and adjacent normal tissues that were randomly selected from the 42 paired tissue samples. The FBP1 protein was expressed at significantly lower levels in the RCC tissues than in the adjacent normal ones (Figure 1F). Furthermore, immunohistochemical staining assays revealed that FBP1 was obviously expressed at lower levels in RCC tissues than in normal tissues (Figure 1G). Since *FBP1* was confirmed to be downregulated in RCC, we assume that it may act as a suppressor of RCC. Therefore, Kaplan–Meier plots of overall survival were analyzed to confirm the effects of *FBP1* expression on patient survival outcomes (Figure 1H). In the TCGA dataset, patients with RCC with lower *FBP1* expression exhibited worse survival outcomes (Figure 1G), suggesting that *FBP1* indeed exhibits a tumor-suppressive effect.

Tumor suppressor gene FBP1 is upregulated by miR-24-1 in RCC cells

Epigenetic regulations like DNA hypermethylation exert significant roles on inactivation of tumor suppressor genes without altering DNA sequence (24). Loss of function of tumor suppressor genes may eventually contribute to

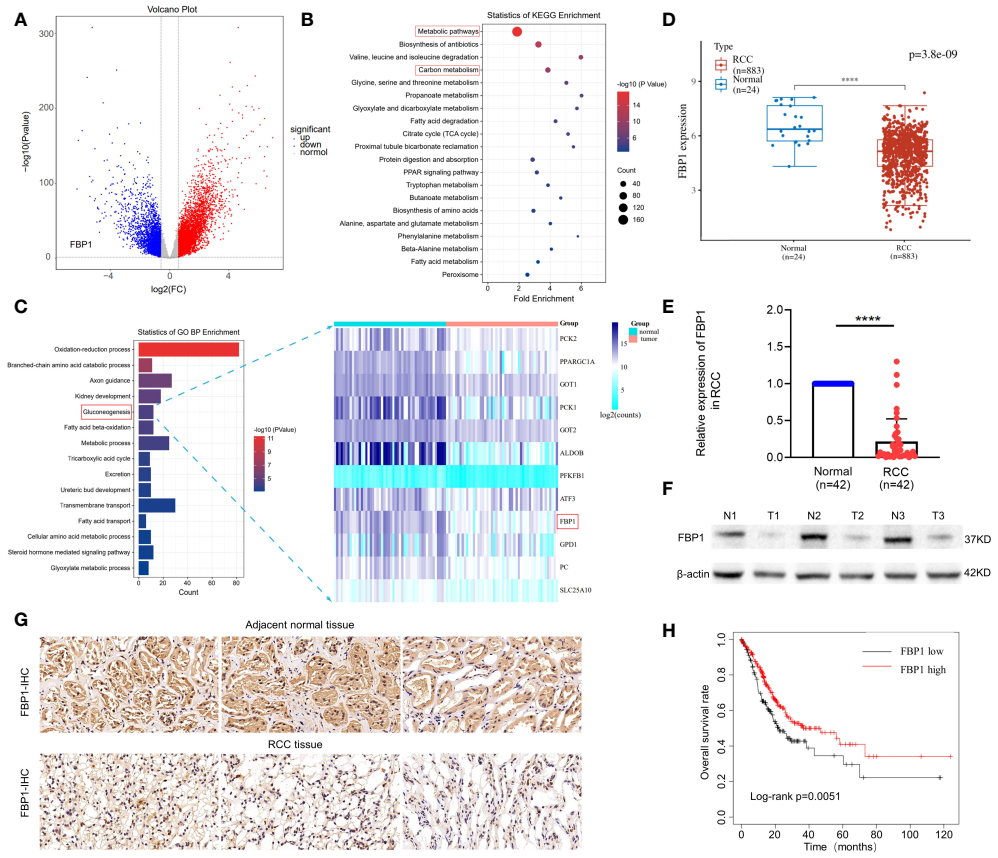

FIGURE 1
FBP1 is reduced in RCC and related to poor survival outcome. **(A)** Volcano Plot of differentially expressed mRNAs associated with glucose metabolism of Warburg effect in RCC and adjacent normal tissues. Blue represents downregulated genes, and red represents upregulated genes. $p < 0.05$. **(B, C)** KEGG pathway and gene oncology (GO) profiling for the downregulated genes in RCC. **(D)** The mRNA expression levels of FBP1 in RCC and adjacent normal renal tissues from TCGA database by bioinformatic analysis. **(E)** The mRNA expression levels of FBP1 in RCC and adjacent normal renal tissues detected by qPCR. **(F)** The protein level of FBP1 in 3 randomly selected paired RCC and adjacent normal renal tissues by western blot. b-actin was used as input control. **(G)** Representative pictures of immunohistochemical (IHC) staining of 3 randomly selected paired RCC tissue and adjacent normal renal tissues. **(H)** Kaplan–Meier plots of overall survival in RCC patients with low expression of *FBP1* (n=166) compared to high expression of FBP1 (n=178) stratified by the expression levels of *FBP1*. The cutoff was confirmed as the threshold with the best performance. Log-rank test p value is shown. Results are shown as mean ± S.D., ****$p < 0.0001$.

tumorigenesis (25). Therefore, we firstly carry on DNA methylation profiling for 491 downregulated tumor suppressor genes in kidney renal clear cell carcinoma (KIRC) from TSGene database (https://bioinfo.uth.edu/TSGene/) (26). Available DNA methylation data with KIRC were downloaded from TCGA database. Interestingly, the results showed 61% tumor suppressor genes exhibited hypomethylation but with no methylation difference as seen in left panel of Figure 2A (red box). Particularly, *FBP1* showed DNA hypermethylation status in promoter regions in both KIRC and normal ones, which is even relatively higher in normal than that in KIRC (right panel of Figure 2A), implying that *FBP1* depletion in renal cell carcinoma is not caused by DNA hypermethylation in promoter.

Based on our previous work, NamiRNA plays positive regulatory function on tumor suppressor genes through enhancer (16) and in particular, miR-24-1 can activate its neighboring gene *FBP1* in 293T cells (13). So, we put our attention to the regulatory function of miR-24-1 on *FBP1* to investigate its potential role in RCC. Subsequently, we examined the mRNA expression level of miR-24-1 in 873 RCC patients and 25 normal controls from TCGA by bioinformatic analysis. Interestingly, miR-24-1 expressed in lower level in RCC tissues than that in adjacent normal tissues (Figure 2B). Next, we detected the expression of miR-24-1 by qPCR. The results confirmed that miR-24-1 was significantly downregulated in the 42 RCC tissues compared to the adjacent normal tissues (Figure 2C). In addition, Kaplan–Meier analysis of overall survival rate showed that patients with low miR-24-1 expression had obviously poor survival outcomes in the TCGA datasets (Figure 2D). Finally, we calculated the correlation coefficient of the expression levels for *FBP1* and miR-24-1 in tumor tissues. The result showed their expressions are

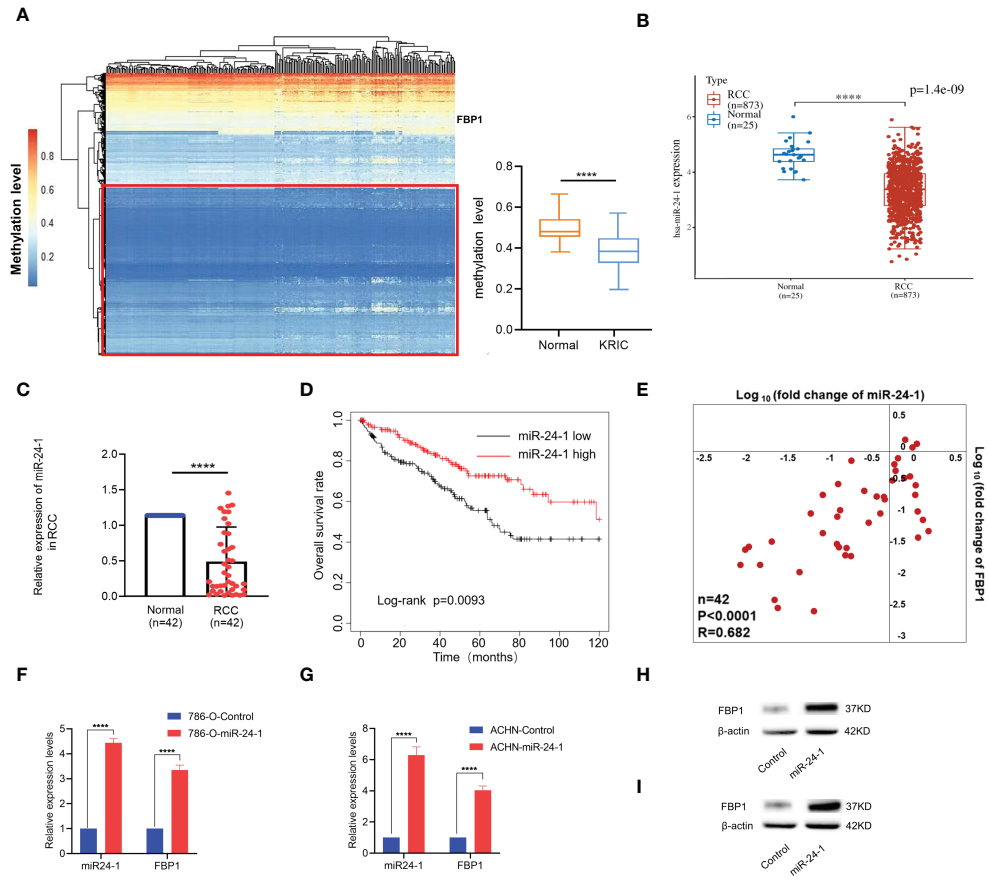

FIGURE 2
Tumor suppressor gene *FBP1* can be activated by miR-24-1 in RCC cells. **(A)** Left panel: DNA methylation profiling for downregulated tumor suppressor genes in RCC, reporting the depletion of *FBP1* in RCC was not caused by hypermethylation in promoter; Right panel: the methylation level of *FBP1* promoter between normal and KIRC ones. **(B)** The expression levels of miR-24-1 in RCC and adjacent normal renal tissues from TCGA database by bioinformatic analysis. **(C)** The expression levels of miR-24-1 in RCC and adjacent normal renal tissues detected by qPCR. **(D)** Kaplan–Meier survival analysis showed miR-24-1 is significantly associated with poor overall survival in RCC patients with low expression of miR-24-1 (n=166) compared to high expression of miR-24-1 (n=265). **(E)** Both miR-24-1 and *FBP1* are downregulated in RCC compared to normal ones. Besides, the expression levels of miR-24-1 and *FBP1* in RCC tissues exhibit a significantly positive correlation. Correlation coefficient = 0.682. **(F, G)** The activation of *FBP1* by miR-24-1 was assessed by qPCR in 786-O **(F)** and ACHN **(G)** cells after transfecting miR-24-1 expression vectors. **(H, I)** The protein levels of FBP1 in 786-O **(H)** and ACHN **(I)** cells were increased after transfecting miR-24-1 confirmed by western blot. Results are shown as mean ± S.D., ****p < 0.0001.

significantly positively correlated (R=0.682), implying *FBP1* may be positively regulated by miR-24-1 (Figure 2E). Taken together, these findings indicated that both *FBP1* and miR-24-1 are downregulated in RCC and that their downregulation can predict poor survival in RCC.

As *FBP1* can be upregulated by miR-24-1 in HEK293T cells (13), we examined whether miR-24-1 exerts an activating effect on *FBP1* in the RCC cell lines 786-O and ACHN. Lentiviruses overexpressing miR-24-1 (GFP+) and empty control vector (GFP+) were transfected into 786-O and ACHN cells to obtain stable cell lines. Accordingly, the expression levels of miR-24-1 in 786-O and ACHN cells were increased by 4-fold and 6-fold, respectively; moreover, *FBP1* expression was increased by 3.2-fold and 4-fold, respectively, after miR-24-1 overexpression (Figures 2F, G). The protein expression levels of FBP1 were confirmed in 786-O and ACHN cells by western blot analysis and were consistent with the above result (Figures 2H, I). These results showed *FBP1* can be upregulated by miR-24-1 in RCC cells.

MiR-24-1 suppresses the proliferation and migration of RCC cells by activating FBP1

To investigate how *FBP1* activation by miR-24-1 affects the proliferation of 786-O and ACHN cells, colony formation assays were performed by utilizing the above stable cell lines. The

observations showed that transfection of miR-24-1 reduced the number of colonies formed by both 786-O and ACHN cells after incubation for 14 days (Figures 3A, B). In addition, a CCK-8 assay was carried out to characterize cell viability at different timing (12, 24, 48, 72 and 96 hours, respectively). 786-O cells with overexpressing miR-24-1 showed a higher growth rate than the corresponding control group at 48, 72, and 96 hours, and ACHN cells overexpressing miR-24-1 showed a higher growth rate than the corresponding control cells at 72 and 96 hours (Figures 3C, D). These results indicate *FBP1* activation by miR-24-1 can repress the proliferation and growth of RCC cells. In turn, transfecting miR-24-1 inhibitor can suppress *FBP1* expression (Supplementary Figures 1A, B) and promotes the proliferation and growth of RCC cells (Supplementary Figures 1C, D).

In addition to validating its effects on the proliferation and growth of RCC cells, we also assessed whether miR-24-1 overexpression affects the migration ability of them. The wound healing assay revealed that the wound areas of 786-O and ACHN cells overexpressing miR-24-1 closed significantly slower than those of the corresponding control cells after incubation for 24 hours (Figures 3E, F). Furthermore, the numbers of 786-O and ACHN cells with miR-24-1 overexpression that migrated and traversed the membrane into

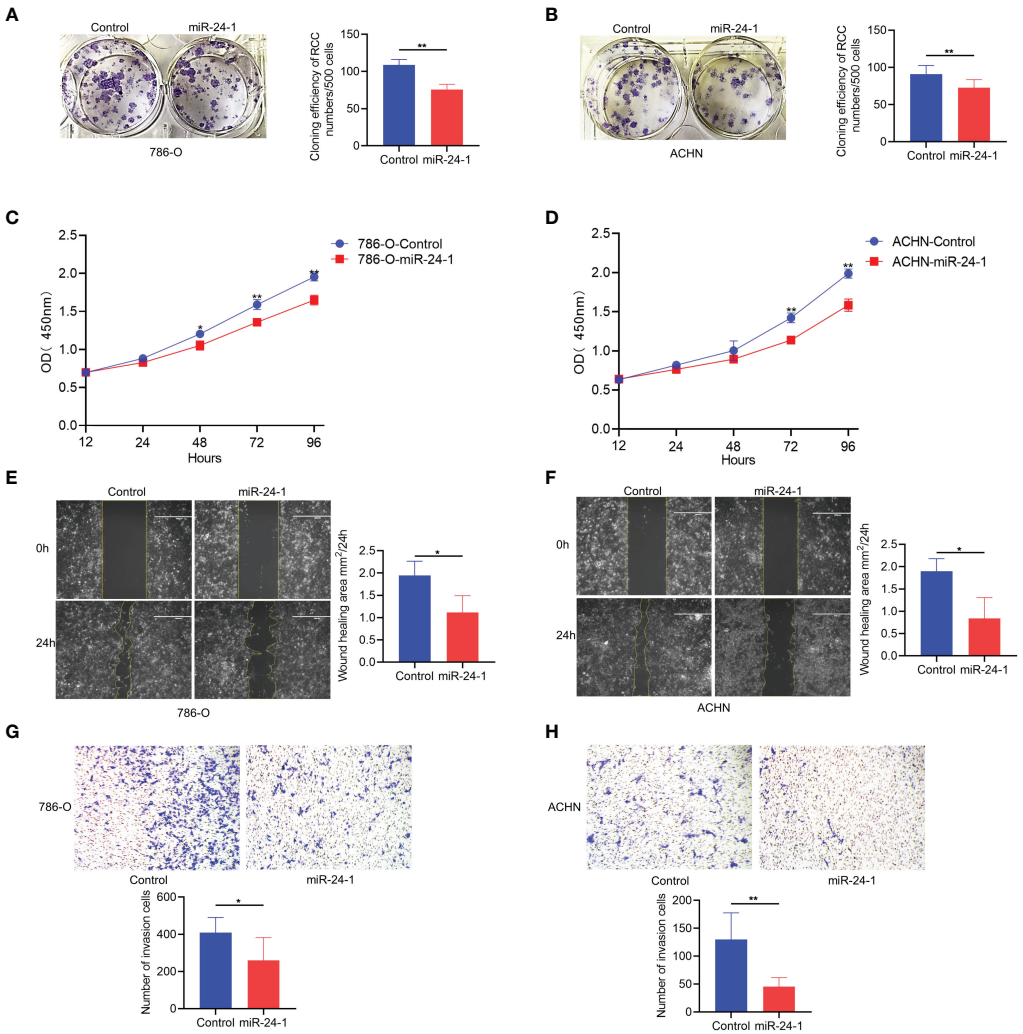

FIGURE 3
FBP1 can be activated by miR-24-1 and inhibit the proliferation and migration of RCC cells. **(A, B)** The colony formation ability of 786-O **(A)** and ACHN **(B)** cells was inhibited after overexpressing miR-24-1 in colony formation assay. **(C, D)** The proliferation ability of 786-O **(C)** and ACHN **(D)** cells was blocked after overexpressing miR-24-1 in CCK8 assay. **(E, F)** The migrating abilities of 786-O **(E)** and ACHN **(F)** cells were inhibited after overexpressing miR-24-1 in would healing assay. **(G, H)** The migrating and invasive abilities of 786-O **(G)** and ACHN **(H)** cells were repressed after overexpressing miR-24-1 in transwell assay. Results are shown as mean ± S.D. of triplicated experiments, $^{**}p < 0.01$, $^{*}p < 0.05$.

the lower chamber were obviously lower than those of the corresponding control cells in the transwell assay (Figures 3G, H), indicating that *FBP1* activation by miR-24-1 overexpression can block the migrating ability of RCC cells. Overall, these results suggest FBP1 activated by miR-24-1 plays an inhibitory role in the proliferation and migration of RCC cells.

Transcriptional activation of FBP1 by miR-24-1 is mechanistically triggered by an enhancer

Enhancers overlapping with miRNA loci crosstalk with the corresponding miRNAs to increase the expression of miRNAs crucial for cell identity (15). Hence, we hypothesized that miR-24-1 increases enhancer activity and, thus, this enhancer activates transcriptional expression of *FBP1*. To test our hypothesis, we first inserted the enhancer region containing the miR-24-1 DNA locus into the pGL3 vector to construct the pGL3 enhancer and detected enhancer activity by a dual luciferase reporter assay (Figure 4A). As shown in Figure 4B, the enhancer sequence indeed exhibited enhancer activity after transfection with the pGL3-enhancer vector compared to the control (Figure 4B). In addition, when the pGL3-enhancer vector was co-transfected with the miR-24-1 expression vector, the reporter activity of was obviously increased compared to that in cells transfected with only the pGL3-enhancer vector (Figure 4B), suggesting that miR-24-1 can boost enhancer activity to activate the reporter.

Furthermore, we evaluated the alterations in H3K27ac and H3K4me1 enrichment at the miR-24-1 locus by ChIP-qPCR, because H3K27ac and H3K4me1 are typical enhancer markers. A greater enrichment of H3K27ac and H3K4me1 at miR-24-1 loci was observed in miR-24-1-overexpressing cells (Figures 4C, D). Taken together, these results demonstrated that miR-24-1 can increase enhancer activity to activate the expression of the target gene FBP1. Conversely, we examined whether deletion of the enhancer region (54 bp) by CRISPR/Cas9 gene editing exerts a negative effect on the regulation of *FBP1* by miR-24-1 (Figures 4E, F). As expected, in wild-type ACHN cells, miR-24-1 overexpression increased the expression of *FBP1*; however, after deletion of the enhancer, overexpression of miR-24-1 no longer activated *FBP1* in ACHN cells compared to wild-type ACHN cells, as determined by qPCR (Figure 4F). Consistent with the alterations in mRNA expression, FBP1 protein expression was not activated, as determined by western blot analysis (Figure 4G).

FBP1 reactivation disrupts Warburg effect to suppress kidney cancer

FBP1, a rate-limiting enzyme in gluconeogenesis, catalyzes the hydrolysis of fructose 1,6-bisphosphate to fructose 6-phosphate, playing a critical role in the energy metabolism of cancer cells. To investigate whether *FBP1* blocks RCC progression through the Warburg effect, the levels of glucose consumption and lactate production were measured in RCC cell lines. It showed that miR-24-1 inhibits aerobic glycolysis by activating *FBP1*, as indicated by the decreases in glucose consumption and lactate production in 786-O and ACHN cells (Figures 5A, B). To further evaluate the impact of miR-24-1 and *FBP1* on aerobic glycolysis in RCC cells, the ECAR was measured with an XFe24 extracellular flux analyzer (Seahorse). The glycolytic ECAR was measured immediately following the addition of glucose after the cells were glucose starved for approximately 2 hours. The maximum glycolytic capacity is equal to the ECAR after oligomycin treatment. Transfection of miR-24-1 can reduce the ECAR (Figures 5C, D) and the maximum glycolytic capacity (Figures 5E, F) of 786-O and ACHN cells. Moreover, we detected the mRNA levels of the glycolysis-related genes *LDHA* and glucose transporter 1 gene *GLUT1* which are two key factors in Warburg Effect after transfecting miR-24-1 in 786-O and ACHN cells. The results showed activation of *FBP1* by miR-24-1 further declined the expression of *LDHA and GLUT1* (Figures 5G, H). Collectively, these findings indicated that overexpression of miR-24-1 activates *FBP1* transcription by targeting active enhancers in the nucleus, and reactivated *FBP1* then inhibits Warburg effect in cancer cells by slowing aerobic glycolysis, which finally blocks RCC progression (Figure 5I).

The *FBP1*/miR-24-1/enhancer axis inhibits kidney tumor growth in mice

Since *FBP1* can be activated by miR-24-1 expression induced by enhancer elements, we further studied the function of the *FBP1*/miR-24-1/enhancer axis in tumor growth *via* xenograft experiments *in vivo*. First, ACHN cells stably expressing miR-24-1 with deletion of the enhancer region and the corresponding control cells were orthotopically injected into the flanks of male nude mice to test the function of miR-24-1 in tumor growth (4×10^6 cells/mouse, three groups of mice, n=6 mice/group). Notably, successful overexpression of miR-24-1 was demonstrated in these stable cells to increase *FBP1* expression (Figures 2F, G) or fail to increase FBP1 expression due to deletion of the enhancer region (Figure 4G). The growth rate was calculated and reported as the tumor volume during the treatment process.

As observed in Figure 6A, the growth of tumors derived from miR-24-1-overexpressing ACHN cells was significantly inhibited compared to that of tumors derived from empty vector-transfected cells or cells with enhancer deletion. After 6 weeks, the mice were sacrificed to obtain tumors for further

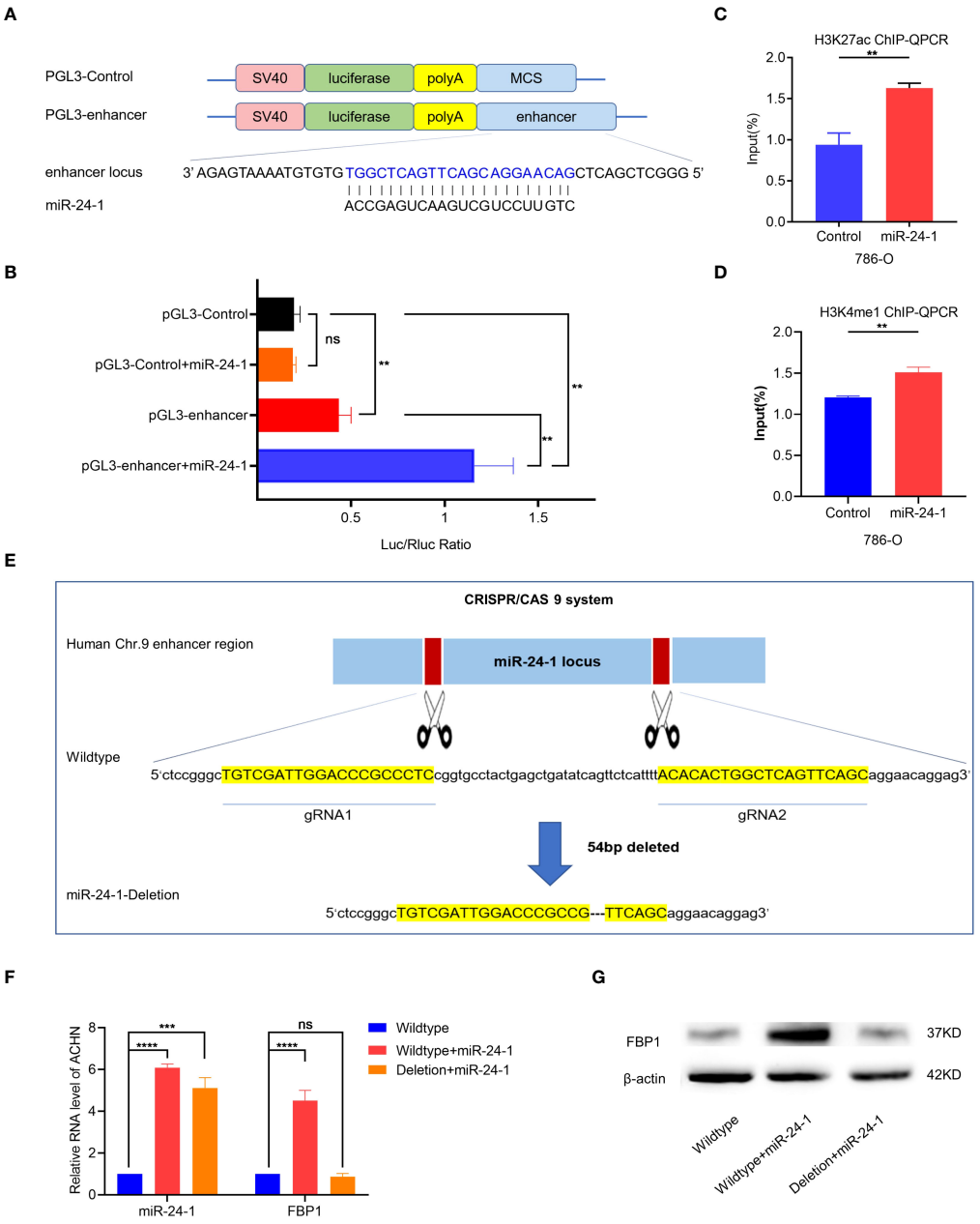

FIGURE 4
MiR-24-1 mechanistically activates *FBP1* through enhancer. **(A)** The schematic diagram of pGL3-enhancer vector construction in dual luciferase reporter gene assay. The enhancer sequence containing miR-24-1 DNA locus located on 60 kb upstream from *FBP1* was inserted into pGL3 vector to construct pGL3-enhancer vector. **(B)** The enhancer sequence containing miR-24-1 DNA locus can increase the activity of reporter gene. Co-transfection of miR-24-1 expression vector and pGL3-enhancer vector induced an increase of enhancer activity in dual luciferase reporter gene assay. **(C, D)** More enrichment of H3K27ac **(C)** and H3K4me1 **(D)** on miR-24-1 locus was observed by ChIP-qPCR after overexpressing miR-24-1. **(E, F)** The schematic diagram of CRISPR/Cas9 system. A deletion of 54bp in enhancer sequence containing miR-24-1 **(E)** was confirmed by Sanger sequencing **(F)**. **(G)** The mRNA expression levels of *FBP1* were detected by qPCR. *FBP1* was increased when overexpressing miR-24-1, yet failed to be activated when enhancer was deleted. **(G)** Similarly, the protein expression levels of FBP1 were detected by western blot. Results are shown as mean ± S.D., ****p < 0.0001, ***p < 0.001, **p < 0.01, ns means not significant.

studies. The tumors from the miR-24-1 overexpression group were smaller and weighed less than those from the empty vector-transfected and enhancer deletion groups (Figures 6B–D), suggesting that miR-24-1 overexpression activated *FBP1* expression to block tumor growth in a manner dependent on enhancer integrity. Moreover, we performed qPCR assay to figure out the expression levels of miR-24-1 in the tumor tissues among three groups. As seen in Figure 6E, miR-24-1

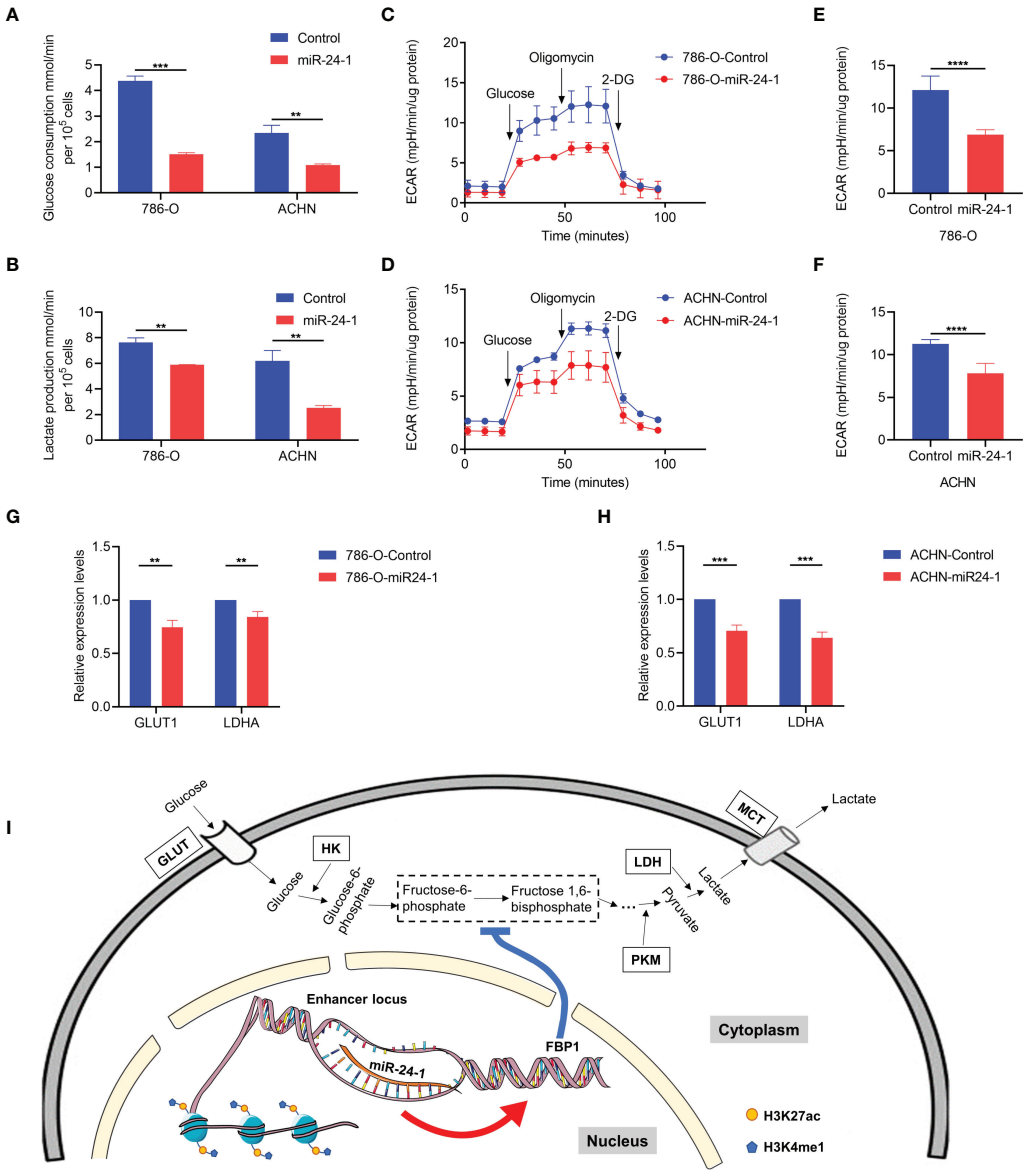

FIGURE 5
FBP1 suppresses Warburg effect in RCC cells. **(A)** Quantification of glucose consumption in miR-24-1-overexpressing 786-O and ACHN cells. **(B)** Lactate production in 786-O and ACHN cells transfected with miR-24-1 was measured by lactate assay. **(C, D)** Extracellular acidification rate (ECAR) of 786-O **(C)** and ACHN **(D)** cells was detected after miR-24-1 overexpression with glucose starved for two hours and subsequently treated with 2 g/L D-glucose, 1 μM oligomycin, and 100 mM 2-Deoxyglucose (2-DG). **(E, F)** ECAR represents maximum glycolytic capacity after oligomycin treatment of 786-O **(E)** and ACHN **(F)** cells. **(G, H)** qPCR analysis of glycolytic related genes in vector control or miR-24-1-overexpressing 786-O **(G)** and ACHN **(H)** cells. **(I)** Schematic diagram of *FBP1* being activated by miR-24-1 to disturb Warburg effect in RCC cells. The enriched modifications of H3K4me1 and H3K27ac represent active enhancer markers. Results are shown as mean ± S.D. of triplicated experiments, ****p < 0.0001, ***p < 0.001, **p < 0.01.

was significantly upregulated in both the overexpressing miR-24-1 group and enhancer-deleted group after transfecting miR-24-1 lentivirus compared to control group, however, *FBP1* was only activated in the over-expressing miR-24-1 group but not in enhancer-deleted group even miR-24-1 was overexpressed. HE staining confirmed that the tumors in each group were indeed RCCs (Figure 6F); IHC staining revealed that there were fewer Ki-67-positive cells in the miR-24-1 overexpression group than in the empty vector-transfected and enhancer deletion groups. In turn, TUNEL-positive cells were significantly more abundant in the miR-24-1 overexpression group than in the other two groups

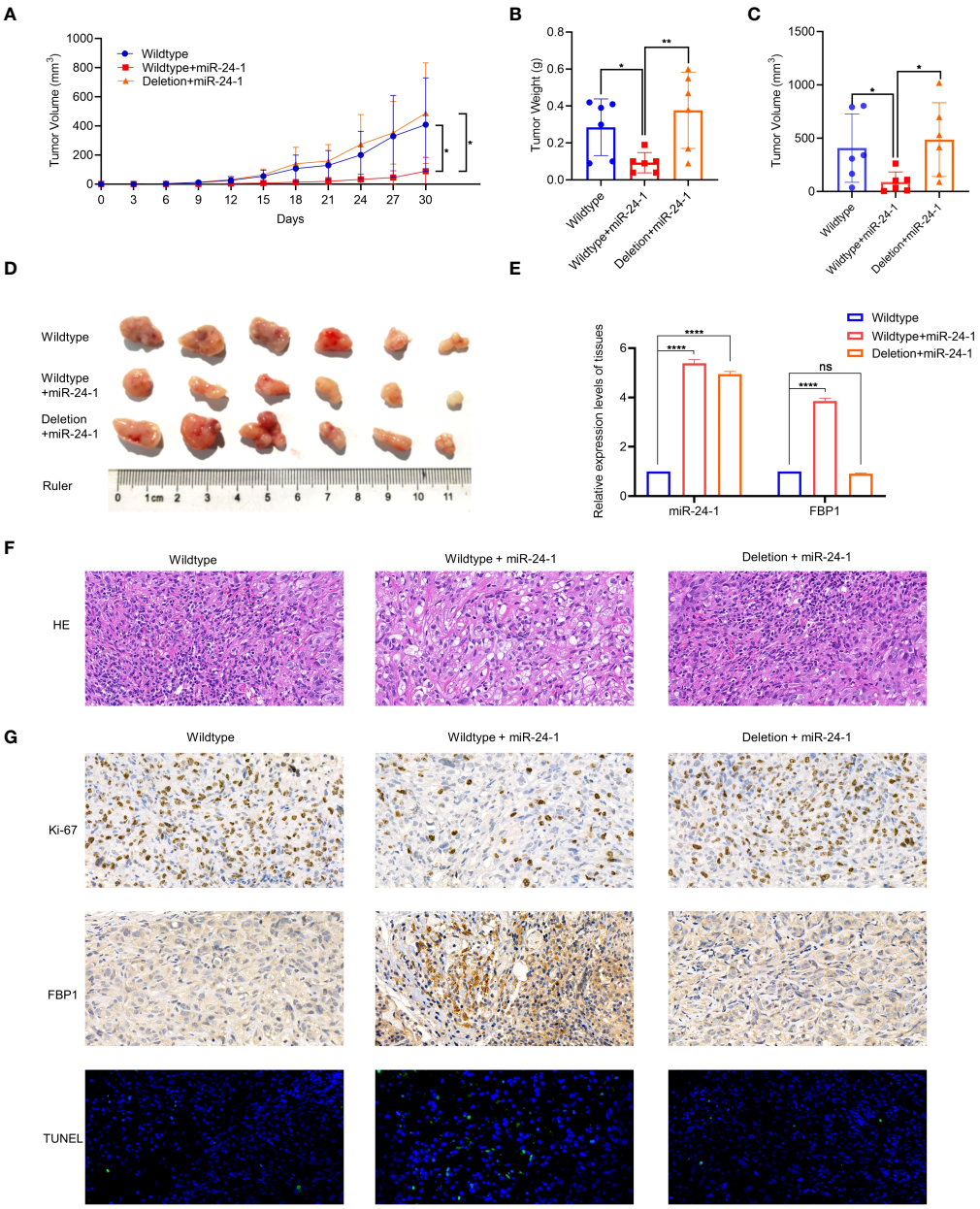

FIGURE 6
MiR-24-1 activates *FBP1 via* enhancer to suppress tumor growth *in vivo*. **(A)** Measuring tumor sizes every 3 days during feeding period. The day when tumors were initially formed marked as day 0. Mice were sacrificed on day 30. **(B, C)** The weight and size of tumors were calculated. **(D)** The dissected tumors from sacrificed mice were photographed. **(E)** qPCR assay was performed to detect the expression levels of miR-24-1 and *FBP1* in the tumor tissues among three groups. **(F)** Representative images of HE staining of tumors. HE staining confirmed that the tumors in each group were indeed RCCs (magnification, 500×). **(G)** Representative images of immunohistochemistry of tumors. The expression of Ki-67 was obviously less in the tumors from overexpressing miR-24-1 group than those from control group and enhancer-deleted group (top). The expression of *FBP1* was increased by overexpressing miR-24-1, but not when enhancer was deleted (middle). The number of TUNEL-positive cells (green fluorescent signal) in the overexpressing miR-24-1 group was significantly increased, indicating an increase of the apoptosis of tumor cells in this group (bottom) (magnification, 500×). Results are shown as mean ± S.D., **p < 0.01, *p < 0.05, ****p < 0.0001, ns means not significant.

(Figure 6G), indicating that miR-24-1 overexpression inhibits tumor growth and increases the number of apoptotic cells. In addition, the protein level of FBP1 was elevated obviously in miR-24-1 overexpression group but not in the enhancer deletion group as seen in Figure 6G. Collectively, these results indicate that *FBP1* can be activated by miR-24-1 and inhibit tumor growth in a manner dependent on enhancer integrity (Figure 6G).

Discussion

Although a myriad of RCC investigations have already been conducted, challenges remain in understanding its underlying mechanism (27). Recent studies have shown that *FBP1* is a critical player in the malignancies (28–31). Glycogen Branching Enzyme 1 (GBE1)-mediated *FBP1* suppression *via* promoter methylation contributes to tumor progression in lung adenocarcinoma (LUAD) (32). Low expression of *FBP1* is directly related to a poor overall survival rate based on JavaScript:; a comprehensive profiling of TCGA dataset, indicating that *FBP1* may be considered a potential prognostic biomarker in RCC as a tumor suppressor (32). Importantly, as a tumor suppressor, *FBP1* is generally depleted in ccRCC (11); thus, upregulating the expression of *FBP1* is a potential therapeutic strategy for cancer. In our study, we found that *FBP1* is depleted in RCC and can be activated by miR-24-1, which implies a potential treatment strategy for RCC.

MiRNAs are tumor hallmarks that are only 21-23 *nt* in length, and play critical roles in immunity (33), metabolism (34), cell proliferation and differentiation (35), and tumor progression (36). Since the discovery of these short RNA molecules in *Caenorhabditis elegans* (37) in 1990s, miRNAs have been recognized to negatively regulate gene expression by degrading or repressing their target mRNAs (38). However, recent studies have also shown that miRNAs are as well involved in gene activation (13, 39, 40). For example, enhancer-overlapped miRNAs can activate target genes through chromatin remodeling at enhancer regions (13). Our work demonstrated that overexpression of miR-24-1 can activate *FBP1* to block RCC proliferation and metastasis (Figures 2F, G), shedding a light on the unconventional role of miRNAs in malignancies. However, there is still a paucity of datasets about the crosstalk between miRNAs and enhancers.

Enhancers are *cis*-acting DNA sequences that can function as transcription factor binding platforms and increase gene transcription levels independent of their orientation and location (41, 42). We verified miRNAs overlapped within enhancer region are capable of activating target genes *via* binding to enhancers in a manner dependent on the enhancer integrity (Figures 4F, G). In addition, our work showed that deletion of miR-24-1 reduces enhancer activity in RCC, nevertheless, enhancer inactivation leads to low expression of *FBP1*, which in turn promoted the Warburg effect. Although Warburg effect phenotype is well established, its role in cancer metabolism progression is still incompletely defined. In our study, we found that activation of the tumor suppressor *FBP1* by miR-24-1 can inhibit Warburg effect in RCC, suggesting that blockade of metabolic processes such as Warburg effect through miR-24-1 constitutes a good therapeutic strategy for RCC.

In conclusion, the current study revealed that low expression of enhancer-associated miR-24-1 can contributes to inactivation of *FBP1*, and that *FBP1* depletion further facilitates Warburg effect, which eventually promotes RCC development. Taken together, our findings provide an alternative mechanism for the low expression of *FBP1* in RCC and a potential therapeutic strategy for RCC treatment.

Data availability statement

The original contributions presented in the study are included in the article/supplementary material. Further inquiries can be directed to the corresponding authors.

Ethics statement

The studies involving human participants were reviewed and approved by ethics committee of Fourth Military Medical University. The patients/participants provided their written informed consent to participate in this study. The animal study was reviewed and approved by Ethics Committee of Fourth Military Medical University.

Author contributions

DJ and YL performed the research and wrote the manuscript. WY and YW provided experimental conditions. JLY contributed to the financial support and administrative support. GH, WZ, and GZ analyzed the data. XD, DW, FY, LZ, and JRY modified the manuscript. DL, YZ, FW, and PM provided the clinical samples. All authors contributed to the article and approved the submitted version.

Funding

Our work was supported by the Xijing Hospital subject booster plan translational medicine research projects (grant number XJZT13Z05), the Military medical innovation project (grant number 16CXZ023) and the National Natural Science Foundation of China (grant number 81672535) and the Shaanxi Provincial Key Research and Development Program (grant number 2021SF-053).

Conflict of interest

The authors declare that the research was conducted in the absence of any commercial or financial relationships that could be construed as a potential conflict of interest.

Publisher's note

Supplementary material

The Supplementary Material for this article can be found online at: https://www.frontiersin.org/articles/10.3389/fonc.2022.928373/full#supplementary-material.

SUPPLEMENTARY FIGURE 1
miR-24-1 inhibitor declines the expression of *FBP1* and promotes the proliferation and migration of RCC cells. **(a, b)** qPCR assay was performed to confirm that the expression of miR-24-1 was successfully declined after transfecting miR-24-1 inhibitor, and *FBP1* was accordingly downregulated in ACHN (a) and 786-O **(b)** cells. **(c, d)** The proliferation ability of 786-O (c) and ACHN (d) cells was promoted after transfecting miR-24-1 inhibitor in CCK8 assay. Results are shown as mean ± S.D. of triplicated experiments, ****p < 0.0001, **p < 0.01, *p< 0.05.

References

1. Hakimi AA, Reznik E, Lee CH, Creighton CJ, Brannon AR, Luna A, et al. An integrated metabolic atlas of clear cell renal cell carcinoma. *Cancer Cell* (2016) 29 (1):104–16. doi: 10.1016/j.ccell.2015.12.004

2. Inamura K. Renal cell tumors: Understanding their molecular pathological epidemiology and the 2016 WHO classification. *Int J Mol Sci* (2017) 18(10):2195. doi: 10.3390/ijms18102195

3. Gnarra JR, Tory K, Weng Y, Schmidt L, Wei MH, Li H, et al. Mutations of the VHL tumour suppressor gene in renal carcinoma. *Nat Genet* (1994) 7(1):85–90. doi: 10.1038/ng0594-85

4. Linehan WM, Schmidt LS, Crooks DR, Wei D, Srinivasan R, Lang M, et al. The metabolic basis of kidney cancer. *Cancer Discovery* (2019) 9(8):1006–21. doi: 10.1158/2159-8290.CD-18-1354

5. Rankin EB, Tomaszewski JE, Haase VH. Renal cyst development in mice with conditional inactivation of the von hippel-lindau tumor suppressor. *Cancer Res* (2006) 66(5):2576–83. doi: 10.1158/0008-5472.CAN-05-3241

6. Wettersten HI, Aboud OA, Lara PN Jr., Weiss RH. Metabolic reprogramming in clear cell renal cell carcinoma. *Nat Rev Nephrol* (2017) 13(7):410–9. doi: 10.1038/nrneph.2017.59

7. Lu J, Tan M, Cai Q. The warburg effect in tumor progression: mitochondrial oxidative metabolism as an anti-metastasis mechanism. *Cancer Lett* (2015) 356(2 Pt A):156–64. doi: 10.1016/j.canlet.2014.04.001

8. Warburg O. On the origin of cancer cells. *Science* (1956) 123(3191):309–14. doi: 10.1126/science.123.3191.309

9. Yang J, Wang C, Zhao F, Luo X, Qin M, Arunachalam E, et al. Loss of FBP1 facilitates aggressive features of hepatocellular carcinoma cells through the warburg effect. *Carcinogenesis* (2017) 38(2):134–43. doi: 10.1093/carcin/bgw109

10. Liu X, Wang X, Zhang J, Lam EK, Shin VY, Cheng AS, et al. Warburg effect revisited: an epigenetic link between glycolysis and gastric carcinogenesis. *Oncogene* (2010) 29(3):442–50. doi: 10.1038/onc.2009.332

11. Li B, Qiu B, Lee D, Walton Z, Ochocki J, Mathew L, et al. Fructose-1,6-bisphosphatase opposes renal carcinoma progression. *Nature* (2014) 513 (7517):251–5. doi: 10.1038/nature13557

12. Dai QC, Li N, Zhou XH. Increased miR-21a provides metabolic advantages through suppression of FBP1 expression in non-small cell lung cancer cells. *Am J Cancer Res* (2017) 7(11):2121–30.

13. Xiao M, Li J, Li W, Wang Y, Wu F, Xi Y, et al. MicroRNAs activate gene transcription epigenetically as an enhancer trigger. *RNA Biol* (2017) 14(10):1326–34. doi: 10.1080/15476286.2015.1112487

14. Liang Y, Zou Q, Yu W. Steering against wind: A new network of NamiRNAs and enhancers. *Genomics Proteomics Bioinf* (2017) 15(5):331–7. doi: 10.1016/j.gpb.2017.05.001

15. Liang Y, Xu P, Zou QP, Luo HB, Yu WQ. An epigenetic perspective on tumorigenesis: Loss of cell identity, enhancer switching, and NamiRNA network. *Semin Cancer Biol* (2019) 57:1–9. doi: 10.1016/j.semcancer.2018.09.001

16. Liang Y, Lu Q, Li W, Zhang DP, Zhang FL, Zou QP, et al. Reactivation of tumour suppressor in breast cancer by enhancer switching through NamiRNA network. *Nucleic Acids Res* (2021) 49(15):8556–72. doi: 10.1093/nar/gkab626

17. McCall MN, Kim MS, Adil M, Patil AH, Lu Y, Mitchell CJ, et al. Toward the human cellular microRNAome. *Genome Res* (2017) 27(10):1769–81. doi: 10.1101/gr.222067.117

18. Suzuki HI, Young RA, Sharp PA. Super-Enhancer-Mediated RNA processing revealed by integrative MicroRNA network analysis. *Cell* (2017) 168 (6):1000–1014 e15. doi: 10.1016/j.cell.2017.02.015

19. Zhang H, Guo J, Mao L, Li Q, Guo M, Mu T, et al. Up-regulation of miR-24-1 is involved in the chemoprevention of colorectal cancer by black raspberry anthocyanins. *Br J Nutr* (2019) 122(5):518–26. doi: 10.1017/S0007114518003136

20. Wang S, Liu N, Tang Q, Sheng H, Long S, Wu W. MicroRNA-24 in cancer: A double side medal with opposite properties. *Front Oncol* (2020) 10:553714. doi: 10.3389/fonc.2020.553714

21. Cui J, Shi M, Xie D, Wei D, Jia Z, Zheng S, et al. FOXM1 promotes the warburg effect and pancreatic cancer progression via transactivation of LDHA expression. *Clin Cancer Res* (2014) 20(10):2595–606. doi: 10.1158/1078-0432.CCR-13-2407

22. Jiang M, Liu S, Lin J, Hao W, Wei B, Gao Y, et al. A pan-cancer analysis of molecular characteristics and oncogenic role of hexokinase family genes in human tumors. *Life Sci* (2021) 264:118669. doi: 10.1016/j.lfs.2020.118669

23. Shi T, Ma Y, Cao L, Zhan S, Xu Y, Fu F, et al. B7-H3 promotes aerobic glycolysis and chemoresistance in colorectal cancer cells by regulating HK2. *Cell Death Dis* (2019) 10(4):308. doi: 10.1038/s41419-019-1549-6

24. Klacz J, Wierzbicki PM, Wronska A, Rybarczyk A, Stanislawowski M, Slebioda T, et al. Decreased expression of RASSF1A tumor suppressor gene is associated with worse prognosis in clear cell renal cell carcinoma. *Int J Oncol* (2016) 48(1):55–66. doi: 10.3892/ijo.2015.3251

25. Morris MR, Latif F. The epigenetic landscape of renal cancer. *Nat Rev Nephrol* (2017) 13(1):47–60. doi: 10.1038/nrneph.2016.168

26. Zhao M, Sun J, Zhao Z. TSGene: a web resource for tumor suppressor genes. *Nucleic Acids Res* (2013) 41(Database issue):D970–6. doi: 10.1093/nar/gks937

27. Barata PC, Rini BI. Treatment of renal cell carcinoma: Current status and future directions. *CA Cancer J Clin* (2017) 67(6):507–24. doi: 10.3322/caac.21411

28. Yang C, Zhu S, Yang H, Fan P, Meng Z, Zhao J, et al. FBP1 binds to the bromodomain of BRD4 to inhibit pancreatic cancer progression. *Am J Cancer Res* (2020) 10(2):523–35.

29. Li F, Huangyang P, Burrows M, Guo K, Riscal R, Godfrey J, et al. FBP1 loss disrupts liver metabolism and promotes tumorigenesis through a hepatic stellate cell senescence secretome. *Nat Cell Biol* (2020) 22(6):728–39. doi: 10.1038/s41556-020-0511-2

30. Cong J, Wang X, Zheng X, Wang D, Fu B, Sun R, et al. Dysfunction of natural killer cells by FBP1-induced inhibition of glycolysis during lung cancer progression. *Cell Metab* (2018) 28(2):243–255.e5. doi: 10.1016/j.cmet.2018.06.021

31. Dong C, Yuan T, Wu Y, Wang Y, Fan T, Miriyala S, et al. Loss of FBP1 by snail-mediated repression provides metabolic advantages in basal-like breast cancer. *Cancer Cell* (2013) 23(3):316–31. doi: 10.1016/j.ccr.2013.01.022

32. Liu M, Pan Q, Xiao R, Yu Y, Lu W, Wang L. A cluster of metabolism-related genes predict prognosis and progression of clear cell renal cell carcinoma. *Sci Rep* (2020) 10(1):12949. doi: 10.1038/s41598-020-67760-6

33. Eniafe J, Jiang S. *MicroRNA-99 family in cancer and immunity*. Wiley interdisciplinary reviews. *RNA* (2020) 12(3):e1635. doi: 10.1002/wrna.1635

34. Subramaniam S, Jeet V, Clements J, Gunter J, Batra J. Emergence of MicroRNAs as key players in cancer cell metabolism. *Clin Chem* (2019) 65 (9):1090–101. doi: 10.1373/clinchem.2018.299651

35. Wüst S, Dröse S, Heidler J, Wittig I, Klockner I, Franko A, et al. Metabolic maturation during muscle stem cell differentiation is achieved by miR-1/133a-Mediated inhibition of the Dlk1-Dio3 mega gene cluster. *Cell Metab* (2018) 27 (5):1026–1039.e6. doi: 10.1016/j.cmet.2018.02.022

36. Garofalo M, Leva G, Croce C. MicroRNAs as anti-cancer therapy. *Curr Pharm design* (2014) 20(33):5328–35. doi: 10.2174/1381612820666140128211346

37. Lee R, Feinbaum R, Ambros V. The c. elegans heterochronic gene lin-4 encodes small RNAs with antisense complementarity to lin-14. *Cell* (1993) 75 (5):843–54. doi: 10.1016/0092-8674(93)90529-y

38. Reinhart B, Slack F, Basson M, Pasquinelli A, Bettinger J, Rougvie A, et al. The 21-nucleotide let-7 RNA regulates developmental timing in caenorhabditis elegans. *Nature* (2000) 403(6772):901–6. doi: 10.1038/35002607

39. Tan H, Huang S, Zhang Z, Qian X, Sun P, Zhou X. Pan-cancer analysis on microRNA-associated gene activation. *EBioMedicine* (2019) 43:82–97. doi: 10.1016/j.ebiom.2019.03.082

40. Place RF, Li LC, Pookot D, Noonan EJ, Dahiya R. MicroRNA-373 induces expression of genes with complementary promoter sequences. *Proc Natl Acad Sci United States America* (2008) 105(5):1608–13. doi: 10.1073/pnas.0707594105

41. Bell R, Golan T, Sheinboim D, Malcov H, Amar D, Salamon A, et al. Enhancer methylation dynamics contribute to cancer plasticity and patient mortality. *Genome Res* (2016) 26(5):601–11. doi: 10.1101/gr.197194.115

42. Chen H, Li C, Peng X, Zhou Z, Weinstein J, Liang H. A pan-cancer analysis of enhancer expression in nearly 9000 patient samples. *Cell* (2018) 173(2):386–399.e12. doi: 10.1016/j.cell.2018.03.027

Frontiers in Oncology

Advances knowledge of carcinogenesis and tumor progression for better treatment and management

The third most-cited oncology journal, which highlights research in carcinogenesis and tumor progression, bridging the gap between basic research and applications to imrpove diagnosis, therapeutics and management strategies.

Discover the latest Research Topics

See more →

Frontiers

Avenue du Tribunal-Fédéral 34
1005 Lausanne, Switzerland
frontiersin.org

Contact us

+41 (0)21 510 17 00
frontiersin.org/about/contact